SECTION 4

Hydrological Analysis

Analyses of hydrological conditions at the PIEP focused on three specific issues: sedimentation, scour, and ice forces. These analyses were primarily for the North Expansion projects shown on Figure 1.2-3. Opinions related to extending the analyses to future phases of the project are also provided. The scope of the analyses included the assumption that existing information was sufficient, and no supplemental investigations were to be performed. Analysis of each of these three issues is documented below. Included is a discussion of the scope and limitations of the analyses, and conclusions relevant to the design of the PIEP.

4.1 Sedimentation Analysis

The U.S. Army Engineer Research and Development Center (ERDC) performed field investigations and a numerical modeling study to evaluate sedimentation and dredging requirements associated with expanding and deepening the POA. These studies are documented in USACE (2010). CH2M HILL was tasked to review the ERDC sedimentation study and assess the impact on the design and performance of the OCSP® system, which is the basis of the POA North Extension and Barge Berth Phase 2. It is CH2M HILL's understanding that the ERDC report is in the process of being finalized. Discussions with the lead author (Smith, 2012) indicated that although some of the sections have been edited for clarity, the data presented in the draft report are still valid. The following subsections summarize the relevant results of the ERDC study and the potential impacts on the design and performance of the as-built North Expansion area. Topics covered include:

- The physical setting related to hydraulics and sedimentation in the area, as well as historical dredging requirements
- Hydrodynamic and sediment transport modeling performed
- Implications for the North Expansion, as well as the future full build-out

4.1.1 Physical Setting

The hydraulics of Knik Arm are dominated by tidal influences. Large tidal swings, with a mean tidal range of 26.2 feet (NOAA, 2012) and a spring tide range of nearly 39 feet (USACE, 2010) result in strong currents through Knik Arm, with the water column vertically well-mixed. Headlands at Cairn Point, Point MacKenzie, and Point Woronzof (Figure 4.1-1) produce pronounced eddies on alternating flood and ebb flows. The POA is located within the eddy produced by Cairn Point during ebb flows which, combined with extremely high suspended sediment loads in the spring and summer, results in a depositional environment.

Most of the suspended sediment load is present during the spring and summer months and is associated with melting snowpack and glaciers. Knik Arm generally has ice cover from November through March, and suspended sediment loads are reduced during this period. USACE (2010) primarily addresses sedimentation during the summer season. Potential effects of reduced sediment loads during the winter season are briefly discussed but were not the focus of the study. These are addressed separately below in Section 4.2, Scour Analysis.

Sedimentation rates during the spring and summer are relatively high, with basin average sedimentation rates of approximately 1.6 inches per day measured in August 2006. The dynamic nature of Knik Arm is also reflected in variations in dredging volumes over time. Between 1980 and 1998, annual dredge volumes at the POA were relatively constant at roughly 260,000 to 390,000 cubic yards (cy). Beginning in 1999, dredging volumes increased to approximately 2 million cy per year before declining to approximately 1.3 million cy per year in recent years.

Construction of the PIEP will alter the hydrodynamics of Knik Arm in the area of the port because of extending the sheet pile dock face approximately 400 feet further into Knik Arm, replacing the pile-supported wharf with a sheet pile structure, eventually extending the wharf to the north and south from its present 2,500-foot length to a total length of approximately 8,200 feet, and expanding and dredging the basin serving the port.

4.1.2 Summary of ERDC Modeling Performed

Modeling was performed and documented by USACE (2010) to evaluate potential future dredging requirements within the POA during five phases of port and basin expansion. Models used to assess sedimentation impacts at the POA included a two-dimensional (2D) ADvanced CIRCulation (ADCIRC) hydrodynamic model of oceanic, coastal, and estuarine waters for the entire Cook Inlet and a more focused three-dimensional (3D) hydrodynamic and sediment transport model (LTFATE) of the upper portion of Cook Inlet. LTFATE combines the 3D Environmental Fluid Dynamics Code (EFDC) hydrodynamic and transport model with the SEDZLJ cohesive and non-cohesive sediment transport model to allow simulation of erosion, transport, and deposition of sediments through the model domain.

4.1.2.1 ADCIRC Hydrodynamic Model

ADCIRC was used by ERDC to simulate the hydrodynamics associated with the propagation of tides from the Gulf of Alaska to the study site and through the estuary. ADCIRC model results were used to establish hydrodynamic boundary conditions for the LTFATE model, as well as to assess hydrodynamic changes in lower Knik Arm resulting from the various phases of the PIEP. The ADCIRC results were also used to provide hydrodynamics for a Lagrangian particle-tracking model to assess dredging operations and to provide hydrodynamic conditions for ship simulation studies. According to discussions with USACE staff, the particle tracking model was never documented; rather it was used as a visual model.

Field measurements of currents using acoustic Doppler current profilers (ADCPs) collected by ERDC over two sampling periods, July/August 2002 and August 2006, were used as calibration data for calibrating and verifying the performance of their model. The 2002 data, consisting of current measurements collected by the National Ocean Service (NOS) over a number of transects, were used to assess the ability of the model to accurately simulate water exchange between upper Cook Inlet and Knik Arm. The 2006 data were collected in the area of the POA and focused on capturing formation and structure of the Cairn Point ebb tide gyre. These data were used to calibrate and verify that the model was representing the gyre development, size, structure, and evolution.

The model was run using the shoreline and bathymetry for the pre-expansion conditions at the POA, as well as modified shorelines and bathymetries representing the different phases of construction, including the shorelines indicative of the existing North Expansion area and the future completed PIEP configuration. Figure 4.1-2 shows the shoreline configurations and bathymetry used by ERDC to represent the pre-expansion and proposed future complete port expansion scenarios.

Model results were presented in USACE (2010) for a number of tide stages in the form of vector and contour plots of current velocities in the area of the port. Frequency distributions of model results of dock-parallel currents at locations 50 feet off the dock faces for existing berths and berths along the proposed expanded port dock face are summarized in USACE (2008b). These results indicate that an increase in magnitude and prevalence of flood-directed currents can be expected along the length of the dock face. Ebb-directed currents are generally weaker in the area of the North Expansion and become stronger towards the south end of the expanded port.

Results for the pre-expansion, North Expansion, and future complete port expansion scenarios for maximum flood and maximum ebb flows are reproduced in Figures 4.1-3 and 4.1-4. These show that the hydraulics in the vicinity of the POA will be modified as a result of extending the shoreline further into Knik Arm. Comparison of plots in Figure 4.1-4 show impacts to the size, location, and strength of the ebb flow gyre that forms off Cairn Point. The "dead space" that can be seen at maximum ebb in the area of the existing port in Figure 4.1-4 (a) is largely gone for the future complete expansion scenario shown in Figure 4.1-4 (c). The North Expansion is located in the area where the ebb tide eddy appears strongest, and extension of the shoreline during the PIEP and subsequent phases limits the development of the eddy.

Model results showed predicted maximum dock parallel velocities of about 1.6 knots (2.7 ft/s, 0.82 m/s) along the dock face for the existing berths. By comparison, maximum velocities ranging from 2.2 to 2.4 knots (3.7 to 4.1 ft/s, 1.1 to 1.2 m/s) were predicted for the expanded port, for an increase of approximately 40 to 50 percent.

4.1.2.2 Sedimentation Modeling

Sedimentation modeling was performed by ERDC using LTFATE, which includes the EFDC hydrodynamic and transport model and the SEDZLJ sediment transport model. The model domain for the LTFATE model extended from an open boundary between East and West Foreland in Cook Inlet up through Knik Arm and Turnagain Arm (Figure 4.1-5).

Calibration of the hydrodynamics was performed using the 2002 and 2006 datasets that were used for calibrating the ADCIRC model. Although EFDC has the capability of modeling 3D hydrodynamics, the model was run in a depth-averaged mode because the water column in the modeled area is well-mixed through most of the tidal cycle.

The model was run to simulate conditions during the August through September 2006 data collection period. The sediment transport model was calibrated by adjusting the critical shear stress for deposition until the average daily sedimentation rate over the 2-month simulation matched the average rate of 1.6 inches/day observed during that period.

Sedimentation over the August-September 2006 period was simulated for the pre-expansion port configuration and for six scenarios representing different phases of expansion and dredging from the initial North Expansion project to full build-out. Twenty dredging polygons, shown in Figure 4.1-6, were defined to monitor the sediment accumulation in both historical and future dredging areas. The polygon labeled H1 contains the existing wharf and extends out to the location of the future expanded OCSP® structure face.

The model results show that sedimentation within the sediment polygons as a whole will increase slightly with the construction of the North Expansion, likely as a result of small-scale eddies caused by discontinuities in the shoreline, then decrease as the full future expansion is complete. Sedimentation along the central berths of the future port (based on results for the H2 polygon) decreased from 1.6 inches/day to 1.3 inches/day (4.1 cm/day to 3.4 cm/day) largely as a result of increased current velocities along the proposed future OCSP® structure face. Although overall sedimentation rates will decrease, the overall volume of sediment and dredging requirements will increase because of the expanded footprint of the areas to be dredged. Model results predicted that the sedimentation volume for the future expanded port could be on the order of 2.1 times the volumes dredged from the historical dredge prism. For the North Expansion phase, sedimentation volume for the dredge polygons in Figure 4.1-6 was estimated to be 2.8 times that for the historical dredge areas under the pre-expansion scenario.

Two additional model runs were made by ERDC: one for the pre-expansion scenario, and one for the full build-out. These runs simulated potential winter conditions by reducing suspended sediment concentrations for the initial conditions and inflows into the model and by increasing the critical shear stress for erosion on mudflats where sediments would be bound up by ice in order to reduce the potential for erosion in those areas. Overall reductions in sedimentation volumes on the order of 25 percent were predicted for these model runs. Details on the distribution of the sedimentation rates over the defined polygons were not provided.

Note that the discussion of sedimentation in the previous paragraphs assumes full build-out of the PIEP with an approximately 8,000-foot OCSP® structure. Because the project is currently in a partially constructed condition, sedimentation is accumulating in the berth currently occupied by Totem Ocean Trailer Express (TOTE). This is being studied separately by USACE.

4.1.3 Summary

The ERDC sedimentation study was focused on changes to hydrodynamics resulting from the PIEP during the various construction phases and the associated impacts these changes would have on dredging requirements. Clearly, the requirements for dredging would increase with the expanded footprint of the basin. However, rates of sedimentation for the specific areas near the OCSP® structure face will likely decrease because of higher current velocities. The sheet pile wall extends the berths further into Knik Arm, changes the shape and timing of the Cairn Point ebb gyre, and reduces the irregularities in the shoreline that otherwise could result in additional dead spots and accelerated sedimentation. Results of the study can be used to guide the POA to ensure that adequate dredging resources are available during the various stages of development.

A number of data gaps and their potential effect on uncertainties associated with results from the sedimentation model are discussed in USACE (2010). These include time-variable sediment loads and erosional properties of sediments throughout the model domain. The model was run based on available and collected data for August and September 2006. It is noted that sediment loads vary both seasonally and over longer periods and, at best, the model provides predictions of sedimentation during the modeled 60-day period. Sedimentation during other periods where the amount and characteristics of sediment delivered to the system vary may be significantly different. However, if hydrodynamics in the system are adequately represented, then the differences among the various scenarios should provide a reasonable representation of relative differences in sedimentation that can be expected.

No negative impacts of future sedimentation at the POA were identified. Potential for scour associated with the PIEP is discussed in Section 4.2. Changes in current velocities near the berths resulting from the PIEP extending further into Knik Arm should not have a negative impact directly on the loads to the structure; however, increased currents can have an impact on berthing operations and mooring forces and on exposure to ice loads.

4.2 Scour Analysis

CH2M HILL was tasked to review design assumptions and calculations that have been developed by PND to assess whether scour at the toe of the sheet pile wall has been adequately assessed. It does not appear that scour was assessed in the previous design to a significant level of detail. The Draft *PIEP Design Criteria* (ICRC, 2011) does not specify a scour allowance. Under the heading of *Open Cell Bulkhead Scour and Dredge Tolerance*, the Basis of Design provided in the Extended Wet Barge Berth (WBB) Design Manual (PND, 2011a) considers a 6-foot tolerance to allow for over-dredging and storage dredging by the USACE maintenance dredging program. Under the heading *Currents* it states:

> Loose silt and sand at the mudline move due to tidal currents that are a maximum average of 3 knots during both ebb and flood. A 3-knot current can move up to a 3-mm sand particle. Scour has not been observed. A scour apron can be added if the problem arises.

This statement indicates that scour was not expected to be a problem based on PND's assessment.

Although scour has not been identified as a significant issue at the existing POA berths, both seasonal bed erosion and more localized scour near the berths can be observed in USACE survey data, although it appears to be mild and the existing pile-supported facility is likely designed sufficiently so that scour is not an issue.

The PIEP differs from the existing facility both in type of construction and the hydrodynamic conditions that it will see. The OCSP® structure of the expanded port, which is fronted by regularly spaced fender piling, is a very different structure than the existing pile-supported dock, and scour around the piling in the vicinity of the OCSP® wall could be an issue. Hydrodynamic modeling by ERDC has shown that moving the berths 400 feet further into Knik Arm will result in increased current velocities along the dock face by as much as 50 percent over the existing facility. These differences can result in different scour mechanisms and magnitudes, and conclusions made by the designer on the potential for scour, if based solely on the observed conditions at the existing facility, are questionable.

4.2.1 Physical Setting

As discussed in Section 4.1, Sedimentation Analysis, the existing port lies within the ebb tide gyre behind Cairn Point which, because of the high suspended sediment concentrations in Knik Arm in the spring and summer, results in a depositional environment. Although the area as a whole is net depositional, localized scour can still occur in this environment based on the placement of specific structures. It is noted that most of the studies reviewed relevant to hydrodynamic and sedimentation issues are focused on the spring and summer months when sedimentation and corresponding dredging requirements in the POA are issues of concern.

In winter months, suspended sediment concentrations within Knik Arm decrease significantly as sediments delivered to the system with runoff and glacial melt no longer flow in and tidal flats freeze, reducing or eliminating erosion of these areas as an additional source of sediment. Figure 4.2-1, reproduced from USACE (2010), shows seasonal variations in suspended sediment concentrations based on samples collected from the POA wharf at lower, mid, and upper water column locations. These seasonal variations likely affect seasonal patterns of erosion and deposition within Knik Arm. Modeling of potential impacts of reduced sediment loads presented in USACE (2010) indicated that sedimentation will be reduced but the area of the POA as a whole may remain depositional; however, detailed results were not available to evaluate potential patterns within the dredging prism. It is also noted that, because winter sedimentation patterns were not the focus of the study, the model was not calibrated with data collected during the winter season, which increases the uncertainty of results and limits the extent of conclusions that can be made.

Erodability of sediments in the area of the POA was investigated by the USACE using a mobile High Shear Stress flume (SEDflume) designed to quantify sediment erosion rates and critical shear stress of fine-grained and mixed fine/coarse grained sediments. SEDflume tests were performed on freshly to weakly consolidated sediment samples collected from the site, slurried with site water, and allowed to consolidate for periods ranging from 2 hours to 100 days. These were used to develop a relationship between erosion rate and bottom shear for freshly to recently deposited sediments at the site to use in sedimentation modeling. Although these may be relevant for modeling the behavior of the recently deposited surface sediments at the site, it is unlikely that buried sediments at the site, which will become exposed after dredging in front of the wall and which will have undergone greater consolidation as a result of overburden pressures, will have similar cohesive properties to the sediments that were tested.

4.2.2 Scour Potential

The depth of the sediment surface in front of the OCSP® wall will depend on seasonal and longer-scale changes in the bathymetry in Knik Arm near the site, as well as localized scour effects resulting from the structure/current interactions. More localized scour holes can also occur as a result of propeller wash from ships and accompanying tug boats during berthing operations.

4.2.2.1 Seasonal or Long-Term Bed Changes

The USACE performed a series of hydrographic surveys documenting the seabed elevation along ten defined baseline profiles within Knik Arm between 2000 and 2010. Of these, four (BP3 through BP6) included the shoreline of the existing or future PIEP footprint (Figure 4.2-2). Table 4.2-1 lists survey drawings that were obtained from the USACE that compare surveyed profiles along each transect with previous surveyed profiles. Table 4.2-2 summarizes grain-size characteristics for geotechnical borings taken in the vicinity of each of the baseline profiles.

These profiles document relatively short-term seabed elevation changes near the site and give an indication of the stability of the bed over this period; however, the profiles may not be representative of possible longer-term changes at the site.

Under present conditions, the POA area is depositional in the spring and summer; however, there was a concern that erosion could occur at the berths during the winter when suspended sediments in the water column are reduced. Profile plots presented in the drawings listed in Table 4.2-1 were reviewed with a focus on changes over the winter season; that is, between the last survey from one year and the first survey of the subsequent year.

TABLE 4.2-1
Baseline Profile Comparison Summary

Survey/Drawing No.	Dates of Surveys Compared
1927-01	Sept 23, 2000 June 15, 2001 Aug 15, 2001
1978-02	Aug 15, 2001 Nov 2, 2001 May 17, 2002 July 16, 2002
2097-03	Sept 21, 2002 May 15, 2003 July 15, 2003 Sept 13 – Oct 13, 2003
2193-04	July 15, 2003 Sept 13 – Oct 13, 2003 June 2004 Sept 16 – 21, 2004
2848-10	Sept 16 – 21, 2004 May 24 – June 2, 2005 Sept 29 – Oct 6, 2005 Oct 28 – 31, 2010

TABLE 4.2-2
Sediment Characteristics from Borings Collected in the Vicinity of Baseline Profiles BP3 through BP6

Profile No.	Borehole No.	Top of Hole (ft, MLLW)	Sample Depth (ft)	Description	% Gravel	% Sand	% Fines
BP3	AP-4627	-24.3	5	Poorly graded GRAVEL with Silt and Sand	74	21	5
			10	Well Graded GRAVEL with Silt and Sand	58	36	6
			15 – 40	Lean CLAY	-	-	-
	AP-4628	-16.8	5	Well Graded GRAVEL with Sand and	56	40	4
			10	Cobbles	30	53	17
			15	Silty SAND with Gravel	22	33	45
			20-25	Clayey SAND with Gravel	-	-	-
			30	Lean CLAY with Gravel	-	-	-
			35	SILT with Sand	-	-	-
			40	Sandy SILT	-	-	-
				Poorly graded SAND with Silt			
	AP-4631	-11.6	5	Clayey SAND	0	84	16
			10	Clayey SAND	0	52	48
			15	Clayey SAND	0	85	15
			20	Clayey SAND	0	82	18
			25-40	Lean CLAY	-	-	-
	AP-4632	-10.6	5	No Recovery	-	-	-
			10	SILT	-	-	-
			15 – 30	Lean CLAY	-	-	-
			35	SILT	-	-	-
	AP-4591	-36.8	5	Lean CLAY	-	-	-
			10	Sandy Lean CLAY/Sandy Silt with Gravel	-	-	-
			15	Silty SAND with Gravel	17	36	47

TABLE 4.2-2
Sediment Characteristics from Borings Collected in the Vicinity of Baseline Profiles BP3 through BP6

Profile No.	Borehole No.	Top of Hole (ft, MLLW)	Sample Depth (ft)	Description	% Gravel	% Sand	% Fines
BP4	AP-4620	-39.1	5	SILT	-	-	-
			10	Lean CLAY with Sand	6	18	76
			15	SILT	-	-	-
	AP-4621	-38.0	5	SILT	0	9	91
			10	Sandy SILT	-	-	-
			15	Sandy SILT	0	34	66
	AP-4622		5	SILT	-	-	-
			10	SILT with Sand	0	26	74
			15	SILT with Sand	0	24	76
	AP-4595	-42.0	5	Sandy SILT	2	43	55
			10	Sandy SILT	15	33	52
			15	Sandy SILT	-	-	-
BP5	AP-4616	-40.7	5	SILT with Sand	0	23	77
			10	SILT	0	12	88
			15	Sandy SILT	-	-	-
	AP-4617	-41.6	5	No Recovery	-	-	-
			10	SILT with Sand	3	17	80
			15	SILT with Sand	0	25	75
BP6	AP-4612	-34.1	5	GRAVEL with Clay and Sand/Lean Clay	55	39	6
			10	Lean CLAY	-	-	-
			15	Lean CLAY	-	-	-
	AP-4613	-41.7	5	SILT/SILT with Sand	0	15	85
			10	Silty SAND with Gravel	39	44	17
			15	Poorly graded GRAVEL with Silt and Sand	-	-	-

Observations for the four profiles that extend into the area of the PIEP footprint are as follows:

- **Profile No. BP3.** The profile extending from the North Expansion area shows little change between surveys over the length of the profile. The one exception is that the profile shows considerable change between stations 24+00 and 36+00 from September 2003 to June 2004 (Figure 4.2-3). It is questionable whether this change is real, because the September 2004 data closely match the September 2003 data in areas that had shown significant changes in the interim survey. It also appears that dredging may have been performed within this area prior to the September 2004 survey. The 2005 surveys in the area that appeared to be dredged showed essentially no change from the dredged condition. Aside from the dredged area fronting the new construction, no significant changes were observed in the 2010 survey compared to previous years. Based on these surveys, it appears that the profiles along BP3 were in equilibrium both seasonally and over the period of the surveys.
- **Profile No. BP4.** Changes between September 2000 and June 2001 and between November 2001 and May 2002 showed similar characteristics (Figure 4.2-4). Profiles were fairly stable for water depths shallower than 80 feet but with decreases in bottom elevation over the winter at two locations: approximately a 5-foot recession at station 31+50 (approximately 40-foot water depth), and 5- to 10-foot decreases at station 19+50 (approximately 70-foot water depth). Overall, the changes seen in profiles along BP4 increased after September 2002 (Figure 4.2-5). Changes across Knik Arm of 5 to 10 feet or more were observed between 2003 and 2005 in water depths shallower than 60 feet with greater changes in water greater than 60 feet deep. It appears that the survey line for May 2003 is shifted to the right and changes between September 2002 and

May 2003 may actually be less than shown. No profile surveys are presented between October 2005 and the final survey from October 2010. It is noted that the seabed elevation in the area along BP4 near the dock face of the future port decreased from approximately -35 feet MLLW to approximately -50 feet MLLW with concurrent increases in bed elevation further offshore, suggesting the possibility of migration of bed material downslope. These changes may be attributed partly to dredging associated with construction of the North Expansion project to the north of BP4, but can also be considered indicative of potential for changes. Significant cross-section changes across Knik Arm are apparent in the profiles taken along BP4 after 2002. It is notable that similar changes do not take place along the other three profile transects.

- **Profile No. BP5.** The profile appears fairly stable (Figure 4.2-6). Seasonal changes over winter were at most approximately 5 feet between September 2000 and June 2001 and between November 2001 and May 2002. No profiles are presented for BP5 between September 2002 and the final survey in October 2010. Comparison of these profiles shows a decrease in bottom elevation over this period of 5 to 10 feet in the area near the future expansion.
- **Profile No. BP6.** The profile appears fairly stable (Figures 4.2-7 and 4.2-8). Seasonal changes over the 2000/2001 and 2001/2002 winters were localized and on the order of about 5 feet. Changes between the October 2005 and final survey in October 2010 show the potential for greater changes with decreases in bottom elevations on the order of 15 feet in the southern portion of the profile. It is noted that these types of changes do not appear over the rest of the profile, and it is not clear what impact dredging for and construction of the PIEP may have had on the elevations along the southern portion of the profile.

Review of the baseline profiles found that localized erosion can occur over the winter months along portions of the profiles. This can result in as much as 5 to 10 feet of recession in some locations along the profiles. Significant changes have occurred in Profile Nos. BP4, BP5, and BP6 near the areas of the PIEP based on the most recent survey. It is unclear whether these are natural changes or a response to recent dredging and construction activities.

Although some areas appear to be susceptible to recession over the winter months, no appreciable erosion was observed in areas in which clear dredging signals were seen in the fall hydrographic surveys. This could be a result of more erosion-resistant material in these locations which, as a result of previous overburden, have a higher degree of consolidation and cohesion. To the degree that cohesive sediments are present at the dredge depths in front of the OCSP® wall, these areas could be less susceptible to seasonal erosion.

Profile data in Figures 4.2-3 through 4.2-8 document bed elevations over a 10-year period, and therefore provide information on relatively short-term changes. In an attempt to observe longer period trends, the USACE obtained hydrographic survey data from the NOS from surveys conducted in 1974, 1982, and 1992, and plotted profiles extracted from these data against profiles collected in September 2000 and October 2005. These are presented for Profile Nos. BP3 through BP6 in Figures 4.2-9 through 4.2-12.

As with the more recent data, the longer-term survey data show little change in bed elevations along Profile No. BP3, suggesting that the bed in the area of the PIEP is relatively stable over the long term. The historical data along the other profiles indicate the potential for greater variability over time with bed elevation differences between 1974 and 2005 of up to 20 feet or more in locations offshore of the PIEP. In the areas in proximity to the PIEP, these longer-term data suggest increasing bed elevations.

4.2.2.2 Localized Scour

Fenders along the face of the OCSP® wall consist of pairs of 36-inch-diameter pipe piles driven approximately 4 feet out from the base of the wall with a cylindrical rubber energy absorber between the tops of the piles and the concrete utilidor structure (Figure 4.2-13). The pipe piles in each assembly are spaced 6 feet, 8 inches from center to center. There are 24 dual-pile fender assemblies, 4 triple fenders (consisting of 3 dual-pile assemblies), and 2 quadruple fenders (consisting of 4 dual-pile assemblies). With a few exceptions, fender assemblies are generally spaced on 54-foot centers and are centered on every second sheet pile cell.

Scour around the mudline of the pipe piles can be expected. Maximum scour depth for design purposes for a single pile can be taken as two times the pile diameter (Sumer and Fredsøe, 2002), representing a mean value of observed scour of 1.3 times the pile diameter plus one standard deviation. These scour depths relate to live bed scour in which the water velocity exceeds the critical velocity for initiation of motion, which is the case for the currents at the site.

Multiple piles or more complex pile configurations can result in additional scour because of changes in flow in the gaps between the piles and turbulence generated by the individual piles. The total scour for a group of piles includes a local component of scour around each pile related to the mechanisms of scour observed for a single pile as well as a global component related to the hydrodynamics around the pile group. Maximum equilibrium total scour depth as a function of the number of piles in an N x N group of piles, where N is the number of piles on each side of the group, are plotted in Sumer and Fredsøe (2002) as a fraction of the scour for a single pile.

Assuming the dual piles in proximity to the sheet pile wall act similar to a 2 x 2 pile group, the total scour depth can be assumed to be on the order of 20 percent greater than that for a single pile. For 36-inch-diameter fender piles, the total localized scour that can be assumed at the pile is on the order of 5 to 7 feet. The mudline at the wall is assumed to be on the order of 1 to 2 feet higher because of decreasing scour away from the piles.

4.2.3 Conclusions

Scour in front of the OCSP® structure face can occur because of seasonal and longer-term erosional trends within Knik Arm, as well as more localized effects such as scour around structures placed at the site. Velocities along the OCSP® structure face will increase as the PIEP is expanded further into Knik Arm; however, it is not clear from the data provided in USACE (2010) that the velocities in any given location will increase significantly over their historical magnitudes and that the locations at the OCSP® wall will, with the exception of localized scour discussed above, be more prone to erosion than they are presently. In addition, the areas fronting the OCSP® wall will be dredged and the exposed sediments may be more consolidated than the surface sediments and have greater cohesive properties as a result of historical overburden on these sediments.

The largest uncertainties with respect to bed elevations fronting the OCSP® structure bulkhead are a result of natural long-term changes in the bathymetry of Knik Arm, or to the response of the system to hydraulic changes caused by extension of the port. Based on available data, the stability of the profile at Profile No. BP3 suggests that bed changes are likely not an issue at the newly constructed PIEP; however, there is some uncertainty because of the limits on available data. The greater historical variability in bed elevations at Profile Nos. BP4, BP5, and BP6, which extend from areas of future phases of expansion, represent an increased uncertainty in future bed elevations for these areas.

Given the dynamic nature seen in the bed profiles at Profile No. BP4 located adjacent to the site, and extension of the berths further into Knik Arm, long-term bed changes should be considered to be a potential issue with the design of the future expansion phases. Significant changes in Profile No. BP4 beyond the areas that were clearly dredged appear more indicative of natural changes, but could be in response to changed hydraulics in the area as a result of the construction in the PIEP. Historical survey data suggest that longer-term variability can also be significant; however, the trend in the data between 1974 and the present appears to be toward increased seabed elevation along the southern portion of the profiles. Assuming the potential for long-term seabed changes, as well as more detailed study on potential impacts of construction on local hydraulics and seabed morphology, are recommended as part of future design phases.

Additional localized scour could occur at the base of the fender piling, which would reduce the elevation of the seabed in front of the sheet pile face. This scour could be on the order of 5 to 7 feet on top of more global seabed elevation changes and would be most concentrated at the base of the pilings, but still could result in additional scour on the order of 5 feet at the base of the wall. Other factors such as propeller wash against the sheet pile bulkhead could exacerbate this.

Once the facility is constructed, the depths along the OCSP® structure face should be monitored at least annually to measure if scour is occurring. If it is found to be significant, then scour mats can typically be used to control it.

4.3 Ice Forces

CH2M HILL was tasked to review the design assumptions and calculations that have been developed by PND to assess whether ice forces on the OCSP® system and moored ships have been adequately addressed in terms of the extension of the wharf face 400 feet further into the inlet. The scope of this work includes the assumption that existing information regarding inlet ice thicknesses and currents in the vicinity of the new OCSP® system are sufficient. No supplemental investigations were to be performed.

4.3.1 Overview of Evaluation

The *PIEP Design Criteria Summary* (ICRC, 2011) lists a 24-inch-thick slab of ice as the basis for the live load and 40 pounds per cubic foot of ice as the basis for dead loads of ice adhered to the structure. Fifty-year design values are listed as 24-inch ice thickness with 150 psi compression strength and 25 to 40 psi strength in bending. The *Wet Barge Berth Design Manual* (PND, 2011a) lists similar values for compression and bending strengths but with an 18-inch thickness, and are listed as ice forces for mooring.

It is unclear how ice loads were used in the design. In the draft report documenting PND's preliminary analysis on currents, ice, and dredging (PND, 2006d), they cite ice buildup on the existing pile-supported structures at the POA as being problematic; however, the designers suggest that the OCSP® system will eliminate most of the ice buildup. They cite crushing strengths of ice in the POA area of 200 to 300 psi, bending strengths of approximately 25 psi, and an ice thickness of 18 inches.

PND (2006d) refers to studies of pan and beach ice at the Port of Anchorage during the 2005-2006 ice season that were the basis of these values, but gives no details of the studies. The *Marine Ice Atlas for Cook Inlet, Alaska*, (USACE, 2001) cites ice thickness calculations performed based on Anchorage freezing degree-days (FDDs), which indicated maximum thicknesses of 2.1 and 2.5 feet (0.66 and 0.79 m), which are close to the 24-inch ice thickness presented in the *PIEP Design Criteria Summary*. Based on these estimates, an ice thickness of 2 feet was assumed for the purposes of ice impact analysis performed in Section 4.3.2.

In a separate *Ice Condition Findings* report for the Knik Arm Crossing planned just north of Cairn Point (PND, 2006a), compressive strengths of 200 to 300 psi are cited for ice in Knik Arm along with bending strengths estimated to be in the 25 to 50 psi range.

Both reports mention the potential for the presence of river ice from the Matanuska and Knik rivers, which would have a higher strength but would be present in smaller masses; however, this is less common and usually occurs during spring break-up when it is released from the rivers.

4.3.2 Ice Loading

Ice propelled by tidal currents presents the greatest danger to structures at the POA. The *Marine Ice Atlas for Cook Inlet, Alaska* (USACE, 2001) lists incidents of damage caused by floating ice in Cook Inlet between 1960 and 1986 based on U.S. Coast Guard records. These included a number of incidents near the POA of both structural damage caused directly by floating ice, and damage caused by ice impeding the navigation of vessels. Direct damage included pilings torn from the petroleum dock, a dock extension torn from its pilings, and a ship coming loose when ice severed its mooring lines. Ice hazards have continued to be a concern with ship's pilots, and the concern is that these will only worsen as the berths are extended into areas with greater currents.

Risks of damage from floating ice will be less for the OCSP® structure compared to a similarly sited pile-supported structure. As opposed to a pile-supported structure where the water flows through the structure, which can result in impacts of ice on the piling as well as additional loads caused by the current acting on ice built up on the piling and ice jams on the upstream side of the structure, currents will flow parallel to the face of the OCSP® wall. As a result, ice impacts to the sheet piles from current-driven ice will at most be oblique.

Currently, procedures are used to clear ice away from the wharf face prior to bringing ships into their berths. This is typically done using a tug's propeller wash to clear the ice away. It is assumed that similar means will be taken to ensure that ice between the ship and the OCSP® face will not result in a significant bearing load on the sheet piles during berthing. Ice buildup is still expected to occur on the fender piles, and ice driven along the face of the OCSP® wharf will result in a load on these piles.

Other loads would be caused by ice interaction with the moored ships, with loads transmitted to the wharf through the mooring lines. Potential loads on the moored ships from ice floes can be estimated in a manner similar to American Association of State Highway and Transportation Officials (AASHTO) specifications for determining ice loads on bridge piers resulting from crushing (PND, 2006a):

$$F_C = \sqrt{\frac{5t}{w} + 1ptw}$$

Where:

t = ice thickness

w = structure width at ice level

p = effective ice crushing strength

Based on the beam of the design ships and the thickness and compressive strength of the ice, potential loads on the ship as a result of ice crushing are on the order of 2,300 to 6,300 tons, depending on the assumed ice thickness (18 or 24 inches), ice compressive strength (200 to 300 psi), or beam of the design ship (106, 118, or 140 feet). The driving force for the ice floe to generate these forces is largely a result of the current acting on the ice and can be calculated as:

$$F_C = F_d = C_d \rho A V^2$$

Where:

C_d = coefficient of drag

ρ = density of water

A = area of ice

V = current velocity

Assuming a coefficient of drag of 0.003, the areal extent of ice that would be required to generate these forces would be on the order of 243 to 664 acres for a current velocity of 2.7 ft/s and 105 to 288 acres for a current velocity of 4.1 ft/s. It is assumed that this amount of ice, if it were present, would not come to bear solely on the berthed ship. The maximum dock parallel velocities obtained from model predictions for the existing docks and proposed future expanded port are 2.7 and 4.1 ft/s, respectively.

More realistic hazards to ships will be from the impact of a large piece of floating ice on the berthed ship rather than an ice floe moving past the ship and failing under compression. A simplified analysis was performed to assess the potential effect that the greater tidal current velocities could have on ships moored at the new and proposed future berths. A full mooring analysis was beyond the scope of this effort; however, the analysis described below should be sufficient to provide an indication of the potential magnitude of changes that could result from the greater current velocities at the new berths. Because of the simplified nature of the analysis, the results should not be considered to be predictive of actual line loads that will be seen, but should be indicative of relative magnitudes of forces resulting from changes in current speeds.

The scenario used in the analysis is similar to an incident described by Captain Bob Ramsey, the current Master on the Horizon Tacoma (Ramsey, 2012). While at berth at the existing POA wharf, a pan of ice he estimated to be on the order of an acre in size was carried down the face of the dock and started pushing the ship aft in the direction of a second vessel. All the synthetic mooring lines fore and aft parted. Tension wire, which included synthetic pennants, did not part but paid out from the overloaded winches. They were able to keep from hitting the second vessel by increasing the tension on the winches to their maximum settings, as well as using the ship's thrusters.

A spreadsheet model was set up to calculate current and ice forces acting on the ship for various combinations of:

- Ice pan size
- Current speed
- Number of mooring lines

For this analysis, a vessel with similar characteristics to the Horizon Kodiak (Table 4.2-3) is at berth and moored against a current. Mooring lines were assumed to be synthetic lines with an ultimate strength of approximately 116,000 pounds each and an elongation at rupture of 15 percent. It was assumed that the relationship between load and elongation for the mooring lines was linear from a zero load to the ultimate strength. Lines were assumed to be 100 feet long with an angle from the longitudinal axis of the ship of 45 degrees, and that all lines shared the loads equally. The ice was assumed to be 2 feet thick, with an area of the pan of both 1 acre and 0.5-acre and a density of 57 pounds per cubic foot (lb/ft^3).

TABLE 4.2-3
Assumed Ship Characteristics for Ice Load Analysis

Characteristic	Value
Length at waterline	676 feet
Beam	78 feet
Draft	34 feet
Displacement	20,883 Long Tons

Three load cases were calculated for each scenario: force from currents acting on the ship only, force from currents acting on the ship combined with an ice impact, and currents acting on the ship and the ice mass (after the ice pan has come to rest following impact). Current forces acting on the ship were calculated using equations presented in the *Unified Facilities Criteria Design: Moorings* (DoD, 2005), which calculate longitudinal current loads resulting from form drag, skin friction, and propeller drag. Ice impact loads were calculated assuming the ice was moving at the speed of the current and all the kinetic energy of the ice mass (as well as another 50 percent added mass of water moving with the ice) was absorbed by the mooring lines based on the following equations:

$$\frac{1}{2}MV^2 = \frac{1}{2}kx^2$$

Where:

$\frac{1}{2}MV^2$	=	the kinetic energy of the ice and added mass of water
$\frac{1}{2}kx^2$	=	energy absorption of the mooring lines
M	=	mass of ice pan plus added mass of water
V	=	initial current/ice velocity
k	=	effective stiffness of the mooring system
x	=	stretch/elongation of mooring lines

Current forces acting on the ice pan were calculated as:

$$F_d = C_d \rho A V^2$$

Where:

C_d = coefficient of drag = 0.003 (assumed)

P = density of water

A = area of ice

V = current velocity

Additional line loads from factors such as preloading the mooring lines were not considered for the purposes of this analysis.

Results are presented in Tables 4.2-4 through 4.2-6. Table 4.2-4 presents calculated line loads as a percent of the breaking strength of each line assuming two mooring lines are used to hold the ship longitudinally. Table 4.2-5 shows results of calculations in which the number of lines was varied in order to keep the peak line loads at less than the line breaking strength. For the scenarios presented in Table 4.2-6, the ice size was varied as the current increased such that the peak combined current and ice impact loads that resulted were maintained at a level equivalent to the impact of either a 1 or 0.5-acre pan of ice moving with a 2.5 ft/s current.

For results presented in each table, calculations were made for current speeds ranging from 2.5 to 4.0 ft/s (approximately 1.5 and 3.0 knots) and ice pan areas of 1 acre and ½ acre. A current speed of 2.5 ft/s is on the order of the maximum ebb tide currents along the dock face predicted by modeling results for the historical port berths in USACE (2008b), and 4.0 ft/s currents are on the order of increased current speeds for the built-out port. A pan ice area of 1 acre was based on anecdotal information from an incident described by Captain Bob Ramsey (Ramsey, 2012). The mass of a half acre, 2-foot thick pan of ice is also on the order of magnitude of the mass of potential river ice at the site discussed in PND (2006a).

For scenarios presented in Table 4.2-4, current forces on the ship accounted for loads at 3 percent of the line capacity for the ship moored in 2.5 ft/s of current and 6 percent of the line capacity for a 4 ft/s current. In contrast, impact of a 1-acre pan of ice resulted in line loads at 94 percent and 152 percent of the rated line capacity for the 2.5 and 4.0 ft/s current scenarios, respectively, with the line capacity exceeded for current speeds of 3.0 ft/s or higher. For a 0.5-acre mass of ice impacting the ship under these conditions, the line load at impact varied from 67 percent to 109 percent of the rated line capacity, with line capacities exceeded at current speeds of 4.0 ft/s or higher.

Table 4.2-5 shows that increasing the current from 2.5 ft/s to 4 ft/s, the number of lines required to resist the ice impact load would need to be increased by a factor of about 2.5. In other words, if two lines are required to resist an impact from a given mass of ice, at the present berths, up to five lines of similar size may be required at the extended berths to resist an impact from a similarly sized ice mass. It is noted that, although adding lines increases the capacity of the mooring system, it also increases the stiffness of the mooring system, and the total force transmitted to the wharf will increase for a given amount of energy that is absorbed.

The results also indicate that ice impact loads could far exceed normal mooring forces. For the cases considered in Table 4.2-4, current forces accounted for 3 to 6 percent of the line capacity depending on the current conditions. These forces increased to 94 to 152 percent of the line capacity for an impact from a 1-acre pan of ice and to 67 to 109 percent for a half-acre pan of ice.

Results presented in Table 4.2-6 are based on calculations made by reducing the size of the ice pan until the combined current and ice impact loads occurring under a given current were approximately the same as those for a given mass of ice under 2.5 ft/s current. These results indicate that for a ship moored in a 4 ft/s current, the mooring loads resulting from the impact of a given mass of ice would be equivalent to the same ship moored in

2.5 ft/s of current impacted by a mass of ice 3 times the size. In other words, it would take an ice pan traveling at 4 ft/s that was only one third the size of one traveling at 2.5 ft/s to have the same impact.

4.3.3 Conclusions

The analysis described above is a simplified analysis based on available and anecdotal information on ice conditions at the site. It does not provide a detailed mooring analysis. Simplifying assumptions are made on general line length and geometry and number of lines. Additional energy absorption resulting from localized crushing of the ice upon impact and additional line loads resulting from wind effects and pre-tensioning of the lines are not included in the analysis. Results should not be taken as predictions of actual loads; however, conclusions can be made based on the analysis results:

1) Mooring loads caused by ice impacts will increase significantly as the wharfs are pushed out into higher current areas.
2) In the absence of implementing mooring components with greater capacities than those on the existing wharf, or other mitigating measures that would break up or redirect the ice from the berths, the frequency of potentially significant ice impacts will increase.

TABLE 4.2-4
Results of Mooring Load Calculations – Line Load Assuming Two Mooring Lines

Current Velocity (feet/second)	Number of Lines	Line Load (% Breaking Strength)		
		Current (Ship Only)	Current (Ship Only) + Ice Impact	Current (Ship + Ice Pan)
		1-Acre Pan of Ice		
2.5	2	3	94	4
3.0	2	4	113	5
3.5	2	5	132	7
4.0	2	6	152	9
		½-Acre Pan of Ice		
2.5	2	3	67	3
3.0	2	4	81	4
3.5	2	5	95	6
4.0	2	6	109	8

TABLE 4.2-5
Results of Mooring Load Calculations – Number of Mooring Lines to Maintain Maximum Line Load Less than Mooring Line Breaking Strength

Current Velocity (feet/sec)	Number of Lines	Line Load (% breaking strength)		
		Current (Ship Only)	Current (Ship Only) + Ice Impact	Current (Ship + Ice Pan)
1-Acre Pan of Ice				
2.5	2	3	94	4
3.0	3	2	92	3
3.5	4	2	93	3
4.0	5	3	95	4
½-Acre Pan of Ice				
2.5	1	5	96	6
3.0	2	4	81	4
3.5	2	5	95	6
4.0	3	4	88	5

TABLE 4.2-6
Results of Mooring Load Calculations – Ice Pan Size to Generate a Load Equivalent to the 2.5 feet/second Case

Current Velocity (feet/second)	Equivalent Ice Pan Size (acres)	Line Load (% Breaking Strength) Current (Ship Only) + Ice Impact
Based On 1-Acre Pan of Ice In 2.5 feet/second Current		
2.5	1.0	94
3.0	0.69	94
3.5	0.49	94
4.0	0.36	94
Based On ½-Acre Pan of Ice In 2.5 feet/second Current		
2.5	0.5	67
3.0	0.33	66
3.5	0.23	66
4.0	0.17	66

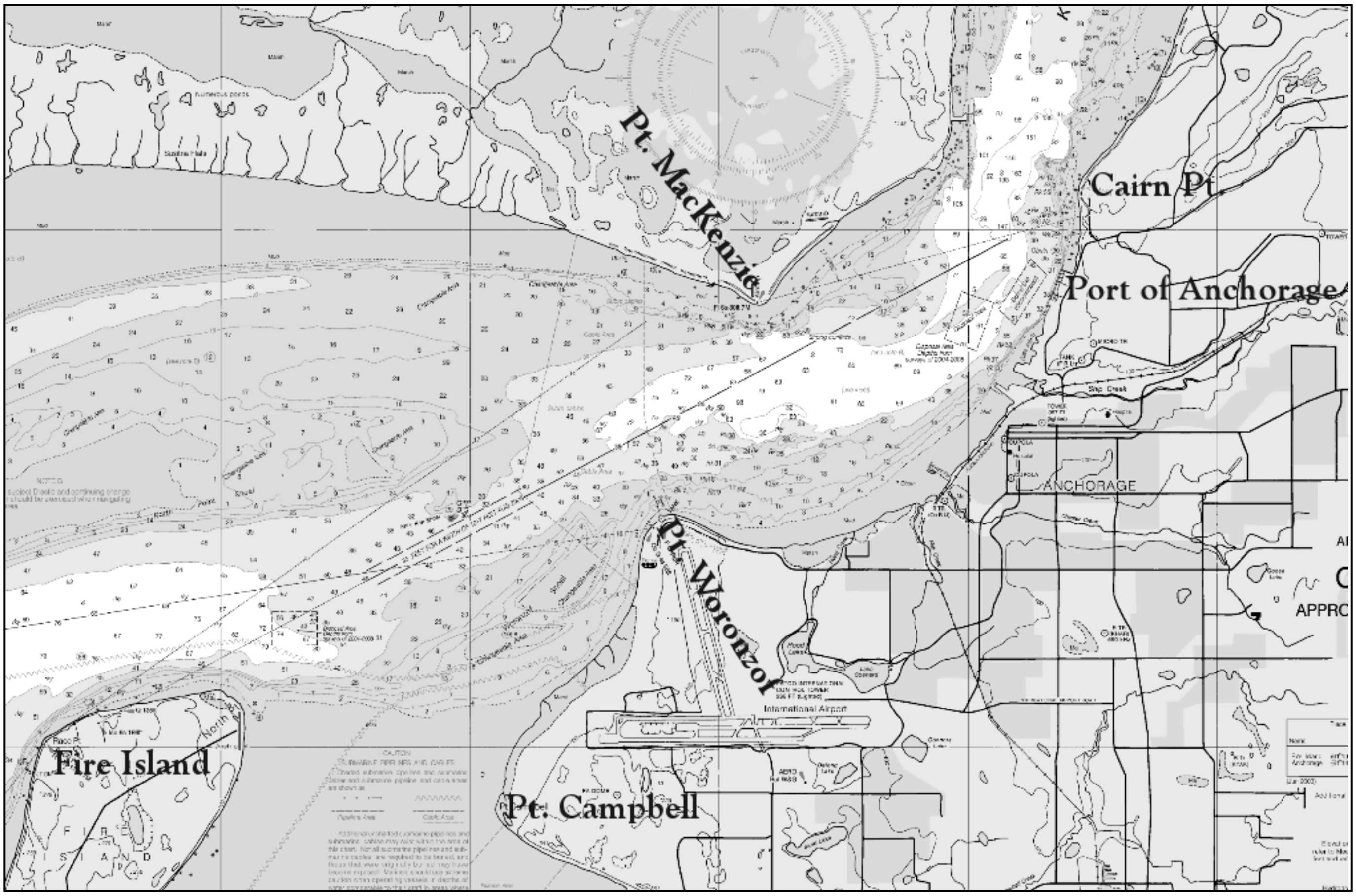

FIGURE 4.1-1. Knik Arm in the Vicinity of the Port of Anchorage

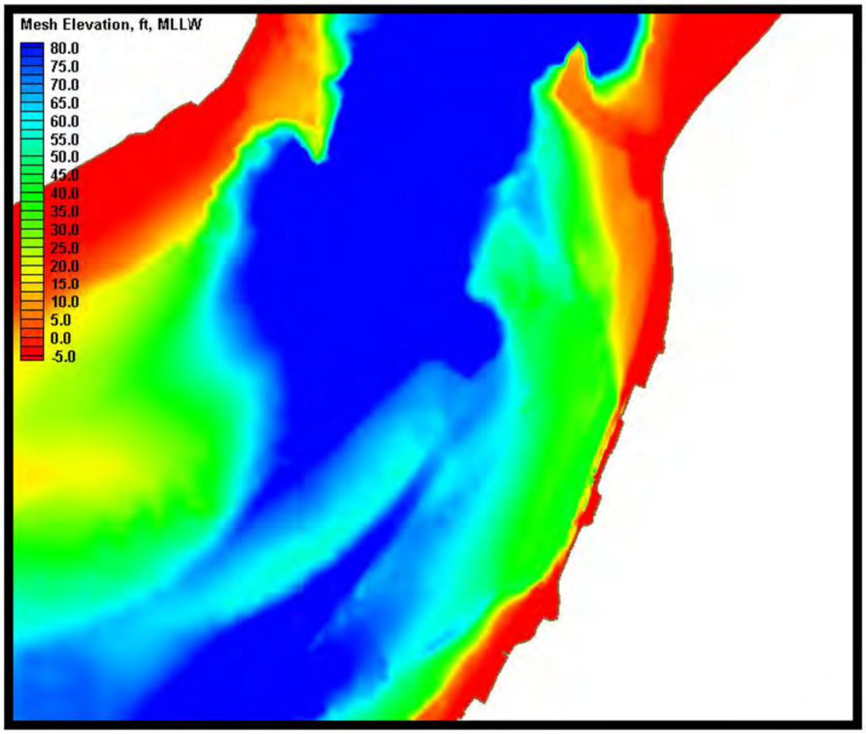

a) Pre-Expansion Bathymetry

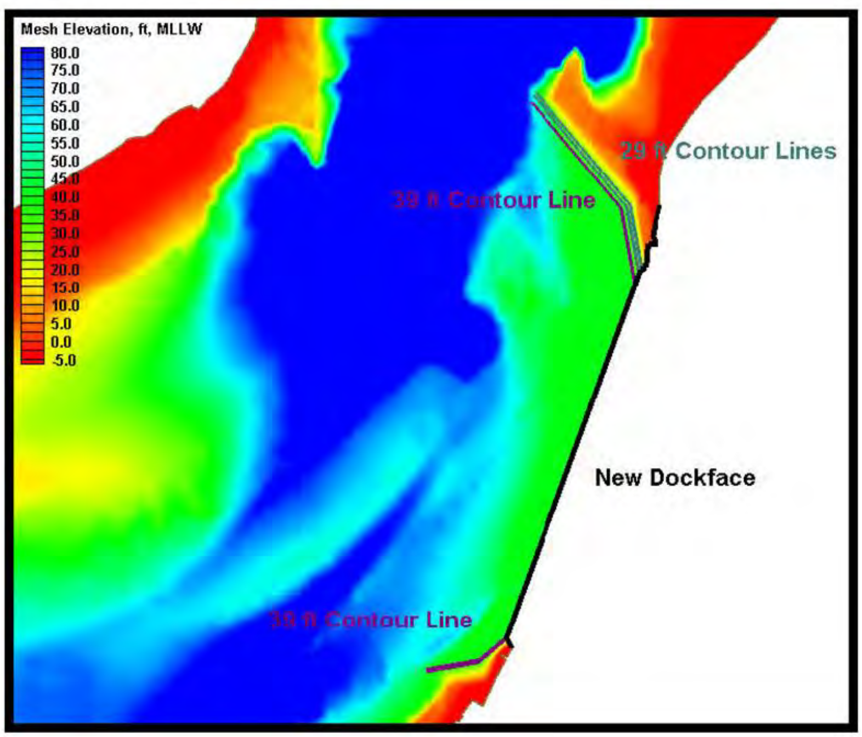

b) Complete Port Expansion Bathymetry

FIGURE 4.1-2. ADCIRC Model Bathymetry Near the POA

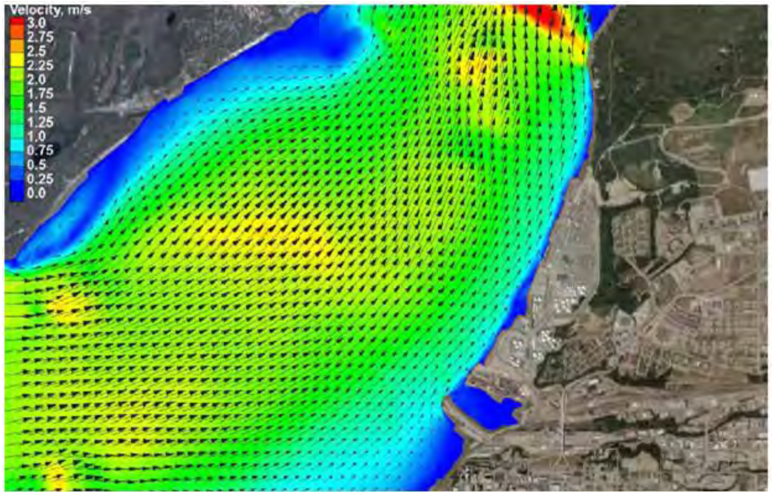

a) Pre-expansion Port Configuration

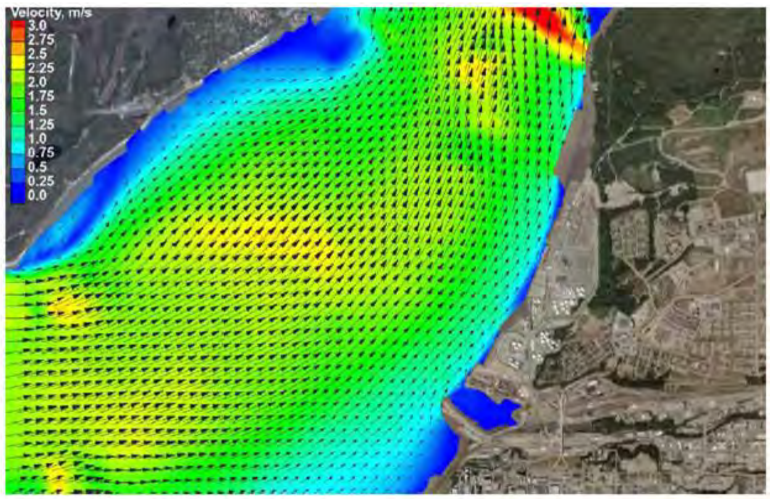

b) North Expansion Phase

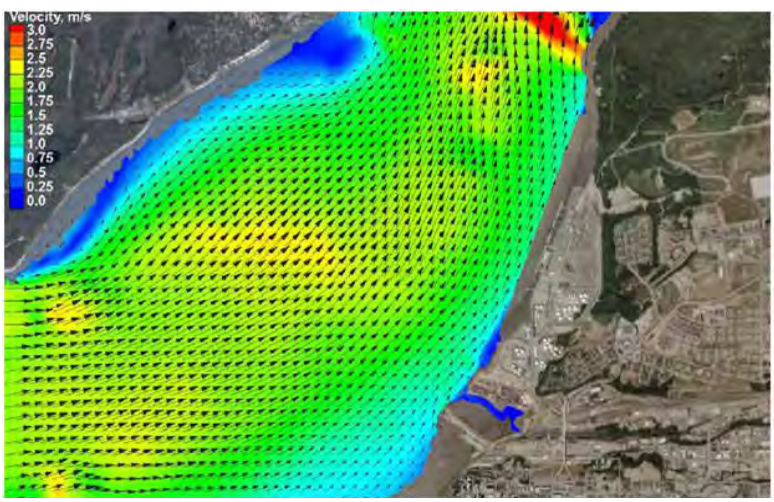

c) Complete Port Expansion

FIGURE 4.1-3. ADCIRC Model Results – Maximum Flood Flow

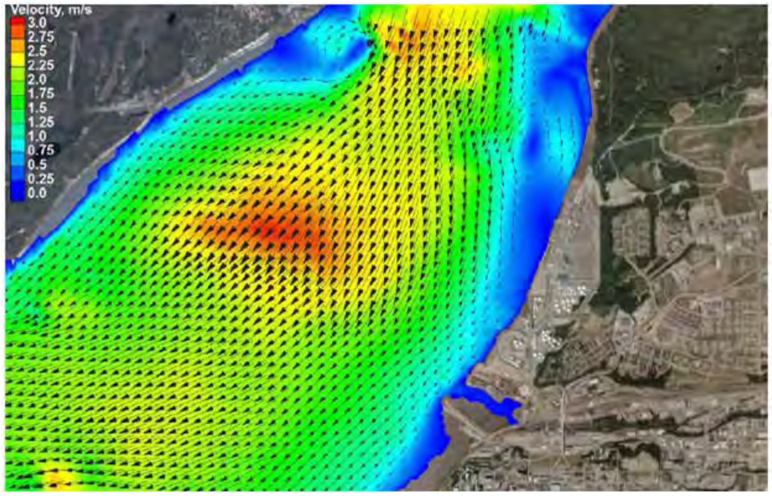

a) Pre-expansion Port Configuration

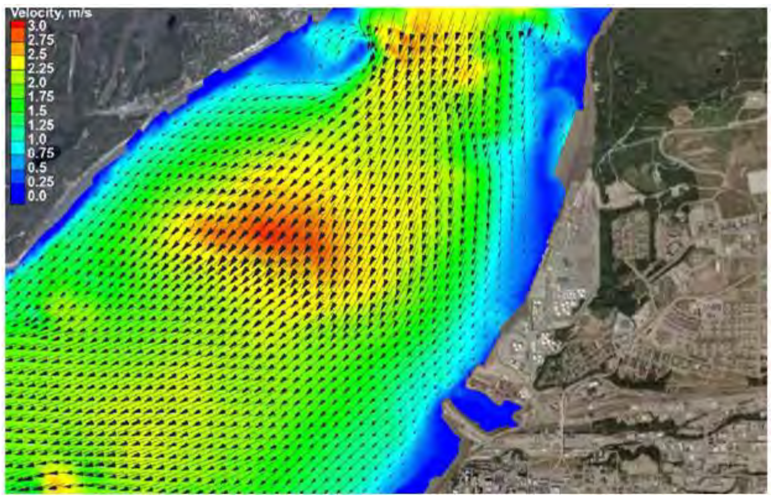

b) North Expansion Phase

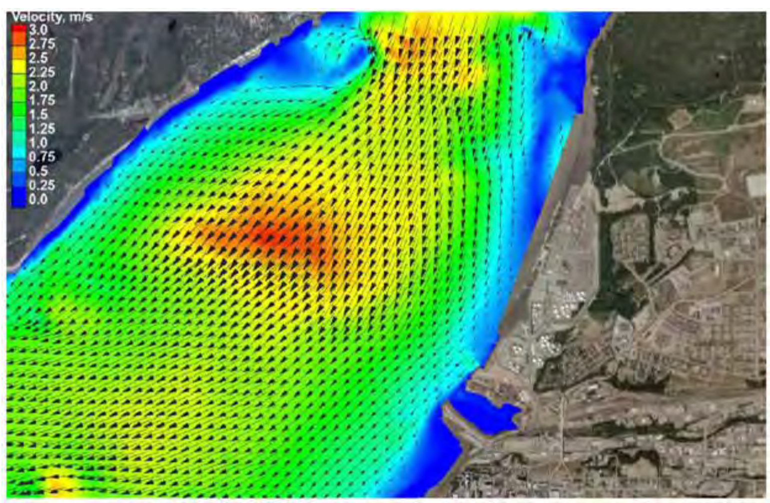

c) Complete Port Expansion

FIGURE 4.1-4. ADCIRC Model Results – Maximum Ebb Flow

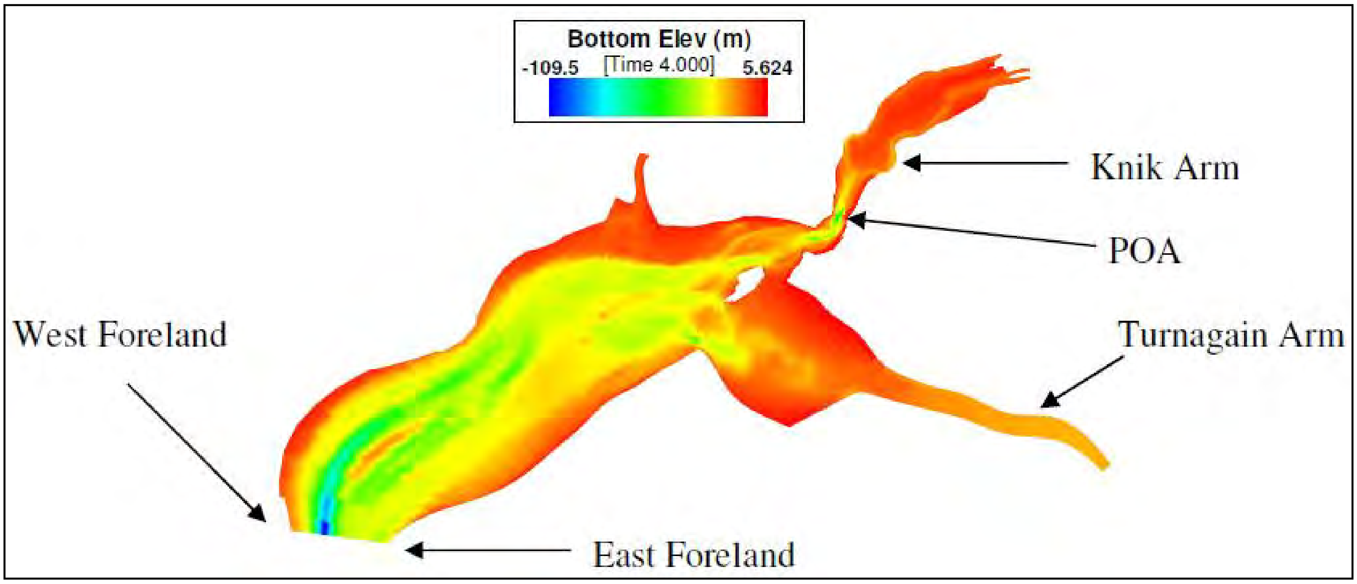

FIGURE 4.1-5. LTFATE Model Domain

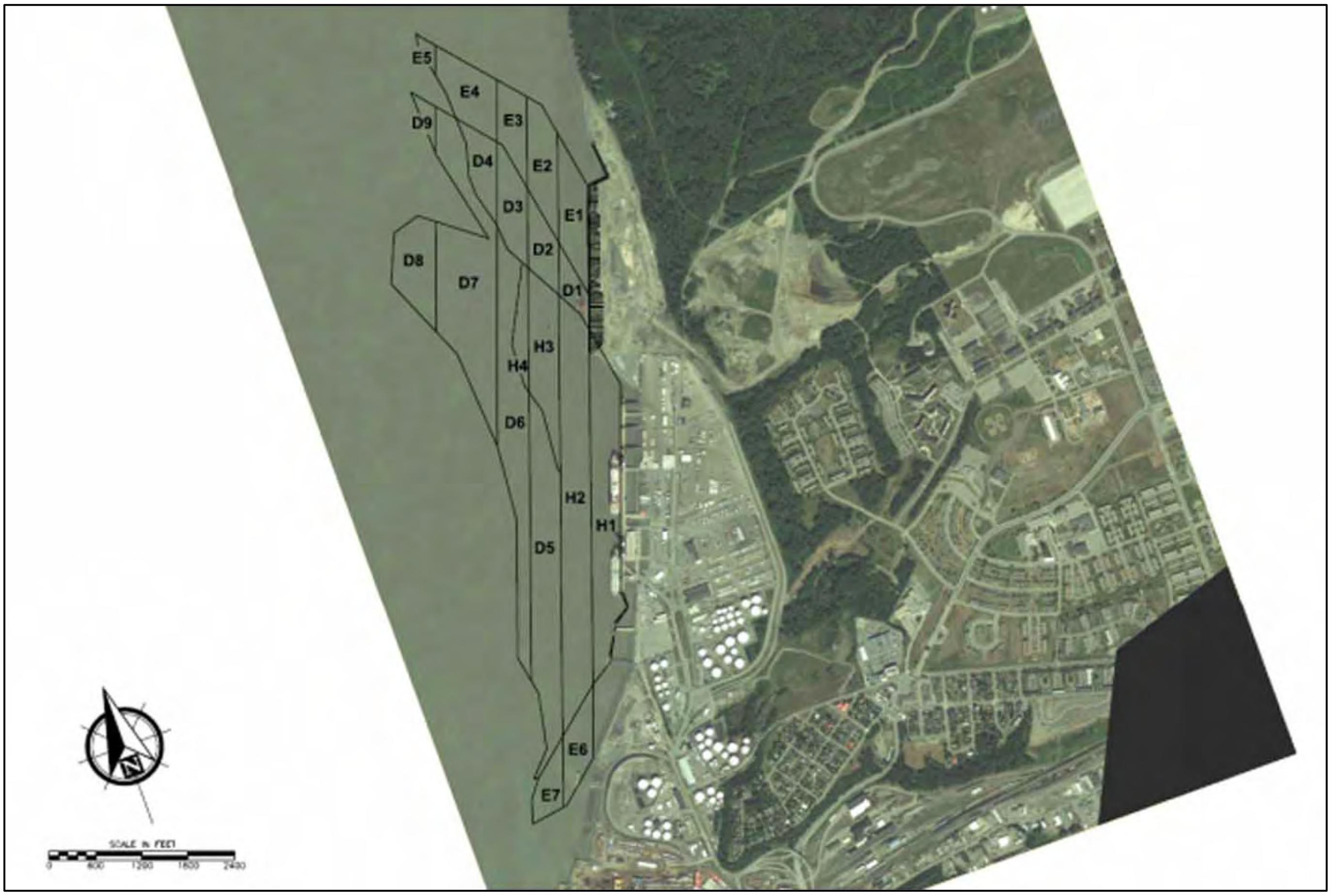

FIGURE 4.1-6. Defined Dredging Polygons

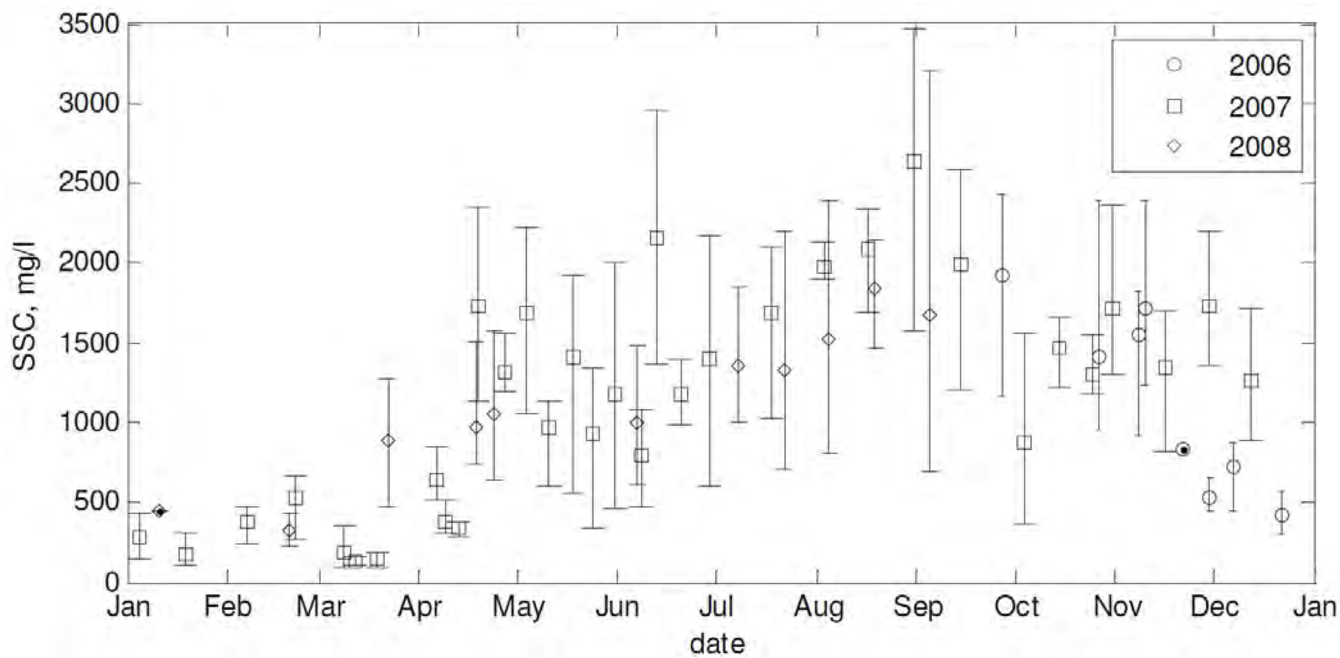

FIGURE 4.2-1. Seasonal Suspended Sediment Concentrations at the Port of Anchorage

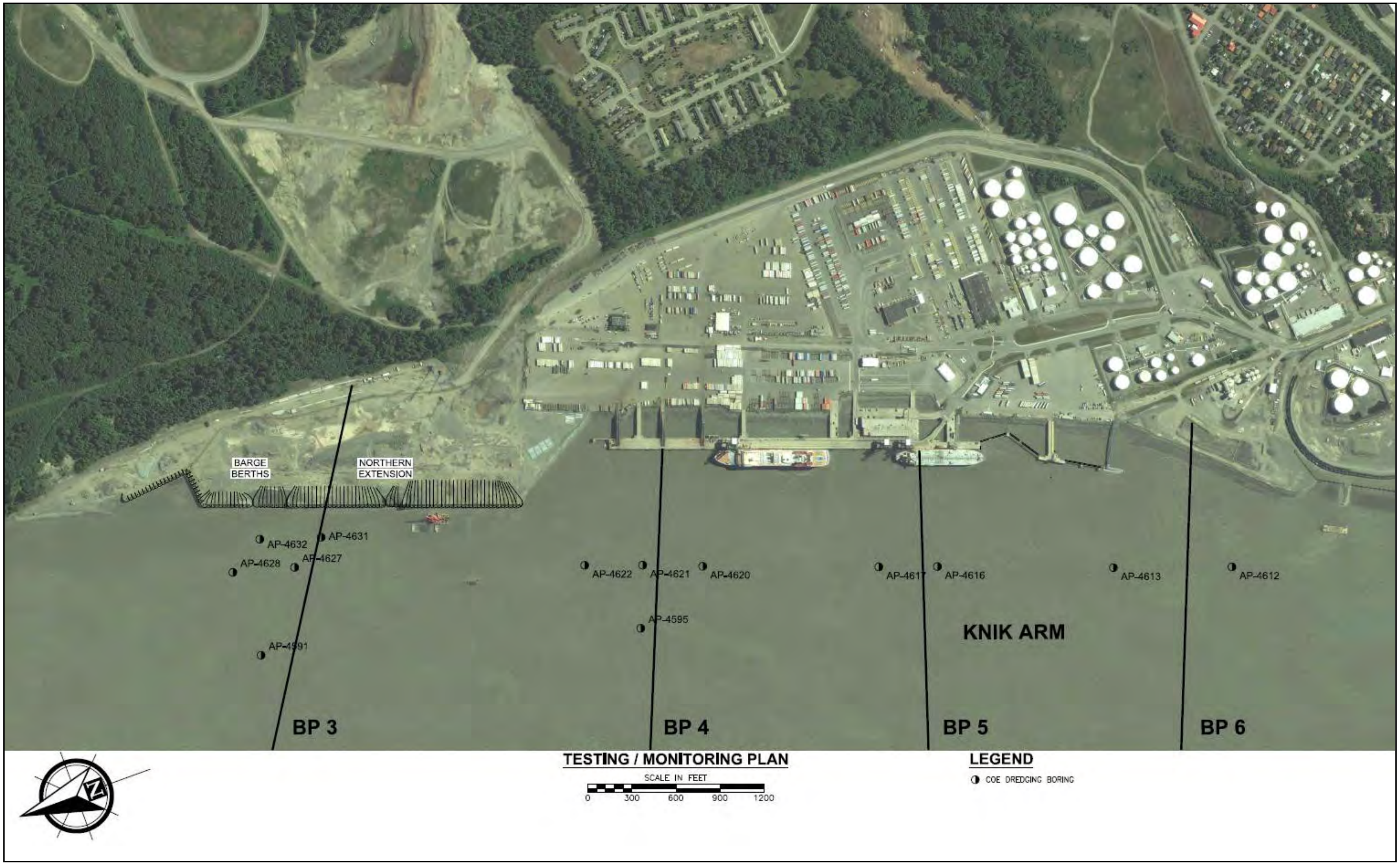

FIGURE 4.2-2. Baseline Profile Locations

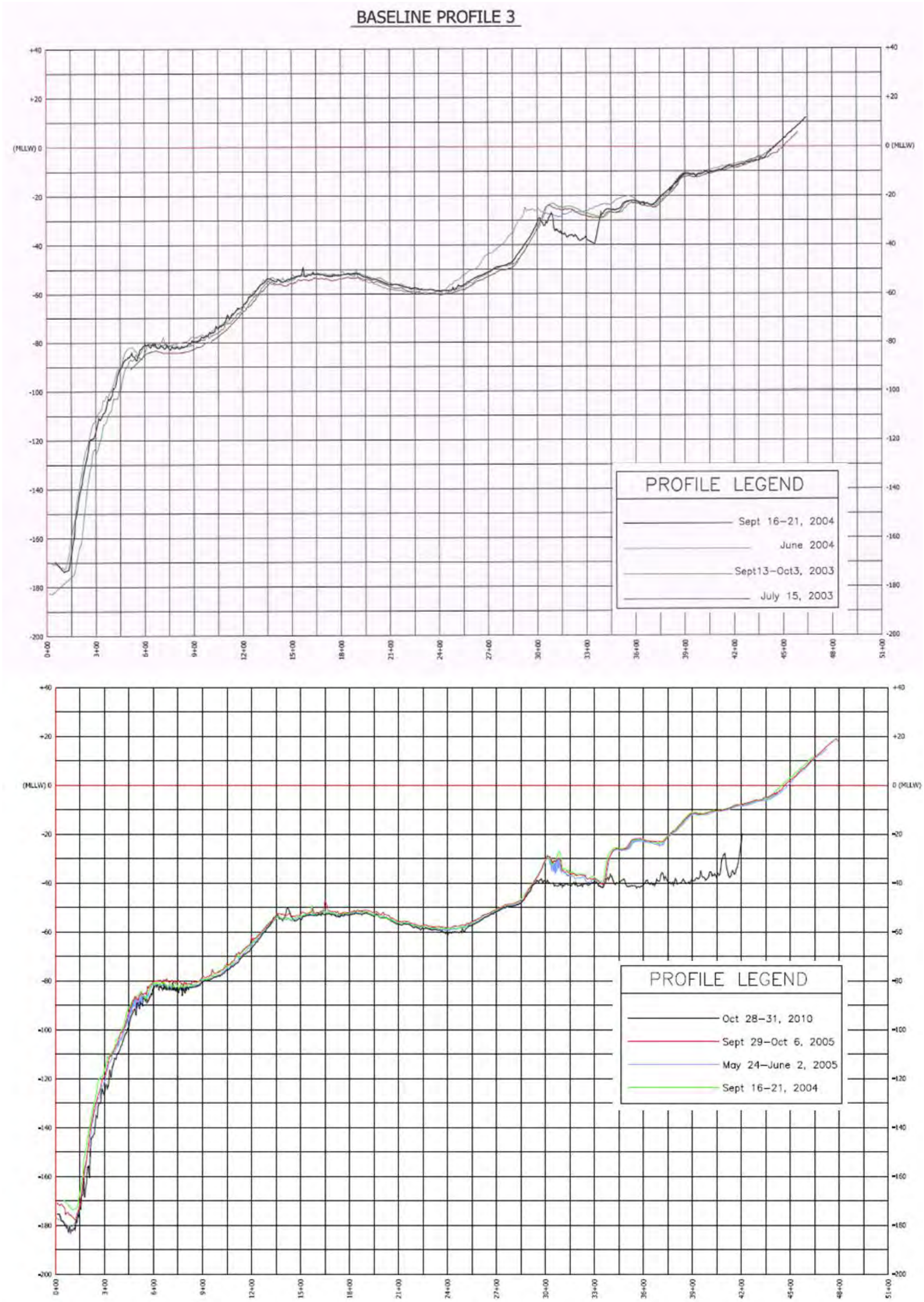

FIGURE 4.2-3. Baseline Profile BP3 – 2003 to 2010 Surveys

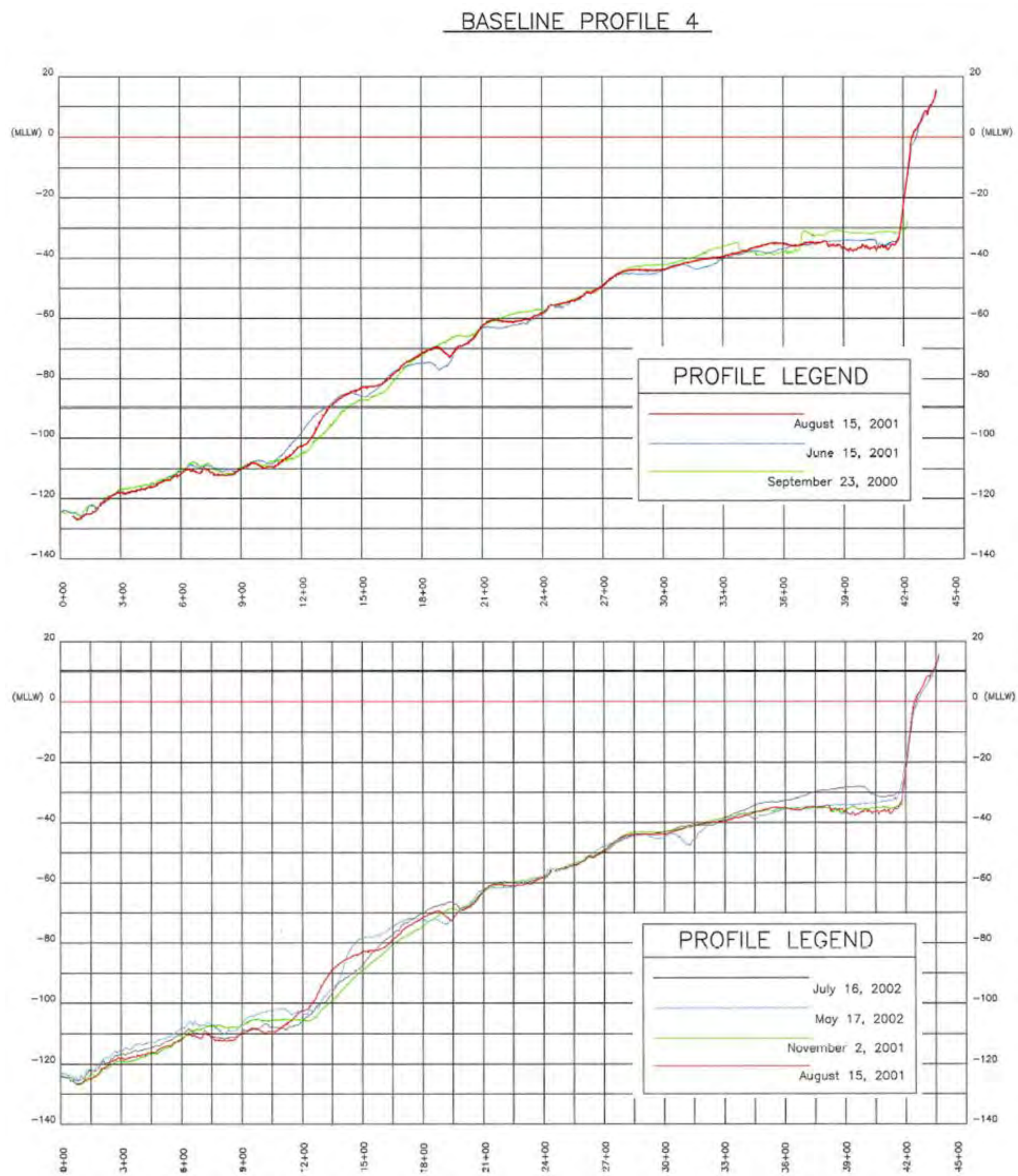

FIGURE 4.2-4. Baseline Profile BP4 – 2000 to 2002 Surveys

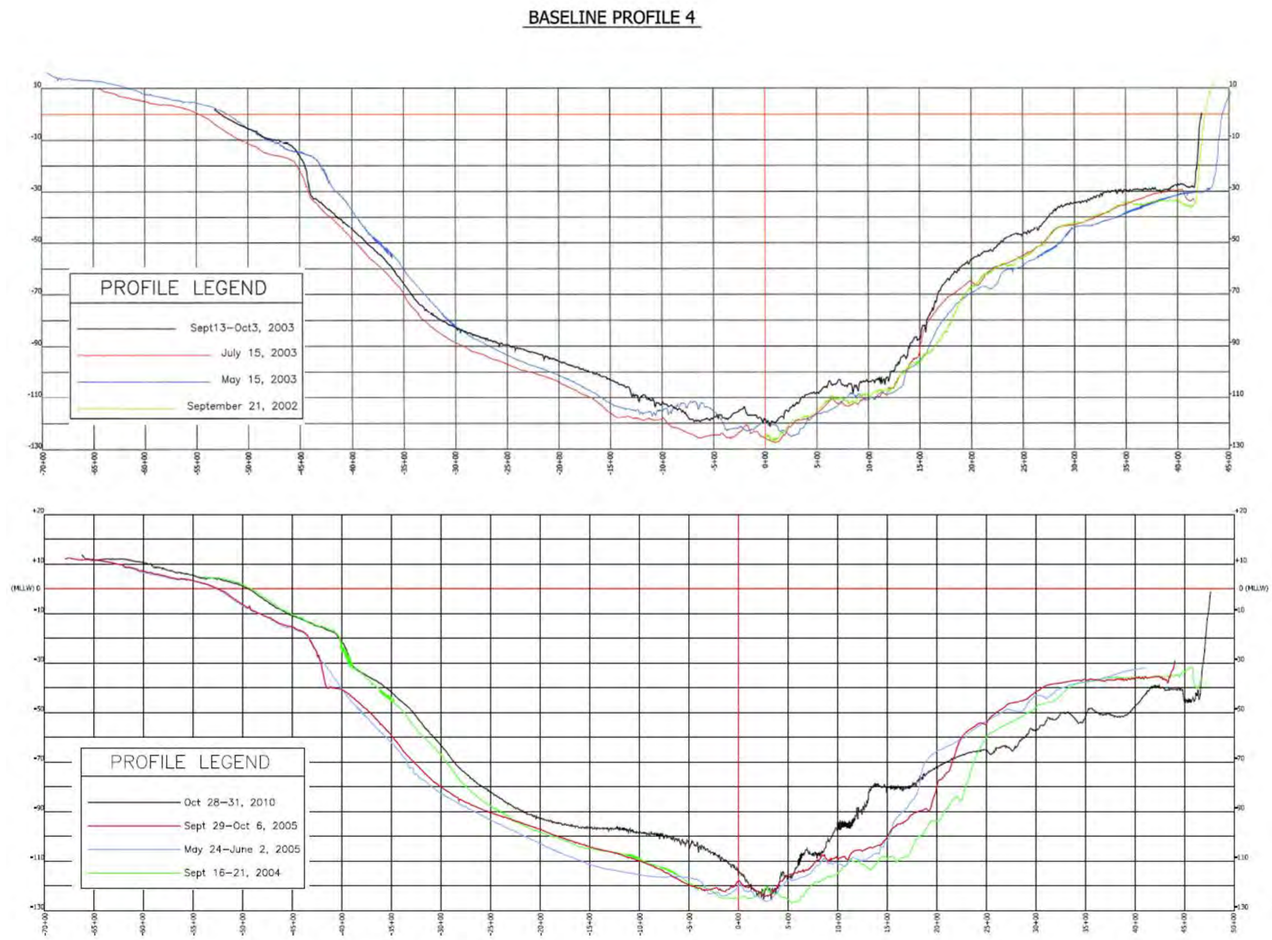

FIGURE 4.2-5. Baseline Profile BP4 – 2002 to 2010 Surveys

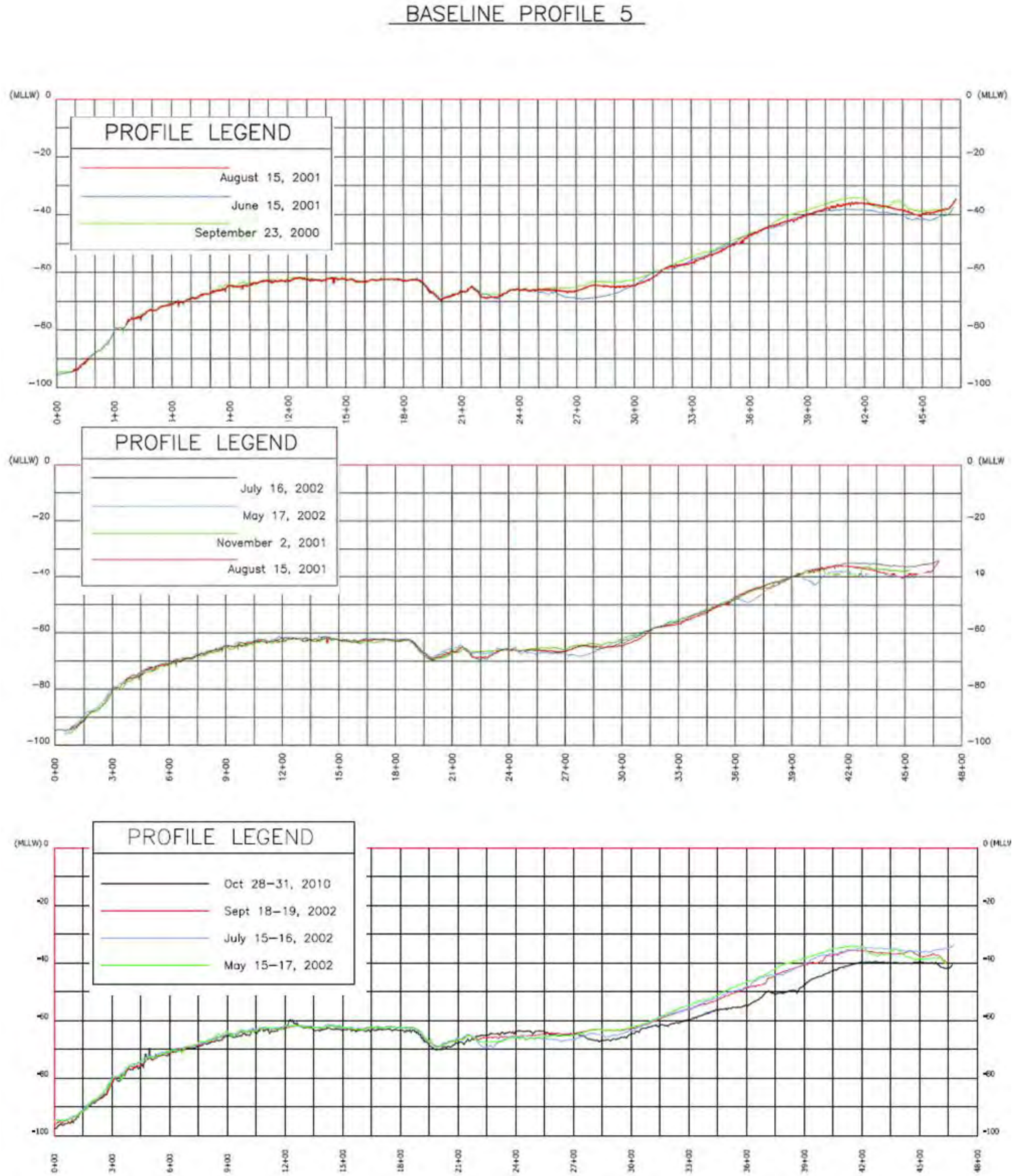

FIGURE 4.2-6. Baseline Profile BP5 2001 to 2010 Surveys

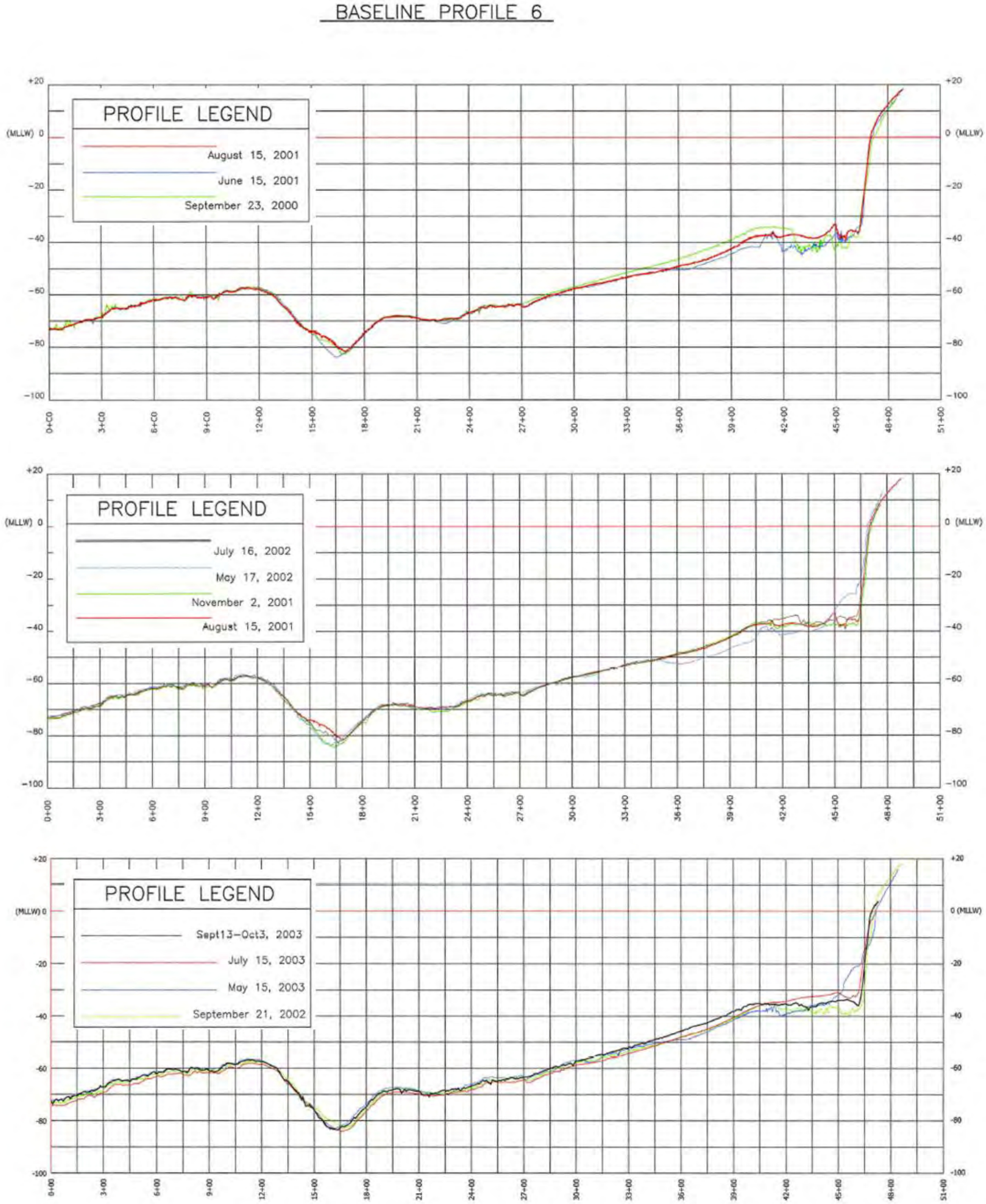

FIGURE 4.2-7. Baseline Profile BP6 – 2000 to 2003 Surveys

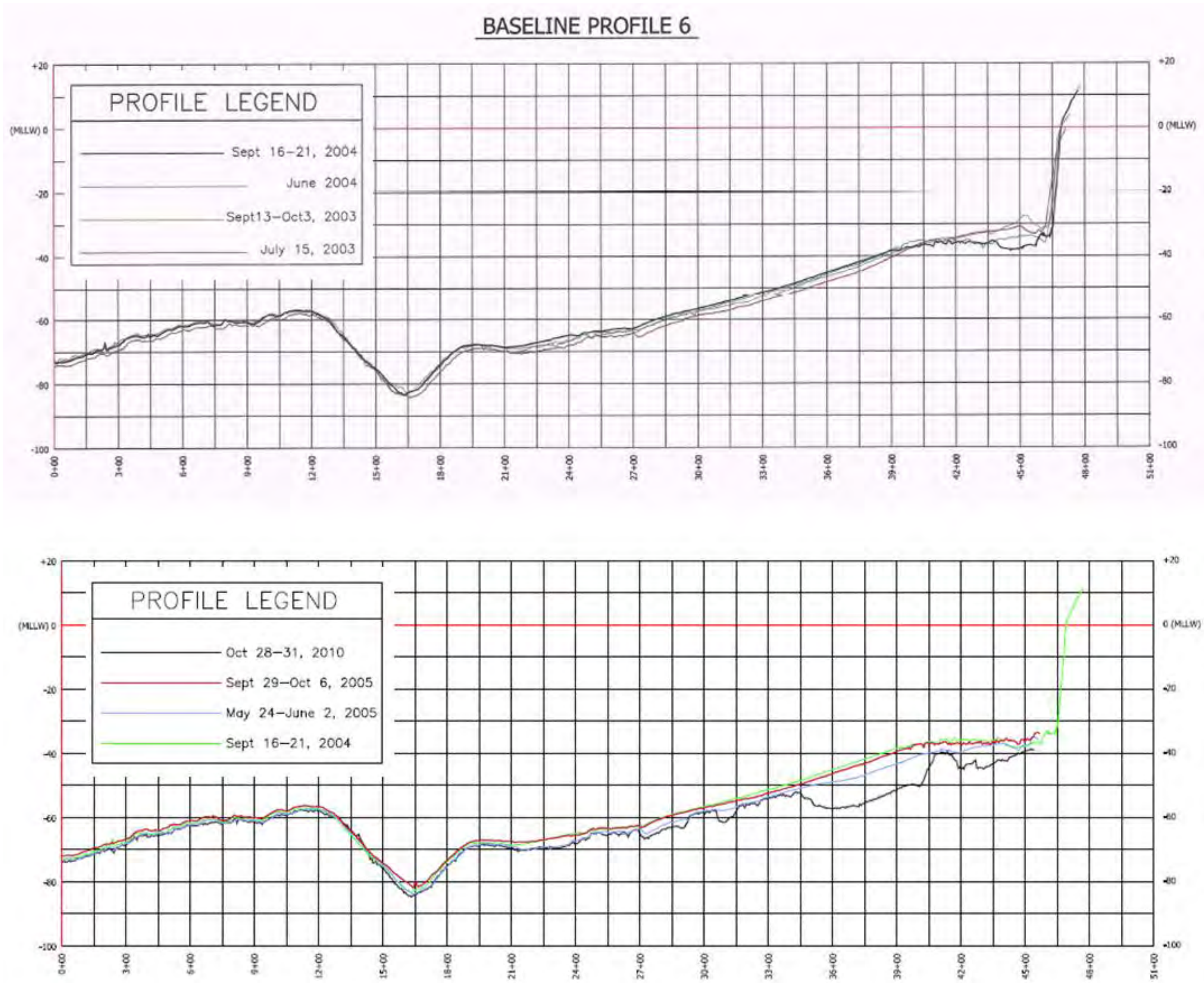

FIGURE 4.2-8. Baseline Profile BP6 – 2003 to 2010 Surveys

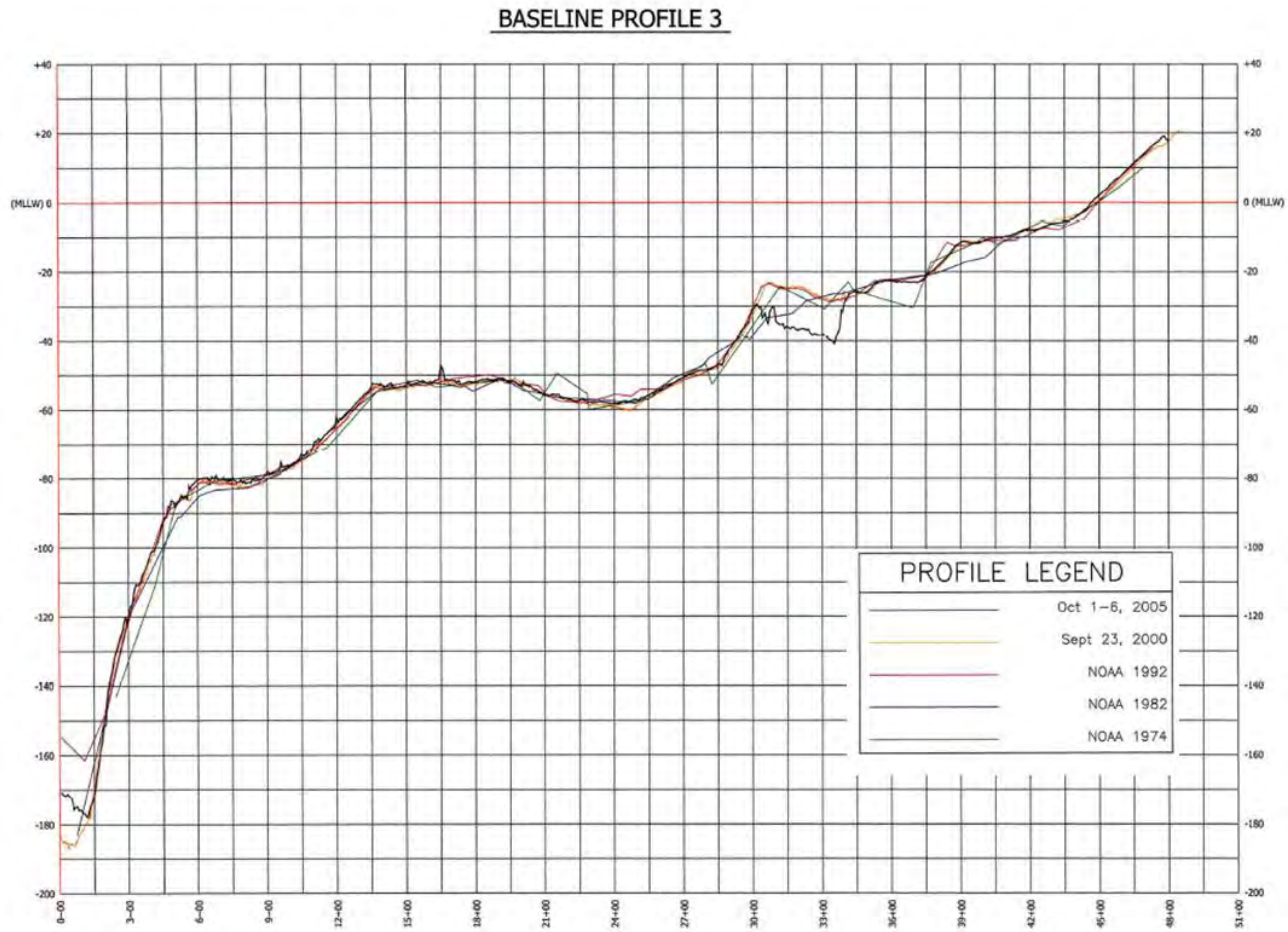

FIGURE 4.2-9. Baseline Profile BP3 Data Including Historical NOS Survey Data

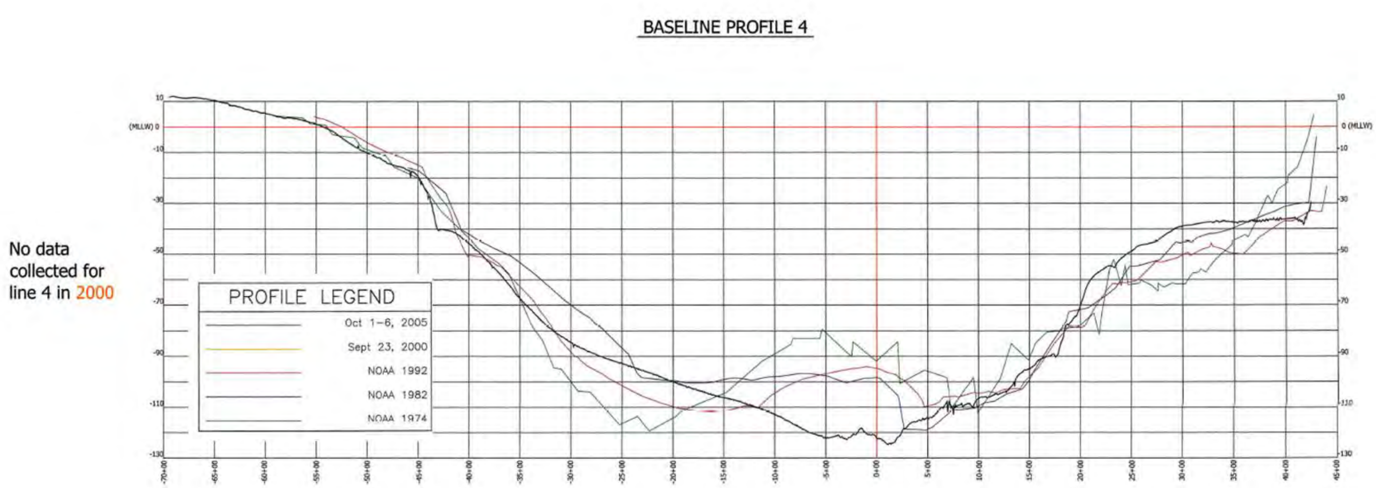

FIGURE 4.2-10. Baseline Profile BP4 Data Including Historical NOS Survey Data

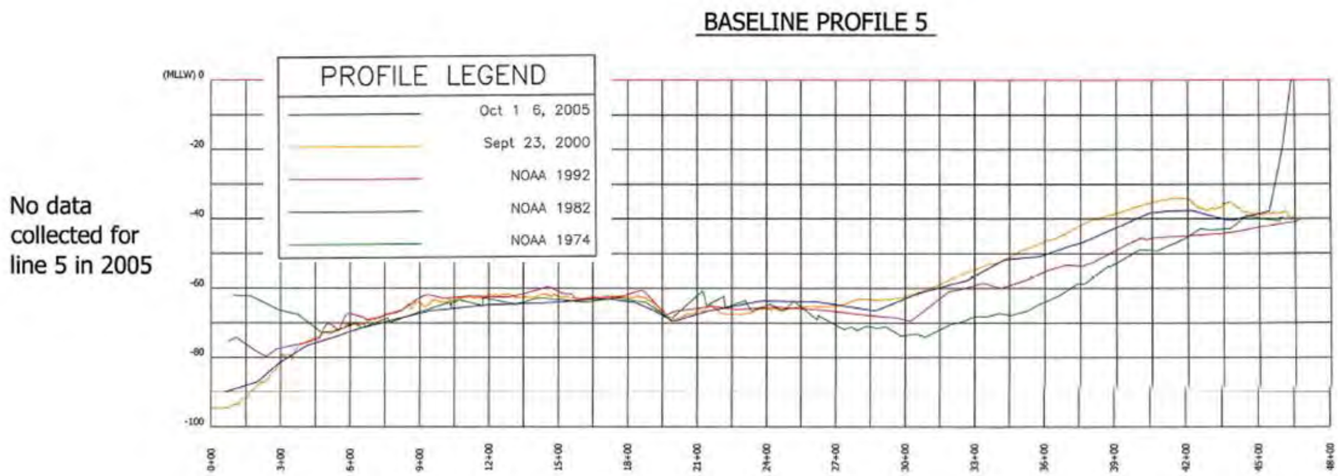

FIGURE 4.2-11. Baseline Profile BP5 Data Including Historical NOS Survey Data

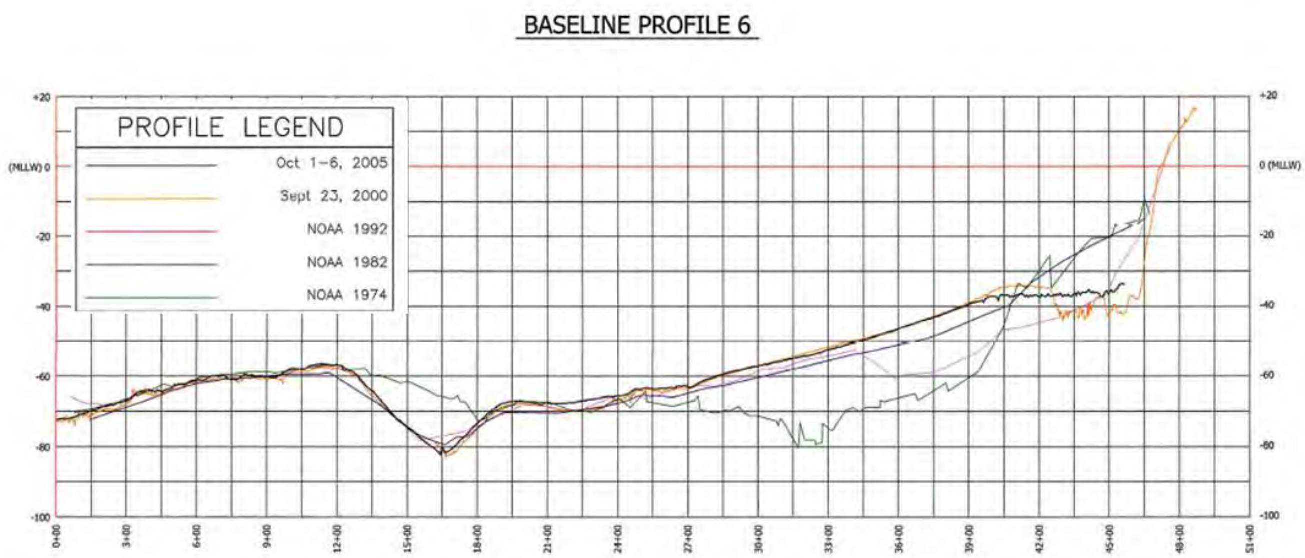

FIGURE 4.2-12. Baseline Profile BP6 Data Including Historical NOS Survey Data

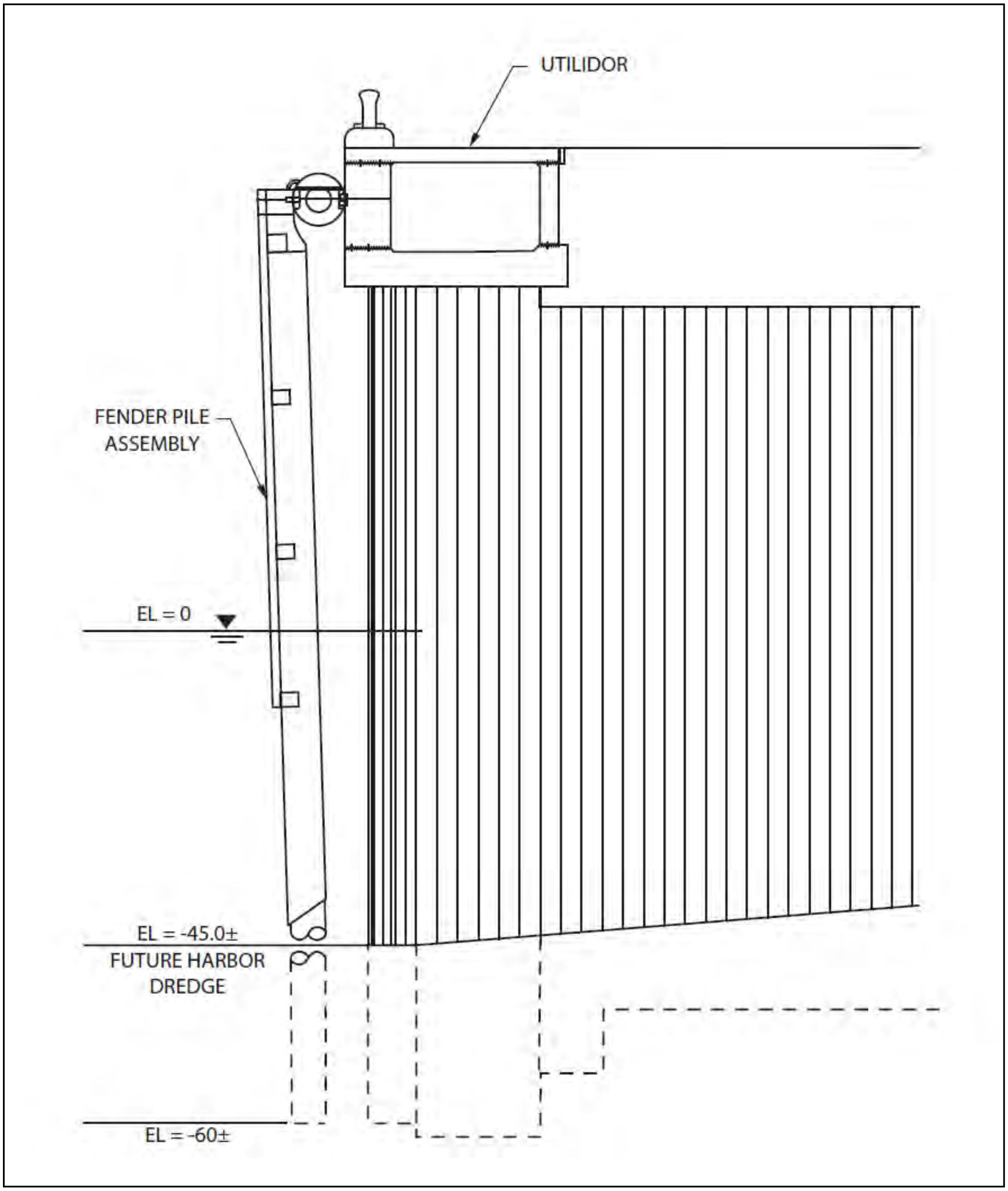

FIGURE 4.2-13. Fender Pile Assembly Fronting the OCSP® Structure Face

SECTION 5

Geotechnical Engineering Analysis

This section summarizes geotechnical engineering analyses conducted in accordance with current state-of-the-practice methods. These state-of-the-practice methods involved use of design equations and standard computer modeling methods. Numerical analyses for investigating soil-structure interaction are discussed in Section 7 of this report. The discussions in the following subsections cover the subsurface conditions used in the analyses and the geotechnical engineering evaluations for the as-built condition. Topics within the engineering evaluations include earth pressures, external stability, settlement, global stability, and sensitivity to variations in site conditions. Results of an evaluation of OCSP® system interlock pullout are also presented.

5.1 Subsurface Conditions Analysis

One of the most significant tasks in the review of the OCSP® system was to understand the geotechnical conditions at the PIEP. Geotechnical information has been collected at the POA by various engineering teams since early 2002. This information includes soil borings, cone penetration test (CPT) soundings, in situ shear wave velocity measurements, as well as results from laboratory testing programs to identify soil index properties and develop parameters for engineering analyses. Geotechnical information has also been collected for the backfill that is used within the OCSP® system walls; post-vibracompaction standard penetration test (SPT) blow counts (N-value) are available. This database of information was reviewed to understand what assumptions the PND design team used in their analyses and to identify alternate interpretations that could be made from the available information.

Two supplemental field investigations were conducted by CH2M HILL as part of this suitability study:

- **February 2012 Field and Laboratory Testing Program.** This investigation (Due Diligence 1) was performed in early 2012 to investigate granular backfill characteristics and the transition from backfill to native materials. Information from this investigation is presented and discussed in Section 5.2. A summary of this granular fill investigation is provided in Appendix D1.
- **May-August 2012 Field and Laboratory Testing Program.** This investigation (Due Diligence 2) was performed between May and September of 2012. This study was focused on the engineering behavior of Bootlegger Cove Formation (BCF) clay within the North Expansion area. The laboratory study was composed of constant rate-of-strain consolidation tests, monotonic direct simple shear and triaxial compression tests, cyclic and post-cyclic direct simple shear tests, and constant volume ring shear tests. Objectives for the testing were to confirm stress history and peak undrained strengths of BCF clay in the North Expansion area and to investigate the behavior of the foundation material under cyclic load application, as well as undrained shear strength under large displacements. The BCF clay investigation is summarized in Appendix D2.

5.1.1 Subsurface Conditions

Several historical geotechnical exploration programs have been performed at the POA. For this study, reports summarizing the geotechnical findings were reviewed to obtain an understanding of the geology and subsurface conditions in the area of development. The focus of the review was on subsurface information derived from explorations completed specifically for the PIEP. Figure 5.1-1 shows original explorations used for site characterization within North Extension 1 and North Extension 2.

The following three reports completed specifically for the PIEP were reviewed to evaluate the subsurface conditions at the Dry and Wet Barge Berths, North Extension 1, and North Extension 2. The subsurface explorations summarized in these reports are considered to be the most relevant to this evaluation because they were performed along the proposed OCSP® wall alignment in the North Expansion area:

- *Port of Anchorage Marine Terminal Redevelopment Geotechnical Analysis Report*, Appendix P, 2010 Sampling Report (PND, 2010e)
- *Marine Geotechnical Exploration Port of Anchorage Intermodal Expansion*, Volume 1 (Terracon, 2004a)
- *Marine Geotechnical Exploration Port of Anchorage Intermodal Expansion*, Volume II, Site Investigation Project Data Presentation (Gregg Drilling & Testing, Inc., 2003)

The subsurface soils encountered in the explorations for the PIEP include three main units. From the mudline down, they are: (1) estuarine deposits, (2) glacio-estuarine or glacio-lacustrine BCF, and (3) glaciofluvial deposits. Characteristics of these units are briefly reviewed in the following subsections. More detailed discussions of the properties of these units are presented later in this section.

5.1.1.1 Estuarine Deposits

The estuarine deposits consist mainly of sands, silts, and clays deposited by tidal action and sedimentation. These deposits extend from the mudline to the top of the BCF clay. The mudline starts at approximately elevation zero mean lower low water (MLLW) near the north end of the Dry Barge Berth and grades down to approximately elevation -45 MLLW at the south end of North Extension 2 along the face of the sheet pile wall.

The estuarine deposits range in thickness from few feet to 20 feet between the north end of the Dry Barge Berth and the south end of North Extension 2. This layer grades from soft/loose at the surface to stiff/medium dense. The layer can vary significantly in composition, density, and consistency due to erosion and reworking by the tides. Most of the Holocene silt deposits have been removed over the years by dredging, and they have been replaced with silts and sands that have been deposited by tidal action and sedimentation (Terracon, 2004b). These silts and sands are relatively loose or soft in consistency and were not expected to be a suitable foundation material for the OCSP® system.

Dredging of the estuarine deposits before placement of the backfill was recommended; however, due to scheduling and construction constraints, this layer was not dredged along the entire site. Construction records indicate that this layer was dredged at the face of the OCSP® wall between Cells 9 and 66 of North Extensions 1 and 2. The depth of dredging at the face of the wall was about elevation -40 feet MLLW between Cells 9 and 32 and about elevation -50 feet MLLW between Cells 37 and 66.

5.1.1.2 Glacio-Estuarine or Glacio-Lacustrine Bootlegger Cove Formation

The Bootlegger Cove Formation deposit is a glacio-estuarine or glacio-lacustrine geological unit that encompasses a variety of sediment textures from numerous depositional regimes in a single glaciomarine-glaciodeltaic system (Updike, 1985). Five cohesive and three cohesionless geologic facies have been identified within the BCF based on their textural characteristics (Ulery and Updike, 1983). Although the BCF includes both cohesive and cohesionless facies, it is commonly referred to as the BCF clay, without regard for facies or soil type. This terminology will be used throughout this report.

The BCF clay encountered between the Dry Barge Berth and the North Extension 2 consists mainly of overconsolidated clay and silts with interbedded lenses composed of dense fine sand and silt. The interbedded lenses generally vary in thickness between 0.5 and 3 inches but could be up to 5-feet thick. The formation encountered along the OCSP® alignment is mainly classified as stiff to very stiff silty clay of low plasticity. The BCF clay typically starts below the estuarine deposits and extends to about elevation -150 to -200 MLLW under the footprint of the of the OCSP® wall.

5.1.1.3 Glaciofluvial Deposits

The glaciofluvial deposits (glacial drift) consist mainly of dense to very dense sand and gravel with interbedded hard clay layers that were consolidated under the effect of glaciers. These deposits are present under the BCF clay and generally extend to over 600 feet in depth. The glacial drift is underlain by undifferentiated pre-Quaternary deposits or metamorphic bedrock.

5.1.2 Subsurface Model Development

Three cross sections labeled in Figure 5.1-1 as 1-1, 2-2, and 3-3 were developed perpendicular to the OCSP® wall alignment to represent the subsurface along the North Expansion area, as shown in Figures 5.1-2 to 5.1-4:

- Section 1-1 was taken in the middle of the constructed section of North Extension 2 in Cell 60.
- Section 2-2 was taken in Cell 54, which is the most southern cell in North Extension 1.
- Section 3-3 was taken in Cell 29 of North Extension 1.

The OCSP® system in the Wet Barge Berth and in North Extension 1 is considered part of an essential facility that should be analyzed for the MCE, as discussed in Section 2 of this report. Sections 1-1 and 2-2 are in deeper water with the bottom of the OCSP® piling extending to about elevation -61 feet MLLW, whereas Section 3-3 is in shallower water with the tip of the piling extending to about elevation -50 feet MLLW.

Boring logs for boreholes drilled closest to the cross sections under investigation were used to represent the subsurface at each of these sections. The existing mudline before placement of the backfill was identified from bathymetric contour lines provided with the project archives. For the seaward side, the design over-dredge elevation, which is below the existing mudline, was used as the basis of design at the face of the wall. The soil units generally included granular fill, common fill, BCF clay (in stress states after dredging [seaside of wall] and fill placement [landside of wall], sand, and glacial drift.

The sections shown in Figures 5.1-2 to 5.2-4 differ somewhat from the sections used by the PND design team in their design (PND, 2008). The closest PND sections were for Analysis Section F Replacement and North Extension, which is similar to North Extension 2, and Analysis Section G North Extension, which covers North Extension 1 and the Wet Barge Berth (see Figure 4.1 in PND, 2008). The differences between PND's sections and CH2M HILL's sections result from the planned dredge depths behind the OCSP® wall used by PND versus the post-construction dredge depths used by CH2M HILL.

The sections shown in Figures 5.1-3 and 5.2-4 were simplified for the geotechnical and numerical analyses described in Section 5 and Section 7 of this suitability study report. The simplified Section 2-2 and Section 3-3 are presented in Figures 5.1-5 and 5.1-6, respectively. The simplifications involved use of straight-line sections to represent the geometry of the soil profile and OCSP® wall. These changes were made to help in the computer modeling for stability and soil-structure interaction analyses. The nature of the simplifications was such that results of the analyses would not be affected.

Section 2-2 was identified as the most critical section in the area being evaluated for the following three reasons:

1. This section has the highest wall section constructed to date on the project, with a top sheet pile elevation of +30 feet MLLW and a bottom elevation of -61 feet MLLW at the face of the wall, resulting in sheet piling that are about 90 feet long.
2. This section is located within the essential facility area, which must be analyzed for the MCE seismic event, as well as for the OLE and CLE events.
3. This section has a thick, soft mud layer consisting of soft estuarine deposits that was not fully dredged during construction.

5.1.3 Soil Profiles

Two subsurface profiles perpendicular to those described in the previous section were also created as labeled in Figure 5.1-1 as A-A and B-B. Profile A-A was cut along the face of the OCSP® wall; Profile B-B was cut 200 feet east of the face of the OCSP® wall. Relative to the existing POA berthing line, the face of the OCSP® wall is 400 feet to the west. In general, the subsurface conditions along these two profiles are consistent with one another except that the mudline for Profile B-B is shallower, especially in the Wet Barge Berth and North Extension 1.

The profiles are presented in Figures 5.1-7 and 5.1-8. The characteristics of these soil profiles are, as follows:

- **Profile A-A, at face of wall (Figures 5.1-7a, b, and c).** The profile along the face of the OCSP® wall (400 feet west of the existing POA berthing line) consists of 10 to 20 feet of estuarine deposits underlain by the BCF clay to approximately elevation -200 feet. The top 40 to 80 feet of the BCF clay includes sand and silt lenses of varying thicknesses. For example, boring TB-56 encountered a 23-foot-thick layer of sand between elevations -37 MLLW and -61 feet MLLW.
- **Profile B-B, 200 feet east of face of wall (Figures 5.1-8a, b, and c).** The profile along the 200-foot line behind the face of the OCSP® wall (200 feet west of the existing POA berthing line) shows about 4 to 20 feet of estuarine deposits underlain by the BCF clay to about elevation -200 feet MLLW. The top 10 to 50 feet of the BCF clay includes sand and silt lenses. The BCF clay becomes more homogeneous with less sand and silt intrusions below -65 feet MLLW. Boring TB-52 encountered sand to silty sand between approximately elevations -150 and -160 feet MLLW.

These profiles show that the soft estuarine deposits at the face of the OCSP® wall (400 feet west of the existing POA berthing line) deepens to the south. The layer is generally about 30 to 40 feet thick in the North and South Replacement areas (see Figure 1.2-2), but could be as much as 50 feet thick as shown in boring B-43 in Appendix P (April 2009) of the PND Report. These thicknesses are greater than the soft estuarine deposit to the north for the North Extension and Wet Barge Berth area, making planned construction of the OCSP® wall in the North and South Replacement areas more challenging.

5.1.4 Groundwater Conditions

Landside groundwater readings were reviewed from Terracon's *Interim Monitoring Summary Report, North Extension Instrumentation* (November 7, 2011). Three sets of readings were typically reported for piezometers installed on the landside of the OCSP® structure as follows:

- Tidal water elevation
- Hydrostatic groundwater elevation in the backfill layer from a shallow piezometer installed in the backfill
- Hydrostatic and excess porewater pressure heads from a deep piezometer installed in the BCF clay

The readings for the deep piezometers installed in BCF clay are artificially high because they show the increased porewater pressure due to consolidation from the placement of the backfill and, therefore, are considered not representative of the landside groundwater elevation at this time. The readings from piezometers installed in the backfill layer were used to estimate the groundwater on the landside.

The groundwater monitoring graphs provided in Appendix B-6 of Terracon's report (2011) show one point for the rolling average of about 24 readings. The automatic data loggers used by Terracon were set up to take readings every 15 minutes between June 17, 2009, and July 2, 2009, and every 30 minutes from July 2, 2009, to date. The rolling average for 24 readings taken at 30-minute intervals represents the average water elevation over a 12-hour period. The locations of the piezometers installed on the landside with their observed maximum groundwater elevation are shown in Figure 5.1-9a.

The individual 30-minute readings for piezometers installed in backfill in Cells 15 and 45 were plotted on graphs shown in Figures 5.1-9b and 5.1-9c, respectively. These graphs show bands of data that represent a point every 30 minutes over a period of 2 years. Since it was hard to identify the water-head elevation variation over a 2-year period, a sample of data extending for 15 days between January 6, 2010, and January 21, 2010, is shown in Figures 5.1-9d and 5.1-9e for backfill piezometers in Cells 15 and 45, respectively. The graphs in Figures 5.1-9d and 5.1-9e include the tidal water elevation and the piezometer readings during the same period and show that the water on the landside is impacted by the tidal variation, as follows:

- There is a synchronized variation in water elevation between the tidal water and the landside water even though the water on the landside does not reach the maximum or minimum tide elevations.
- A slight delay is also observed between the tidal and landside water elevation variation. This lag likely reflects the hydraulic conductivity through the interlocks and through gaps in the OCSP®.

The graphs presented in Terracon's report (2011), shown in Figures 5.1-9f and 5.1-9g for piezometers installed in backfill in Cells 15 and 45, respectively, were the average of about 24 readings performed at 30-minute intervals. When presented as one point, these readings mask the peak tidal and landside elevations shown in Figures 5.1-9b through 5.1-9e. The average tidal water in Terracon's report is around elevation +16.5 feet MLLW. In Appendix B-6 of Terracon's report, average landside water elevations in Cell 15, Cell 30, and EP1 are generally higher than the average tidal elevation, whereas the average landside water elevations in Cell 45, Cell 61, and EP2 are generally lower than the average tidal elevation. This indicates that water elevation on the landside of the face of the OCSP® wall may not be the same in different cells.

Based on the data provided in Terracon's report (2011), a landside groundwater elevation of +20 feet MLLW was assumed for the evaluation of the OCSP® wall. A sensitivity analysis that varies the landside water elevation from +17 to +23 feet MLLW was performed and is presented in Section 5.3 of this report. The assumed backfill or landside groundwater elevation of about +20 feet MLLW was later verified during the field exploration program conducted as part of the CH2M HILL suitability study in February 2012. Groundwater readings performed during the February 2012 exploration program are included in Appendix D1 of this report.

The relatively high groundwater elevation on the landside of the wall is also thought to be influenced by surface water runoff from the east of the site, as well as from rainfall infiltration. Since runoff and rainfall are seasonal in the area, some variation in groundwater elevation is likely. Available data suggest that this variation could be up to 5 feet. Groundwater data in the North Extension backfill presented in Appendix B-6 of Terracon's report suggest that the highest water elevation is observed between April and May and may be due to the spring runoff from the hillside to the east and the thaw process.

In addition to groundwater readings obtained from Terracon's report (2011), groundwater information obtained from Appendix Q of PND's report (2010d) was evaluated. Appendix Q (PND) summarizes groundwater readings obtained in piezometers PZ 24 through PZ 29, which were installed in 2008 prior to the construction of the cells in the North Extension. Piezometer PZ 29, which was installed in the backfill behind the riprap, shows a high groundwater elevation of +29 feet MLLW as summarized in Appendix Q (PND). However, since Appendix Q (PND) data do not represent groundwater readings behind the OCSP® wall system, the groundwater readings from 2008 and early 2009 reported in Appendix Q (PND) were disregarded for this analysis.

5.1.5 Engineering Properties of Native Soils

Engineering properties of the native material were determined on the basis of information collected during the field explorations and laboratory testing. The field exploration included blow counts from SPTs, as well as tip resistance and sleeve friction measurements from CPT soundings. The laboratory testing included classification and engineering property testing. By using these results, either directly or in empirical relationships, engineering properties required for design were developed. The following two subsections summarize these engineering properties. This summary is followed by a discussion of the potential shear strength reduction of the BCF clay at large displacements, as this particular behavior could control the stability of the OCSP® system during seismic loading.

5.1.5.1 Estuarine Deposits

The engineering properties of the estuarine deposits were collected from the following sources:

- *Preliminary Marine Geotechnical Exploration Report for the Port of Anchorage Intermodal Expansion Project* (Terracon, 2004b)
- *Geotechnical Report for the Port of Anchorage Intermodal Expansion Project,* Appendices A-M (PND, 2008b)
- *Geotechnical Report for the Port of Anchorage Intermodal Expansion Project,* Appendix N (PND, 2010i), Appendix O (PND, 2009c), Appendix P (PND, 2010e), Appendix Q (PND, 2010d), and Appendix R (PND, 2010g)
- *Geotechnical Finding Report for the Anchorage Harbor Deepening Project* (USACE, 2008a)

In general, there is a lack of information on the engineering behaviors of the estuarine deposits from the Terracon (2004b) report, as it was apparently assumed that this layer would be removed, and therefore, the soil layer was not sampled during the exploration program. Exploration work done by the USACE for their dredging program and by PND in 2008 to supplement previous Terracon work provided information about the estuarine deposits. All test borings conducted by USACE in 2008 were offshore (west of the project alignment).

Data from these additional investigations indicated that the estuarine deposits encountered below the mudline mainly consist of clay and silt (CL, ML) with fines content ranging from 80 to 89 percent and moisture content ranging from 20 to 43 percent. Results from Atterberg limits tests gave a range of liquid limits (LL) from 21 to 40 percent and plasticity index (PI) from non-plastic to about 18 percent. The blow counts obtained from SPTs were typically less than 5 blows per foot (bpf), with consistency ranging from very soft to firm. The unconfined compressive strength obtained from pocket penetrometer tests varied between 1 and 9 kips per square foot (ksf). Field vane shear testing (VST) conducted by USACE (2008) in three borings near the northern, center, and southern parts of the project area gave a range of undrained shear strengths from 0.6 to 1.95 ksf with the peak over residual undrained shear strength ratio ranging from 1.8 to 4.3. The average of the normalized peak undrained shear strength (S_u/σ'_v) estimated from the VST results is about 1.1, where σ'_v is the effective overburden stress. The VST was unsuccessfully conducted by PND in the 2008 exploration. It was reported by PND (2010a) that the results from VST were not reliable as the capacity of the equipment was exceeded during the tests.

According to PND (2008b), the estuarine deposits mainly consist of very fine sand with 2 to 10 percent non-plastic, clay-size “rock dust.” The term “rock dust” was used to differentiate between clay minerals and clay-size particles of other rock minerals. PND (2008b) also reported that the effective stress friction angle of the estuarine deposits, obtained from triaxial compression tests under the estimated consolidation pressure of the fill material, varied from 32 to 40 degrees. Based on CH2M HILL’s experience with soils of similar origin (estuarine silts) and blow counts, the range of friction angles reported by PND (2008b) is relatively high. Therefore, the lower bound value of 32 degrees was assumed for the effective stress friction angle of the estuarine deposits.

Table 5.1-1 shows all engineering parameters that were used by CH2M HILL for the estuarine deposits in this suitability study. These engineering parameters were estimated by CH2M HILL using the existing field and laboratory testing data, empirical-based correlations published in the literature, previous practice, and engineering judgment. The estuarine deposits were assumed to behave in an “undrained” manner for the end-of-construction, long-term static-undrained, and seismic loading cases. The undrained shear strength of the estuarine deposits in the seismic loading conditions was assumed to be 80 percent of the static undrained shear strength to account for the temporary strength reduction of soft soils under cyclic loading. The effective stress parameters (E', ν', ϕ') were assumed for the estuarine deposits in the long-term static drained condition.

TABLE 5.1-1
Engineering Summary of the Estuarine Deposits

Total Unit Weight, γ (kcf)	Effective Cohesion, c’ (ksf)	Effective Friction Angle, ϕ' (degree)	Undrained Shear Strength, S_u	Drained Elastic Modulus, E’ (ksf)	Undrained Elastic Modulus, E_u (ksf)	Poisson’s Ratio, ν (--)
0.12	0	32	$0.55*\sigma'_v$ [b]	40[c]	45[d]	$\nu' = 0.3$ $\nu_u = 0.49$

[a] S_u^{VST} varies from 0.6 to 1.95 ksf at depth from 7.5 to 14 feet below the mudline.
[b] The post-construction S_u/σ'_v ratio was assumed to be a half of the in situ S_u/σ'_v ratio, where σ'_v was estimated by including the live load.
[c] Estimated from Table 29 of Sabatini et al. (2002) using the relationship $E' = 8*(N1)_{60}$ ksf with $(N1)_{60}$ assumed to be 5 blows per foot.
[d] Calculated from E’ using the relationship $E_u = E'*(1+\nu_u)/(1+\nu')$ where ν' and ν_u are Poisson’s ratio in drained and undrained conditions, respectively.
kcf = kips per cubic foot
ksf = kips per square foot

5.1.5.2 Bootlegger Cove Formation Clay

According to the *Preliminary Marine Geotechnical Exploration Report for the POA Intermodal Expansion Project* (Terracon, 2004b), the BCF clay was classified as low-plasticity silty clay (CL) with a consistency ranging from stiff to very stiff. Within the North Extension and North Replacement areas, the BCF clay is typically encountered at depth of 10 to 20 feet below the mudline with thicknesses varying from 50 to about 100 feet. In the upper 50 feet, the BCF clay contains numerous interbedded sand layers (1- to 5-feet thick) that are located approximately 10 to 20 feet apart from each other (facies F.IV). The BCF clay in the lower 50 feet, which is believed to belong to facies F.I, appears to be relatively homogeneous (without the interbedded sand layers).

Based on the results obtained from the one-dimensional consolidation and the consolidated undrained triaxial compression tests, the BCF clay at the project site appears to be lightly to moderately overconsolidated with the preconsolidation stress (σ'_P) increasing from 9 ksf at the top of the BCF clay to about 16 ksf at a depth of 120 feet below the mudline (Figure 5.1-10). As a result, the pre-construction (in situ) overconsolidation ratio (OCR) was estimated to vary from about 10 at the top of the layer to about 2 at 120 feet below the mudline (Figure 5.1-11). Because the effective overburden stress in the BCF clay increases after placement of the backfill, the OCR values in the BCF clay in the post-construction stage were estimated to range from about 1.2 to 1.3. New constant rate-of-strain consolidation tests confirm this original design assumption regarding stress history, as documented in Appendix D2.

The average re-compression index over the compression index ratio (C_R/C_C) of the BCF clay was found to be about 0.2, which is considered to be typical for natural clays (Kulhawy and Mayne, 1990). The average coefficient of consolidation at 90 percent degree of consolidation, c_{V90}, was estimated to be about 0.2 foot square per day, which is considered reasonable for lightly overconsolidated clays (Sabatini et al., 2002).

Table 5.1-2 summarizes the representative consolidation parameters for the BCF clay in the North Extension and North Replacement areas used by CH2M HILL for the evaluation of the long-term settlement.

TABLE 5.1-2
Representative Consolidation Parameters of the BCF Clay

Total Unit Weight, γ (kcf)	Average Initial Void Ratio, e_0 (--)	Assumed Preconsolidation Stress at the Mudline EL., σ'_P (ksf)	Average Compression Index, C_C (--)	Average Re-Compression Index, C_R (--)	Secondary Compression Index, C_α (--)	Average Coefficient of Consolidation, c_{V-90} (ft^2/day)
0.125	0.78	8.0[a]	0.25	0.05	0.002[b]	0.2[c]

[a] Assumed by Professor Paul Mayne by extrapolating the data obtained from one-dimensional consolidation tests.
[b] Assumed to be equal to 0.04*C_R for overconsolidated clays (Terzaghi et al., 1996).
[c] Calculated at 90 percent degree of consolidation and under a range of effective overburden stress from 4 to 8 ksf.
ft^2/day = square feet per day

The in situ peak undrained shear strength and the effective stress shear strength parameters of the BCF clay were initially characterized using the data collected from cone penetration tests with porewater pressure measurements (CPTu), field vane shear tests conducted within one boring near the existing terminal, and a laboratory testing program composed of isotropically consolidated undrained compression (CIUC) and direct simple shear (DSS) tests. The shear strength recommendations described herein for North Expansion areas are based on the existing information, as well as the results of the supplemental investigation summarized in Appendix D2. An effective friction angle of 30 degrees (with no cohesion) was selected for long-term, effective-stress analyses. This friction angle is reasonable for clays with average PI of 20 percent and is just slightly higher than the value of 29 degrees more commonly reported for the BCF clay at other locations in Anchorage. The higher effective friction angle (compared with 27 degrees assumed by the PND design team for design) represents approximately 13 percent increase in shear strength, much of which is offset by the use of no cohesion.

After construction of the OCSP® structure, the undrained shear strength of the BCF clay increases with time as the excess porewater pressure in the clay dissipates. The change in the undrained shear strength of the BCF clay was characterized by using the Stress History And Normalized Soil Engineering Properties (SHANSEP) method (Ladd and Foott, 1974). In the SHANSEP approach, the undrained shear strength of the clay (S_u) is correlated with the effective overburden stress (σ'_v) and the overconsolidation ratio—both are changed from the in situ condition to the time when the BCF clay, under the weight of the backfill on the land side of the facewall, is fully consolidated (that is, post-construction condition), or when the existing stress state decreases on the sea side of the facewall from dredging.

The SHANSEP correlation has the following form:

$$(S_u/\sigma'_v)_{OC} = (S_u/\sigma'_v)_{NC}*(OCR)^m$$

where $(S_u/\sigma'_v)_{NC}$ and *m* are estimated from one-dimensional consolidation and triaxial compression and/or DSS tests.

Professor Paul Mayne of the Georgia Institute of Technology, who served as a member of ICRC's independent advisory committee for the project, developed the SHANSEP correlations for the BCF clay using the CIUC and DSS test results provided by Terracon (2004b). These initial SHANSEP strength ratios for DSS and triaxial compression shearing modes were:

Triaxial compression: $S_u/\sigma'_v = 0.33*(OCR)^{0.77}$

Simple shear: $S_u/\sigma'_v = 0.23*(OCR)^{0.70}$

According to PND (2008b), only the post-construction, undrained shear strength of the BCF clay in the North Extension and North Replacement areas was calculated using the triaxial compression-based SHANSEP correlation. The in situ undrained shear strength of the seaside BCF clay was estimated by PND (2008b) from the CPT data using N_{kt} values of 20.

In the recent CH2M HILL suitability study, the undrained shear strengths of the BCF clay for both in situ and post-construction stages were also calculated using SHANSEP correlations. Based on new testing, the peak undrained strengths were found to be just slightly higher. The revised shear strength ratios are shown in Figure 5.1-13 as a function of OCR, and the following SHANSEP correlations were used for estimating the undrained shear strength of the BCF clay encountered in the North Extension and North Replacement areas:

Triaxial compression: $S_u/\sigma'_v = 0.34*(OCR)^{0.79}$

Simple shear: $S_u/\sigma'_v = 0.25*(OCR)^{0.79}$

The shear strength profiles, after multiplying by the estimated vertical effective stress (σ'_v) for the seaside and landside BCF clays used in the CH2M HILL suitability study, are shown in Figure 5.1-12. For comparison, the shear strength profiles used by PND (2008b) for Section F (North Replacement) and Section G (North Extension) are also shown in Figure 5.1-12. As can be seen in this figure, the shear strengths used by PND (2008b) for the seaside BCF clay at Analysis Sections F and G were significantly higher than those used by CH2M HILL for Sections 2-2 and 3-3 in this study. It is important to note that the shear strength profiles developed by PND (2008b) for the seaside BCF clay were calculated from CPT soundings, which were conducted in the in-situ condition (that is, prior to dredging work). Since the overburden effective stress in the seaside BCF clay will significantly reduce after dredging, the undrained shear strength used by PND (2008b) for the seaside clay will likely be overestimated. The CIUC-based shear strength profiles used by PND (2008b) for landside clay, as shown in Figure 5.2-12, are generally more similar with the shear strength used by CH2M HILL for Sections 2-2 and 3-3 in this study.

Comparisons of BCF clay shear strengths used for the original design and this suitability study are provided in Table 5.1-3.

TABLE 5.1-3
BCF Clay Shear Strength Comparison

Shear Strength	Terracon (2004), PND (2008)	Suitability Study (2012)
Effective-stress friction angle	$\phi' = 27$ degrees	$\phi' = 30$ degrees
Peak undrained strength ratio for simple shear	$(s_u/\sigma'_v)_{DSS} = 0.23\ OCR^{0.70}$	$(s_u/\sigma'_v)_{DSS} = 0.25\ OCR^{0.79}$
Peak undrained strength ratio for triaxial compression	$(s_u/\sigma'_v)_{TC} = 0.33\ OCR^{0.75}$	$(s_u/\sigma'_v)_{TC} = 0.34\ OCR^{0.79}$
Peak undrained strength ratio for triaxial extension (seaside only)	Used pre-dredging CPTu with N_{kt} = 20 (see Figure 5.1-12)	$(s_u/\sigma'_v)_{TE} = 0.5\ (s_u/\sigma'_v)_{TC}$
Cyclic/residual undrained shear strength for seismic loading cases	Peak undrained strengths used	• Pseudo-static analyses optimistically assumed peak undrained strength. • FLAC analyses assumed 90 percent of peak undrained strength. • Estimates of permanent deformation (Newmark analyses) assumed displacement-dependent undrained strength from 30 to 100 percent of peak strength (see Section 5.2.7.2).

σ'_v = vertical effective stress
OCR = overconsolidation ratio
CPT = cone penetration test

The elastic deformation of the BCF clay in the static, undrained loading condition can be modeled by using either the initial elastic undrained modulus (E_{ui}) or the secant undrained modulus (E_{u50}) obtained from the CIUC tests. The E_{u50} in this study is defined as the ratio of the stress on the stress-strain curve that is equal to 50 percent of the ultimate shear stress over the corresponding shear strain. Figure 5.1-14 shows the undrained modulus of the BCF clay normalized by the undrained shear strength (E_{ui}/S_u and E_{u50}/S_u) over a range of OCRs. As can be seen in this figure, the average E_{ui}/S_u and E_{u50}/S_u ratios for the BCF clay were estimated to be about 505 and 125, respectively. According to PND (2008b), E_u/S_u ratios of 600 and 800 were assumed for the BCF clay on the sea side of the wall and on the land side of the wall, respectively. These assumed E_u/S_u ratios from PND (2008b) appear to be higher than the E_{ui}/S_u ratio shown in Figure 5.1-14. It is also noted that PND (2008b) did not use the secant modulus in modeling the undrained static deformation of the BCF clay. As a result, the static deformations calculated by PND (2008b) could be underestimated.

For the long-term, static drained loading condition, either the effective stress initial modulus (E'_i) or the effective stress secant modulus (E'_{50}) must be used for the BCF clay. Ideally, the effective stress modulus of soils should be obtained from the consolidated isotropically drained compression (CIDC) tests. However, the E'_i and E'_{50} were estimated from the undrained modulus values (E_{ui} and E_{u50}) and Poisson's ratio in this suitability study.

Similar to the estuarine deposits, the BCF clay was assumed by CH2M HILL to behave in an "undrained" manner for the end-of-construction, long-term static-undrained, and seismic loading cases. For the long-term static loading condition with mean tidal elevation, the BCF clay was assumed to be fully drained, and thus the effective stress parameters (E', ν', ϕ') were used. Stress-strain parameters developed by CH2M HILL for the BCF clay are summarized in Table 5.1-4. Discussions on the potential reduction in the undrained shear strength of the BCF clay during and after earthquake shaking are provided in the next section, as well as in Sections 5.2.2, 5.2.6, and 5.2.7. The seismic stress-strain parameters of the BCF clay are also discussed in Chapter 7.

TABLE 5.1-4
Stress-Strain Parameters of the BCF Clay in Static Loading Condition from CH2M HILL Analysis

Effective Stress Cohesion, c' (ksf)	Effective Stress Friction Angle, ϕ' (degree)	Static Undrained Shear Strength, S_u [a] (ksf)	Normalized Drained Initial Modulus, E'_i/S_u [b] (--)	Normalized Drained Secant Modulus, E'_{50}/S_u [b] (--)	Normalized Undrained Initial Modulus, E_{iu}/S_u (--)	Normalized Undrained Secant Modulus, E'_{u50}/S_u (--)	Poisson's Ratio, ν (--)
0.0	30	SHANSEP	505	125	560	140	$\nu' = 0.35$ $\nu_u = 0.49$

[a] The triaxial compression-based SHANSEP correlation was used in the FLAC^{3D} analyses. Both triaxial compression-based and DSS-based SHANSEP correlations were used in the global stability analyses.
[b] Calculated from the undrained modulus (E_u) using the relationship $E' = E_u*(1+\nu')/(1+\nu_u)$ where ν' and ν_u are Poisson's ratio in drained and undrained conditions, respectively.

5.2 Geotechnical Engineering Analysis

Properties of native soils described in the previous section were used to evaluate the as-built response of the OCSP® system (the as-built design case). As noted in Section 2, the as-built conditions represent conditions after the construction of the OCSP® system. They differ from the as-designed case by the changes in OCSP® geometry, soil conditions, and the assumptions regarding tidal elevation, groundwater elevation, and scour depth. Therefore, the as-built analyses represent CH2M HILL's best effort to characterize and evaluate the existing conditions for the constructed OCSP® system for likely response to operational and seismic loading.

5.2.1 As-Built Backfill Characteristics

The engineering characteristics of the granular backfill material are important for understanding the behavior of the OCSP® bulkhead structure, as these properties determine the forces imposed on the facewall of the OCSP® system, the pullout capacity of tailwalls, the potential for liquefaction within the materials during seismic loading, and the overall stability of the system under operational and seismic loads. For these reasons, this suitability study included a detailed, independent review of the characteristics of the backfill material with emphasis on estimating relative density and internal friction angle.

5.2.1.1 Backfill Source, Gradation, and Placement Method

The OCSP® system was constructed by filling from the top of native soil (that is, estuarine deposits or BCF clays) to elevation +30 MLLW using an unprocessed (that is, no sorting or crushing) granular material obtained from a borrow source at Joint Base Elmendorf-Richardson (JBER), formerly called the Elmendorf Air Force Base North End Borrow Pit. The borrow source, which is part of the Elmendorf moraine, was not processed because of the cost of processing and the good quality of the material (that is, a minimum amount of material passing the No. 200 sieve) and limited amount of oversized material (greater than 4 inches).The material is generally classified as silty gravel with sand or silty sand with gravel (Clarus Technologies, 2008). The material has been noted by PND to be fairly consistent in its gradations; however, local variation has been observed. Table 5.2-1 summarizes the characteristics of the granular fill placed in the North Extension.

Some backfill was placed before sheet piling installation to build a temporary access dike for equipment used to install the sheet piles. The backfill was also deposited after the OCSP® system piling was driven. Backfill was placed underwater without compaction until the top was above water, and then it was compacted. Contract documents required that the placement method avoid segregation of the finer portion of the fill when placing underwater. Once the backfill reached elevation +30 feet MLLW, it was further densified using a vibratory probing system called vibracompaction. Vibracompaction was performed on approximately 10-foot centers to the bottom of the backfill. Additional granular fill was added to the probe location as the backfill was densified. Post-ground-improvement SPTs were then conducted to confirm that a minimum density existed within the backfill. Based on this planned construction process, the PND design team used a friction value of 36 degrees to represent the backfill material in their design evaluations. The densified backfill was also assumed to be non-liquefiable.

TABLE 5.2-1
Summary of Granular Fill Gradations for North Extension Cell Construction (after PND, 2011c)

No. Samples	Location	% Gravel	StDev	% Sand	StDev	% Fines	StDev
45	2008 NE trench	45	7	49	6	6	2
65	2009 NE north cells	59	6	37	6	4	2
43	2009 NE south cells	63	7	33	6	4	2

StDev = standard deviation

5.2.1.2 Relative Density

Relative density of the as-built granular fill material was estimated by CH2M HILL using the post-vibracompaction SPT results from tests within the North Extension section composed of Cells 9 to 32. The field test results were documented by PND (2010b). Based on the PND summary of SPT verification results, the mean energy-corrected N-value (N_{60}) was about 59 bpf. The mean energy- and overburden-corrected N-value [$(N_1)_{60}$] was about 55 bpf. Standard deviation for these two parameters was about 16 bpf.

The evaluation of relative density considered three empirical correlations that relate N-values to relative density, Terzaghi and Peck (1967), Holtz and Gibbs (1979), and Skempton (1986):

- The Terzaghi and Peck (1967) relationship between N-value and relative density is shown in Figure 5.2-1; based on the mean N_{60} value, relative density is approximately 90 percent.
- The N_{60} value is plotted against normalized vertical effective stress in Figure 5.2-2. The plotted data superimposed on the Holtz and Gibbs (1979) guidance for relative density show relative density for the compacted granular fill exceeding 90 percent.
- The Skempton (1986) procedure to estimate relative density accounts for particle size. For gravel, the defined parameter $(N_1)_{60}$ $[D_r^2]^{-1}$ can range from 60 to 70. Based on the mean $(N_1)_{60}$ value of 55 bpf, relative density can range from about 88 to 96 percent.

With consideration given to each of the above methods, engineering evaluations assumed a relative density value of 90 percent for compacted granular fill. The as-built condition assessment does not include evaluation of the stability of the system prior to vibracompaction. Therefore, relative density of uncompacted granular fill is not discussed in this section.

5.2.1.3 Internal Friction Angle Based on Empirical Correlation

Internal friction angle for cohesionless soils depends on relative density, particle size and shape, gradation, particle strength, and confining pressure. At the beginning of the suitability study, in the absence of laboratory strength tests conducted on the North Extension backfill materials, an empirical method proposed by Koerner (1970) was used to estimate friction angle. Koerner (1970) offers guidelines for estimating friction angle using systematic recommendations to account for the above factors. The following equation represents the recommended design value for internal friction angle of cohesionless soils:

$$\phi_f = 36^o + \Delta\phi_1 + \Delta\phi_2 + \Delta\phi_3 + \Delta\phi_4 + \Delta\phi_5$$

Where:

$\Delta\phi_1$ = correction for particle shape; $\Delta\phi_1 = -6^o$ for high sphericity and subrounded shape, and $\Delta\phi_1 = +2^o$ for low sphericity and angular shape.

$\Delta\phi_2$ = correction for particle size (effective size, d_{10}); $\Delta\phi_2 = -11^o$ for $d_{10} > 2.0$ mm (gravel), $\Delta\phi_2 = -9^o$ for $2.0 > d_{10} > 0.6$ (coarse sand), $\Delta\phi_2 = -4^o$ for $0.6 > d_{10} > 0.2$ (medium sand), and $\Delta\phi_2 = 0^o$ for $0.2 > d_{10} > 0.06$ (fine sand).

$\Delta\phi_3$ = correction for gradation (coefficient of uniformity, C_u); $\Delta\phi_3 = -2^o$ for $C_u > 2.0$ (well graded), $\Delta\phi_3 = -1^o$ for $C_u = 2.0$ (medium graded), and $\Delta\phi_3 = 0^o$ for $C_u < 2.0$ (poorly graded).

$\Delta\phi_4$ = correction for relative density (D_r); $\Delta\phi_4 = -1^o$ for $0 < D_r < 50$ percent (loose), $\Delta\phi_4 = 0^o$ for $50 < D_r < 75$ (intermediate), and $\Delta\phi_4 = +4^o$ for $75 < D_r < 100$ (dense).

$\Delta\phi_5$ = correction for mineral type; $\Delta\phi_5 = 0^o$ for quartz, $\Delta\phi_5 = +4^o$ for feldspar, calcite and chlorite, and $\Delta\phi_5 = +6^o$ for mica.

The following approach was used for estimating friction angle of compacted granular fill within the North Extension:

- $\Delta\phi_2$ and $\Delta\phi_3$ were selected using the above criteria with reference to specific QC/QA gradation tests conducted on placed material.
- $\Delta\phi_4$ was estimated using the above criteria with assumed relative density equal to 90 percent (discussed previously in this section).
- $\Delta\phi_5$ was assumed to be 0^o; mineral type is not anticipated to have a significant effect on shear strength of the granular material within the sheet pile cells because the confining pressures are not high enough to cause significant particle breakage during shearing.
- $\Delta\phi_1$ was "calibrated" to the material type using direct shear tests with accompanying soil gradations—tests conducted on materials from the JBER pit during a gravel extraction study for the PIEP (Terracon, 2006a). The correction factors for particle size, material gradation, and relative density were determined using the Koerner (1970) criteria, and $\Delta\phi_1$ was adjusted until a best fit was achieved between the estimated and measured friction angles. The resulting $\Delta\phi_1$ was about -2 to -3 degrees, which is consistent with Koerner (1970) criteria for subrounded particles. Considering how particle shape between the source and destination of the granular fill should be similar, if not identical, this $\Delta\phi_1$ value was assumed to apply to granular fill within the OCSP® cells.

Using the above approach, the internal friction angle for compacted granular material was estimated to be about 35 degrees. This value is about 1 degree less than assumed for PND analyses of the structure and about 5 degrees less than the "specified" value in the construction documents. Note that as discussed in the next subsection, results of supplemental large-size (that is, 12-inch by 12-inch) direct shear tests gave a friction value greater than 35 degrees.

5.2.1.4 Supplemental Investigation of Granular Backfill and Recommended Internal Friction Angle

A supplemental geotechnical investigation of the granular backfill within the OCSP® system and overlying the estuarine deposits and BCF soils was conducted by CH2M HILL in February and March 2012 as a parallel task to the engineering and numerical analyses. In the absence of backfill strength and stiffness information for the as-built backfill, the supplemental investigation was conducted as part of this suitability study to confirm assumed soil engineering properties discussed above. The supplemental investigation included in situ and laboratory testing.

The in situ testing consisted of SPTs and large penetration tests (LPTs) conducted within boreholes. The SPTs followed ASTM standards; the large penetration test involved use of a 3-inch outside diameter sampler with a 2.4-inch inner diameter. This sampler was driven with a 340-pound weight falling 30 inches. An auto hammer was used to lift the hammer for each drop. Blow counts recorded in the final 12 inches of penetration were recorded as the LPT blow count. These blow counts were multiplied by a conversion factor to obtain an equivalent SPT blow count (see Appendix D1 for this discussion). This larger hammer was used in an attempt to reduce the effects of large gravel particles that occur in the backfill on the blow count measurement.

Laboratory testing of the collected samples was conducted to define intrinsic soil characteristics (for example, gradation); direct shear tests were also conducted on granular backfill samples. The shear box used for these tests was approximately 12 inches by 12 inches in surface area. The shear strength testing results provided a direct measure of the shear strength of the as-built granular backfill as a function of relative density and normal stress.

A summary of the supplemental geotechnical investigation is provided in Appendix D1 of this report. These results suggest that the granular backfill has a friction angle ranging from 40 to 45 degrees. For engineering analyses, the granular fill friction angle was assumed to be 40 degrees. This value is higher than estimated using the Koerner (1970) empirical method, but lower than measured in the direct shear tests (which included some scalping of oversize portion that may have impacted the test results). The impact of this recommendation/assumption is evaluated in the sensitivity study provided in Section 5.3.

5.2.2 Liquefaction Susceptibility and Cyclic Strength Degradation Assessment

Liquefaction susceptibility was evaluated for the granular backfill, and cyclic strength degradation was evaluated for the BCF clay. The potential for liquefaction is of interest in the granular backfill soil, as the development of excess porewater pressures during a seismic event could result in reduction of the operable friction angle of granular material. In this situation, the stability of the backfill during or following seismic loading could be controlled by a friction angle of less than 40 degrees. Although BCF clay was not expected to be susceptible to liquefaction in the same sense as cohesionless materials, repeated cycles of shear loading during a seismic event can result in a reduction of the undrained strength of the BCF clay, which will lead to a higher potential for instability. The following sections discuss the analysis methods and results from the liquefaction susceptibility evaluation of granular backfill and the cyclic degradation of the BCF clay.

5.2.2.1 Liquefaction Potential Evaluation for the Granular Backfill

The potential for liquefaction within the granular backfill placed behind the OCSP® facewall was evaluated. The primary intent of this evaluation was to determine whether reduced soil strengths had to be considered in the backfill for seismic design, and if liquefaction were to occur, the effects on backfill strength and the potential for post-liquefaction settlement.

Methods Used in Liquefaction Assessment

Liquefaction-triggering potential in the backfill layer was determined through SPT-based procedures. The analysis followed the procedures described in Youd et al. (2001) for the OLE, CLE, and MCE design seismic events. Liquefaction-triggering potential was evaluated by estimating the cyclic stress ratio, CSR (that is, a measure of the seismic stress acting on a soil layer) and the cyclic resistance ratio, CRR (that is, a measure of the capacity of the soils to resist liquefaction). The factor of safety (FS) against the occurrence of liquefaction at each evaluation depth was determined by comparing the computed value of CRR to the CSR caused by the design earthquake, with PGA values coming from site response analyses in Section 3.

Liquefaction susceptibility was analyzed for each seismic design case at the magnitude determined from a deaggregation of the uniform seismic hazard for each event. The magnitude from the deaggregation is based on results of the URS (2008) probabilistic seismic hazard analyses. The magnitudes from the URS deaggregation represent the modal magnitude for the OLE, CLE, and MCE return period (that is, 72 years, 475 years, and 2,475 years) based on all seismic sources. A check on liquefaction potential was also conducted for magnitude 7.5, which URS reported as representing the maximum seismic event on the intraslab source, based on their deterministic seismic hazard analysis. This magnitude (that is, $M_w = 7.5$) is only slightly less than URS's estimate of the magnitude for a seismic event on the Castle Mountain fault (that is, $M_w = 7.7$). Liquefaction analyses for a mega-thrust event (that is, $M_w = 9.2$) were also performed. This liquefaction analysis would be generally consistent with a repeat of the 1964 Alaska earthquake.

A magnitude scaling factor (MSF) was applied when the design magnitude was not equal to 7.5 using the MSF adjustment recommended by Youd et al. (2001). For the SPT-based analysis, the soil was identified as having a high potential for liquefaction triggering during a design earthquake if the FS was less than 1.1.

Results of Liquefaction Potential Assessment

Borings used for the liquefaction potential analyses of the granular materials at Sections 2-2 and 3-3 are shown in Figure 5.1-1. Eight borings were used at Section 2-2, and 14 borings were used at Section 3-3 for the liquefaction potential analyses. These borings include the most recent borings conducted by CH2M HILL in 2012 for this study and borings drilled by PND in 2010 to determine the effectiveness of the vibracompaction in the backfill. The CH2M HILL borings were accompanied by a combination of SPT and LPT (3-inch-diameter sampler) samplings, as described previously. The N-values obtained from the LPT samplings were correlated to SPT N-value values by using a factor of 1.5. This factor was found by averaging the correlations proposed by Burmister (1948), Lacroix and Horn (1973), Winterkorn and Fang (1975), and Alaska Department of Transportation (Hemstreet, 2012).

The CH2M HILL borings were drilled along Sections 2-2 and 3-3 for this suitability study. These borings were terminated at a depth below the BCF clay layer. Locations of these borings can be found in Appendix D1 of this report. The vibracompaction borings conducted by PND in 2010 used N-values obtained from SPT sampling. Only the post-vibracompaction N-values were considered in this analysis. The post-vibracompaction borings were drilled to the bottom of the granular backfill and were terminated when native soils were encountered. These borings are shown in Figure 5.2-3. Further discussion of the post-vibracompaction borings can be found in PND (2010b).

Results from the liquefaction analyses show that liquefaction potential exists in some limited zones within the backfill. A summary of the findings is as follows:

- Section 2-2 shows liquefaction potential in seven of the eight borings analyzed for the MCE (M_w = 7.5) event. Only one of the eight borings shows liquefaction potential for the OLE (M6.1) event. The potentially liquefiable zones were encountered between approximately elevations +16 and -20 feet MLLW for the MCE (M_w = 7.5) event. For the OLE (M_w = 6.1) event, the potentially liquefiable zones were encountered between elevations 0 and -5 feet MLLW. Random zones of liquefaction are also predicted for a repeat of the 1964 Alaska earthquake (M_w = 9.2). This prediction is generally consistent with observations of liquefaction at the POA following the 1964 Alaska earthquake.
- Section 3-3 shows liquefaction in 13 of the 14 analyzed borings for the MCE (M_w = 7.5) event. Only two of the 14 borings analyzed for the OLE (M_w = 6.1) event show liquefaction potential. The potentially liquefiable zones were encountered between approximately elevations 10 and -27 feet MLLW. For the OLE (M_w = 6.1), the potentially liquefiable zones were encountered between approximately elevations -5 and -20 feet MLLW. Similar to Section 2-2, random zones of liquefaction are also predicted for a repeat of the 1964 Alaska earthquake (M_w = 9.2).

Results from the liquefaction potential analyses for the modal magnitude and the M_w = 7.5 and 9.2 deterministic events are summarized in Table 5.2-2. The FSs against liquefaction versus elevation are shown in Figures 5.2-4 through 5.2-9 for both Sections 2-2 and 3-3.

Although PND (2010b) stated that low SPT values typically occurred at locations of soft silt or clay pockets, the CH2M HILL borings (Appendix D1) indicate some zones in the granular backfill layer that have low SPT N-values. In particular, boring B-18 located near the wall face shows a zone of continuously low SPT N-values with thickness up to 20 feet. The liquefaction potential of these zones will reduce as the design PGA and earthquake magnitude decrease. During the OLE event, the liquefaction potential of the granular backfill is very low.

It was concluded from these evaluations that some localized zones of either partial liquefaction, where FS values for liquefaction triggering range from 1.1 to 1.4, or full liquefaction, where FS is 1.1 or lower, could develop. However, because of the proximity of adjacent layers that are non-liquefiable, the consequences of these random zones of liquefaction are expected to be small, as any build-up in porewater pressure during liquefaction will tend to redistribute into adjacent dense soil layers. Zones of excess porewater pressure that do not redistribute could cause reduction in the pullout capacity of the tailwalls or increased loading to the OCSP® facewall; however, these effects are expected to be small. The impact of shear strength loss in the compacted backfill due to liquefaction is evaluated in a sensitivity study described in Section 5.3.

TABLE 5.2-2
Summary of Liquefaction Analysis

Seismic Case	Magnitude, PGA	Section	Liquefiable Layer Thickness Range (ft)	No. of Liquefiable SPT N-value / No. of Total SPT N-value
MCE	M=7.5, PGA=0.39g	Section 2-2	0 to 40	35 / 175
		Section 3-3	0 to 35	41 / 189
	M=6.6, PGA=0.39g	Section 2-2	0 to 25	22 / 175
		Section 3-3	0 to 30	27 / 189
CLE	M=7.5, PGA=0.29g	Section 2-2	0 to 25	23 / 175
		Section 3-3	0 to 30	28 / 189
	M=6.3, PGA=0.29g	Section 2-2	0 to 10	9 / 175
		Section 3-3	0 to 20	19 / 189
OLE	M=7.5, PGA=0.16g	Section 2-2	0 to 10	6 / 175
		Section 3-3	0 to 20	10 / 189
	M=6.1, PGA=0.16g	Section 2-2	0 to 7.5	2 / 175
		Section 3-3	0 to 10	3 / 189
MT	M=9.2, PGA=0.25g	Section 2-2	5 to 45	37 / 175

Note: Borings used a combination of SPT and LPT samplers. LPT N-values were adjusted to SPT N-values using a factor of 1.5.
MT = mega-thrust event

Residual Strength of Liquefied Granular Fill

The residual shear strength ratio (S_{ur}/σ'_v) for liquefiable soils was calculated by CH2M HILL using SPT-based empirical methods. The SPT-based empirical methods used in this suitability study included Olson and Stark (2002), Idriss and Boulanger (2007), and Kramer (2008). In general, the empirical methods were developed by back correlation to observed cases of lateral spreading and liquefaction-related flow observed after earthquakes. Since there is currently no consensus on the preferred method for determining the residual strength of liquefied soil using the empirical-based approach, an average of the methods was used in this study.

The calculated S_{ur}/σ'_v ratios are summarized in Table 5.2-3. The S_{ur}/σ'_v ratios were found to be similar for both Sections 2-2 and 3-3. In general the results show that the S_{ur}/σ'_v ratios tended to decrease as the earthquake magnitude and the design PGA decreased.

Liquefaction-Induced Settlement of the Granular Fill

Liquefaction-induced settlement was calculated using the Tokimatsu and Seed (1987) method. This method estimates the volumetric strain as a function of CSR and corrected SPT blow counts. Data from borings B-53200 and B-18 were used for the liquefaction-induced settlement analysis for Sections 2-2 and 3-3, respectively. These borings showed the worst condition for liquefaction-induced settlement.

Results from the liquefaction-induced settlement analyses are summarized in Table 5.2-3; the results in this table represent an upper-bound settlement. The actual amount of liquefaction-induced settlement will depend heavily upon the location and thicknesses of the loose material within the backfill at the project site. The design earthquake could produce differential settlements if the thickness of the potentially liquefiable layers varies greatly within a small area.

TABLE 5.2-3
Residual Strength S_{ur}/σ'_v Values and Liquefaction Induced Settlement

Seismic Case	Magnitude, PGA	Section	$(N_1)_{60}$	S_{ur}/σ'_v Range	Average S_{ur}/σ'_v	Liquefaction-Induced Settlement (in)
MCE	M=7.5, PGA=0.39g	Section 2-2	1 to 28	0.15 to 0.40	0.29	< 8
		Section 3-3	5 to 27	0.06 to 0.34	0.24	< 10
	M=6.6, PGA=0.39g	Section 2-2	1 to 24	0.07 to 0.32	0.24	< 7
		Section 3-3	5 to 22	0.06 to 0.28	0.21	< 10
CLE	M=7.5, PGA=0.29g	Section 2-2	1 to 24	0.07 to 0.34	0.24	< 7
		Section 3-3	5 to 24	0.06 to 0.31	0.21	< 9
	M=6.3, PGA=0.29g	Section 2-2	1 to 16	0.07 to 0.21	0.13	< 7
		Section 3-3	5 to 18	0.06 to 0.27	0.17	< 8
OLE	M=7.5, PGA=0.16g	Section 2-2	1 to 12	0.07 to 0.12	0.12	< 7
		Section 3-3	5 to 12	0.06 to 0.13	0.13	< 7
	M=6.1, PGA=0.16g	Section 2-2	1 to 4	0.04	0.04	< 7
		Section 3-3	5	0.05 to 0.06	0.06	< 5
MT	M=9.2, PGA=0.25g	Section 2-2	1 to 28	0.15 to 0.4	0.3	< 7
		Section 3-3	5 to 28	0.08 to 0.34	0.26	< 8

(N1)60 = normalized SPT blow count
S_{ur}/σ'_v = normalized residual strength
MT = mega-thrust event

Other Potential Consequences of Liquefaction

Another issue that was identified for the OCSP® system was the potential for liquefaction behind the facewall. Granular backfill within approximately 10 feet of the facewall was not densified, leading to an increased potential for liquefaction. This liquefaction could result in either flow beneath the wall or flow through damaged interlocks.

The potential for flow failure below the OCSP® system is unlikely, as the sheets are driven at least 10 feet into the BCF clay. This depth of embedment provides enough distance that a critical flow gradient between the liquefied soil behind the face of the wall and the seabed on the outside of the face is small. However, at locations where sheets are out of interlock, flow of liquefied backfill through gaps in the wall could occur. The amount of flow will depend on the size of the gap. This flow could lead to sinkholes forming at the ground surface, much like what was observed during construction.

To avoid flow through interlocks, it will be important to maintain the interlock of all sheet piles. Interlock integrity is also required to avoid loss of backfill during tidal cycles; therefore, this has to be considered as a critical construction requirement.

5.2.2.2 Cyclic Strength Behavior of BCF Clay

The seismic-induced shear strength degradation of the BCF clay was independently evaluated by CH2M HILL in this suitability study. This evaluation considered the effects of cyclic loading on the BCF clay as well as the effects of large-shear displacements that develop from movement of soil along a shear plane. As discussed later in this section, accumulated movement is determined by the combination of earthquake shaking level and the strength of the soil. When the margin of capacity over demand (that is FS for stability) is low, small amounts of strength degradation during cyclic loading can lead to significant losses in strength from soil displacements, and this mechanism can lead to large earthquake-induced land movement. Findings from this evaluation are discussed in the following sections.

Undrained Shear Strength of the BCF Clay under Cyclic Loading

The effect of cyclic loading on undrained shear strength of the BCF clay has been previously documented in the literature (Woodward-Clyde, 1982; Idriss, 1985; Lade et al., 1988), sometimes with conflicting conclusions drawn. Testing results from some of these studies have indicated that the cyclic undrained shear strength of the BCF clay was not significantly affected by the cyclic loading, even under conditions where significant excess porewater pressure was generated.

The study conducted by Idriss (1985) on the BCF clay showed that the cyclic degradation of the undrained shear strength was about 20 percent when the excess porewater pressure ratio (R_u) was about 0.75. Through extrapolation of his test results to the maximum R_u ratio of 1.0, the maximum shear strength reduction during cyclic loading was estimated to be about 30 percent (strength 70 percent of peak).

Based on the results from cyclic triaxial tests, Lade et al. (1988) concluded that cyclic loading and generation of excess porewater pressure did not significantly affect the cyclic shear strength of the BCF clay. In fact, results from Lade et al. (1988) even showed that the ratio of the cyclic over static undrained shear strength was greater than unity. This behavior is likely related to the loading rate used in cyclic shear tests where the peak shear stress causing failure is typically reached within 0.25 second, as opposed to 10 to 20 minutes for a conventional monotonic-loading undrained shear test.

Thiers and Seed (1969) studied the cyclic behavior of BCF clay and found that the post-cyclic shear strength of the material was dependent on the strain mobilized during cyclic load application. A nonlinear relationship between post-cyclic strength (normalized by peak monotonic undrained shear strength) and cyclic strain (normalized by static shear strain at failure) was observed, with the normalized strength equal to about 1.0 at very low cyclic strains and the normalized strength approaching 0.3 at large cyclic strains.

Similar observations on the cyclic-to-static undrained shear strength ratio were provided in Seed and Chan (1966) for various compacted sandy and silty clays. More recent studies by Boulanger and Idriss (2006) also found that the cyclic-to-static undrained shear strength ratio for various silts and clays varied from 0.75 to 1.01 (average of 0.87 based on DSS tests), dependent on the level of shear stress application.

Port of Anchorage Cyclic Testing Programs for BCF Clay

Seven CyDSS tests were conducted by Terracon (2004b) and PND (2010a) to evaluate the potential for strength loss during and following cyclic loading. These tests were conducted on undisturbed BCF clay samples obtained from two zones: (1) within 20 feet of the mudline and (2) greater than 50 feet below the mudline. Post-cyclic direct simple shear tests were also performed to evaluate the post-cyclic undrained shear strength of the BCF clay. Details of the CyDSS tests conducted by Terracon (2004b) and PND (2010a) are as follows:

- Terracon (2004b) conducted two stress-controlled CyDSS tests at 20 and 40 cycles of loading on BCF clay samples obtained at 110 and 125 feet below the mudline. The vertical consolidation pressure for both tests was about 60 psi, and the CSR for both tests was about 0.21.
- PND (2010a) conducted six stress-controlled CyDSS tests: four test series on estuarine silt deposits and two on BCF clay samples. The CyDSS tests conducted by PND (2010a) were performed at cyclic stress ratios ranging from approximately 0.15 to 0.35 to simulate the cyclic stress level induced by the OLE, CLE, and MCE events.

Sample results obtained from the available CyDSS tests are shown in Figure 5.2-10 (a though c). The following observations were made from these initial tests:

- Limited cyclic testing was conducted on the BCF clay. A majority of the CyDSS tests documented in PND (2010) were actually conducted on the estuarine silt deposits.
- The test consolidation stresses for many of the tests were very low, from about little as 14 kilopascals (kPa) (about 2 psi) up to 359 kPa (52 psi). While some of these test pressures may represent the in situ stress condition of the samples (that is, high OCR conditions), the post-construction stress states are not well

represented. The high OCR values for test samples, resulting from low test pressures, may give different cyclic behavior than clay with the granular fill placed up to elevation +38 feet MLLW.

- The post-cyclic DSS tests exhibited some shear strength reduction (compared with monotonic peak shear strength) with some additional strain-softening ranging up to 30 percent at maximum strain levels. In general, the post-cyclic strengths seemed to follow the Thiers and Seed (1969) relationship which relates cyclic strength to cyclic strain.

Given the limitations of the aforementioned cyclic testing, additional CyDSS tests were conducted in 2012 as part of the CH2M HILL suitability study. The complete results are summarized in Appendix D2. Degradation in shear modulus and post-cyclic strength was observed as CSR values approached about 0.2 (for normally consolidated samples), roughly corresponding to CLE event. Results are consistent with the relationship identified by Thiers and Seed (1969), which relates post-cyclic undrained strength to cyclic strain. Normal-consolidation post-cyclic strength ratios (that is, cyclic strength divided by peak undrained strength) ranged from about 0.10 to about 0.28, depending on the cyclic loading.

These findings suggest that the undrained strength of BCF clay is affected by cyclic load applications and indicated that the cyclic behavior of the BCF clay at POA was not very different than the BCF clay associated with ground failures occurring at other locations around Anchorage during the 1964 earthquake.

Large-Displacement Strength Loss during the 1964 Alaska Earthquake

As a result of the above finding regarding cyclic strength behavior of BCF clay, CH2M HILL reviewed the published analyses of ground failures from the 1964 Alaska earthquake. Published back-analyses of landslides in the Anchorage area (for example, Fourth Avenue, L Street, Turnagain Heights) following the 1964 Alaska earthquake show that considerable displacement-softening behavior was operable during and immediately following seismic shaking. This displacement-softening has been attributed primarily to excess porewater pressure generation and, in part, to re-orientation of clay particles, both of which occur under large deformations.

Idriss (1985) appears to be the first to recognize the significant reduction in undrained shear strength of the BCF clay at large displacements. Noting that ground displacements during the 1964 Alaska earthquake were either very large (greater than 10 feet) or relatively small (less than about 6 inches), Idriss (1985) concluded that the undrained shear strength of the BCF clay at the Fourth Avenue slide in Anchorage dropped to the residual shear strength level (based on DSS, CPT, and VST) when the displacement at the base of the slide increased beyond 6 inches. Accordingly, Idriss (1985) proposed a two-level chart that relates the undrained shear strength of the BCF clay with the displacement at the ground surface. According to Idriss (1985), when the ground displacement is less than 6 inches, the undrained shear strength should be *at least* equal to 70 percent of the static undrained shear strength. As the ground displacement increases beyond 6 inches, the residual shear strength that is equal to about 30 percent of peak undrained shear strength should be assumed.

The undrained shear strength of the BCF clay at the Fourth Avenue slide was later studied by Stark and Contreras (1998) using data from constant-volume ring shear tests. Results from Stark and Contreras (1998) analyses also showed that the undrained shear strength of the BCF clay was reduced to about 70 percent of the static undrained shear strength when the ground displacement was 0.15 m (6 inches). The residual undrained shear strength equal to 30 percent of the static undrained shear strength was mobilized when the ground displacement was beyond 2.5 m (100 inches). According to Stark and Contreras (1998), at large deformation the soil structure may have collapsed, causing generation of excess porewater pressures and reorientation of some clay particles on the shear plane parallel to the direction of the shear stress. The generation of excess porewater pressures results in the reduction of the effective stress and, consequently, the shear strength of the soils.

Sensitivity versus Large-Displacement Softening of BCF Clay

The apparent inconsistency between the limited strength degradation observed during previous cyclic laboratory tests on BCF clay versus the displacement softening that led to the large landslides observed during the 1964 Alaska earthquake, as well as Stark and Contreras ring-shear tests, results from two separate mechanisms that are occurring, although both are often lumped together and referred to as soil sensitivity. Sensitivity defines the ratio of peak undrained strength of an intact sample to the peak strength of a remolded (or fully softened) sample. Both the peak and remolded strengths occur at relatively small strains, less than 5 to 10 percent. If shear strains continue to develop consistent with large ground displacements that occur during a landslide, the residual strength is developed. This strength is normally lower than the remolded strength. In general the behavior of clay at large displacements (that is, residual strength) is unaffected by sensitivity and the past stress history. This dependence of strength on the amount of movement is what Idriss postulated and what Stark and Contreras observed in their laboratory tests.

The difference between residual strength and the remolded strength defined by sensitivity often leads to overestimation of the residual strength, where CPT soundings or field vane shear tests (VST) are used to estimate sensitivity, and the resulting strength from the sensitivity determination is used as a proxy for residual strength. Dr. P.K. Robertson, in his letter to Terracon dated September 29, 2003, stated that the BCF clay appeared to have sensitivity of around 2 to 3, based on his interpretation of CPT soundings, and this sensitivity significantly decreased the likelihood of strain softening due to cyclic loading. The PND design team made the assumption from this statement, as well as their observations from cyclic test results, that the BCF clay would maintain most if not all of its strength throughout seismic shaking.

While this interpretation of cyclic strength degradation was valid, it did not account for the second “mechanism” of strength reduction that Idriss and Stark and Contreras noted: the post-peak strength reduction due to large displacement. This type of strength reduction was not considered at the POA, despite the historical evidence from the 1964 Alaska earthquake that such softening occurred in BCF clay at other locations in Anchorage. In the past, the common interpretation in the Anchorage area was that large post-peak strength reductions were limited to Facies III within the BCF clay, which is considered geologically as “sensitive” (Updike, 1986), and would not occur in deeper facies at the POA (that is, Facies IV and Facies I), which were not identified as sensitive. However, results of large displacement tests on clays obtained for the Port MacKenzie project by Dr. Timothy Stark (USACE, 2002) exhibited similar large-displacement strength reduction, suggesting that large-displacement strength reduction is a kinematically feasible mechanism at the POA and, therefore, needs to be evaluated during seismic design.

Undrained Shear Strength of BCF Clay Under Large Ground Displacements

To investigate peak and residual undrained shear strengths at the POA, CH2M HILL had a series of constant volume ring shear (RS) tests conducted by Dr. Timothy Stark, University of Illinois at Urbana-Champaign, on 12 intact samples of BCF clay recovered from the POA. Results of these special tests are reported in Appendix D2.

In general, the behavior of BCF clay at the POA was consistent with test results for BCF clay at Fourth Avenue and Port MacKenzie, that is, large post-peak strength reductions were observed when the ring shear tests were conducted under constant volume conditions to simulate undrained shear. The recommended post-peak strength used for Newmark seismic deformation estimation, therefore, followed the back-analysis strength for Fourth Avenue, L-Street, and Government Hill landslides (see Stark and Contreras, 1998).

Since it is not certain whether the similarity of the BCF clay at Fourth Avenue and the BCF clay within the upper 50 feet at the POA is indicative of the potential losses in strength during earthquake-induced ground movement, two design scenarios were considered by CH2M HILL in this suitability study:

1. **Best-Case Scenario.** Limited strength reduction will be encountered in the BCF clay at the PIEP during and after the design earthquakes. This approach is consistent with that used by the PND design team.

2. **Worst-Case Scenario.** The large deformation induced by the design earthquakes will cause significant loss in the undrained shear strength of the BCF clay at the POA. In this case the shear strength loss will be similar to that experienced at the Fourth Avenue slide (Idriss, 1985; Stark and Contreras, 1998).

In this study, the seismic-induced permanent deformation for the best-case scenario was calculated using several empirical-based methods assuming constant yield acceleration. A modified Newmark analysis which considers the yield acceleration as a function of soil displacement was used to estimate the seismic-induced permanent deformation for the worst-case scenario. Details of each analysis approach are discussed in the later sections addressing global stability.

5.2.3 Internal Stability

The internal stability of the OCSP® system was evaluated with respect to tailwall pullout resistance and interlock tensile stress capacity. This type of stability evaluation differs from external stability or global stability that will be discussed later in Section 5. It involves sheet pile failure by either yielding in tension of the steel forming the sheet pile or pullout of the tailwall in the granular backfill as loads are imposed on the facewall. The tailwall pullout being evaluated occurs in the backfill material above the tip of the tailwall sheet piles. It differs from both global stability and the sliding mechanism for external stability by the relative location of the movement, with pullout being limited to areas where there is relative movement between the granular fill material and the face of the tailwall. As will be discussed, internal stability meets most FS requirements, and therefore is not a critical stability mechanism. The following subsection discusses static and seismic lateral earth pressure as inputs into local OCSP® stability calculations, as well as the determination of FS values against tailwall pullout and interlock tension capacity exceedance.

5.2.3.1 Static and Seismic Lateral Earth Pressures

Static and seismic lateral earth pressures were calculated for the as-built section as input for evaluating the structural stability of the OCSP® sheet piling. For each loading case considered, the following components of lateral pressure were provided, as depicted in Figure 5.2-11:

- Surcharge loading
- Hydrostatic water pressures (with differing landside and seaside water levels)
- Hydrodynamic water pressure
- Static active earth pressure
- Static passive earth pressure
- Seismic earth pressure

The resultant lateral force on the wall for static and seismic loading was determined using the generalized limit-equilibrium (GLE) method described in Anderson et al. (2008). This procedure includes setting up a limit-equilibrium model, adding an external load to the wall face to represent the resultant lateral force, and adjusting this lateral force until a FS of 1.0 is achieved. Consistent with classical methods, the failure surface is forced through the bottom of the wall and extends upward in the direction of the active wedge. The advantage of this method is the easy incorporation of varied geometry, soil layering, groundwater conditions, surface surcharges, and seismic coefficients for a pseudo-static analysis. An example GLE model with solution is shown in Figure 5.2-12 for the long-term static-undrained loading case. For OLE, CLE, and MCE seismic cases, seismic coefficients (k_h) equal to half the PHGA were used. The 0.5 factor is applicable as long as small amounts of permanent movement are acceptable during seismic loading, as discussed by Anderson et al. (2008).

With the resultant lateral force determined from the GLE method for each loading case, classical methods were used to separate the force into individual pressure distributions (for example, hydrostatic, static earth pressure, etc.). These pressure distributions account for the various assumed water conditions and the layering of granular fill and BCF clay. The following assumptions were used in this evaluation:

- The passive earth pressure was not modeled in the limit-equilibrium analyses. The passive earth pressure distribution was computed separately using the Rankine passive lateral pressure coefficient with applied FS of 2.0. The assumption of Rankine earth pressure is considered to be insignificant given that this contribution to resistance was small relative to the active pressures.

- The distribution for the seismic incremental earth pressure was triangular, with the largest earth pressure observed at the tip of the face sheet. This distribution, recommended in the sixth edition of the AASHTO LRFD Bridge Design Specifications (2012), differs from the inverted trapezoidal distribution associated with the Mononobe-Okabe method. The triangular distribution is noted to be conservative for this analysis, because the critical loading for structural stability is where the sum of superimposed pressures is greatest, usually occurring near the dredge elevation or bottom of the wall. The revised distribution recommended in the

AASHTO LRFD Bridge Design Specifications (2012) is based on centrifuge laboratory tests conducted on scaled retaining walls during seismic loading, as well as observations during recent large earthquakes.

5.2.3.2 Tailwall Sheet Pile Pullout Resistance

The OCSP® tailwall sheet pile pullout resistance was determined using a combination of classical methods and numerical analyses that addressed the influence of the sheet pile knuckles on the pullout resistance. A $FLAC^{3D}$ model of the tailwall (see Section 7) identified the governing, "large-strain" friction coefficient to be about equal to the shear strength of the granular fill (that is, tan ϕ). The contribution to pullout resistance from intermediate and end anchor piles was conservatively ignored. Therefore, the total pullout resistance of the sheet piling was represented by:

$$P_{pullout} = \Sigma[(\tan \phi_i)\ K_{0i}\ (\sigma'_{vi})\ A_i]$$

Where:

ϕ_i = internal friction angle of soil adjacent to a particular area of the tailwall

K_{0i} = at-rest lateral coefficient, computed as $K_0 = 1 - \sin(\phi_i) = 0.36$ based on ϕ_i = 40 degrees

σ'_{vi} = vertical effective stress at depth of a particular area of the tailwall

A_i = area of effective pullout resistance

Only the area behind the active wedge identified using the GLE method was used for calculating pullout resistance. With increasing seismic coefficient in pseudo-static analyses, the failure angle flattens (more horizontal); therefore, the lowest pullout resistance (and highest demand) was observed for the MCE loading condition. The FS against tailwall pullout was calculated as the total pullout resistance provided by a tailwall divided by the total (net) lateral driving force acting on the face sheets of one cell. Computed FS values exceeded 2.0 for all design loading cases (see Table 5.2-4), except the MCE event for Section 3-3.

TABLE 5.2-4
Factors of Safety Against Tailwall Pullout

Loading Case	Section 2-2	Section 3-3	Required
End of Construction	3.2	2.9	1.3
Long-Term Static-Drained	4.4	4.4	1.5
Long-Term Static-Undrained	3.1	3.0	1.5
OLE	3.3	3.0	1.3
CLE	2.6	2.1	1.1
MCE	2.2	1.8	1.0
Post-Earthquake	3.2	2.8	1.3

In the above analyses, the potential for loss of frictional resistance from build-up in porewater pressures during seismic loading was not explicitly considered. As discussed in the liquefaction potential assessment of the backfill, there is a potential for localized build-up in porewater pressure within the backfill. The potential for build-up in porewater occurs primarily between elevation -10 and +10 feet MLLW in Section 2-2 and between elevation 0 and -20 feet MLLW in Section 3-3. It appears that the occurrence of porewater pressure build-up is localized and random enough that the FS values given in Table 5.2-4 will be sufficient to compensate for any localized porewater pressure build-up. The higher friction values observed during the supplemental field exploration and laboratory test programs conducted by CH2M HILL in February and March of 2012 also appear to support the assumption that there will be adequate pullout resistance even with some build-up in porewater pressure or localized liquefaction.

5.2.3.3 Interlock Tension Strength

An OCSP® bulkhead system must be stable against the bursting pressure exerted by the retained backfill. The FS for interlock tension is defined as the ratio of allowable interlock strength guaranteed by the sheet pile manufacture (or the yielding strength of the web of the sheet pile, whichever is lower) to the maximum computed interlock tension. The interlock tension developed in the face sheets of the OCSP® is a function of the internal cell pressure and cell radius. The following equation links internal cell pressure to the interlock tension:

$$t = p*r$$

Where:

t = interlock tension
p = internal pressure
r = cell radius

The internal pressure "p" at any given depth in the cell is the combination of active and passive earth pressures, hydrostatic water pressures, hydrodynamic water pressures, and incremental seismic earth pressures, as described in Section 5.2.3. Because the interlock strength is a constant, a cell will experience the highest interlock tension and, hence, the lowest FS for interlock tension at the depth where the combined pressure is the largest. Table 5.2-5 presents the FS for interlock tension. These results show that interlock tension strength is acceptable for all loading cases, except the long-term static-undrained case at Section 2-2 (higher-wall section).

TABLE 5.2-5
Factors of Safety Against Interlock Tension

Loading Case	Section 2-2	Section 3-3	Required
End of Construction	1.9	2.1	1.5
Long-Term Static-Drained	2.7	3.1	2.0
Long-Term Static-Undrained	1.9	2.2	2.0
OLE	1.9	2.3	1.5
CLE	1.6	1.9	1.3
MCE	1.4	1.7	1.1
Post-Earthquake	1.9	2.1	2.0

5.2.4 External Stability

Three external modes of failure are normally considered for the design of wall systems: sliding, overturning, and bearing capacity. Overturning is not discussed in this section, because the large tailwall width-to-face height and the general flexibility of this structure preclude this failure type. Both bearing and sliding failure were considered as part of this suitability study. The bearing failure occurs when the weight of the backfill exceeds the bearing capacity of the underlying BCF clay; sliding failure occurs when the entire block of backfill soil and native soil above elevation -61 feet MLLW move as a coherent mass, as opposed to tailwall pullout were the tailwall moves relative to the granular backfill.

5.2.4.1 Bearing Failure

Local deformation of the foundation soil (that is, BCF clay) near the OCSP® bulkhead face was implicitly investigated in the global FLAC^{3D} model. The check against bearing capacity failure is included in the observed deformations from this numerical modeling effort.

Global stability using limit-equilibrium methods and estimation of seismic-induced permanent deformation are discussed separately in Section 5.2.6.

5.2.4.2 Sliding Failure

The sliding failure mode is characterized by excessive lateral movement of the OCSP® system towards the water. The lateral movement occurs along a horizontal shear plane beneath the structure at the approximate elevation -61 feet MLLW in the BCF clay. An FS value for external stability in sliding is computed as the sum of forces resisting the lateral movement divided by the sum of driving forces. The following assumptions were used in the sliding analyses:

- The driving forces acting on any vertical plane a distance away from the OCSP® bulkhead face are about constant and equal to the sum of resultant forces associated with surcharge pressure, landside hydrostatic water pressure, static lateral earth pressure, and seismic incremental earth pressure, as applicable to the loading case. An active earth pressure condition was assumed when checking sliding stability because of the flexibility of the facewall of the OCSP® system.
- The resisting forces are equal to the sum of resultant forces associated with water-side hydrostatic water pressure, the passive lateral earth pressure below the dredge elevation, the shear strength of soil at the base of the wall between the bulkhead and the vertical plane on which driving forces act, and the pullout resistance of the tailwall area behind this vertical plane. The sliding surface is defined at elevation -61 feet MLLW in the BCF clay. Pullout resistance was estimated using the method described in Section 5.2.3 for tailwall sheet pile resistance.
- The force balance on several vertical planes was computed. As the vertical plane moves closer to the face sheets, the soil shearing resistance below the fill is less, but the pullout resistance is greater. As the vertical plane moves towards the tailwall extension, the soil shearing resistance below the fill increases, but the pullout resistance decreases. The FS was determined using the vertical plane for which the ratio of resistance to demand (that is, FS) was minimum.

The FS values against sliding for all loading cases are provided in Table 5.2-6 for both Sections 2-2 and 3-3. For all loading cases, the computed FS values exceeded the global stability FS criteria, which were also assumed to apply to the sliding failure mode. The lowest FS values were observed for the vertical planes located behind the primary tailwall, but in front of the tailwall extension. These conditions are also acceptable.

TABLE 5.2-6
Factors of Safety Against Sliding

Loading Case	Section 2-2	Section 3-3	Required
End of Construction	1.5	1.4	1.3
Long-Term Static-Drained	2.7	2.6	1.5
Long-Term Static-Undrained	1.8	1.6	1.5
OLE	1.6	1.5	1.2
CLE	1.5	1.4	1.1
MCE	1.4	1.3	1.0
Post-Earthquake	1.5	1.4	1.3

5.2.5 Evaluation of Long-Term Settlement

The construction of the OCSP® system involves placement of 50 feet or more of granular fill on the BCF clay or on the estuarine deposits in locations where the estuarine deposits were not removed by dredging. One consequence of the new backfill placement is consolidation of the underlying cohesive soils. As these soils consolidate, the granular backfill settles. If this settlement continues to occur after final construction of the OCSP® facility, this settlement can affect utilities and surface pavements in the backlands. Whether long-term settlement becomes an issue is a function of the time between placement of the backfill and the consolidation characteristics of the soil below the backfill. The following subsections discuss these issues.

5.2.5.1 Methodology for Settlement Analyses

The total settlement of the compressible soils consists of three components:

- Elastic (or immediate) settlement from the backfill and the native soils, which can be assumed to occur during or immediately after construction of the structure. The immediate settlement can be estimated as the elastic deformation of the soils under the static loads (due to effective weight of the backfill).
- Primary consolidation settlement, which is a volume-reducing process caused by the expulsion of porewater under the long-term static loads. The magnitude of the primary consolidation settlement and time for this process to complete were estimated using the one-dimensional consolidation theory (Terzaghi et al., 1996).
- Secondary compression, which is a process caused by creep/viscous behavior of the soil-water system and/or compression of the organic matter in the soil without any change in the porewater pressure regime. The secondary compression was estimated using the Terzaghi et al. (1996) method, which takes into account the initial degree of overconsolidation in the soil.

As previously discussed, Section 2-2 was identified by CH2M HILL as the most critical section for the evaluation of the as-built structure because of the height of the OCSP® wall. For this reason, the settlement analyses discussed in this subsection focus on the area around Section 2-2, which is located between Cells 53 and 63. The soil profile assumed for the settlement analyses was developed based on the data collected from CPT soundings in the area. The total thickness of the BCF clay at this location is approximately 100 feet. Based on the CPT data, the upper 50 feet of the BCF clay was divided into five sub-layers, each 10 feet thick. Drained boundaries were created between these sub-layers to represent the interbedded sand seams encountered in the BCF clay at these depths. The lower 50 feet of the BCF clay was assumed to be homogeneous. The time-dependent compressibility of the BCF clay was evaluated using the parameters shown in Table 5.1-2 and the pre-construction OCR profile shown in Figure 5.1-11. The settlement analyses were conducted using the computer program Settle3D, version 2.013 (Rocscience).

The construction sequence and history of the OCSP® structure between Cells 53 and 63 was obtained from the "1-Year Instrumentation Monitoring Summary Report" (Terracon, 2011). The access embankment was assumed to be built 3 months before the OCSP® structure was constructed. According to Terracon (2011), it took at least 9 months to construct the OCSP® structure between Cells 53 and 63. Assuming that the construction of the initial dike took 3 months, then by the time the OCSP® structure at this location was completed, the BCF clay under the backfill had already been surcharged for about a year. The future settlement of the OCSP® structure discussed in the following section was estimated from present time, which is about a year after the OCSP® structure between Cells 53 and 63 was completed. Only long-term settlement of the BCF clay (that is, primary consolidation and secondary compression) was considered in this study. The elastic settlement of the soils was assumed to occur immediately after the construction of the as-built OCSP® structure and was not considered in the settlement analyses.

The Settle3D model developed for the as-built OCSP® structure was checked by comparing the calculated settlement with field-measured instrumentation data provided in the Terracon (2011) report. The instrumentation used for this comparison includes two settlement points in Cell 61 and one piezometer in Cell 48. The settlement points in Cell 61 were attached to the top of the bulkhead face and the tailwalls, which is located approximately 40 feet from the face. The piezometer in Cell 48 was installed at elevation -57 feet MLLW, which is approximately 16 feet into the BCF clay layer.

Figures 5.2-13 and 5.2-14 show the normalized excess porewater pressure and settlement computed by Settle3D and those obtained from instrumentation. The close match between the calculated and the measured values suggests that the Settle3D model developed for this study provides an adequate tool for estimating the long-term settlement potential of the as-built OCSP® structure.

5.2.5.2 Findings from Settlement Analyses

The main findings from the Settle3D settlement analyses are as follows:

- The calculated degree of consolidation with depth is shown in Figure 5.2-15. About 90 percent of the consolidation settlement in the upper 50 feet of the BCF clay would be completed in about 3 months after the construction of the OCSP® structure. The consolidation in the lower 50 feet of the BCF clay may take as long as 6 years to complete due to the absence of connected, interbedded sand layers. PND (2008b) estimated that 90 percent of the consolidation settlement in this area would be completed in about 5 months to 3 years after the placement of the backfill. This estimate of consolidation time is comparable with the finding in this suitability study.
- The total long-term settlement of the BCF clay due to the weight of the backfill was estimated to be about 33 inches. However, our analysis indicated that about 75 percent of this settlement could have already occurred during the past year, as shown in Figure 5.2-16(a) and 5.2-16(b). The remaining long-term settlement of the BCF clay layer is estimated to be about 8 inches, which may occur over the next 20 years (Figures 5.2-16c and 5.2-17). The total long-term settlement of the BCF clay estimated by PND (2008b) is between 28 and 31 inches, which is comparable with the estimate by CH2M HILL in this suitability study. It is expected that this settlement may be uneven and will require periodic maintenance.
- The long-term differential settlement of the BCF clay in the direction parallel to the wall alignment is expected to be minor. The long-term differential settlement of the BCF clay in the direction perpendicular to the wall alignment is about 1.5 inch per 50 feet, with maximum differential settlement occurring within 75 feet from the face of the wall. Because the BCF clay is approximately 75 feet below the top of the backfill, the impact of this differential settlement on the superstructure should be negligible.

5.2.5.3 Implications of Settlement

The settlement estimates provided above will have some effect on utilities and pavements located near or at the ground surface and could affect any building or other structures supported on shallow foundations. Although it is possible to mitigate settlements using, for example, prefabricated vertical (wick) drains to accelerate the consolidation process or other types of ground improvement or even pile support, for most facilities the estimated amounts of settlement are within levels that can be handled during detailed design or through regular maintenance.

The depth of the compressible BCF clay layer at the POA is deep, making methods of ground improvement and use of wick drains expensive, though feasible. If settlement-sensitive utilities or facilities are identified, pile support appears to be the most successful method of controlling these settlements.

Crane rails planned for the PIEP will be pile-supported, and therefore, the consequence of fill-induced settlement on crane operations will be limited, as long as piles are installed deep enough that settlement is within acceptable limits. Consideration will have to be given to drag loads and settlement of the neutral plane for the pile foundations when assessing settlement. Approaches for dealing with these issues are well defined.

5.2.6 Evaluation of Global Stability

This section discusses the global stability of the as-built OCSP® structure based on the results obtained from limit-equilibrium analyses. The global stability assessment evaluates whether the total shear resistance of the soils is sufficient to resist the driving forces generated by a variety of sources, including the weight of the retained backfill, the operating surcharges, the hydrostatic and hydrodynamic forces, and the seismic-induced inertial force. The following section discusses findings from the global stability evaluation of the as-built OCSP® structure.

5.2.6.1 Methodology for Global Stability Analyses

Global stability is one of the potential failure mechanisms that must be thoroughly evaluated, especially for tall retaining structures such as the OCSP® system at POA. In the global stability analysis, the failure (slip) surface is assumed to be below the base of the wall (that is, deep-seated type failure) as opposed to the active failure surface that typically initiates from the tip of the sheet pile wall. The main purpose of the global stability analysis is to search for the most critical slip surface that results in the lowest FS, where the FS is defined as the ratio of available shear resistance (or shear strength) from the soils to the total driving shear force (or demand).

The global stability analyses presented in this section were performed using a conventional limit-equilibrium methodology, in which the most critical slip surface with the lowest FS was identified from numerous trial slip surfaces. To enhance the search process for the critical slip surface, a Monte-Carlo type optimization technique, which is also known as the “random walking” method (Greco, 1996), was employed.

The critical slip surface was assumed to have a non-circular shape that consists of multiple linear segments defined by a finite number of vertices. During the optimization search process, each trial slip surface was treated as a mathematical function in which the inputs are the coordinates of the vertices, and the output is the FS associated with that trial slip surface. The critical slip surface was identified as the “function” that yields the lowest FS. The advantage of using an optimization search technique such as the “random walking” method is that the critical failure surface found by the end of the search process is unique and unbiased as the solution does not require an assumption for the location of the failure surface at the beginning. This type of analysis is usually preferred to a circular slip surface when representing locations where horizontal bedding planes exist, such as the POA. In this case, non-circular slip surface will generally coincide with natural bedding planes over much of the slip surface length, meaning that slip occurs on the bedding plane as is often observed in slope instabilities. When using this approach, a check must be made at the end of the optimization process to ensure that the critical slip surface is kinematically admissible (for example, the slip surface cannot "reverse" direction at any point, or include vertical segments). By using the random walking feature, all viable failure surfaces within a search area are considered. For example, if the horizontal sliding surface for external stability analysis discussed in Section 5.3.4 were more critical, then it would have been identified in the search process.

The FS values for global stability were determined primarily using Slide (version 6.015a), a computer program developed by Rocscience (http://www.rocscience.com/products/8/Slide). Three well-known “methods of slices” were employed within Slide to calculate the FS, including Bishop’s Simplified, Spencer’s, and GLE/Morgenstern-Price methods. The Spencer and GLE/Morgenstern-Price methods satisfy both force and moment equilibrium condition, while the simplified Bishop’s method only satisfies moment equilibrium. The FS values reported in this study are the lowest FS values calculated by these methods. Typically either Bishop’s simplified or sometimes GLE/Morgenstern-Price methods resulted in the lowest FS values. The difference in FS calculated by these methods was very small for the long-term static undrained case (less than 2 percent), but it was more significant in the long-term static drained case (up to about 9 percent).

Discussions in PND (2008b) state that limit-equilibrium stability analyses for their work were performed using the computer program SLOPE/W, a computer program provided by Geo-Slope International (http://www.geo-slope.com/). This computer program has most of the same features as Slide. However, to confirm that FS values were not affected by the software used for the global stability analyses, a series of SLOPE/W and Slide analyses were conducted on the same soil cross-section from the POA to demonstrate similarity in results (Appendix E).

5.2.6.2 Assumptions Regarding the Shape and Location of the Critical Slip Surface

The conventional approach used for evaluating stability of mechanically stabilized wall and similar structures is to assume that the soil within the reinforced zone is a rigid block, forcing the slip surface in the global stability analysis to be outside the reinforced zone. This approach was used by the PND design team (PND, 2008b) and by CH2M HILL for the evaluation of the OCSP® system. However, it was also apparent from the 3D numerical modeling (see Section 7) that the slip surface could also be located within the tailwall [extension] zone. This condition can be triggered by several factors such as tailwall configuration (length, depth, and spacing), site conditions (such as backfill and foundation soils), and loading type (static or seismic).

The assumption that the slip surface in the global stability analyses is located outside the tailwall zone is made because conventional limit-equilibrium methods are incapable of modeling the soil-wall interaction, which occurs on the vertical tailwall planes. This soil-tailwall interaction, which must be properly accounted for when analyzing slip surfaces within the tailwall zone, can only be modeled by using numerical methods. However, since there is a possibility that a portion of the slip surface could be within the tailwall zone, a set of analyses were also conducted with the restriction on slip plane location removed to evaluate the sensitivity to this basic assumption. Results from these analyses were recognized as being too conservative, as they did not account for the resistance to movement that would be provided by the tailwall.

The following approach was used in the global stability analyses regarding the shape and location of the critical slip surface:

- The tailwall zone was modeled as a material with infinite shear strength for most cases. This condition prevents the failure surface from going through the tailwall zone. One set of analyses was conducted with the tailwall zone modeled as a frictional material.
- The global failure surface was assumed to be non-circular, as confirmed with factor-of-safety calculations using numerical methods (for example, FLAC, Plaxis), for the baseline evaluations. However, a set of analyses was also conducted using circular slip surfaces to confirm that these surfaces would result in higher FS values, and therefore represented a less critical condition.

5.2.6.3 Modeling the Anisotropic Undrained Shear Strength of the BCF Clay

The undrained shear strength of overconsolidated, anisotropic clays will depend on the angle of maximum shearing stresses and strains. Depending on the angle of shearing, the undrained shear strength of the clay can be quite different. For the BCF clay at the POA, the laboratory test data (triaxial compression and DSS) have shown that the undrained shear strength can be highly anisotropic. Because the angle of shearing changes along the failure surface, appropriate undrained shear strength must be used to calculate the shear resistance of the BCF clay at different locations on the failure surface. The undrained shear strength obtained from the DSS test should be applicable for the clay at the base of the failure surface as the direction of shearing in this zone is close to horizontal, which is similar to the loading condition applied in the DSS test. Similarly, the undrained shear strength of the clay more landside of the failure surface base should be obtained from the triaxial compression test, and the undrained shear strength from the triaxial extension test should be used for the clay on the seaside of the failure surface base. Each of these test conditions defines a different shear strength—by up to 50 percent for some modes of shear—and these differences must be appropriately represented in the stability analysis to obtain realistic estimates of stability.

In this study, the anisotropic undrained shear strength of the BCF clay was modeled in Slide using the following approach:

- For the BCF clay on the landside of the facewall sheets, the triaxial compression-based SHANSEP correlation was used to estimate the shear strength when the angle at the base of the failure surface was greater than 10 degrees from horizontal direction.
- For the BCF clay on the seaside of the facewall sheets, a shear strength that is equal to half of the triaxial compression-based shear strength was used when the angle at the base of the failure surface was greater than 10 degrees from horizontal direction.
- When the angle at the base of the failure surface was less than 10 degrees from horizontal, the DSS-based SHANSEP correlation was used to estimate the shear strength for the BCF clay.

This assignment of anisotropic shear strength was completed automatically using Slide. Therefore, the user was not forced to pre-identify those zones for compression, simple shear, or extension strengths – a process that can affect computed results.

5.2.6.4 Static Global Stability Analyses

The static global stability analyses conducted for the as-built OCSP® structures (Sections 2-2 and 3-3) consisted of the following loading cases:

- **Case 1 - End-of-Construction Condition.** In this case, the global stability of the as-built OCSP® structures at the end of construction was evaluated without the operating loads. The BCF clay under the backfill was modeled using the consolidated-undrained shear strength, whereas the shear strength of the BCF clay in front of the wall was also modeled as undrained but with adjustments for changes in effective confining pressure and OCR from removal during dredging. The sea level was assumed to be at lowest tidal elevation of -5 feet MLLW. The as-built OCSP® structures were assumed to be built to elevation +35 feet MLLW (without the 3-foot surfacing) with a construction surcharge of 0.2 ksf. The over-dredge elevation was assumed to be at elevation -51 ft.

- **Case 2 - Long-Term Static-Drained Condition.** In this case, the global stability of the as-built OCSP® structures was evaluated at the long-term condition when the excess porewater pressure in the BCF clay generated by the backfill surcharge has been fully dissipated. All fine-grained soils were assumed to behave in a "drained" manner with shear strength modeled by using effective shear strength parameters (effective friction angle). The sea level was assumed to be at elevation +7.5 feet MLLW. The as-built OCSP® structures were assumed to be fully built to elevation +38 feet MLLW (including the 3-foot surfacing) with a full live load of 1,000 psf to represent facility operations. The over-dredge elevation was assumed to be at elevation -51 ft.
- **Case 3 – Long-Term Static-Undrained Condition.** In this case, the global stability of the as-built OCSP® structures was evaluated when a rapid drop in the sea level creates a short-term additional load on the structures. The failure mechanism caused by this type of loading is similar to the global failure mechanism of the open cell structure at Skagway Harbor (Alaska) in 1994 (Cornforth, 2004; Cornforth, 2005). The BCF clay in this case was modeled using undrained shear strengths, which is similar to the approach used in the End-of-Construction case. The sea level was assumed to be nearly at the lowest elevation of -5 feet MLLW. The as-built OCSP® structures were assumed to be fully built to elevation +38 ft with a full live load of 1,000 psf. The over-dredge elevation was assumed to be at elevation -51 ft.

Details on the input parameters and assumptions for each static case are summarized in Table 5.2-7. Locations of the critical failure surfaces for all static load cases are shown in Figures 5.2-18 to 5.2-20. The global FS values for the static load cases obtained by CH2M HILL and reported by PND (2008b) are summarized in Table 5.2-8.

TABLE 5.2-7
Summary of the Static Global Stability Analyses for the As-Built OCSP® Structures (Sections 2-2 and 3-3)

Case No.	Description	Shear Strength of BCF Clay		Shear Strength of Estuarine Deposits	Water Elev. (ft MLLW)		Loads
		Seaside	Landside		Seaside	Landside	
1	End-of-Construction	Consolidated-Undrained [a]	Consolidated-Undrained [b]	$S_u/\sigma'_v = 0.55$	-5	20	DL + CL + HS
2	Long-Term Static-Drained	Consolidated-Drained [c]	Consolidated-Drained [c]	$\phi' = 32$	7.5	20	DL + LL + HS
3	Long-Term Static-Undrained	Consolidated-Undrained [a]	Consolidated-Undrained [b]	$S_u/\sigma'_v = 0.55$	-5	20	DL + LL + HS

[a] Calculated by using SHANSEP correlation assuming in situ (post dredging) overburden effective stress and OCR profile.
[b] Calculated by using SHANSEP correlation assuming post-construction overburden effective stress and OCR profile.
[c] Assumed: $\phi' = 30^{o}$ based on triaxial compression results.
DL = dead load
CL = construction load (= 0.2 ksf)
LL = live load (= 1 ksf)
HS = hydrostatic load

TABLE 5.2-8
Results from the Static Global Stability Analyses for the As-Built OCSP® Structure

Case No.	Description	Global Factor of Safety (FS)				FS Criteria
		Section 2-2		Section 3-3		
		CH2M HILL	PND (2008b)	CH2M HILL	PND (2008b)	
1	End-of-Construction	1.1	1.3[a]	1.1	1.6[b]	1.3
2	Long-Term Static-Drained	1.5	N/A[c]	1.4	N/A[c]	1.5
3	Long-Term Static-Undrained	1.1	1.5[a]	1.1	1.8[b]	1.5

[a] Using FS values calculated for Section F in the North Extension area (Figure 4.1, PND, 2008b) using Spencer method with circular failure surface. PNDN FS values from Analysis Section F in Appendix J.[1]
[b] Using FS values calculated for Section G in the North Extension area (Figure 4.1, PND, 2008b) using Spencer method with circular failure surface. PND FS values from Analysis Section G in Appendix J.
[c] The long-term static-drained case was not considered by PND (2008b) in the global stability analyses for the North Extension area.

The following observations can be made based on the results of the static global stability analyses:

- The FS value calculated by CH2M HILL for the End-of-Construction case is 1.1 for both Sections 2-2 and 3-3. This FS value is significantly lower than the FS criterion of 1.3.
- The FS value calculated by CH2M HILL for the Long-term Static-Undrained case is 1.1 for both Sections 2-2 and 3-3. Based on the tidal elevation data collected in Knik Arm between 1983 and 2001, the extremely low tide condition (that is, when the sea level dropped to elevation -5 feet MLLW or below) occurs at least once a year and lasts for about an hour each time it occurs. Per USACE (2005), loading events with a return period of 10 years or less are considered as "usual" and should be designed with a minimum FS of 1.5. On this basis, the FS value of 1.1 calculated for the Long-Term Static-Undrained case is too low.
- The critical slip surfaces defined by CH2M HILL for the End-of-Construction and Long-term Static-Undrained cases have a relatively flat base that resembles a translational-type failure movement.
- The as-built OCSP® structures have adequate FS in the Long-Term Static-Drained condition with the full live load of 1.0 ksf based on CH2M HILL's analyses. This case, however, rarely controls the design of slopes or walls in high-seismicity area.

As can be seen in Table 5.2-8, CH2M HILL's stability evaluations produced lower FS values than determined by PND (2008b). Based on CH2M HILL's review of the PND (2008b) results, the following two factors were the primary cause of the difference:

- **Shape of Slip Surface.** Part of the explanation for this difference is the shape of the slip surface used in the PND analyses. PND (2008b) assumed the critical slip surface to be circular. To evaluate the potential impact of this assumption on the FS value, CH2M HILL conducted a comparative study in which the PND's global stability models for Sections F (North Replacement) and Section B/D (South Replacement) were duplicated and analyzed using both circular and non-circular slip surface assumptions. Results from these analyses indicate that non-circular slip surfaces were always more critical, meaning that the FS values associated with the

[1] Sections used for slope stability analyses in PND (2008) differ from sections in as-built drawings. Analysis Section F used for slope stability assessments is in the general area of Section G-G in as-built drawings, and Analysis Section G used for slope stability assessment is in the general area of Section F-F in as-built drawings. Section 5 of this suitability study is based on analysis sections; Section 6 shows copies of the as-built drawings.

non-circular slip surfaces were lower than those associated with the circular slip surfaces. The amount of this difference was at least 10 percent. It is important to note that non-circular slip surfaces were later considered by PND and their consultant, GeoEngineers, in the global stability analyses for the OCSP® system in the South Extension (PND, 2010a), and the shapes of the non-circular failure surfaces presented in PND (2010a) are similar to those found by CH2M HILL in this study.

- **Soil Strength Assumptions.** Further investigation also revealed that PND (2008b) assumed the shear strength of the landside BCF clay was only governed by the Triaxial Compression (TXC) loading condition. In other words, the shear strength from the Direct Simple Shear (DSS) loading condition was not considered by PND (2008b) in the global stability analyses for all sections. For soils that exhibit significant anisotropic shear strength behavior, such as the BCF clay, using only the TXC-based shear strength for the landside BCF clay in the global stability analysis will overstate the FS as the TXC-based shear strength of the BCF clay is typically 30 to 40 percent higher than the DSS-based shear strength. In the sensitivity study conducted by PND (2008b) for Section B/D (South Replacement), the global FS only decreased by about 5 to 7 percent when the BCF clay within 30 feet from the face of the wall was modeled using shear strength equal to 80 percent (landside clay) and 40 percent (seaside clay) of the TXC-based shear strength. While the assumption regarding the shear strength of the seaside BCF clay appears to be reasonable, the shear strength of the landside BCF clay within 30 feet from the wall face must be reduced further by at least 10 percent (that is, 70 percent of the TXC-based shear strength) in order to match the DSS-based SHANSEP correlation presented in PND (2008b). As a result, the reduction in the FS when considering the DSS-based shear strength of the landside BCF clay should be more than 5 to 7 percent.

Based on the above observations, it is very likely that the FS values calculated by PND (2008b) assuming a circular slip surface and using only TXC-based shear strength for the landside BCF clay are overestimated. Rather than meeting the FS criteria, the proposed design appears to be inadequate relative to current standards of geotechnical engineering practice. As discussed in the next section, these low FS values result in poorer seismic performance. Perhaps more importantly for continued construction, they could mean that excessive wall face displacements could occur as the dredge depth is increased from its current elevation to the final elevation.

5.2.6.5 Pseudo-Static Global Stability Analyses

The global stability of the as-built OCSP® structures during the design seismic events (OLE, CLE, and MCE) was evaluated using a pseudo-static stability analysis. In these analyses, a horizontal static force was applied at the centroid of each slice to represent the earthquake-induced inertial force. This inertial force was calculated as the product of the weight of the soil mass within each slice and a lateral seismic coefficient (k_h). Acceptable conditions were defined if the resulting FS was greater than the prescribed design criteria.

In this study, the lateral seismic coefficient was assumed to be half of the peak horizontal ground acceleration (0.5 x PHGA). By using k_h = 0.5 x PHGA, a lateral movement of at least several inches must be anticipated during the seismic event when the FS is equal to 1.0 (Anderson et al., 2008). As the FS increases above 1.0, the amount of movement associated with the seismic coefficient decreases, while lower FS values imply more movement. Likewise, although the 0.5 x PHGA is commonly used, other seismic coefficient reduction factors can be used to modify the PGHA; values lower than 0.5 imply larger seismic deformation when the FS is 1.0, while larger factors imply less movement. A value of 0.5 was selected, rather than higher or lower factors, based on recommendations in AASHTO (2012).

The following additional assumptions and methodologies were used during these analyses:

- For each design seismic event, the average PHGA obtained from the site-specific ground response analyses (Chapter 3) was used.
- All fine-grained soils including the BCF clay and the estuarine deposits were assumed to behave in "undrained" manner during the design seismic events. A small cohesion of 0.1 ksf was added to the frictional shear strength (ϕ') component to estimate total shear strength of the cohesionless soils (compacted fill,

common fill, and cap material) to represent the short-term “undrained” behavior of these soils in a seismic event.

- The as-built OCSP® structures were assumed to be fully built to elevation +38 feet MLLW with a surcharge equal to 20 percent of the live load (0.2 ksf).
- The sea level for all seismic cases was assumed at the elevation of +7.5 feet MLLW, which is approximately 9 feet below the sea level assumed by PND (2008b) in the pseudo-static global stability analyses and 3.5 feet below the value used in their Plaxis numerical modeling. Groundwater on the land side of the face was assumed to be located at +20 feet MLLW, which is 2 feet higher than assumed by the PND design team.
- The hydrodynamic force exerted by the seawater during the seismic events was estimated using the Westergaard equation (see Section 2.1.3). In this suitability study, the hydrodynamic force was applied as a concentrated horizontal force at a height equal to $0.4*H_w$ from the long-term dredge line, where H_w is the depth of seawater in front of the wall. The hydrodynamic force was also assumed to act in the direction that undermines the global stability of the OCSP® structure (seaward direction). The hydrodynamic force was not considered in the global stability analyses conducted by PND (2008b).

For all pseudo-static loading cases, the cyclic degradation of the shear strength was considered for soils that were potentially affected by cyclic loading, such as the BCF clay, estuarine deposits, and the common fill layers. The following assumptions were made regarding the shear strength reduction of these soils in the cyclic loading condition:

- **BCF Clay.** The cyclic undrained shear strength was assumed to be the same as the static undrained shear strength (that is, no cyclic strength degradation). This assumption, however, was considered “optimistic” given the evidence of mobilization of undrained residual strength of BCF clay under steep slopes in Anchorage, such as during the 1964 Alaska earthquake. Undrained strength reductions under large displacement conditions were also verified with constant volume ring shear testing of BCF clay at POA.
- **Estuarine Deposits.** The S_u/σ'_v ratio of the estuarine deposits was assumed to reduce by 20 percent (from 0.55 to 0.44). Considering the low SPT blow counts observed in the layer, this assumption is also considered to be “optimistic.”
- **Common Fill.** The friction angle of the common fill below the landside water table elevation (+20 feet MLLW) was assumed to reduce from 32 to 27 degrees (tangent of the friction angle reduced by 20 percent). This assumption is also considered “optimistic” for uncompacted and cohesionless material such as the common fill.

Details on the input parameters and assumptions for each pseudo-static loading case are summarized in Table 5.2-9.

TABLE 5.2-9
Summary of the Pseudo-Static Global Stability Analyses for the As-Built OCSP® Structures

Case No.	Description	Shear Strength of BCF Clay: Seaside	Shear Strength of BCF Clay: Landside	Shear Strength of Estuarine Deposits	Water Level (ft, MLLW): Seaside	Water Level (ft, MLLW): Landside	Loads	Lateral Seismic Coefficient k_h
4	OLE	Consolidated-Undrained[a]	Consolidated-Undrained[b]	$S_u = 0.44\sigma'_v$	7.5	20	DL + 0.2*LL + HS + HD[c]	0.08g
5	CLE				7.5	20		0.15g
6	MCE				7.5	20		0.20g

[a] Calculated by using SHANSEP correlation assuming in situ (post dredging) overburden effective stress and OCR profile.
[b] Calculated by using SHANSEP correlation assuming post-construction overburden effective stress and OCR profile.
[c] DL = dead load, LL = live load (= 1 ksf), HS = hydrostatic load, HD = hydrodynamic load.

Results from the pseudo-static global stability analyses obtained by CH2M HILL and reported by PND (2008b) are shown in Figures 5.2-21 to 5.2-24. The FS values calculated for all pseudo-static cases are summarized in Table 5.2-10.

TABLE 5.2-10
Results from the Pseudo-Static Global Stability Analyses for the As-Built OCSP® Structure

Case No.	Description	Global Factor of Safety (FS)				FS Criteria
		Section 2-2		Section 3-3		
		CH2M HILL	PND (2008b)[a]	CH2M HILL	PND (2008)[b]	
4	OLE Event	0.8	1.3	0.8	1.7	1.2
5	CLE Event	0.6	1.1	0.6	1.5	1.1
6	MCE Event	0.5	0.9	N/A	1.2	1.0

[a] Using FS values calculated for Section F in the North Extension Area (Figure 4.1, PND, 2008b) using Spencer method with circular failure surface. PND FS values from Analysis Section F in Appendix J.
[b] Using FS values calculated for Section G in the North Extension Area (Figure 4.1, PND, 2008b) using Spencer method with circular failure surface. PNN FS values from Analysis Section G in Appendix J.[2]

The following observations can be made based on the results of the pseudo-static global stability analyses:

- The FS values calculated by CH2M HILL for all seismic events are less than 1.0, which do not meet the design criteria defined by PND (2008b).
- The shape of the critical slip surfaces in all seismic cases evaluated by CH2M HILL appears to be similar to that obtained from the static undrained loading cases (Cases 1 and 3).
- The critical slip surfaces identified by CH2M HILL for the End-of-Construction and Long-term Static-Undrained cases have a relatively flat base that resembles a translational-type failure movement.

Considering that the FS values are less than 1.0 for all seismic cases using "optimistic" assumptions, it is very likely that the as-built OCSP® structures will move during the design seismic events. The potential seismic-induced permanent deformation of the as-built OCSP® structures will be discussed in the next section.

5.2.6.6 SLOPE/W Stability Evaluations

A comparison of FS values obtained by SLOPE/W and Slide was made to confirm that the software used for the global stability analyses was not introducing bias into the global stability evaluation. This comparative study was conducted for Section F referenced in Table 4-4 of PND (2008). For the initial analyses, the soil profile, OCSP® geometry, strength properties, and seismic coefficient were taken from information published in PND (2008). Subsequent analyses considered variations in the shape of the slip surface and variations in soil strength properties to determine if SLOPE/W gave the same reduction in FS values as observed with Slide.

Results from this comparative study are provided in Appendix E. These results show that both computer programs give comparable, although not identical, FS values when the same geometry, strength, and external loading assumptions are used in each program. Variations in the FS values between the two programs are attributed to differences in the algorithms used to define critical slip surfaces, as well as small variations in material property assumptions. The variations in FS values were also generally similar as assumptions regarding the shape of the slip surface changed from circular to non-circular and the soil model changed from a two- or three-zone strength model. The conclusion from the SLOPE/W comparative study was that low FS values obtained using the computer

[2] Sections used for slope stability analyses in PND (2008) differ from sections in structural as-built drawings. Analysis Section F used for slope stability assessments is in the general area of Section G-G in as-built drawings, and Analysis Section G used for slope stability assessment is in the general area of Section F-F in as-built drawings. Section 5 of this suitability study is based on analysis sections; Section 6 shows copies of the as-built drawings.

program Slide were not due to the computer program that was used, but rather were primarily a function of the assumptions made regarding slip surface geometry and soil strength.

5.2.7 Simplified Evaluation of Seismic-Induced Permanent Deformation

In the CH2M HILL suitability study, the seismic-induced permanent deformation of the as-built OCSP® structures was estimated using both simplified and numerical analyses. Results obtained from the numerical analysis are discussed in Chapter 7. In this section the seismic-induced permanent deformation estimated by simplified methods are discussed. The simplified methods used in this study involved use of a conventional Newmark sliding-block method and a modified sliding-block analysis performed for the set of time histories discussed in Chapter 3. Because seismic-induced permanent deformation calculated by these methods are approximate in nature, the magnitude of the deformation provided in the following subsections should be viewed as an index of seismic performance of the structures (Bray and Travasarou, 2007).

5.2.7.1 Seismic-Induced Permanent Deformation Using Simplified Newmark Method

The simplified Newmark sliding-block method involves correlations or charts that relate the permanent seismic-induced deformation with parameters such as the yield acceleration (or the ratio of the yield acceleration over PGHA), earthquake magnitude, peak ground velocity, or the Arias intensity (Kramer, 1996). These correlations or charts have been developed by various researchers (for example, Hynes-Griffin and Franklin, 1984; Ambraseys and Menu, 1988; Bray and Travasarou, 2007; and Rathje and Saygili, 2008) using statistical and/or regression analyses between predicted deformations and different characteristics of earthquake records, rather than by correlating to observed displacements after earthquake events. Displacements are estimated based on the Newmark sliding-bock method, where the soil mass above the sliding surface is usually assumed to be rigid. In some correlations the flexibility of the soil mass is included. The correlations or charts have evolved over the years as the number of earthquake records has increased and as factors such as peak ground velocity, earthquake magnitude, and peak ground acceleration have been evaluated (Anderson et al., 2008).

The common parameter that is used in all simplified Newmark methods is the yield acceleration, which is determined by interactively employing different horizontal earthquake accelerations in a pseudo-static limit-equilibrium analysis until the global FS of the structure approaches 1.0. When using the simplified sliding-block methods, the yield acceleration is normally assumed to be constant throughout the seismic event. The use of constant yield acceleration simply implies that the undrained shear strength of the foundation soils is unchanged with increasing deformation. This is an optimistic (unconservative) assumption for many cohesive soils, including the BCF clay, as the undrained shear strength of the clay often decreases with increasing deformation (Section 5.2.2). As a result, the seismic-induced deformations estimated by using a constant yield acceleration should be considered as lower bound values, unless the shear strength is modified to include the effects of cyclic loading.

The simplified sliding-block methods used in this study include Hynes-Griffin and Franklin (1984), Ambraseys and Menu (1988), Bray and Travasarou (2007), and Rathje and Saygili (2008). A summary of these methods is as follows:

- The Hynes-Griffin and Franklin (1984) method is a chart-based method. This method is the only method used in this study that did not provide the lower bound for the seismic-induced deformation. In the absence of a predictive equation for the charts, relationships were developed by statistically fitting an equation to the published charts.
- Ambraseys and Menu (1988) method was the first to use the regression technique to develop equations that could be used to estimate the seismic-induced deformation. This development was based on the analyses of 50 strong-motion records from 11 earthquakes.
- Both Bray and Travasarou (2007) and Rathje and Saygili (2008) methods are widely considered as the current state-of-the-practice. These methods are based on more analyses with a wider range of earthquake magnitudes, PHGAs, and frequency contents.

Of the four empirical-based methods used in this study, the Bray and Travasarou (2007) is the only method that considers the earthquake magnitude in the regression equation. Rathje and Saygili (2008) proposed several predictive models including the scalar, the 2-parameter, and the 3-parameter models. In this study, only the scalar model of the Rathje and Saygili (2008) method was used.

The seismic-induced permanent deformation estimated by the empirical-based methods is shown as a range with the weighted average value calculated using the following equation:

$$D = 0.15*D_1 + 0.15*D_2 + 0.35*D_3 + 0.35*D_4$$

Where:

D = weighted average seismic-induced permanent deformation

D_1 = seismic-induced permanent deformation estimated by Hynes-Griffin and Franklin (1984)

D_2 = seismic-induced permanent deformation estimated by Ambraseys and Menu (1984)

D_3 = seismic-induced permanent deformation estimated by Bray and Travasarou (2007)

D_4 = seismic-induced permanent deformation estimated by Rathje and Saygili (2008)

The yield accelerations calculated from the pseudo-static global stability analysis are 0.035g and 0.03g for Sections 2-2 and 3-3, respectively (Figures 5.2-24a and 5.2-24b). These yield accelerations were determined based on the assumption that the undrained shear strength of the BCF clay under seismic loading was equal to the static undrained shear strength (no cyclic or post-cyclic degradation in the undrained shear strength). This assumption was optimistic based on observations from cyclic laboratory and ring shear tests conducted on the BCF clay. Since the yield acceleration values computed for both Sections 2-2 and 3-3 are very low, the as-built OCSP® structures are predicted to experience large deformation during earthquake events.

The seismic-induced deformation for the MCE event was only estimated for Section 2-2 as this section is located within the essential facility area. Since Section 3-3 is located outside the essential facility area, this section does not have to be designed to withstand the MCE earthquake. Results obtained from the deformation analyses using the simplified Newmark method are summarized in Table 5-2-11.

The following observations can be made based on the results calculated by the simplified Newmark method:

- **OLE Event.** The estimated seismic-induced permanent deformation ranges from several inches to about a foot for both Sections 2-2 and 3-3. This range of deformation is approaching the level that would cause strength degradation during cyclic loading, and therefore, permanent deformation could be higher if strength degradation effects are introduced into the analysis. This amount of deformation is greater than the deformation criterion of 3 inches defined by PND (2008b) for the OLE event. While deformation of this magnitude is not anticipated to result in substantial damages to the as-built OCSP® structures, this amount of deformation could cause service interruption as significant repairs should be expected.
- **CLE and MCE Events.** The estimated seismic-induced permanent deformation can be up to several feet for both Sections 2-2 and 3-3. This range of deformation exceeds the level that causes strength degradation during cyclic loading, and therefore, permanent deformation would be expected to be higher if strength degradation effects are introduced into the analysis. These estimated deformations exceed the deformation criteria used by PND (2008b) for the CLE and MCE events. While deformation of this magnitude can cause substantial damage to the as-built OCSP® structures, this amount of movement probably would not result in collapse of the structures.

TABLE 5.2-11

Seismic-Induced Permanent Deformation Calculated by Simplified Newmark Sliding-Block Methods

Section	Seismic Event	Magnitude	Avg. PHGA from SHAKE2000 (g)	Seismic-Induced Permanent Deformation (in) H-G&F[a] (1984)	A&M[b] (1988)	B&T[c] (2007)	R&S[d] (2008)	Weighted Average
2-2	OLE	6.1	0.16	11 (N/A – 20)	9 (4 – 18)	4 (2 – 8)	5 (2 – 17)	6
	CLE	6.3	0.29	20 (N/A – 42)	23 (11 – 45)	14 (7 – 26)	19 (6 – 58)	18
		7.5				19 (10 – 37)		20
	MCE	6.6	0.39	28 (N/A – 61)	34 (17 – 68)	24 (13 – 47)	29 (9 – 91)	28
		9.2				50 (26 – 97)		37
3-3	OLE	6.1	0.16	13 (N/A – 24)	11 (6 – 23)	5 (3 – 10)	7 (2 – 22)	8
	CLE	6.3	0.29	24 (N/A – 51)	28 (14 – 56)	16 (9 – 32)	21 (7 – 66)	21
		7.5				23 (12 – 45)		23

Note: Values shown in parentheses are equal to the mean ± one standard deviation. The weighted average value was calculated based on the best-estimate values. The average PHGA was obtained from SHAKE2000 analyses using all ground motion records considered for each design seismic event.

[a] Hynes-Griffin and Franklin (1984).

[b] Ambraseys and Menu (1988).

[c] Bray and Travasarou (2007).

[d] Rathje and Saygili (2008).

g = ground acceleration, measured in terms of “g” where 1g is 32 ft/sec^2.

5.2.7.2 Seismic-Induced Permanent Deformation Using Modified Newmark Method

As discussed in the previous section, the yield acceleration is typically assumed to be constant throughout the earthquake event in a conventional deformation analysis using simplified Newmark sliding-block method. For soils that exhibit significant shear strength reduction with increasing deformation, the assumption of constant yield acceleration is not appropriate, as the yield acceleration will decrease with the decreasing undrained shear strength. To overcome this shortcoming, Matasovic et al. (1998) proposed a modified approach in which the yield acceleration was treated as a function of seismic-induced deformation. During the analysis, the yield acceleration value is continuously updated as the seismic-induced deformation accumulates. Depending on the amount of shear strength reduction, earthquake intensity, and duration of shaking, the yield acceleration can reduce to zero during the earthquake event. When this occurs, the seismic-induced permanent deformation becomes excessively large, which is indicative of a global failure.

The modified Newmark sliding-block analysis proposed by Matasovic et al. (1998) was adopted for this study. In this analysis, a pseudo-static global stability analysis was carried out first to calculate the initial yield acceleration value. The seismic-induced deformation was then determined by double integration of the acceleration time history data above the initial yield acceleration. Based on this calculated seismic-induced deformation, the yield acceleration was updated and used in the subsequent integration. This iterative process was repeated until either the end of the acceleration time history was reached or when the yield acceleration dropped to zero (which was indicative of global failure).

The following two approaches were used in this study to define the relationship between the yield acceleration and the seismic-induced deformation:

- **Non-Linear Strength Reduction Approach.** The first approach used the form of the relationship between the yield acceleration and the seismic-induced deformation developed by Stark and Contreras (1998) for BCF clay at the Fourth Avenue, L Street, and Government Hill landslides in Anchorage, Alaska during the 1964 Alaska earthquake. From the data published in Stark and Contreras (1998), a power function was used to define the relationship between the cyclic over peak undrained shear strength ratio ($S_{u\text{-}cyc}/S_{u\text{-}p}$) and the yield acceleration (Figure 5.2-25a). By performing a series of pseudo-static global stability analyses, the relationship between the $S_{u\text{-}cyc}/S_{u\text{-}p}$ ratio and the yield acceleration was established (Figure 5.2-25b). The results shown in Figures 5.2-25a and 5.2-25b were then combined to define the relationship between yield acceleration and the seismic-induced deformation shown in Figure 5.2-25c. As can be seen in Figure 5.2-25c, the yield acceleration of both Sections 2-2 and 3-3 rapidly reduced from the initial value to zero when the seismic-induced deformation was very small—about 2 inches. Since it only takes a very small amount of deformation (2 inches) to reduce the yield acceleration to zero, this relationship is considered to be conservative. Yet, given that the non-linear strength reduction is based on back-analyses of three separate failures in BCF clay and is substantiated with constant volume ring shear tests, this approach is not unreasonable.
- **Linear Strength Reduction Approach.** In lieu of a power function, a linear relationship was assumed between the $S_{u\text{-}cyc}/S_{u\text{-}p}$ ratio and the seismic-induced deformation (Figure 5.2-26a). The yield acceleration and the seismic-induced deformation relationship were then developed in a similar fashion compared to the above approach (Figures 5.2-26b and 5.2-26c). Compared to the above approach, the yield acceleration reduced with increasing deformation at a much slower rate (Figure 5.2-26c). For both Sections 2-2 and 3-3, the yield acceleration dropped to zero when the seismic-induced deformation was about 30 inches. Compared to the above approach, the relationship shown in Figure 5.2-26c is considered optimistic and likely underestimates the estimated displacement.

The modified Newmark sliding-block analyses described above were conducted for the earthquake time histories selected for the seismic design of this project. The input acceleration time histories were obtained from the SHAKE2000 analyses at elevation -50 feet MLLW, which is near the base of the potential slip surfaces obtained from the pseudo-static global stability analyses. The list of the acceleration time histories used for the modified rigid-block analyses is provided in Chapter 3 of this report.

Results obtained from the modified Newmark sliding-block analyses are shown in Figures 5.2-27 through 5.2-36. The following observations can be made based on the analysis results:

- **OLE Event.** All OLE acceleration time histories produced less than 3 inches of deformation when the linear approach was used in the modified sliding-block analyses (best-case scenario). However, when the non-linear approach was used (worst-case scenario), only two OLE acceleration time histories (Michoacan and Peru Coast) resulted in less than 3 inches of the deformation. The Puget Sound time history was strong enough to cause the reduction in the yield acceleration after about 13 seconds (Section 3-3) and 15 seconds (Section 2-2). The yield acceleration dropped to zero after about 16 seconds (Section 3-3) and 30 seconds (Section 2-2), which indicated that the as-built OCSP® structure was on the verge of global failure following these times within the seismic shaking event.
- **CLE Event.** For the linear strength reduction approach, three of six CLE earthquake time histories (Cascadia 05, Cascadia-09, and Western Washington) resulted in global failure of the as-built OCSP® structures. The other three CLE earthquake time histories (Michoacan, Nisqually-00 and Nisqually-90) produced deformation ranging from 9 to 24 inches (for both Sections 2-2 and 3-3), which still exceeded the design criterion of 6 inches defined by PND (2008b). For the nonlinear strength reduction approach, all earthquake time histories considered in the analyses caused the as-built OCSP® structures to fail after 6 to 13 seconds.
- **MCE Event.** The modified rigid-block analyses were only performed for Section 2-2 using the MCE earthquake time histories, as Section 3-3 is located outside the essential facility area. All MCE earthquake time histories

caused the as-built OCSP® structures to fail regardless of the assumption used in the analyses (that is, for both linear and nonlinear strength reduction approaches). The time when the structures became unstable was estimated to be about 4 to 12 seconds (nonlinear) and 10 to 33 seconds (linear).

These simplified methods of estimating seismic displacements involve a number of assumptions and simplifications that affect the precision of the displacement estimate. For example, the soil above the slip surface is assumed to be a rigid mass, and it is assumed that there is no incoherency of ground motions within the sliding mass. These factors could reduce the amount of deformation from the estimated values given above. Therefore, these deformation estimates are considered an index of likely performance, as noted by Bray and Travasarou (2007). However, despite these and other limitations within these simplified methods, the consensus by experts in geotechnical earthquake engineering is that displacement estimates provide a reasonable indication of the order of magnitude of displacements, and in this case a warning that displacements during seismic loading, particularly for CLE and MCE events, could be large—exceeding displacements defined in the OCSP® design criteria—and potentially exceeding 10 feet.

The potential for large displacements during the CLE and MCE events should come as no surprise based on the observations during the 1964 Alaska earthquake. The amounts of predicted displacements by CH2M HILL's simplified Newmark analyses are much higher than estimated by PND (2008b), primarily because of differences in analysis methods and soil strength assumptions. These differences resulted in much lower yield accelerations than estimated by the PND design team, and the consequence of these low yield accelerations is large predicted displacement. These displacements appear to be greater than can be accepted without some type of mitigation.

5.3 Sensitivity Evaluation: Effects of Groundwater and Tidal Variation, Dredge, and Granular Backfill Friction Angle on Internal and Global Stability

A number of variables are anticipated to have an effect—sometimes significant—on internal, external, and global stability. These variables include internal friction angle of the granular backfill, landside groundwater conditions, seaside (tidal) water elevation, and assumed dredge/scour elevation. The effect of variations in these parameters on internal and global stability was investigated by conducting a sensitivity study with the geotechnical engineering analysis methods described previously. The sensitivity analyses were performed using the geometry and soil profile of Section 2-2.

Table 5.3-1 summarizes the scope of the sensitivity evaluation. In total, 62 cases were considered, with the first seven representing the baseline loading conditions. The remaining cases represent the long-term static-undrained, OLE, CLE, or MCE loading case with one variable altered. Internal friction angle of the granular fill ranged from 32 to 42 degrees, landside groundwater elevation ranged from +17 to +23 feet MLLW, tide elevation ranged from -5 to +34 feet MLLW, and dredge/scour elevation ranged from -47 to -55 feet MLLW.

TABLE 5.3-1
Scope of Sensitivity Evaluation Using Limit-equilibrium Methods

Case Number	Loading Case[a]	Live Load (psf)	Seismic Coefficient (g)	Granular Fill Friction Angle (deg)	Landside Water Elevation (ft)	Seaside Water Elevation (ft)	Dredge/ Scour Elevation (ft)
1	End-of-Construction	200	0.00	40	20	-5	-51
2	Static-Drained	1000	0.00	40	20	7.5	-51
3	Static-Undrained	1000	0.00	40	20	-5	-51
4	OLE	200	0.08	40	20	7.5	-51
5	CLE	200	0.15	40	20	7.5	-51
6	MCE	200	0.20	40	20	7.5	-51

TABLE 5.3-1
Scope of Sensitivity Evaluation Using Limit-equilibrium Methods

Case Number	Loading Case[a]	Live Load (psf)	Seismic Coefficient (g)	Granular Fill Friction Angle (deg)	Landside Water Elevation (ft)	Seaside Water Elevation (ft)	Dredge/ Scour Elevation (ft)
7	Post-Earthquake	200	0.00	40	20	-5	-51
8	Static-Undrained	1000	0.00	32	20	-5	-51
9	Static-Undrained	1000	0.00	34	20	-5	-51
10	Static-Undrained	1000	0.00	36	20	-5	-51
11	Static-Undrained	1000	0.00	38	20	-5	-51
12	Static-Undrained	1000	0.00	42	20	-5	-51
13	OLE	200	0.08	32	20	7.5	-51
14	OLE	200	0.08	34	20	7.5	-51
15	OLE	200	0.08	36	20	7.5	-51
16	OLE	200	0.08	38	20	7.5	-51
17	OLE	200	0.08	42	20	7.5	-51
18	CLE	200	0.15	32	20	7.5	-51
19	CLE	200	0.15	34	20	7.5	-51
20	CLE	200	0.15	36	20	7.5	-51
21	CLE	200	0.15	38	20	7.5	-51
22	CLE	200	0.15	42	20	7.5	-51
23	MCE	200	0.20	32	20	7.5	-51
24	MCE	200	0.20	34	20	7.5	-51
25	MCE	200	0.20	36	20	7.5	-51
26	MCE	200	0.20	38	20	7.5	-51
27	MCE	200	0.20	42	20	7.5	-51
28	Static-Undrained	1000	0.00	40	17	-5	-51
29	Static-Undrained	1000	0.00	40	23	-5	-51
30	OLE	200	0.08	40	17	7.5	-51
31	OLE	200	0.08	40	23	7.5	-51
32	CLE	200	0.15	40	17	7.5	-51
33	CLE	200	0.15	40	23	7.5	-51
34	MCE	200	0.20	40	17	7.5	-51
35	MCE	200	0.20	40	23	7.5	-51
36	Static-Undrained	1000	0.00	40	20	0	-51
37	Static-Undrained	1000	0.00	40	20	4	-51
38	Static-Undrained	1000	0.00	40	20	12	-51
39	Static-Undrained	1000	0.00	40	20	34	-51
40	OLE	200	0.08	40	20	-5	-51
41	OLE	200	0.08	40	20	0	-51
42	OLE	200	0.08	40	20	4	-51

TABLE 5.3-1
Scope of Sensitivity Evaluation Using Limit-equilibrium Methods

Case Number	Loading Case[a]	Live Load (psf)	Seismic Coefficient (g)	Granular Fill Friction Angle (deg)	Landside Water Elevation (ft)	Seaside Water Elevation (ft)	Dredge/ Scour Elevation (ft)
43	OLE	200	0.08	40	20	12	-51
44	OLE	200	0.08	40	20	34	-51
45	CLE	200	0.15	40	20	-5	-51
46	CLE	200	0.15	40	20	0	-51
47	CLE	200	0.15	40	20	4	-51
48	CLE	200	0.15	40	20	12	-51
49	CLE	200	0.15	40	20	34	-51
50	MCE	200	0.20	40	20	-5	-51
51	MCE	200	0.20	40	20	0	-51
52	MCE	200	0.20	40	20	4	-51
53	MCE	200	0.20	40	20	12	-51
54	MCE	200	0.20	40	20	34	-51
55	Static-Undrained	1000	0.00	40	20	-5	-47
56	Static-Undrained	1000	0.00	40	20	-5	-55
57	OLE	200	0.08	40	20	7.5	-47
58	OLE	200	0.08	40	20	7.5	-55
59	CLE	200	0.15	40	20	7.5	-47
60	CLE	200	0.15	40	20	7.5	-55
61	MCE	200	0.20	40	20	7.5	-47
62	MCE	200	0.20	40	20	7.5	-55

[a] Static-Drained and Static-Undrained loading cases both represent long-term, operational conditions with target FS equal to 1.5.
[b] Baseline BCF clay strength varies for the different loading cases. See the Global Stability section for a description of the shear strengths assumed for each loading case.

Results of the sensitivity evaluation are provided in Figures 5.3-1 to 5.3-4. The observations regarding the sensitivity of internal, external, and global stabilities to the various parameters include the following:

- The internal friction angle has largest impact on pullout and sliding FS values, the last of which also includes a pullout component in its resistance. Both of these FS values satisfy design criteria, even with the lowest considered granular backfill friction angle. The interlock stress and global stability FS values are not highly sensitive to granular backfill internal friction angle. The slight increase in global stability FS with increasing friction angle is accompanied by slight reduction in seismic deformation.
- The landside groundwater elevation also has a large impact on pullout and sliding FS values, because the groundwater level affects calculation of effective stress of the material for estimating frictional strength in pullout resistance. The interlock stress and global stability FS values show little impact of groundwater elevation.
- The tidal water elevation has an impact on all FS values. The seismic deformation is very sensitive to assumed tidal water elevation with a nonlinear trend observed between tidal water elevation and deformation.

- The FS for interlock stress and the estimated seismic deformation are most sensitive to the assumed dredge/scour elevation. However, lowering the dredge elevation below elevation -51 feet MLLW does not seem to significantly affect the internal or external stabilities significantly. In these latter cases, the passive resistance provided by BCF clay below the dredge elevation (and above the face sheet tips less than 10 feet lower) is negligible; the OCSP® structure simply becomes a free-standing wall supported only internally.

5.4 Stability of Wet and Dry Barge Berth Sections

Following completion of the limit-equilibrium stability analyses for the as-built case at Sections 2-2 and 3-3 in the North Extension (Figure 5.1-1), a series of additional limit-equilibrium stability analyses was conducted for the Wet Barge Berth and Dry Barge Berth areas. The purpose of these analyses was to determine whether either of these areas would meet the PIEP design criteria for gravity and seismic loading. The Wet Barge Berth and Dry Barge Berth areas involve shallower water depths, and therefore, the OCSP® facewall height in these areas was less than at Sections 2-2 and 3-3. Further, results of recent soil explorations conducted for this study found that the top of the BCF clay was at a higher elevation than at Sections 2-2 and 3-3. The following subsections summarize results of these additional stability analyses.

5.4.1 Methodology for Global Stability Analyses

Methods used to conduct the global stability analyses at the Wet Barge Berth and Dry Barge Berth areas are the same as those described in Section 5.2.6. The “random walking” method within the computer program Slide was used to perform the stability analyses. The analyses used the same three “methods of slices” as described in Section 5.2.6.

The geometry of each section used in the stability analyses was taken from Drawings 13 and 14 of the PND Barge Berth Phase 2 as-built drawings for the Dry Barge Berth and Wet Barge Berth areas, respectively, as described below:

- **Section C-C (Dry Barge Berth Area).** The berth mudline elevation is + 10 feet MLLW, sheet pile tips are located approximately at elevation – 10 feet MLLW, and the final grade behind the OCSP® wall face is + 36 feet MLLW. The length of the tailwall appears to be approximately 30 feet. The resulting exposed wall height of the sheet piles is 26 feet. The live load for this section will be 1,000 psf, similar to other sections of the project.
- **Section D-D (Wet Barge Berth Area).** The berth dredge depth for this section is -25 feet MLLW, sheet pile tips are located approximately at elevation – 40 feet MLLW, and the final grade is +38 feet. The length of the tailwall appears to be approximately 105 feet. The resulting exposed wall height of the sheet piles is 63 feet. The live load for this section will be 1,000 psf, similar to other sections of the project.

The reduced wall height for these two sections will reduce the force demand on the OCSP® structure. Stresses in the wall will decrease from those determined for Sections 2-2 and 3-3. The lower force demand will improve global stability and reduce static and seismic deformations, as long as soil conditions supporting the OCSP® system are equal to or better than conditions at Sections 2-2 and 3-3.

Soil strengths for the stability analyses were obtained from results of the recent exploration and laboratory testing program carried out by CH2M HILL between May and September of 2012. The boreholes in the area included BH-004-12 and BH-005-12. The locations of these boreholes are shown in Figure 2.1-1 of Appendix D2. Boring logs for these boreholes are also found in Appendix D2. The top of the BCF clay is located at approximate elevation -19 and -5 MLLW for BH-004-12 and BH-005-12, respectively.

5.4.2 Assumptions Regarding the Critical Slip Surface and Undrained Shear Strength

The assumptions regarding the critical surface during gravity and seismic loading, as well as the undrained strength of the BCF clay, were assumed to be the same as those described earlier in Section 5.2.6 of this report. As noted above, a non-circular slip surface with a “random walking” search mechanism was used to identify the slip surface with the lowest FS. Previous analyses have shown that non-circular slip surfaces are more critical than circular slip surfaces.

The SHANSEP equations identified in Section 5.2.2 were used to define the strength within the zones of maximum shear. Adjustments were made to account for portions of the slip surface that should be modeled with direct shear, triaxial compression, and triaxial extension as described previously. The following assumptions were made regarding the shear strength reduction of these soils in the cyclic loading condition:

- **BCF Clay.** The cyclic undrained shear strength was assumed to be the same as the static undrained shear strength (that is, no cyclic strength degradation). This assumption, however, was considered “optimistic” given the evidence of mobilization of undrained residual strength of BCF clay under steep slopes in Anchorage, such as during the 1964 Alaska earthquake. Undrained strength reductions under large displacement conditions were also verified with constant volume ring shear testing of BCF clay at POA.
- **Estuarine Deposits.** The S_u/σ'_v ratio of the estuarine deposits was assumed to reduce by 20 percent (from 0.55 to 0.44). Considering the low SPT blow counts observed in the layer, this assumption is also considered to be “optimistic.”
- **Common Fill.** The friction angle of the common fill below the landside water table elevation (+20 feet MLLW) was assumed to reduce from 32 to 27 degrees (tangent of the friction angle reduced by 20 percent). This assumption is also considered “optimistic” for uncompacted and cohesionless material such as the common fill.

The water level within the OCSP® retaining structure was assumed to be +20 feet MLLW. Tidal elevations ranged from -5 feet MLLW to +7.5 feet MLLW, depending on the specific loading case. Seismic coefficients were assumed to be the same as those that had been computed for Sections 2-2 and 3-3 (that is, 0.08g, 0.15g, and 0.20g for the OLE, CLE, and MCE, respectively). As noted above, the live load for operations was assumed to be 1,000 psf for the static cases and 200 psf during the seismic events. The friction angle value was based on the assumption that the backfill will be improved by using vibracompaction. If vibracompaction is not performed, a lower friction angle will occur, and more importantly, the potential for liquefaction within the backfill will increase.

Soil layering and strengths for the soil cross-sections at the Dry Barge and Wet Barge Berths were used in the computer program Slide to estimate FS values at the three different stages of gravity loading (that is, end of construction, long-term drained, and long-term undrained). For seismic loading the FS values were determined with the added inertial force caused by seismic loading. Estimates of permanent displacement resulting from seismic loading were also made. The same earthquake records as described previously were integrated to estimate the displacement. Values of the yield acceleration were determined from the pseudo-static global stability analyses.

5.4.3 Results of the Global Stability Analyses

Results from the global stability analyses are summarized in terms of FS in Table 5.4-1.

TABLE 5.4.1
Results from the Static Global Stability Analyses for Dry and Wet Barge Berth Areas with OCSP® Structure

Case No.	Description	Global Factor of Safety (FS)		FS Criteria
		Section C-C (Dry Barge Berth)	Section D-D (Wet Barge Berth)	
1	End-of-Construction	1.6	1.2	1.3
2	Long-Term Static-Drained	1.7	1.5	1.5
3	Long-Term Static-Undrained	1.5	1.2	1.5

These results show that the Dry Barge Berth area meets the PIEP design criteria for factors of safety during gravity and operational loading. However, the Wet Barge Berth area does not meet all design requirements. Specifically, both the short-term undrained (end of construction) and the long-term undrained case with FS of 1.2 are less than the required FS of 1.3 and 1.5. These lower FS values occur during extreme low tides. For the end-of-construction case, the required FS = 1.3 is only slightly greater than the estimated value, FS = 1.2. For the long-term undrained case, the difference between the required FS = 1.5 and the estimated FS = 1.2 is more significant. Since the FS is less than 1.5 but greater than 1.0, the Wet Barge Berth margin of safety is lower than desired.

Factors of safety during the seismic events are summarized in Table 5.4-2. A seismic coefficient equal to 0.5 times the PHGA was used in these analyses, consistent with some expected deformation. For cases where the FS values are greater than the FS criteria, acceptable conditions will exist—although several inches of permanent displacement can occur (in accordance with the assumption to use only half of PHGA). For those cases with the FS values less than the design criteria, larger permanent displacement will occur. Section 5.4.4 provides an estimate of these displacements. As noted above, optimistic interpretations of soil strength reduction were used in these analyses, and therefore, these FS values are considered optimistic.

TABLE 5.4.2
Results from the Pseudostatic Global Stability Analyses for Dry and Wet Barge Berth Areas with OCSP® Structure

Case No.	Description	Global Factor of Safety (FS) Section C-C (Dry Barge Berth)	Global Factor of Safety (FS) Section D-D (Wet Barge Berth)	FS Criteria
1	OLE Event	1.4	1.0	1.2
2	CLE Event	1.1	0.8	1.1
3	MCE Event	NA	0.7	1.0

Note: The Dry Barge berth is not an essential facility and therefore it is not evaluated for the MCE.

Plots showing the results of these stability analyses are provided in Figures 5.4-1 to 5.4-7.

5.4.4 Seismic-Induced Deformations

Estimates of deformation during the OLE, CLE, and MCE were made by integrating each earthquake record above the yield acceleration to estimate the permanent deformation. The MCE event was not considered for the Dry Barge Berth, as this area is not included within the essential facility limits. The yield acceleration for each cross-section was determined from the Slide analyses, as described in Section 5.2.6. Results of these evaluations defined yield accelerations of 0.145g and 0.076g for the Dry Barge Berth and Wet Barge Berth areas, respectively. The higher yield acceleration for the Dry Barge Berth cross-section results from the much shorter height of the exposed sheet pile wall.

Results of the deformation estimates are summarized in Table 5.4-3. These results show that the deformations in the Dry Barge Berth are expected to be very small. However, for the Wet Barge Berth area, deformations could be large and could exceed the PIEP design criteria. The range of deformations shown in the table represents the two different assumptions regarding strength degradation during displacement. When degradation is small, deformations will be small. However, when degradation in strength is more consistent with measurements obtained in the ring shear tests conducted for this project and observations made during the 1964 Alaska earthquake throughout the Anchorage area (that is, Fourth Avenue, L Street, Turnagain Heights), large displacements could result. With some earthquake records, such as the 1965 Puget Sound earthquake, even larger deformations were estimated. These larger deformations are not included in this evaluation, as they would seem to be an unlikely occurrence.

TABLE 5.4-3
Results from the Seismic Deformation Estimates for Dry and Wet Barge Berth Areas

Seismic Event	Moment Magnitude	Avg. PHGA from SHAKE 2000 (g)	Estimated Displacement (inches)	
			Section C-C (Dry Barge Berth)	Section D-D (Wet Barge Berth)
OLE	6.1	0.16	<1	1
CLE	6.3 - 7.5	0.29	<6	6-28
MCE	6.6 - 9.2	0.39	N/A	14-28

Note: Range in Wet Barge Berth represents difference between constant yield and yield based on updated, displacement-dependent shear strength.

5.4.5 General Conclusions

It was concluded from these stability analyses that the Dry Barge Berth facility will meet design requirements even under the more severe CLE loading condition; MCE loading conditions are not applicable. Static FS values are acceptable for all loading conditions at this location.

The FS for the Wet Barge Berth area during short-term undrained (end-of-construction) and after long-term undrained loading (operations at extreme low tide) are lower than the required criteria; however, the FS values are greater than 1.0 and therefore do not represent a failure condition. The margin of safety is lower than desired for these cases. During a CLE or MCE seismic event, the Wet Barge Berth facility could undergo large displacements, particularly during an MCE. These displacements could exceed levels that could be easily repaired.

5.5 Summary and Conclusions

This section addressed the as-built condition of the OCSP® structure at POA. Summarized in this section are geotechnical engineering analyses conducted in accordance with current state-of-the-practice methods involving use of design equations and standard computer modeling methods. Specific topics within the engineering evaluations include earth pressures, external stability, settlement, global stability, and sensitivity to variations in site conditions. This section also includes a discussion of methods of analysis, highlighting differences between those used for this study and those used previously for the design of the PIEP.

The following conclusions have been made regarding the subsurface conditions and performance of the as-built OCSP® structure with respect to design criteria:

- Independent assessment of the subsurface conditions is generally consistent with those assumed for the design of North Expansion projects. Estuarine deposits of variable thickness are found to overly BCF clay and glacial drift; no major differences in assumed elevations of the contacts of these layers were identified.
- Based on available piezometer measurements, groundwater levels are interpreted as having some tidal-influenced fluctuation and influence of site drainage characteristics; the variations are small relative to the tide fluctuations. Best-estimate groundwater elevation for engineering analyses was +20 feet MLLW. This level is slightly higher than the original assumed value for design.
- Relative density and effective friction angle for compacted granular fill were estimated to be higher than assumed for original design calculations. Relative density was assumed to be approximately 90 percent, and effective friction angle was estimated to be 40 degrees (compared with 36 degrees). The effective friction angle value is supported by large-size direct shear tests conducted as part of the CH2M HILL backfill investigation.

- The effective-stress friction angle and peak undrained shear strengths (triaxial compression and DSS) of the BCF clay were found to be roughly 5 to 15 percent higher than assumed for design. However, cyclic DSS testing conducted by MEG Consulting, Richmond, BC, and constant volume ring shear testing conducted by Dr. Timothy Stark, University of Illinois at Urbana-Champaign, indicated the possibility of large undrained shear strength reductions resulting from generation of excess porewater pressures and soil fabric reorientation at large strains or displacements. The strength reductions are consistent with behavior of BCF clay associated with landslides at Fourth Avenue, L Street, Turnagain Heights, and Government Hill (Anchorage, Alaska) occurring during the 1964 Alaska earthquake.
- Internal stability checks for tailwall pullout and interlock tension indicated that the design with respect to these failure modes is satisfied for early-life performance of the structure. This conclusion does not address life-cycle performance issues (see Section 6), primarily due to corrosion or construction-related defects (see Section 8), such as sheet piles driven out of interlock.
- The methods used to evaluate global stability are notably different than used for design. Non-circular slip surfaces (consistent with numerical modeling shear strain concentrations) with anisotropic shear strength assigned based on location and orientation of the slip surface resulted in significantly lower FS values. The PIEP static FS criteria are not satisfied using the recommended methods of analysis.
- Following from the low static FS values, the estimated permanent deformations from seismic loading are well over the PIEP design criteria for OLE, CLE, and MCE loading conditions. When post-peak undrained strength reductions from ring shear and back analyses of Fourth Avenue slide data are considered, very large displacements are estimated. The displacements are greater than can be accepted without some level of mitigation; failure to mitigate would subject the constructed facility to risk of an extended-period operational loss following CLE or MCE seismic loading.
- The Dry Barge Berth and Wet Barge Berth areas were investigated with respect to global stability and seismic deformation. OCSP® geometry and subsurface conditions for the Wet Barge Berth combine to give inadequate performance for CLE and MCE loading conditions. The as-built OCSP® structure at the Dry Barge Berth satisfies design criteria; the MCE loading was not considered for Dry Barge Berth, as this area is not included with the essential facilities. The ability of the OCSP® structure to withstand static and seismic loading at Dry Barge Berth is attributed to significantly reduced wall heights compared with other more critical sections.

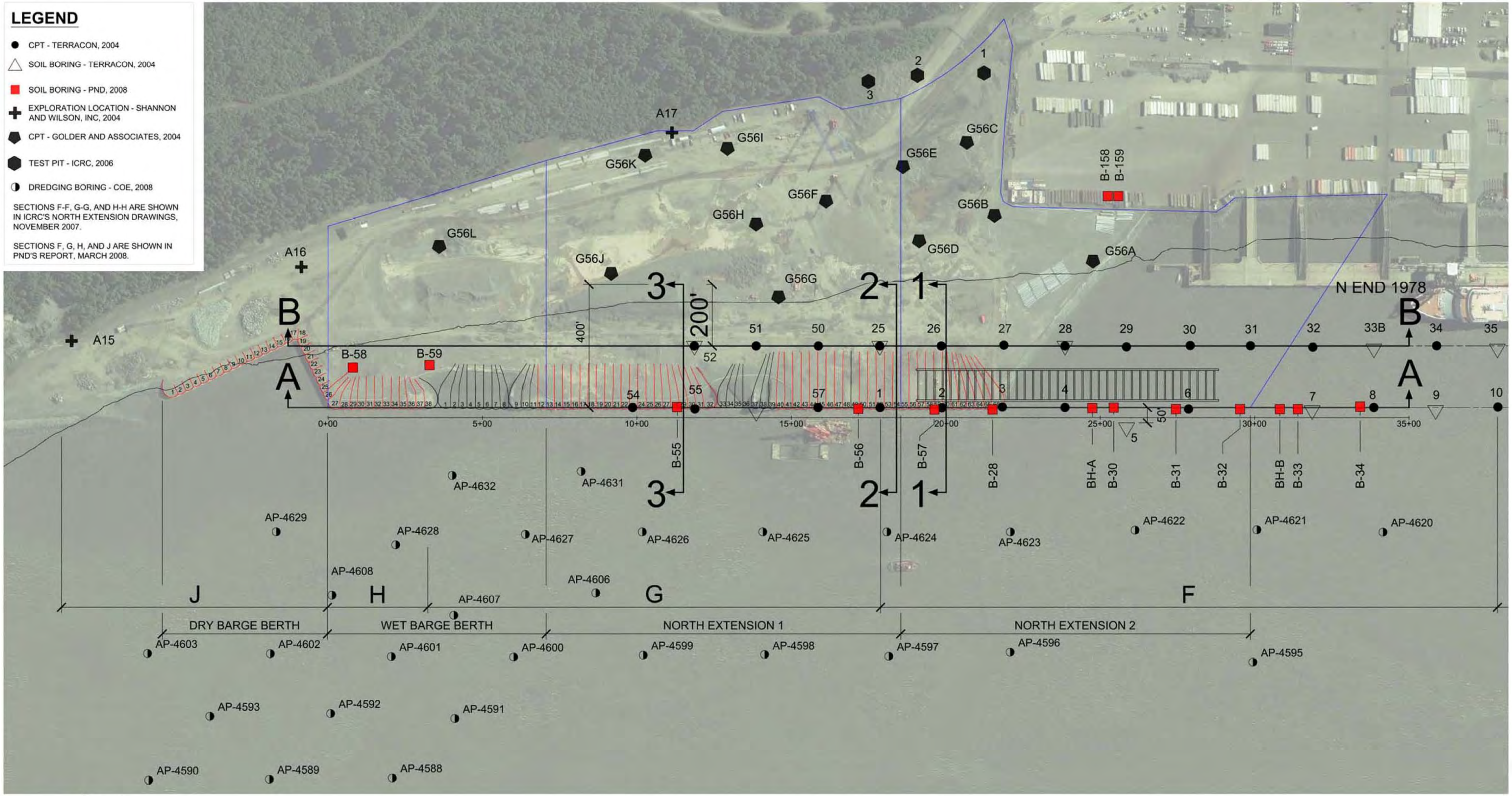

EXISTING EXPLORATIONS

SCALE IN FEET

0 150 300 450 600

FIGURE 5.1-1. Existing Explorations

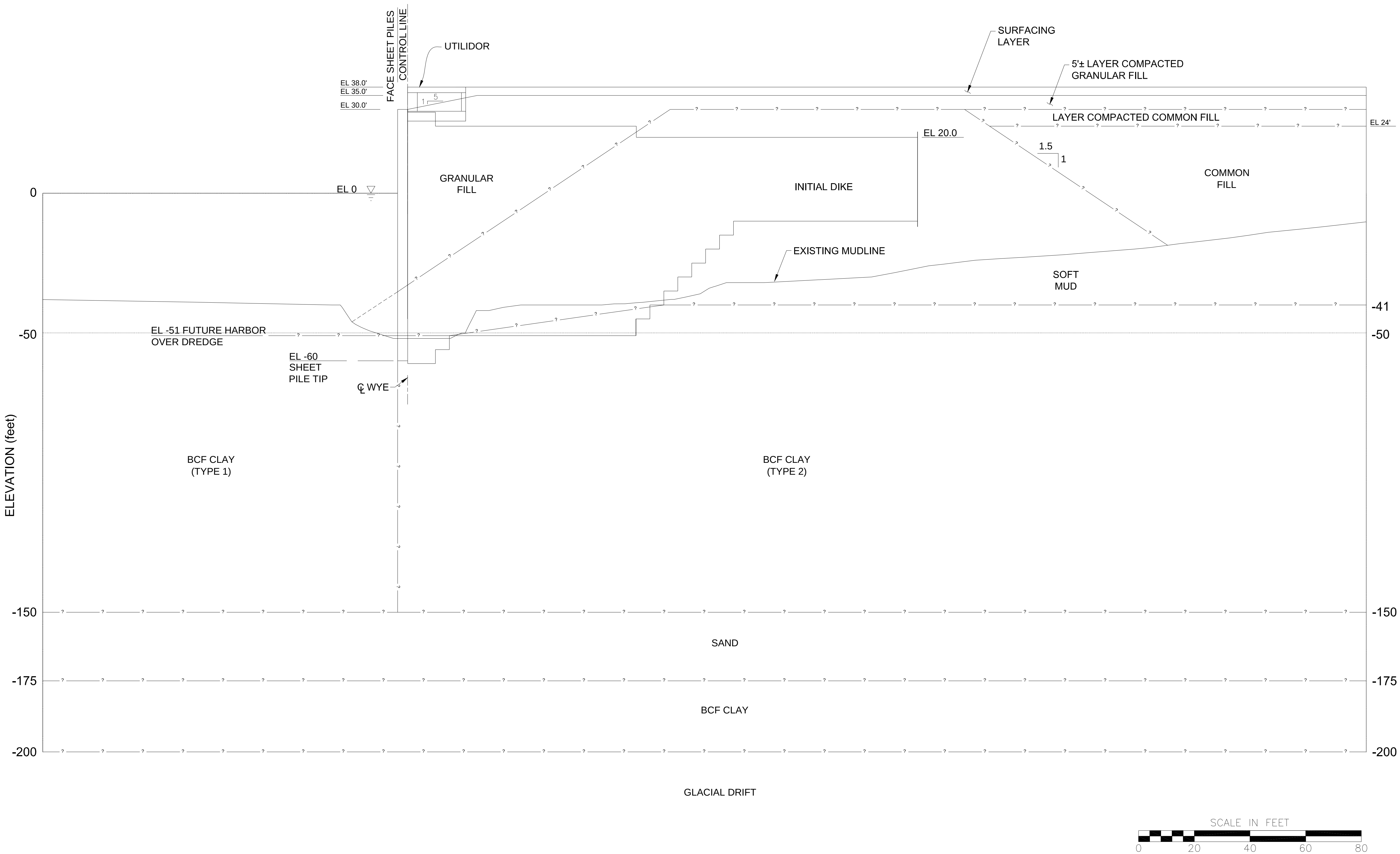

FIGURE 5.1-2. Cross-Section 1-1

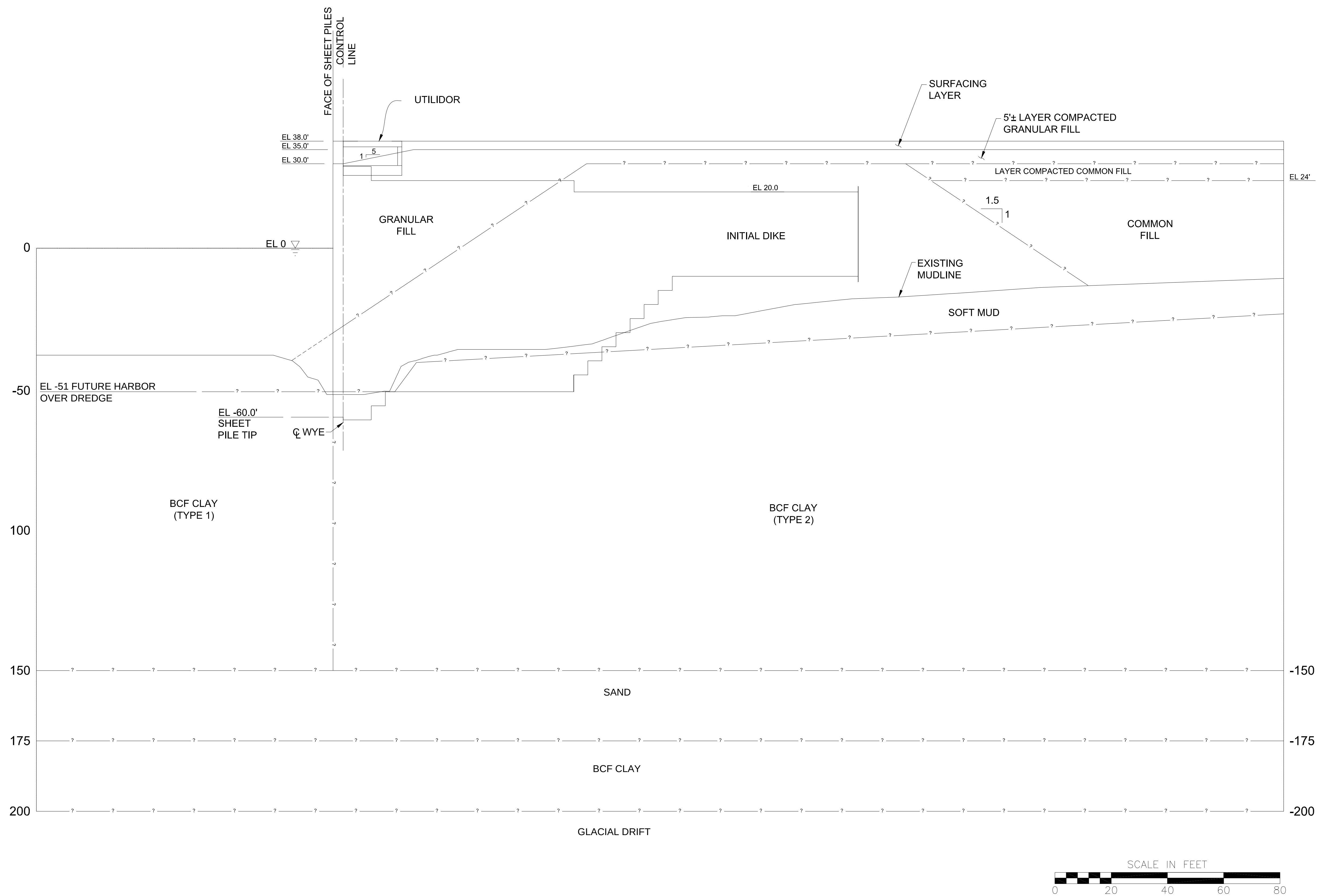

FIGURE 5.1-3. Cross-Section 2-2

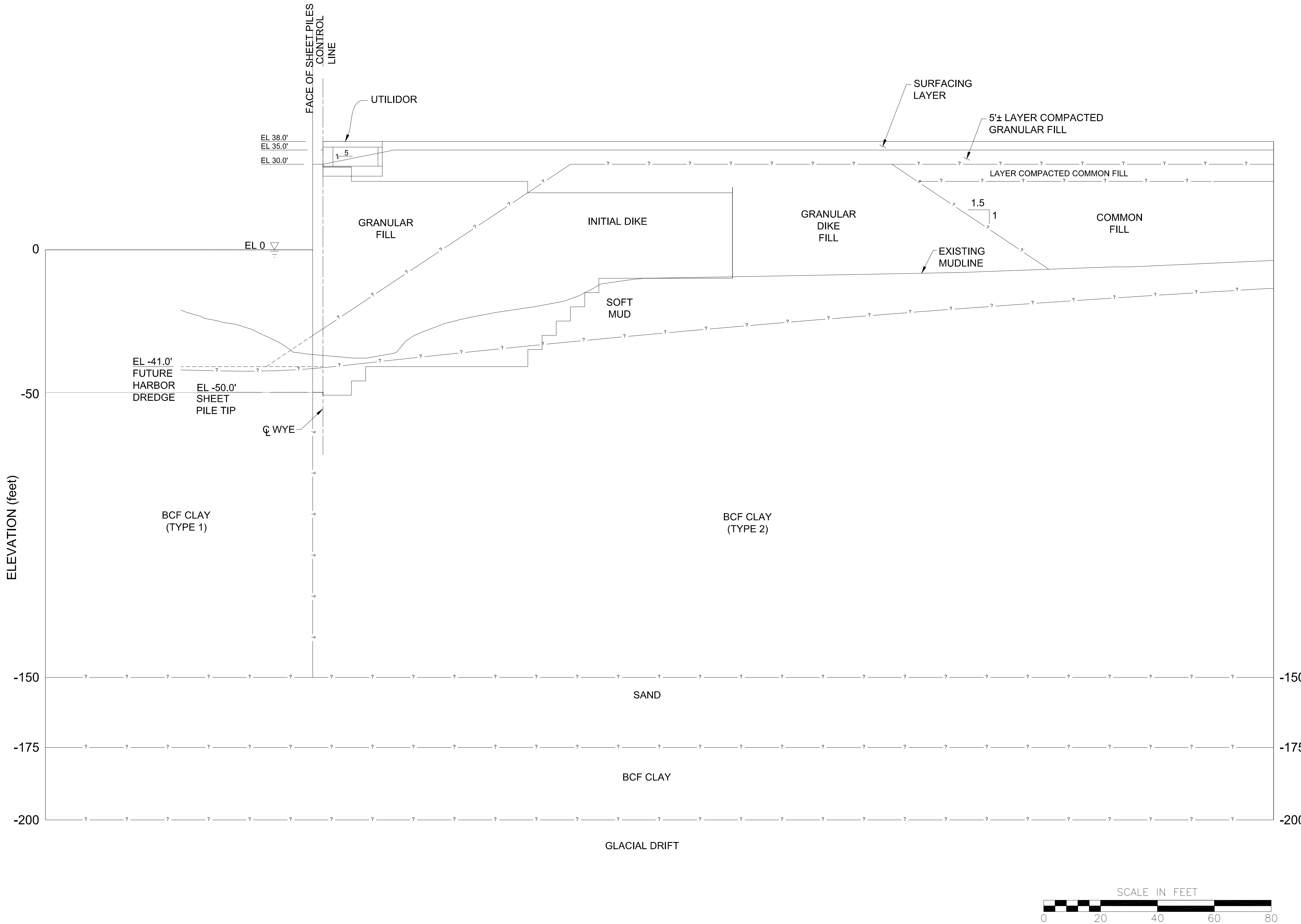

FIGURE 5.1-4. Cross-Section 3-3

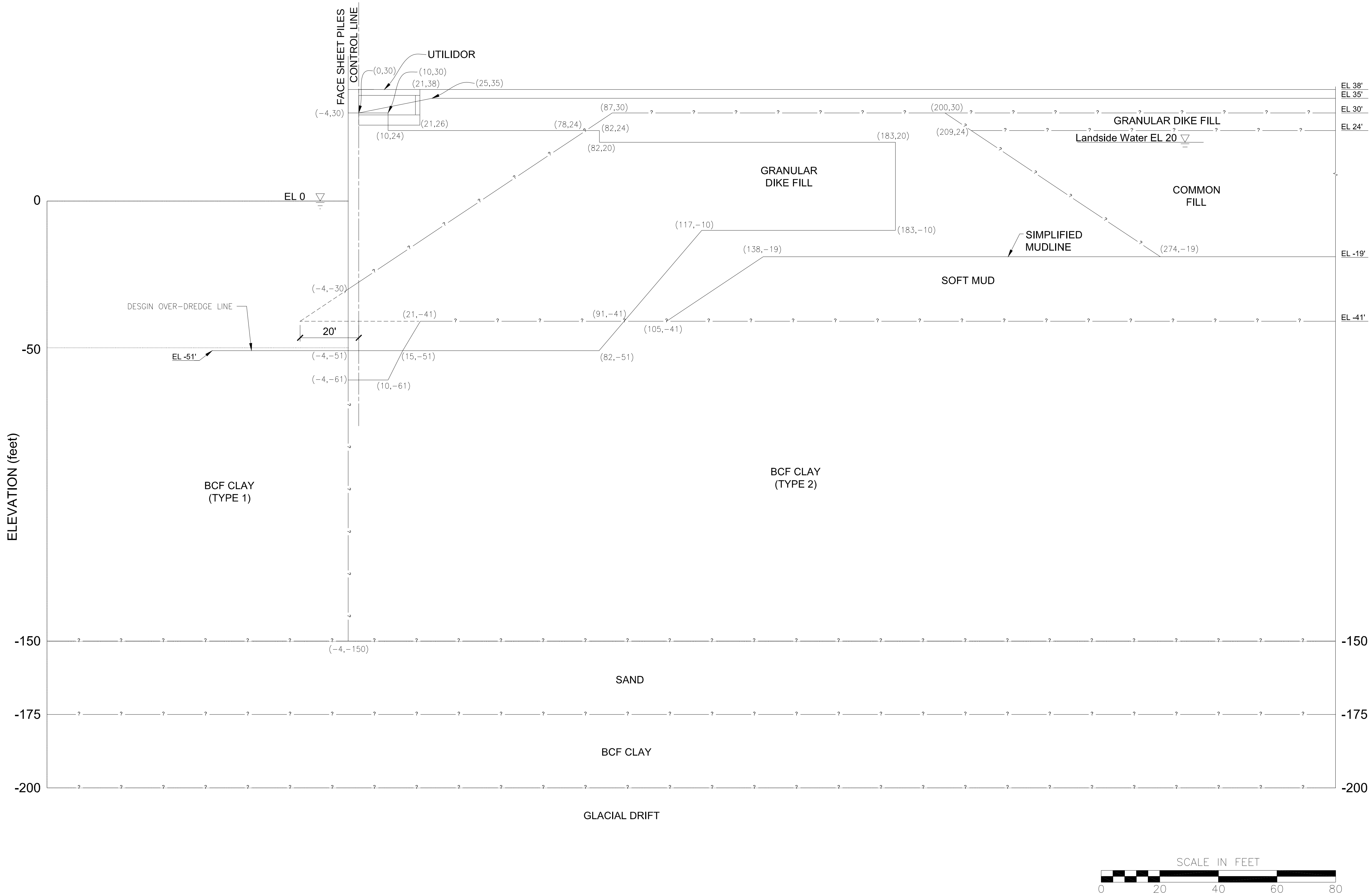

FIGURE 5.1-5. Simplified Cross-Section 2-2

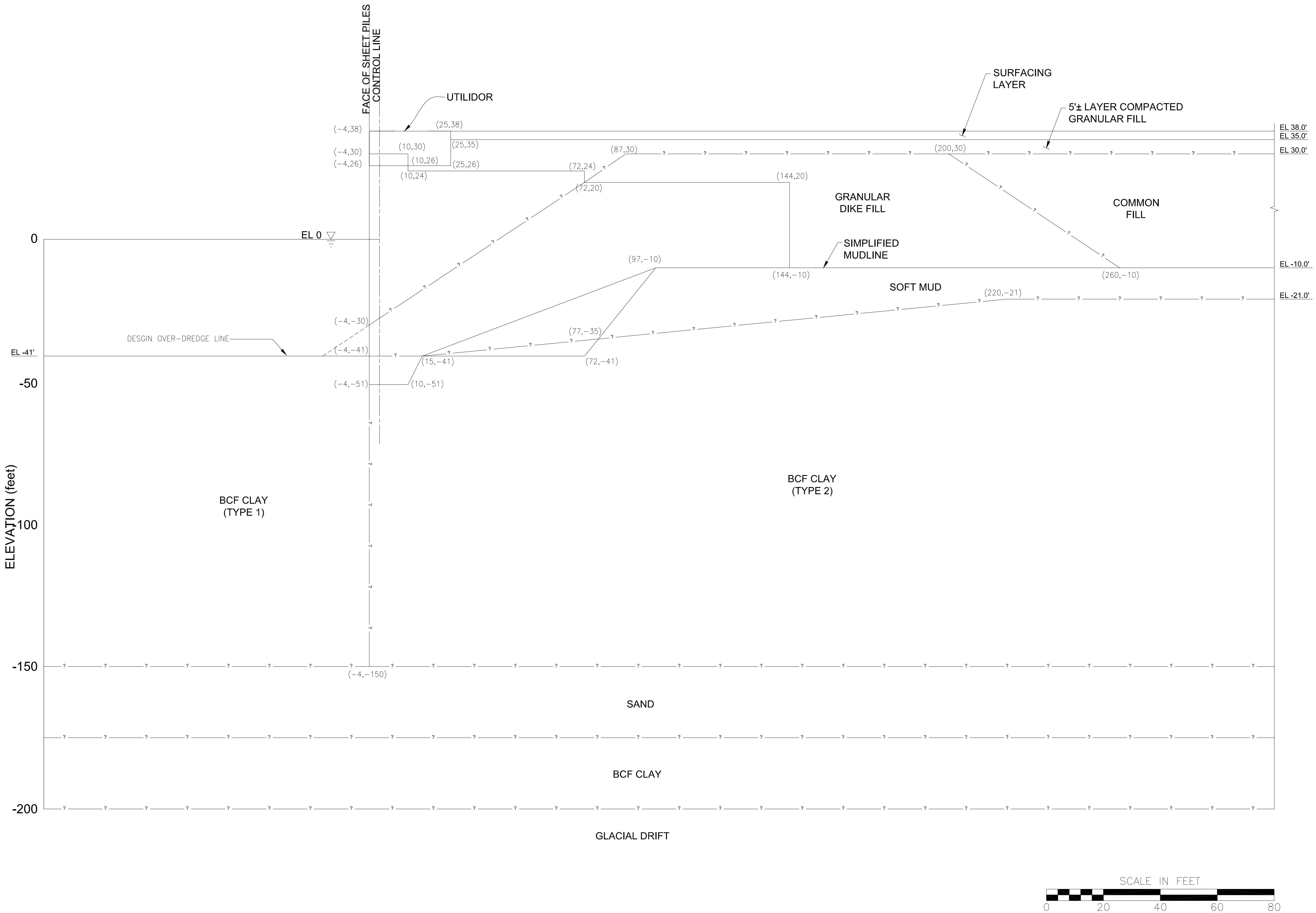

FIGURE 5.1-6. Simplified Cross-Section 3-3

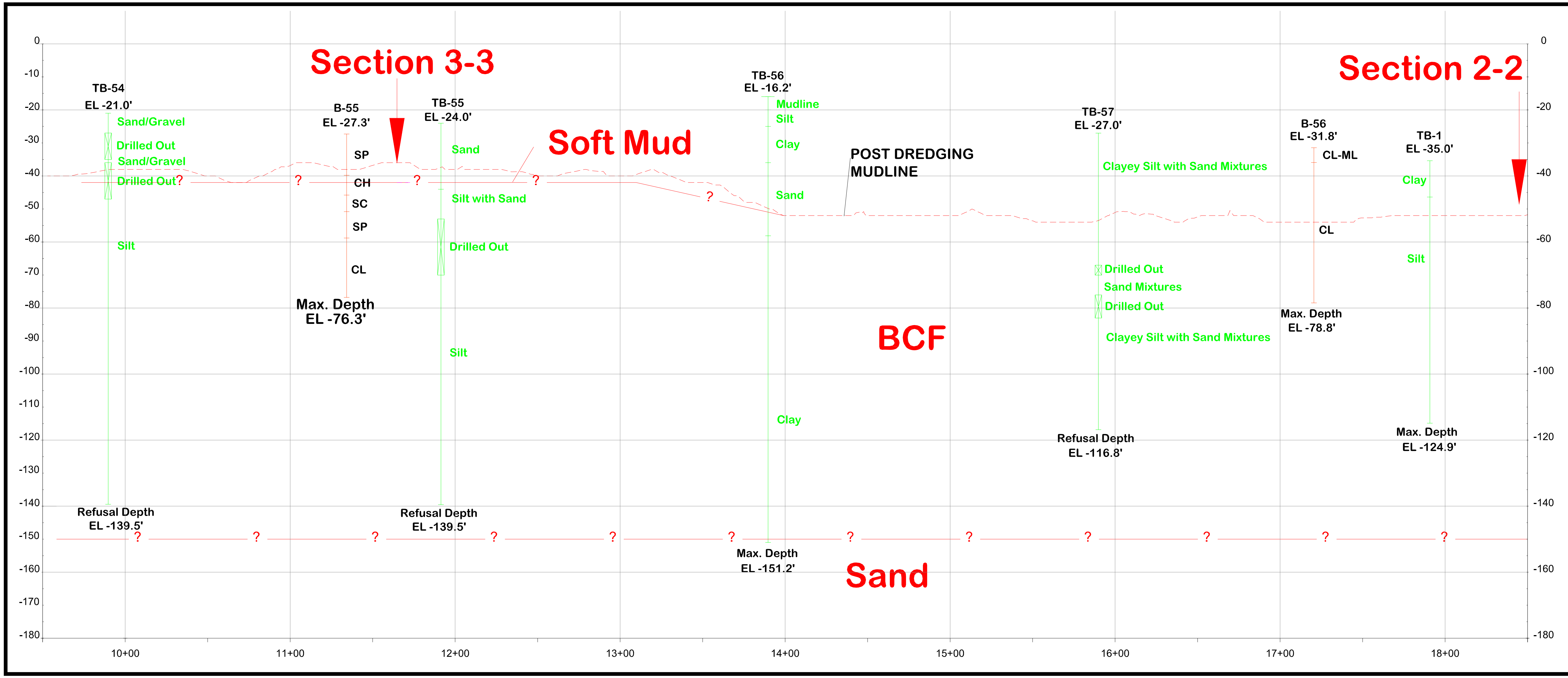

FIGURE 5.1-7a. Profile A-A, Longitudinal Profile at Proposed OCSP® Wall Face

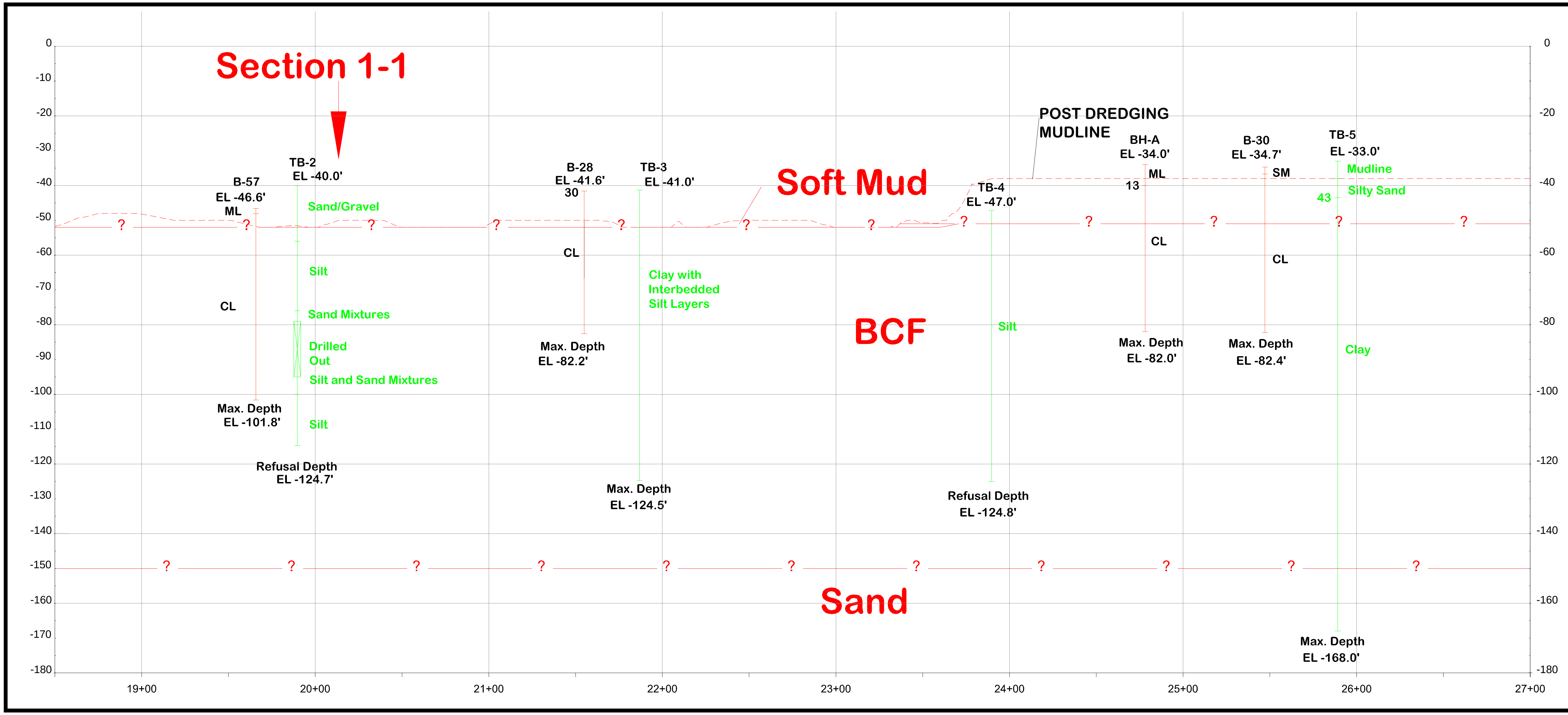

FIGURE 5.1-7b. Profile A-A, Longitudinal Profile at Proposed OCSP® Wall Face

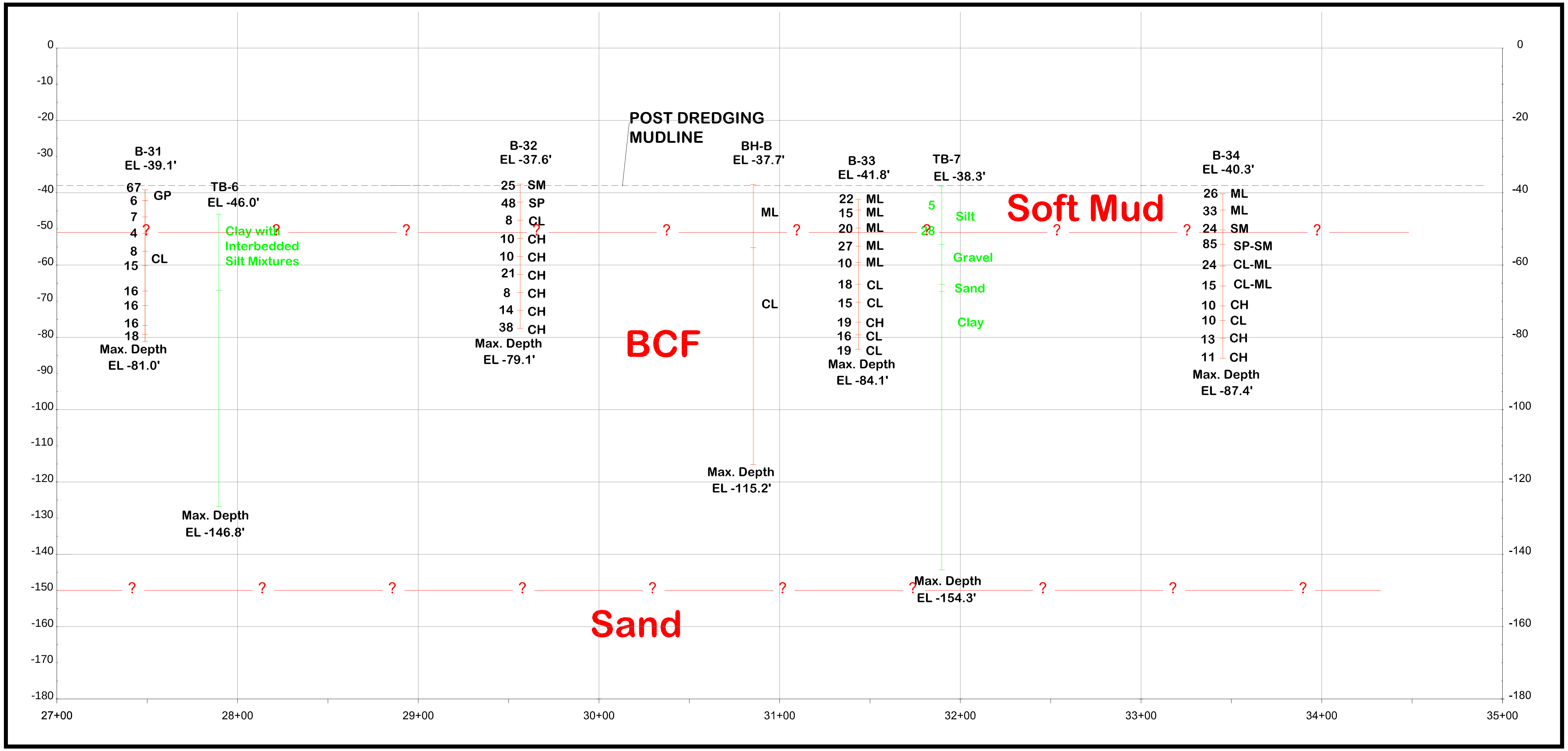

FIGURE 5.1-7c. Profile A-A, Longitudinal Profile at Proposed OCSP® Wall Face

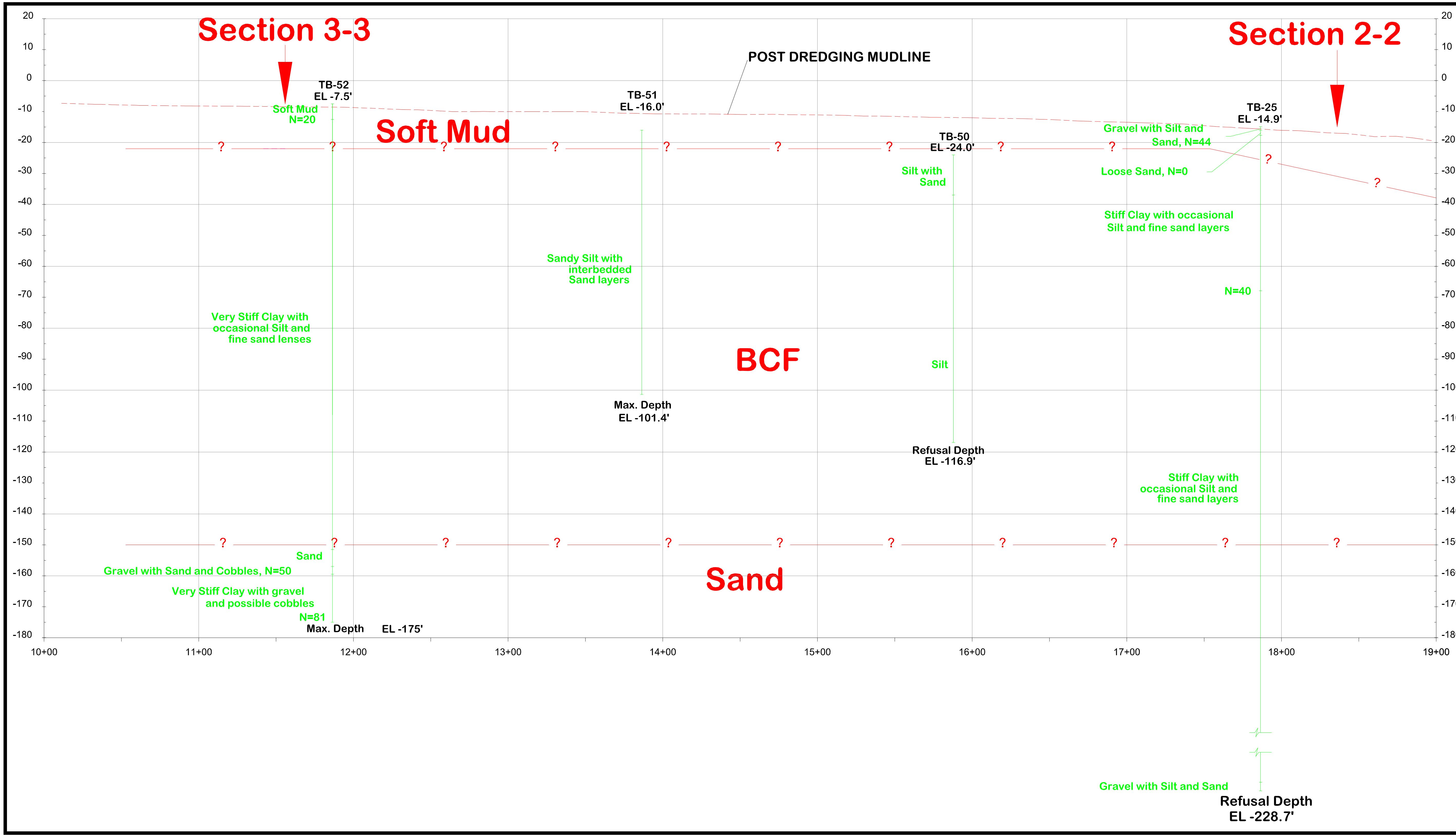

FIGURE 5.1-8a. Profile B-B, Longitudinal Profile 200 feet East of Proposed OCSP® Wall Face

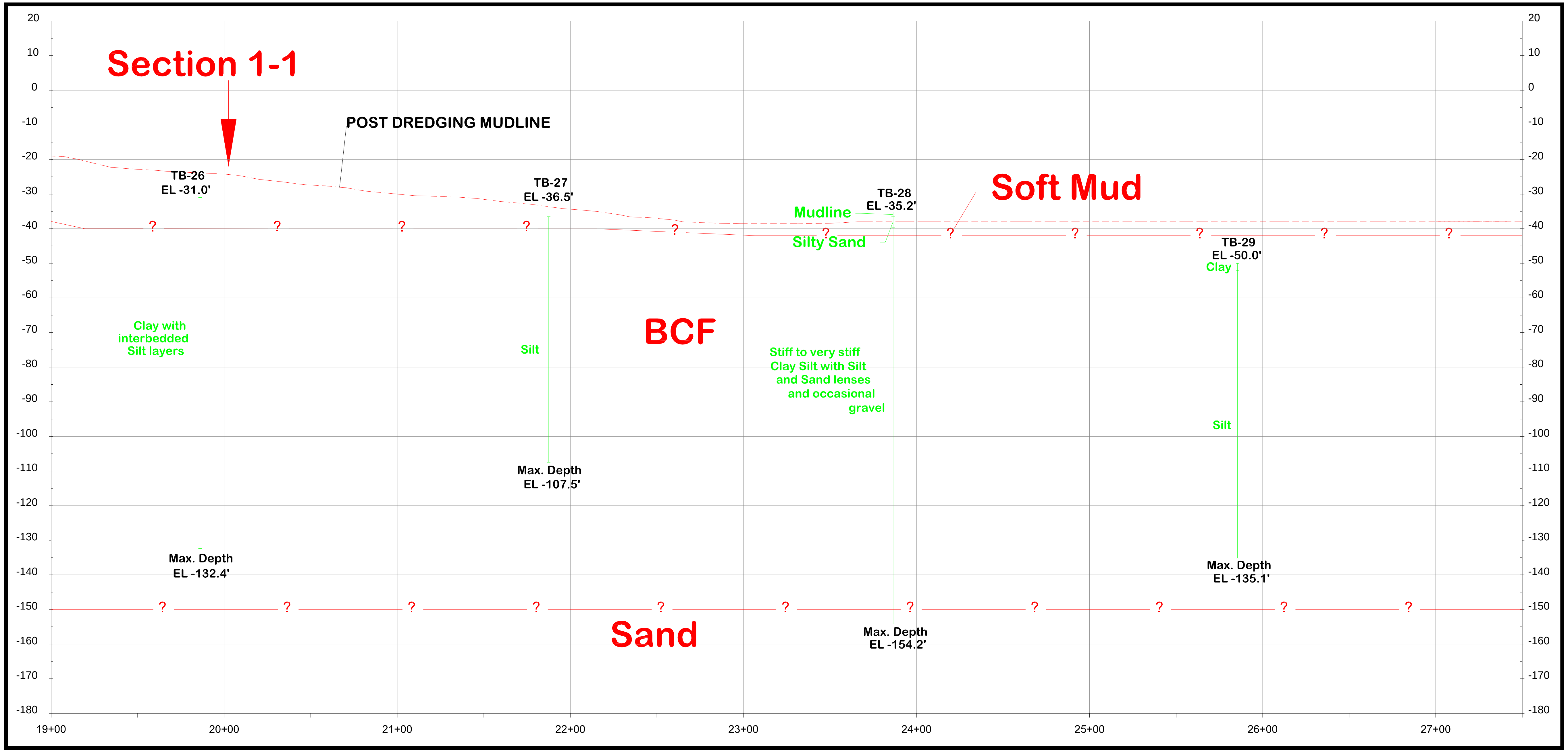

FIGURE 5.1-8b. Profile B-B, Longitudinal Profile 200 feet East of Proposed OCSP® Wall Face

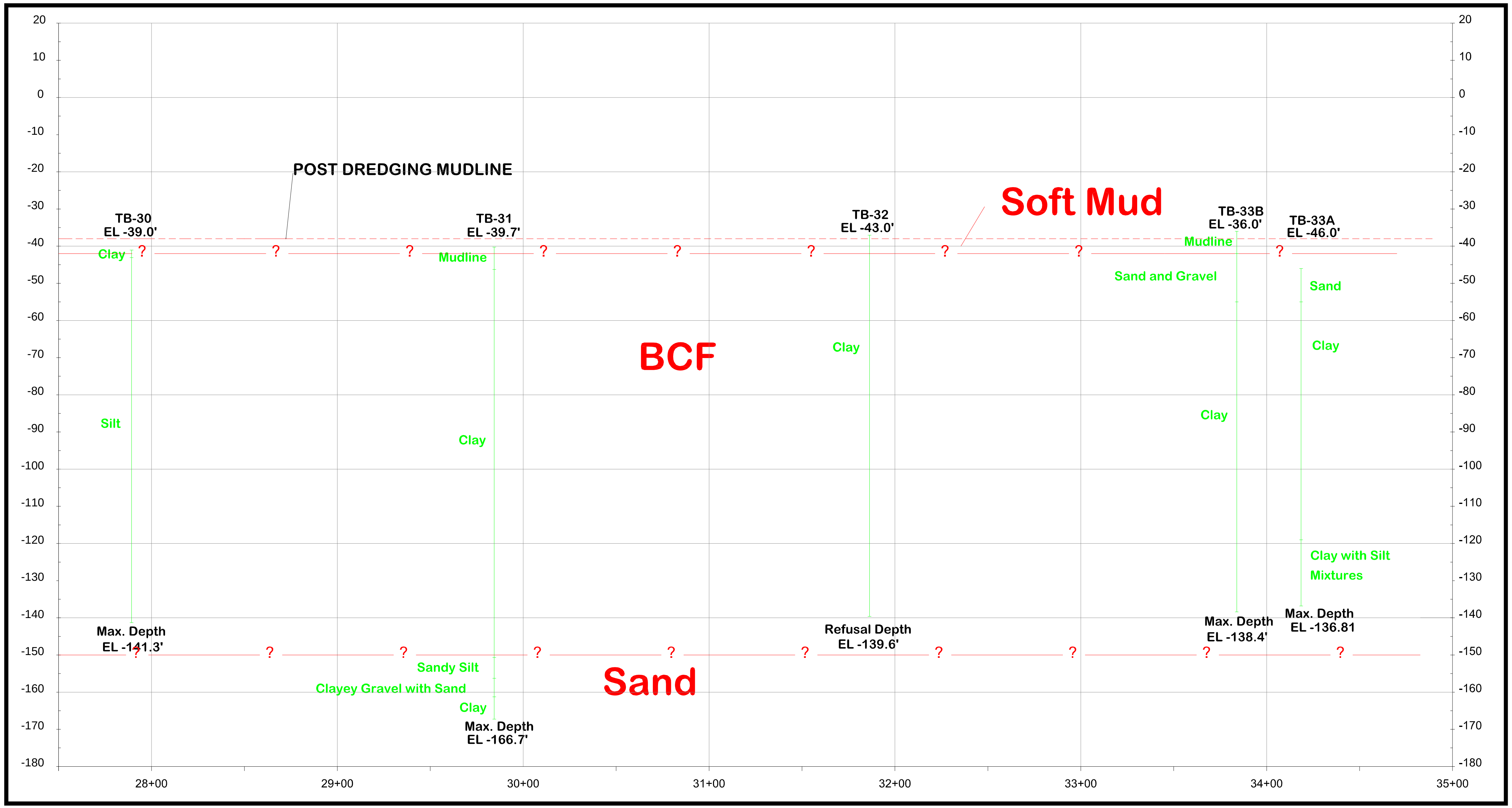

FIGURE 5.1-8c. Profile B-B, Longitudinal Profile 200 feet East of Proposed OCSP® Wall Face

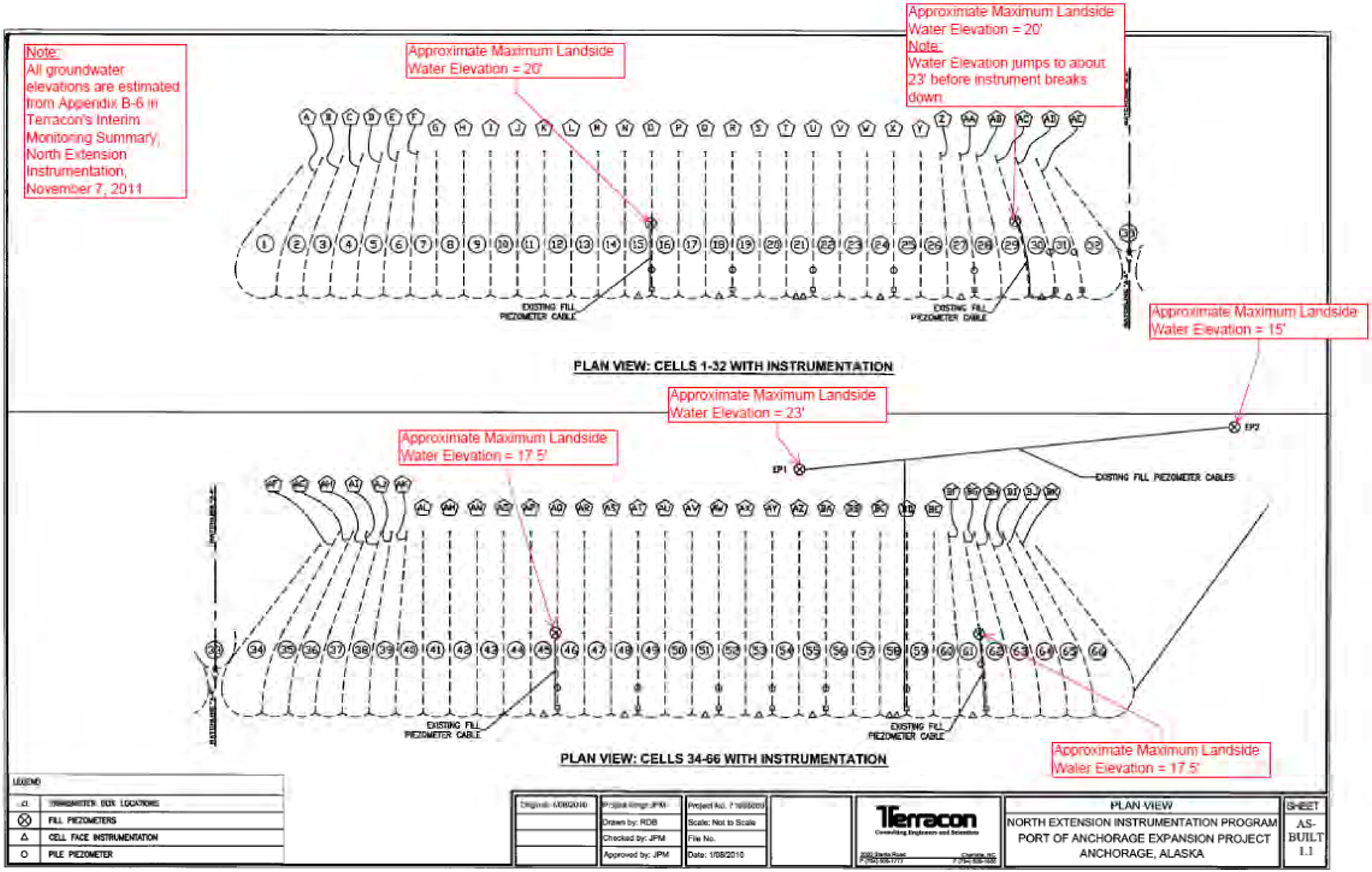

FIGURE 5.1-9a. Summary of Maximum Landside Groundwater Readings (Terracon, 2011)

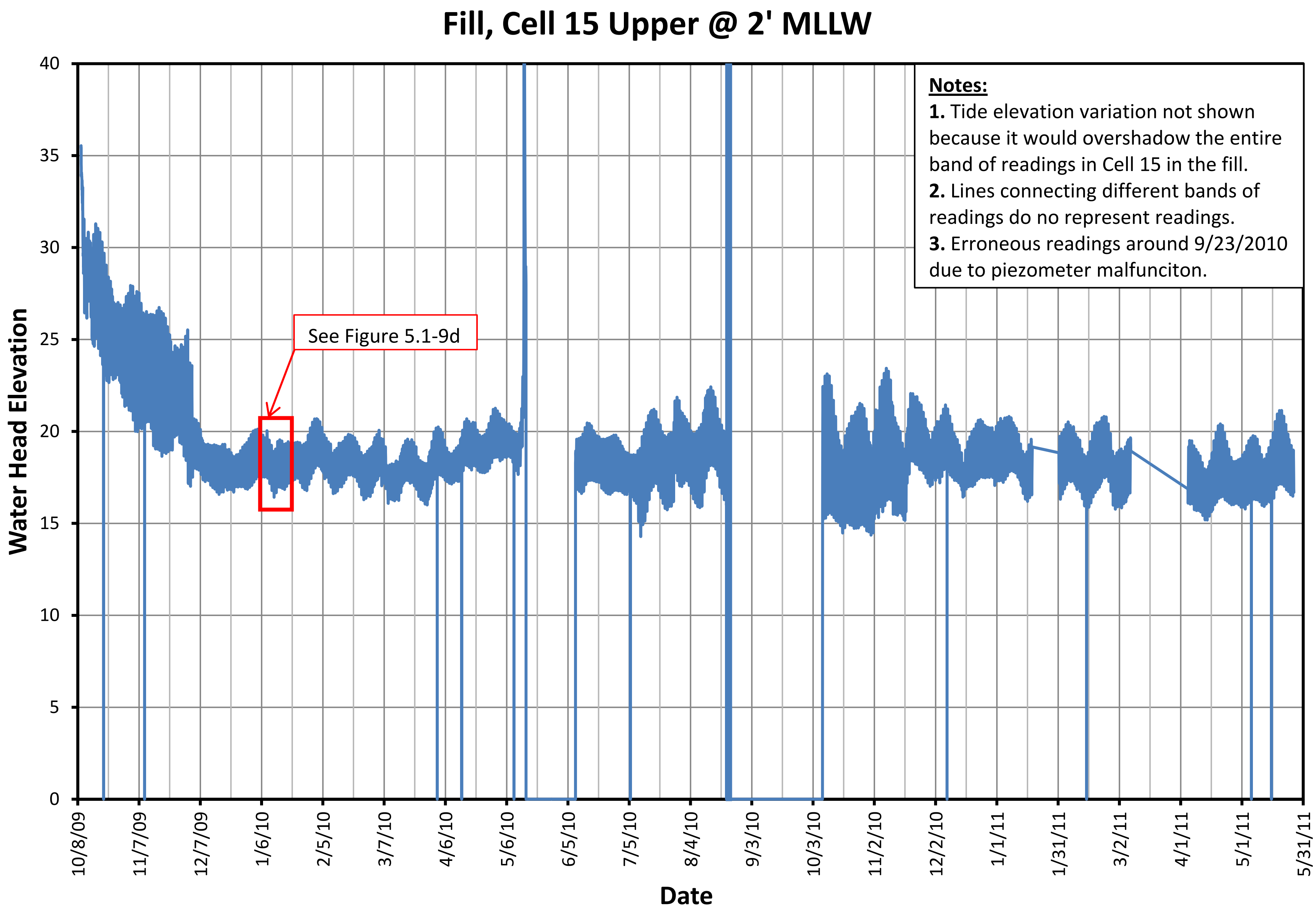

FIGURE 5.1-9b. Landside Groundwater Readings in Cell 15 Fill Piezometer (2 readings/hr)

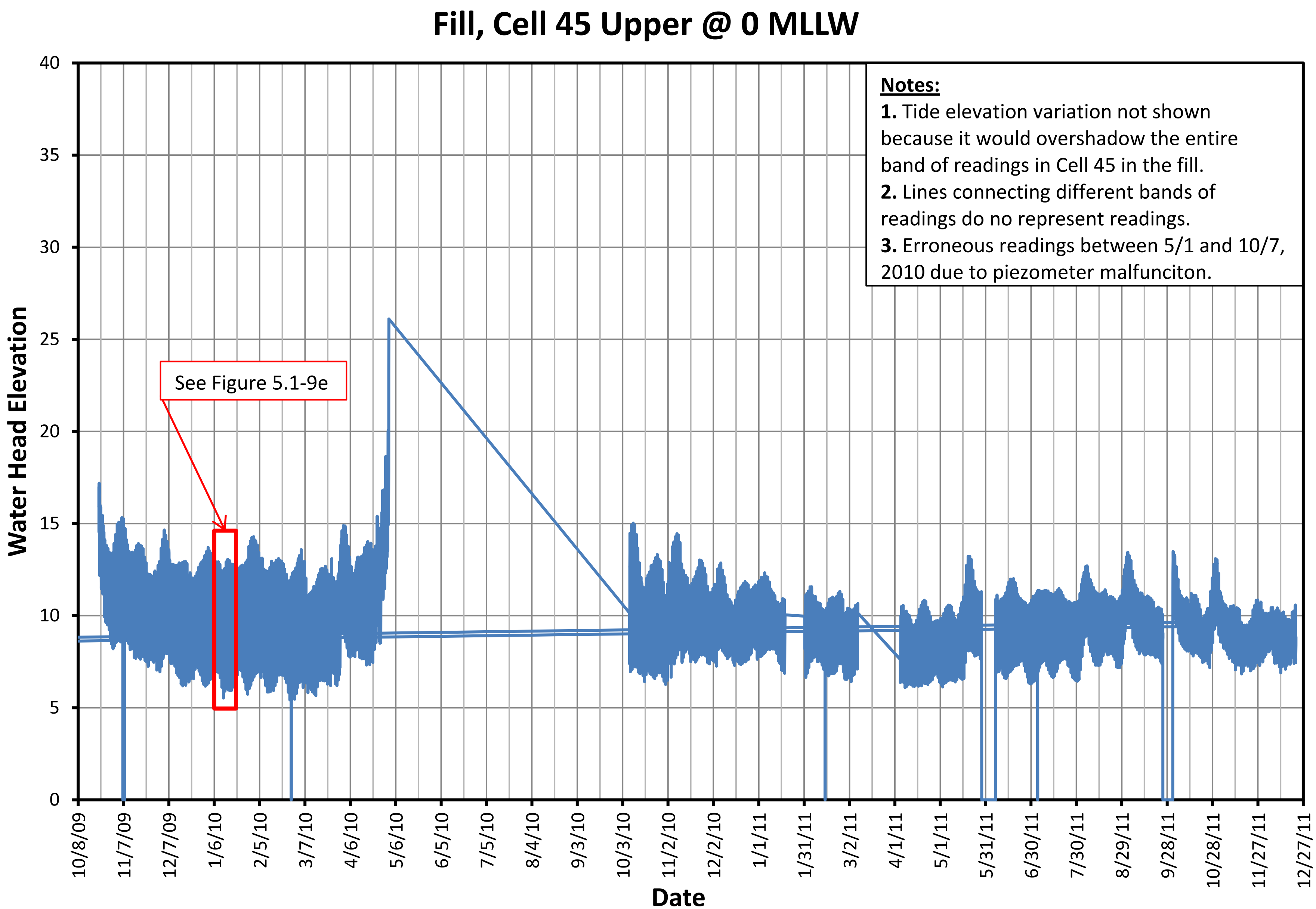

FIGURE 5.1-9c. Landside Groundwater Readings in Cell 45 Fill Piezometer (2 readings/hr)

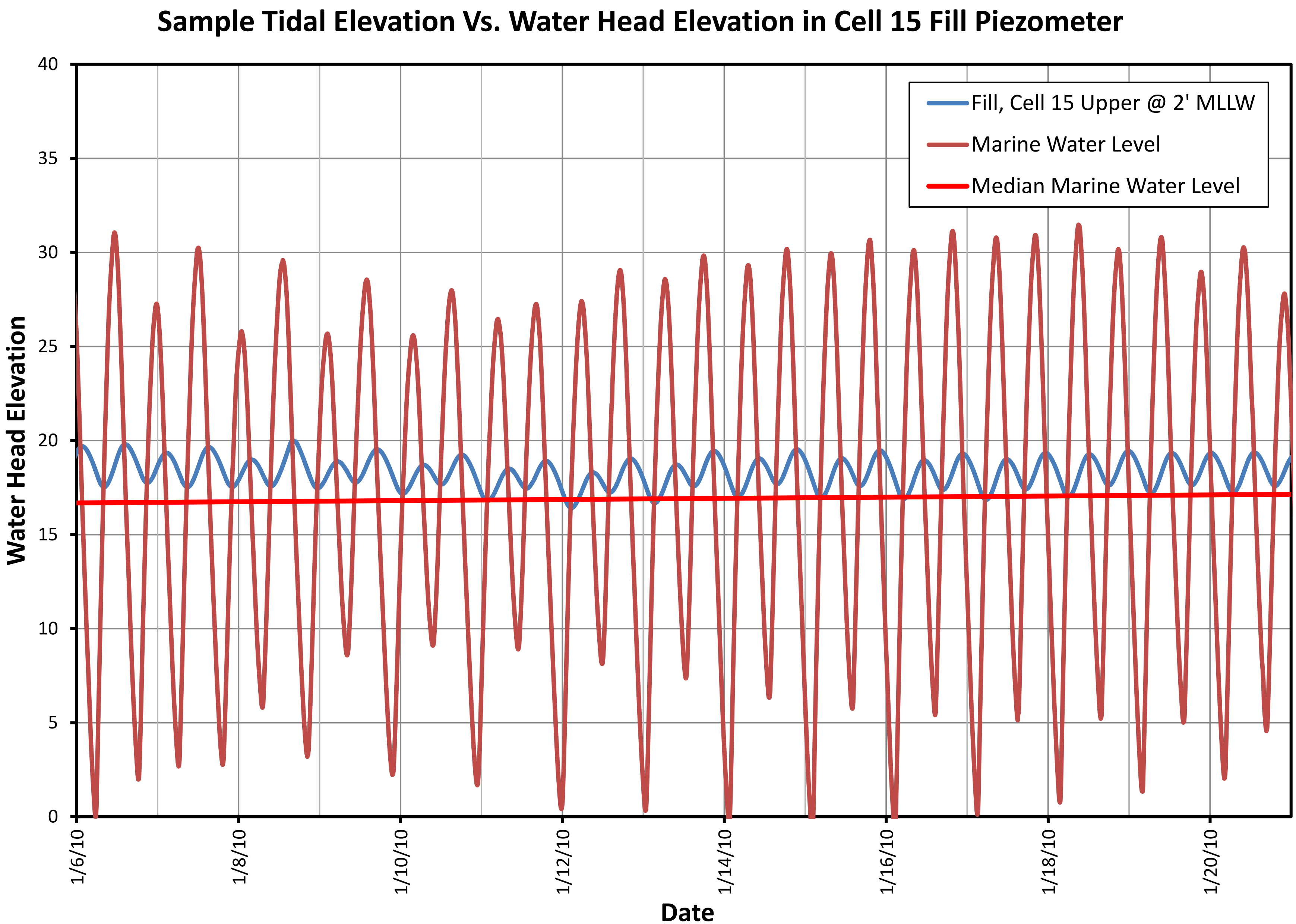

FIGURE 5.1-9d. Variation of Tide Water Elevation with Cell 15 Fill Piezometer Elevation (2 readings/hr over 2 weeks)

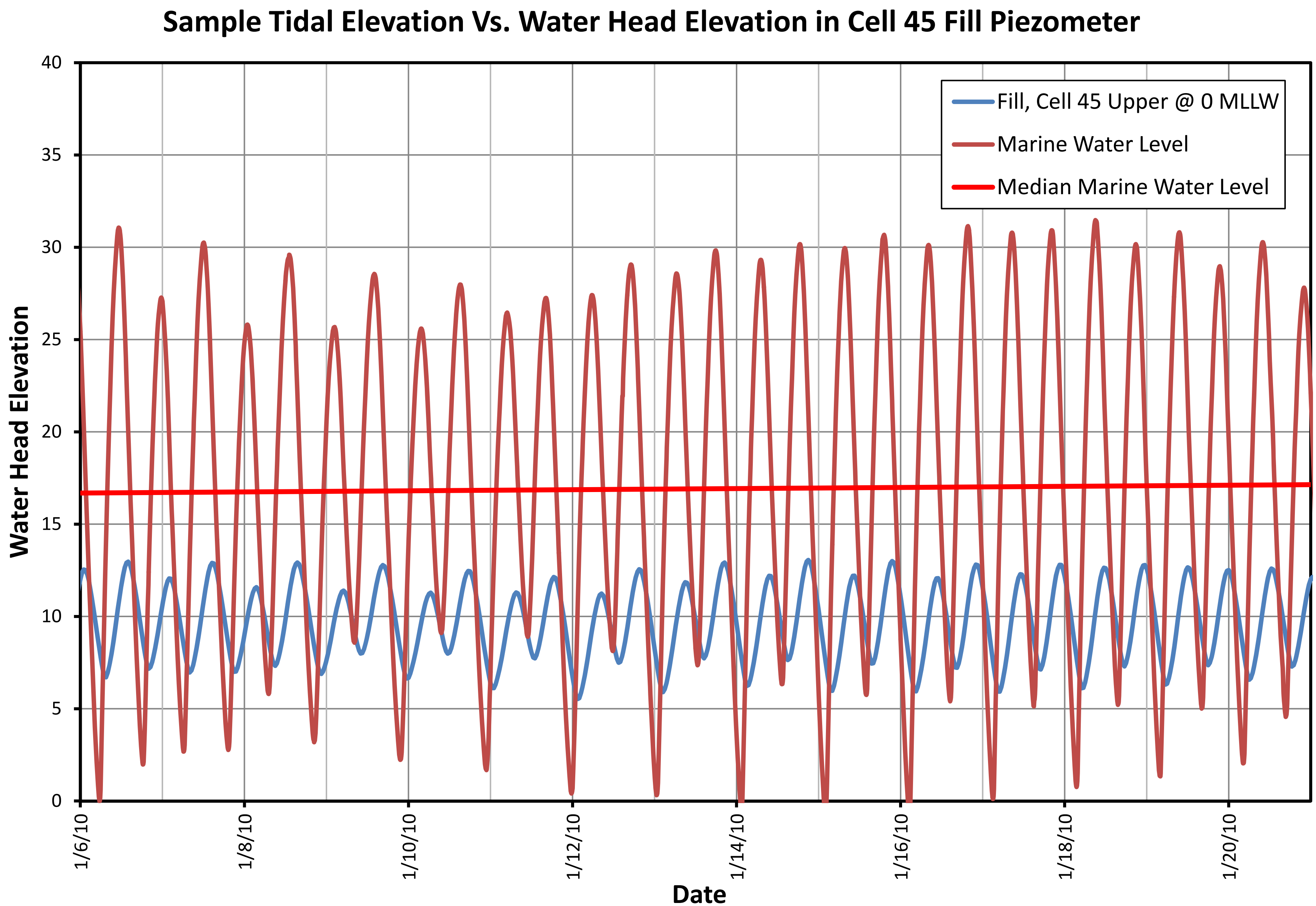

FIGURE 5.1-9e. Variation of Tide Water Elevation with Cell 45 Fill Piezometer Elevation (2 readings/hr over 2 weeks)

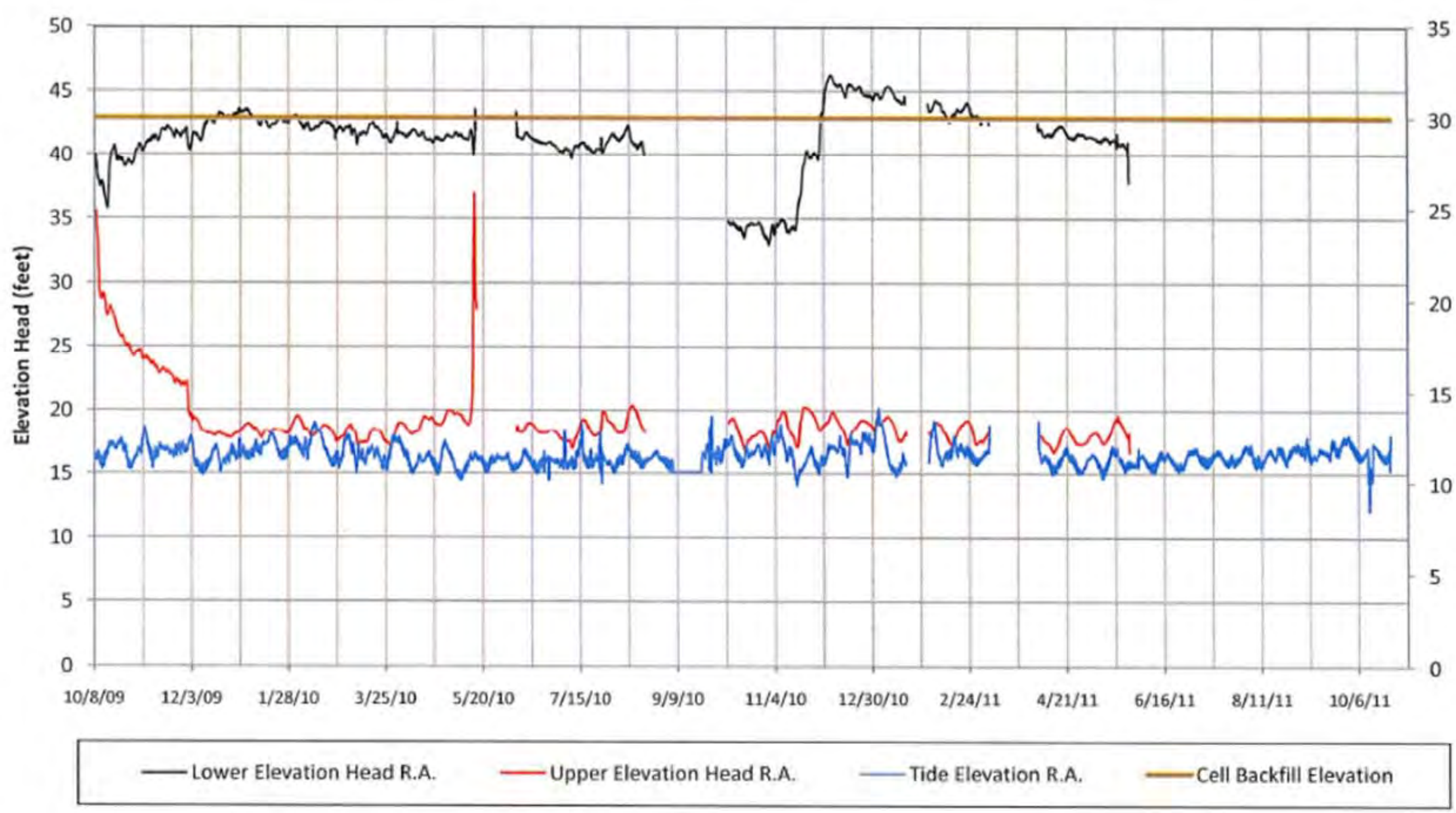

Notes*:

1. Piezometer monitoring began on October 9, 2009
2. Piezometer elevations (MLLW): Upper ~ +2 ft, Lower ~ -72 ft
3. R.A. = Rolling average of +/-24 readings

*Additional notes in Appendix B-1

Terracon

Port of Anchorage Expansion - North Extension

Terracon Project No. 71095009, Task 300

Cell 15 Fill Piezometers

Pore Pressure vs. Time

November 7, 2011 | Figure No. FP-01

FIGURE 5.1-9f. Cell 15 Fill Piezometer Pore Pressure vs. Time (Terracon, November 2011)

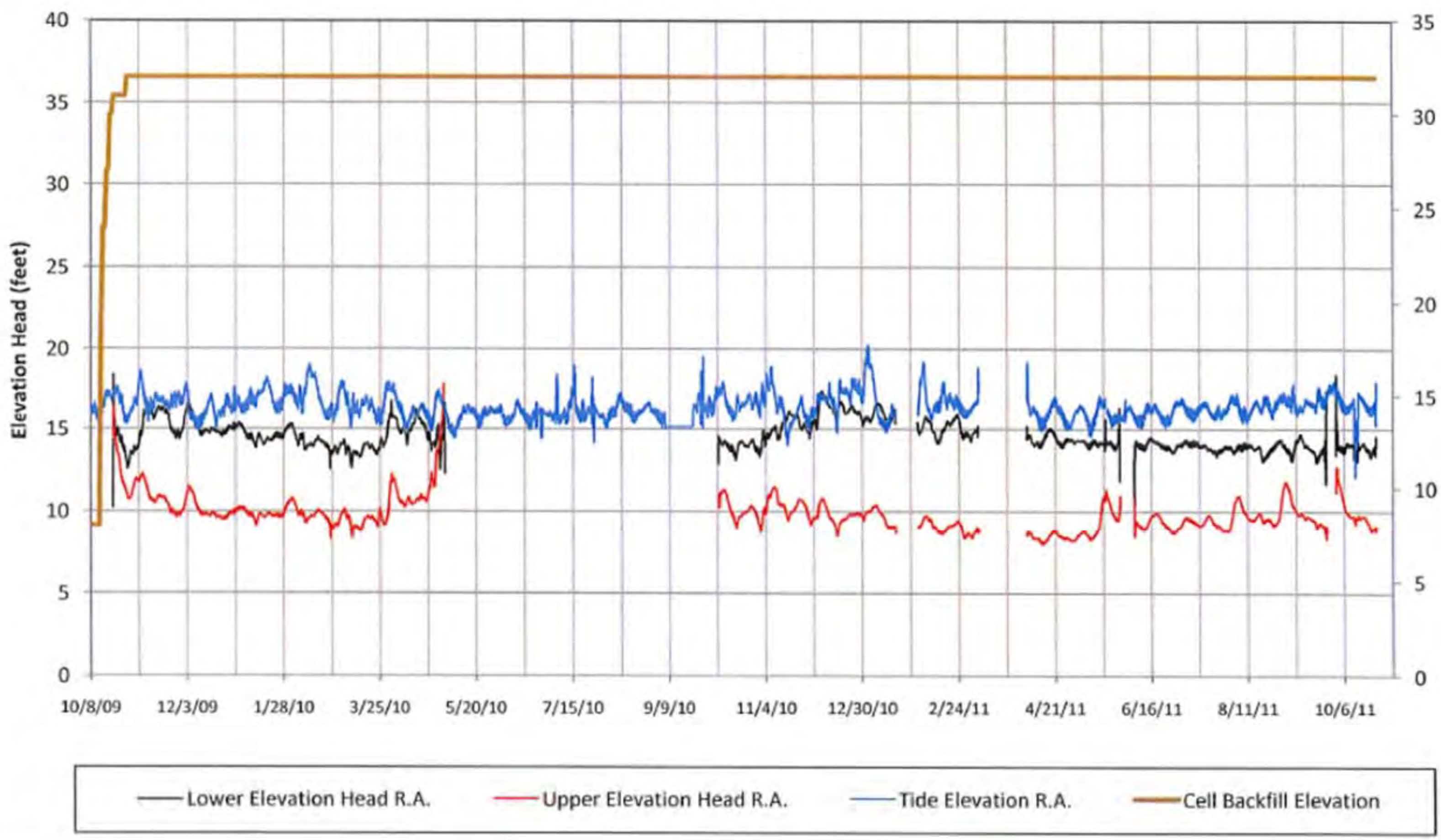

Notes*:

1. Piezometer monitoring began on October 21, 2009
2. Piezometer elevations (MLLW): Upper ~ 0 ft, Lower ~ -45 ft
3. R.A. = Rolling average of +/-24 readings

*Additional notes in Appendix B-1

Terracon

Port of Anchorage Expansion - North Extension	
Terracon Project No. 71095009, Task 300	
Cell 45 Fill Piezometers	
Pore Pressure vs. Time	
November 7, 2011	Figure No. FP-03

FIGURE 5.1-9g. Cell 45 Fill Piezometer Pore Pressure vs. Time (Terracon, 2011)

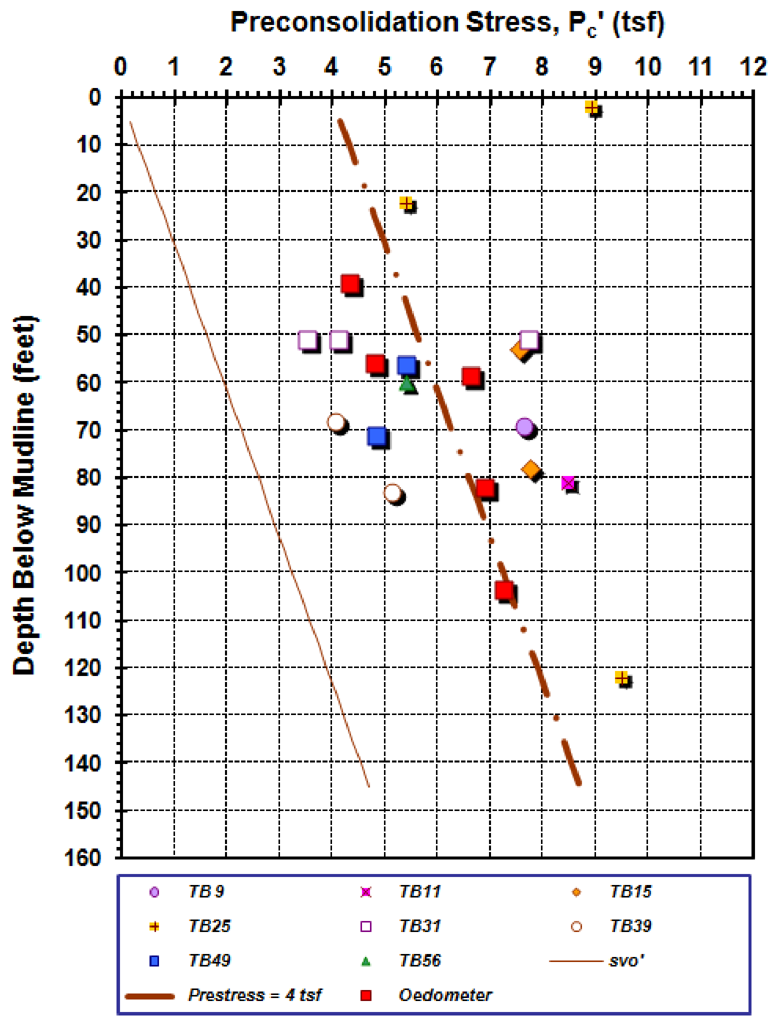

FIGURE 5.1-10. Interpretation of Pre-consolidation Stress from CICU and One-Dimensional Consolidation Tests (Developed by Paul Mayne, 2004)

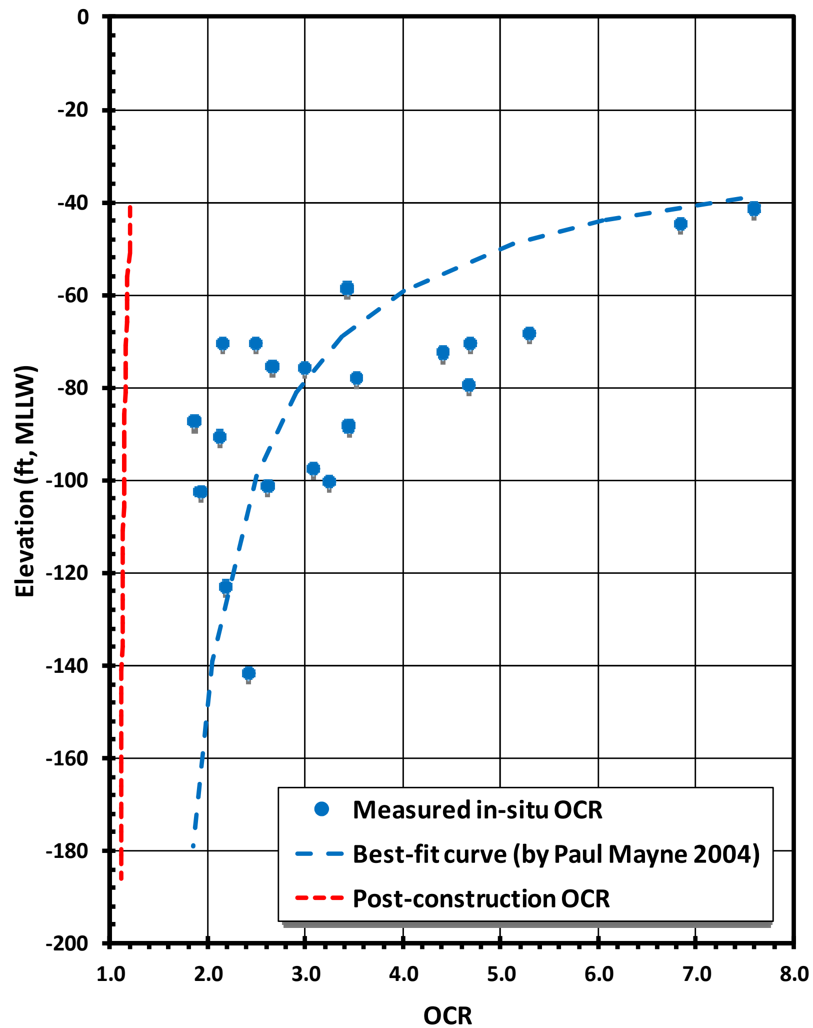

FIGURE 5.1-11. In-situ and Post-Construction OCR Profile of the BCF Clay

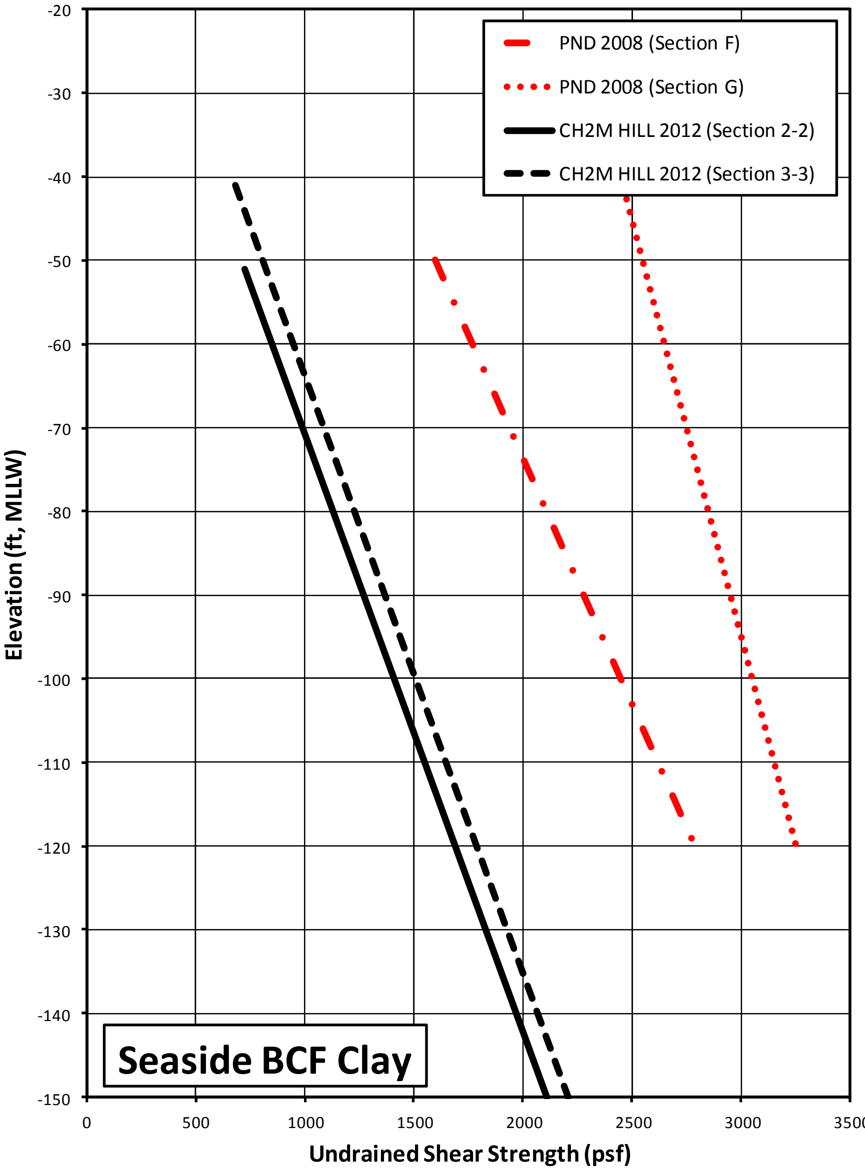

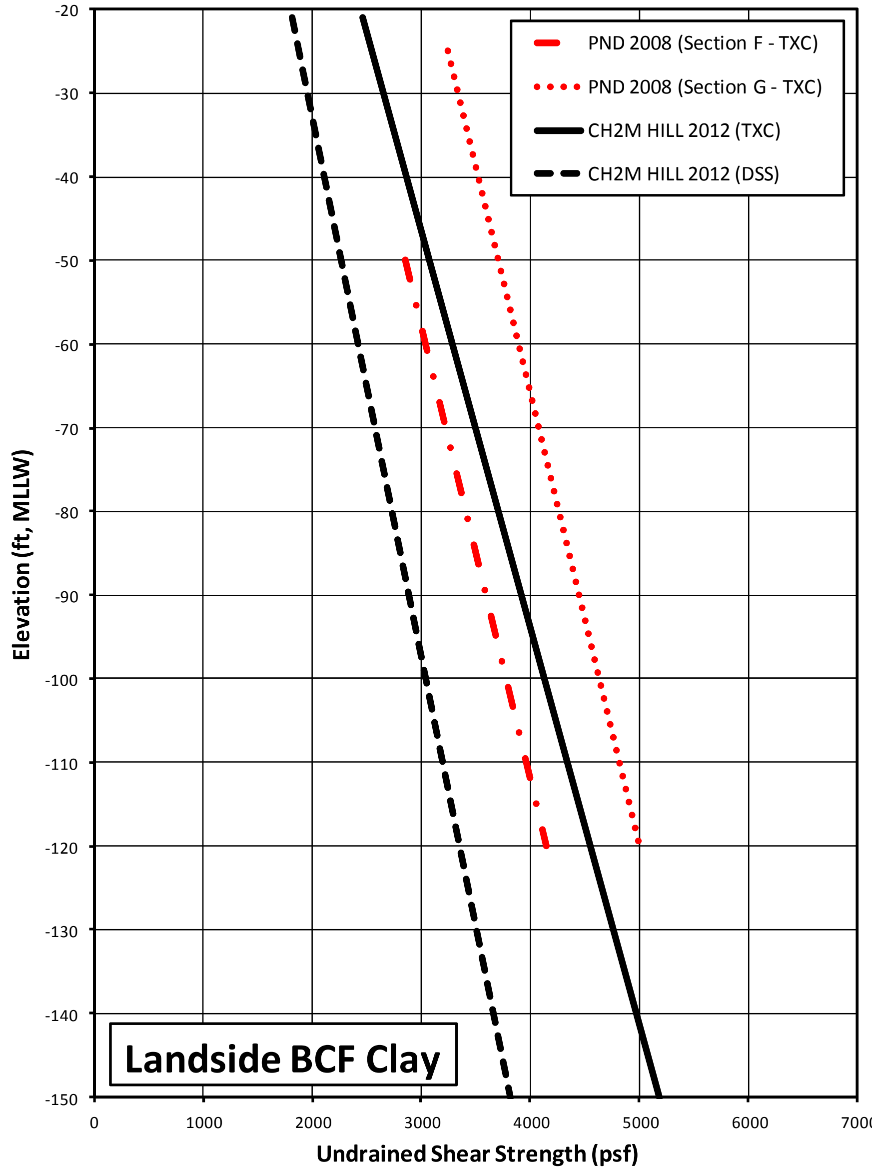

FIGURE 5.1-12. Undrained Shear Strength (S_u) of the BCF Clay

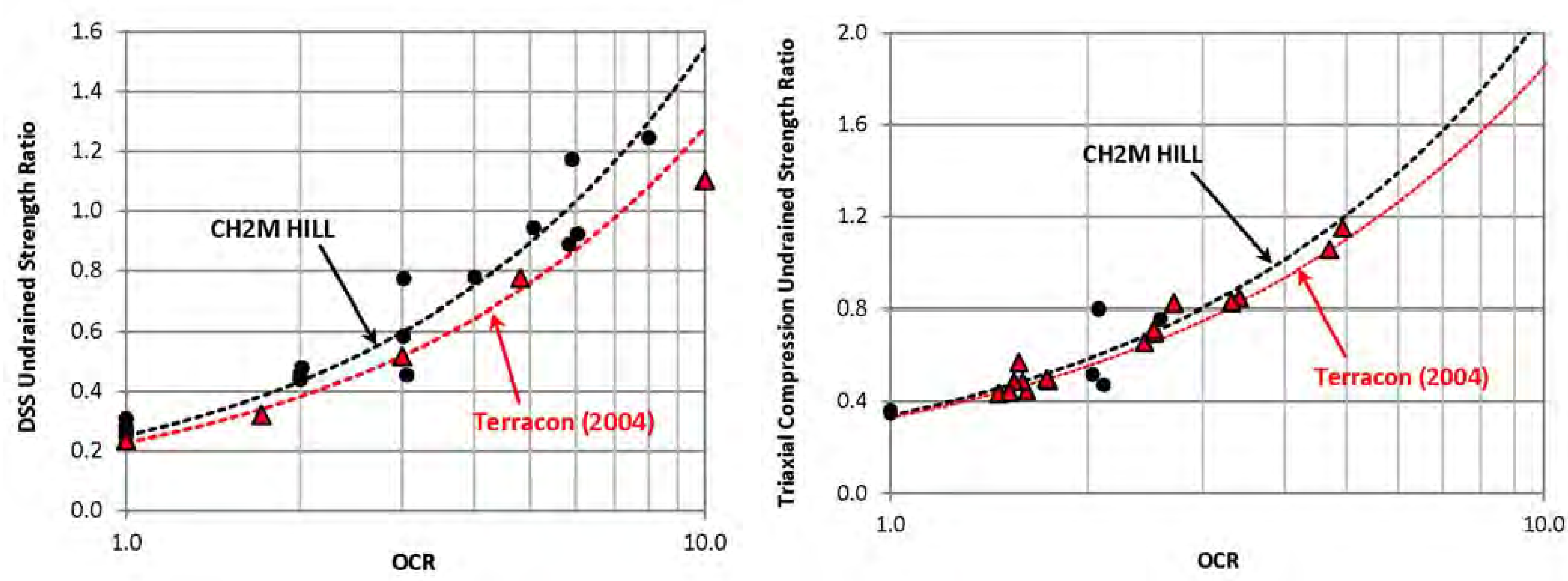

FIGURE 5.1-13. SHANSEP Correlations for the BCF Clay based on DSS and Triaxial Compression Test Results

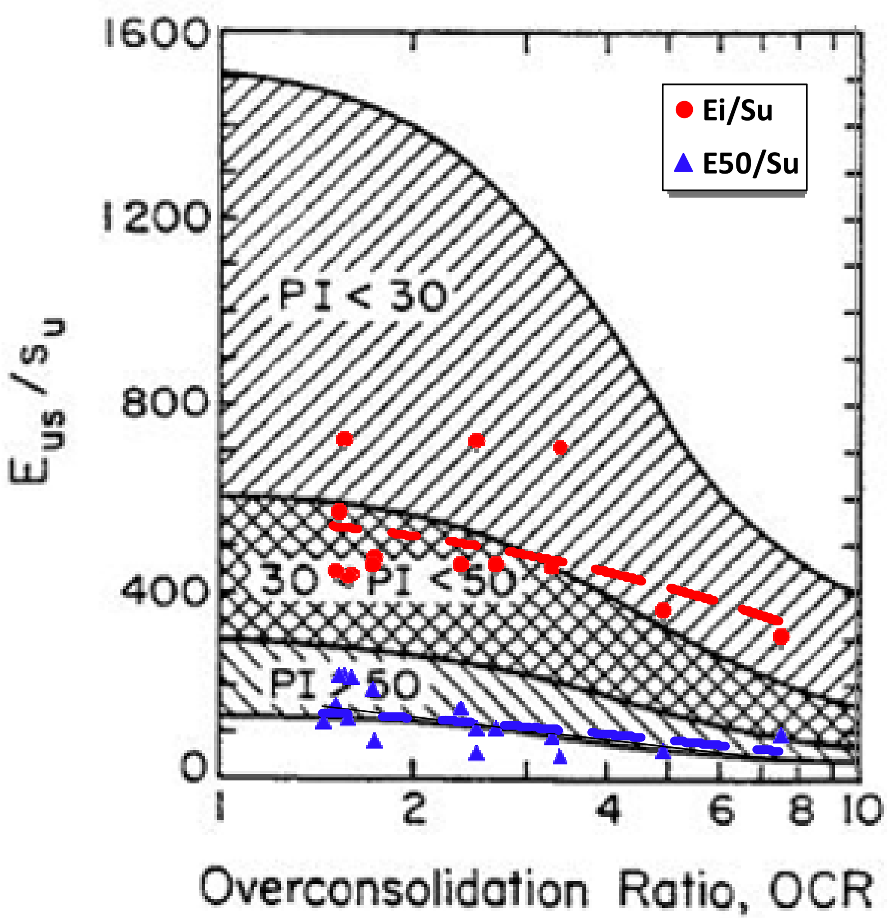

FIGURE 5.1-14. Undrained Moduli (E_i and E_{50}) of the BCF Clay as a Function of OCR (Duncan and Buchignani, 1976)

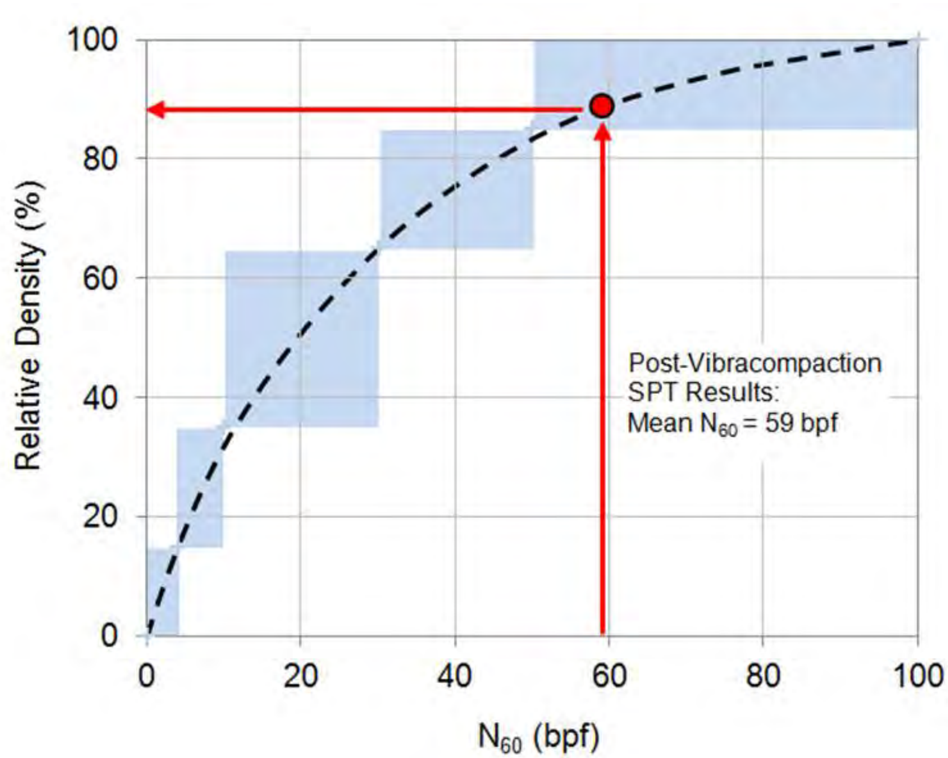

FIGURE 5.2-1. Empirical Relationship between Relative Density and SPT N60 Value (Terzaghi and Peck, 1967)

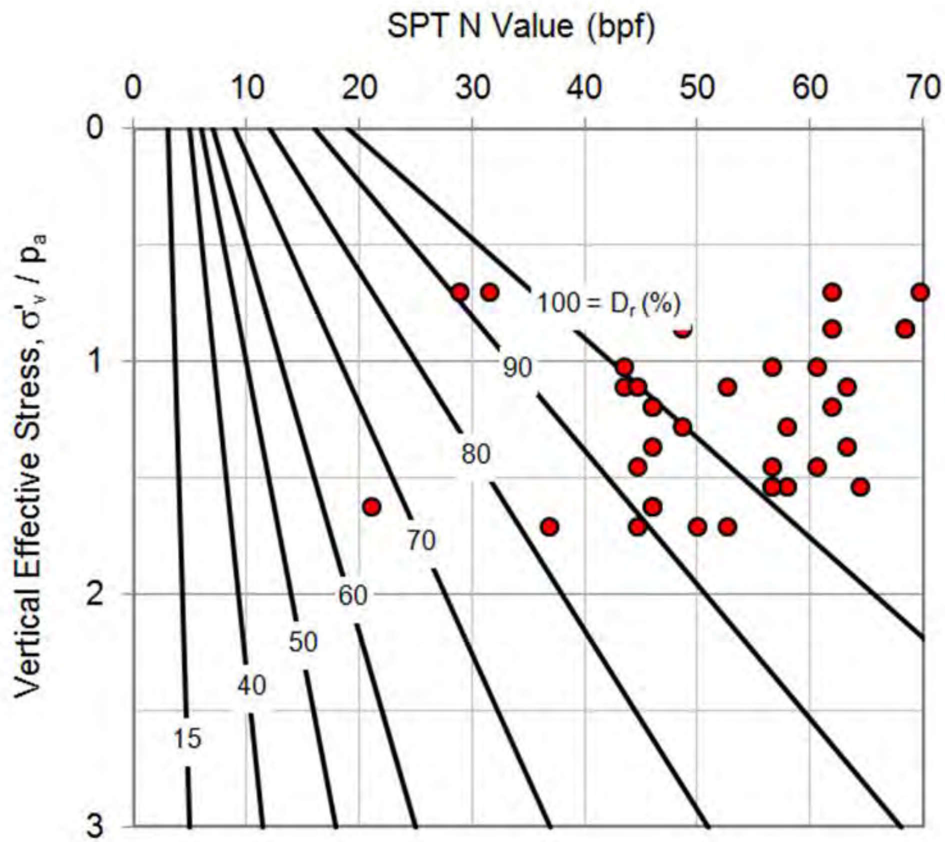

FIGURE 5.2-2. Empirical Relationship Between Relative Density, SPT N Value, and Vertical Effective Stress (Holtz and Gibbs, 1979)

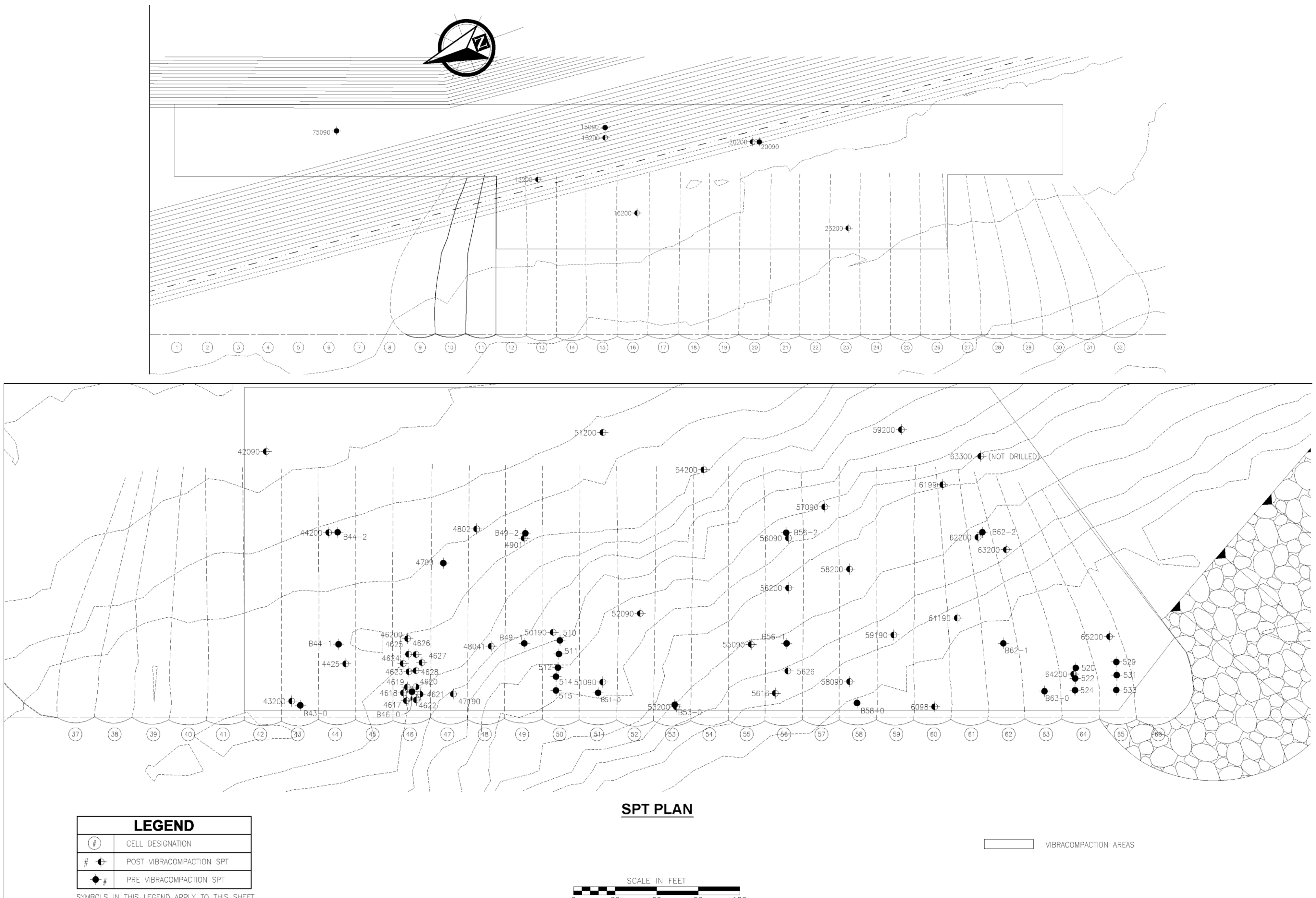

FIGURE 5.2-3. Post-Vibracompaction Boring Locations

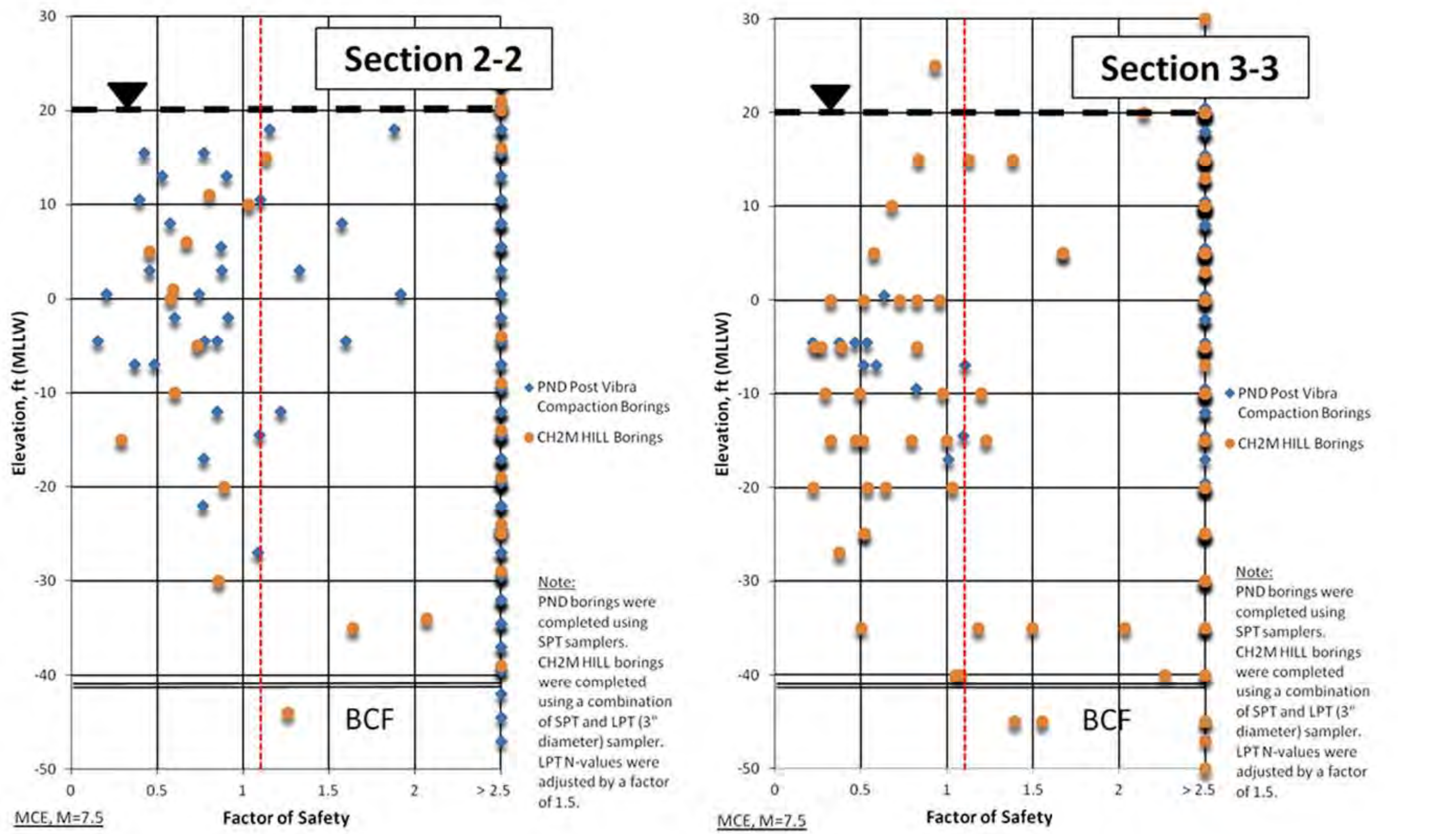

FIGURE 5.2-4. Liquefaction Factor of Safety for Granular Backfill at MCE Event (M7.5)

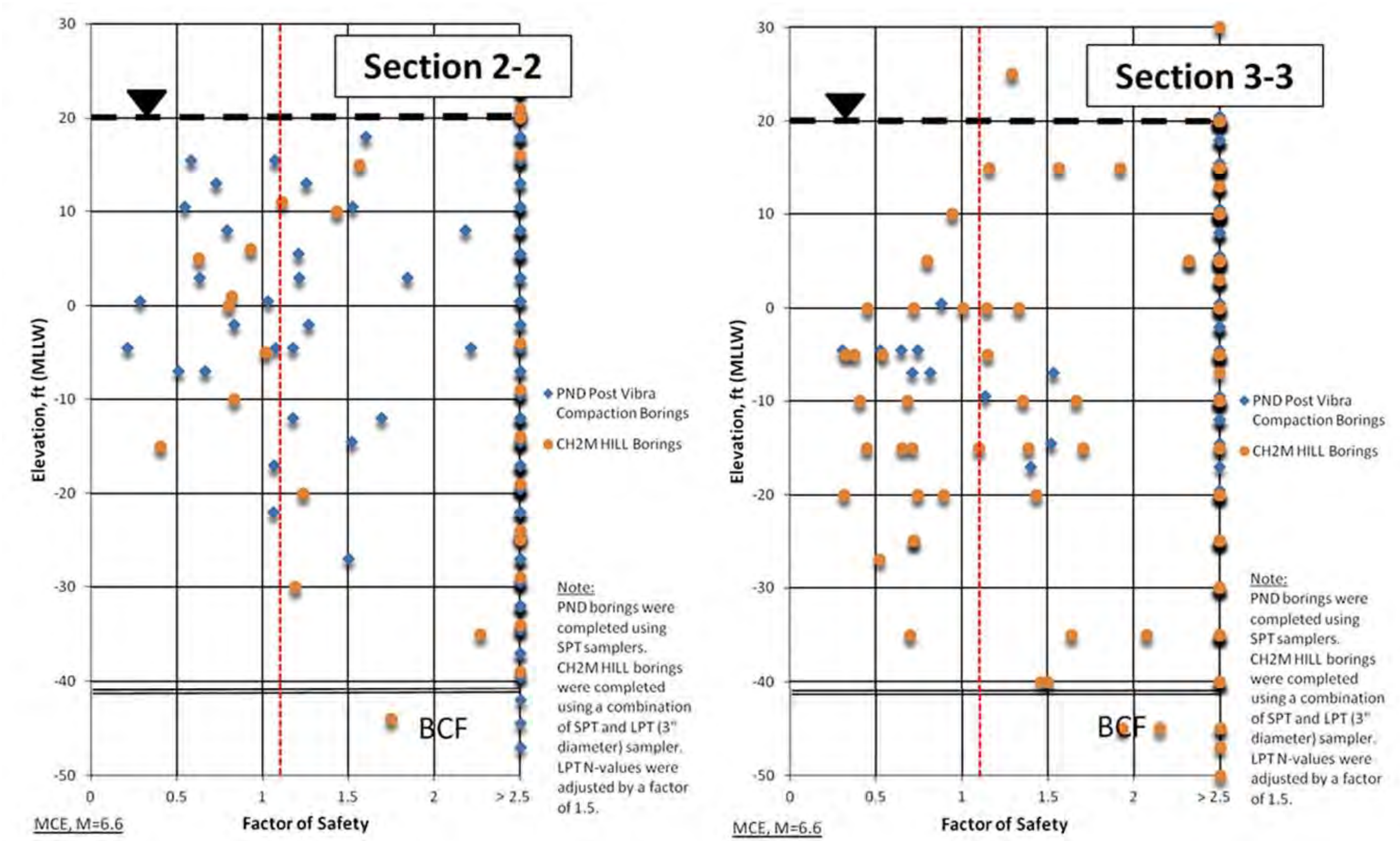

FIGURE 5.2-5. Liquefaction Factor of Safety for Granular Backfill at MCE Event (M6.6)

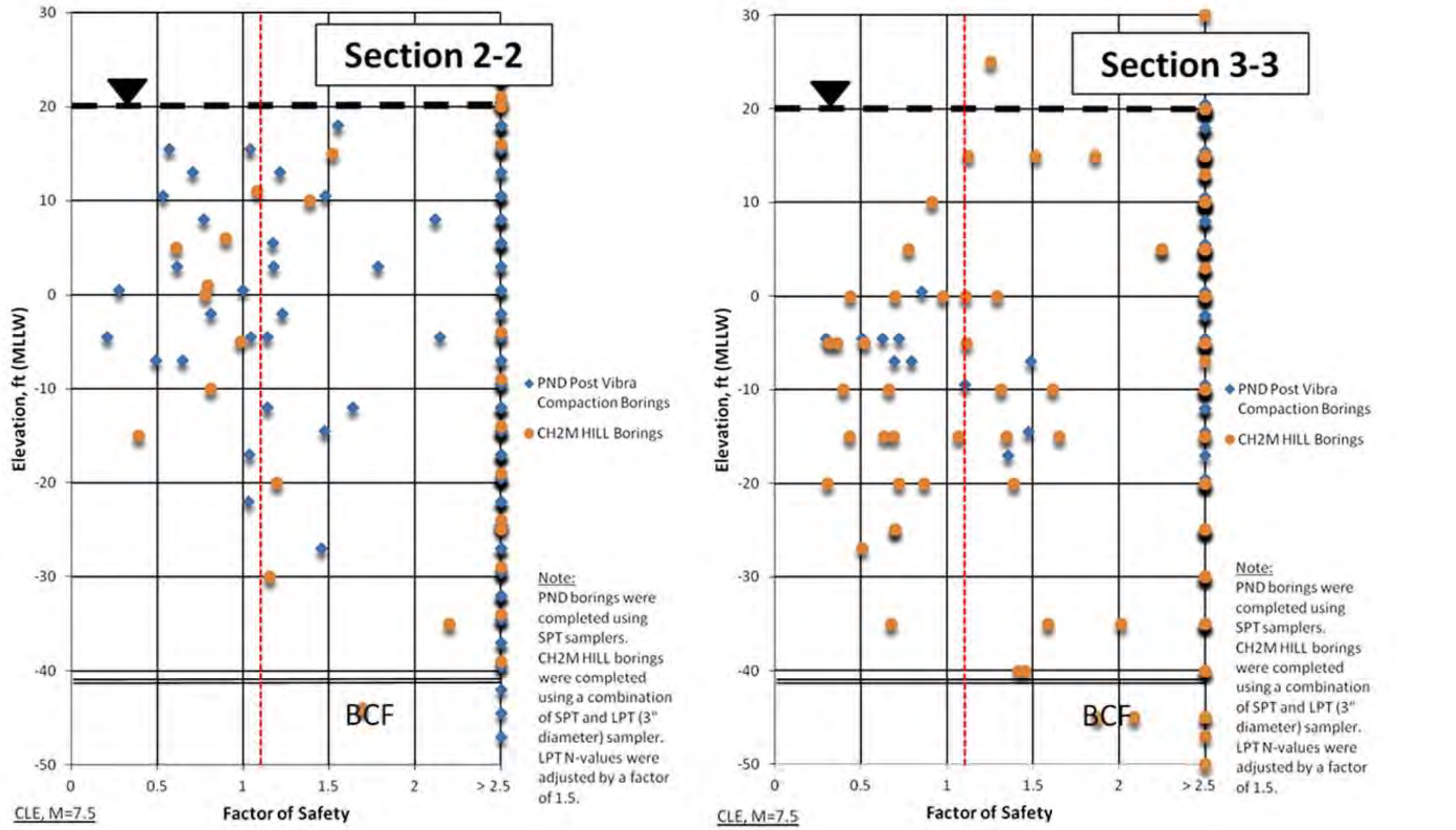

FIGURE 5.2-6. Liquefaction Factor of Safety for Granular Backfill at CLE Event (M7.5)

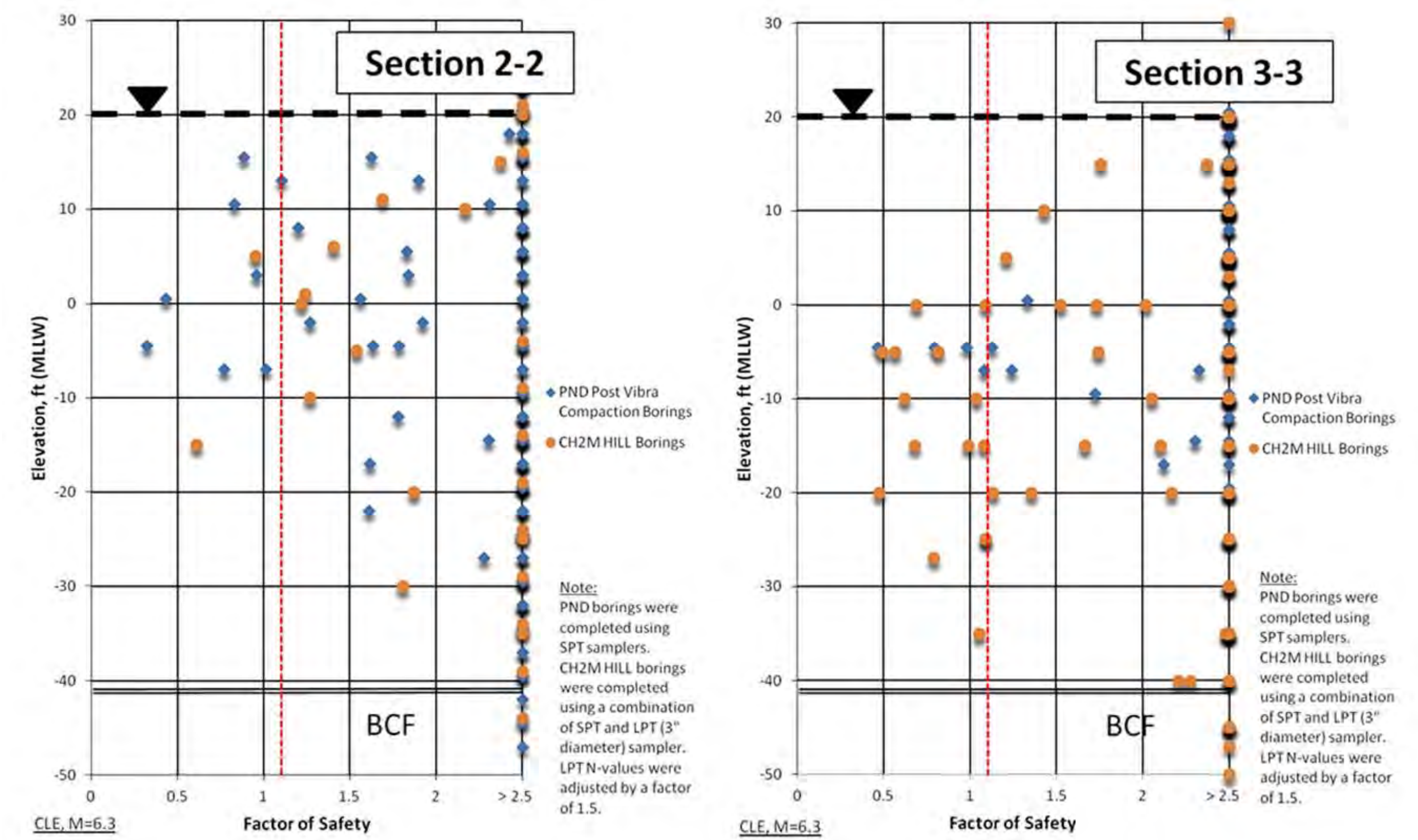

FIGURE 5.2-7. Liquefaction Factor of Safety for Granular Backfill at CLE Event (M6.3)

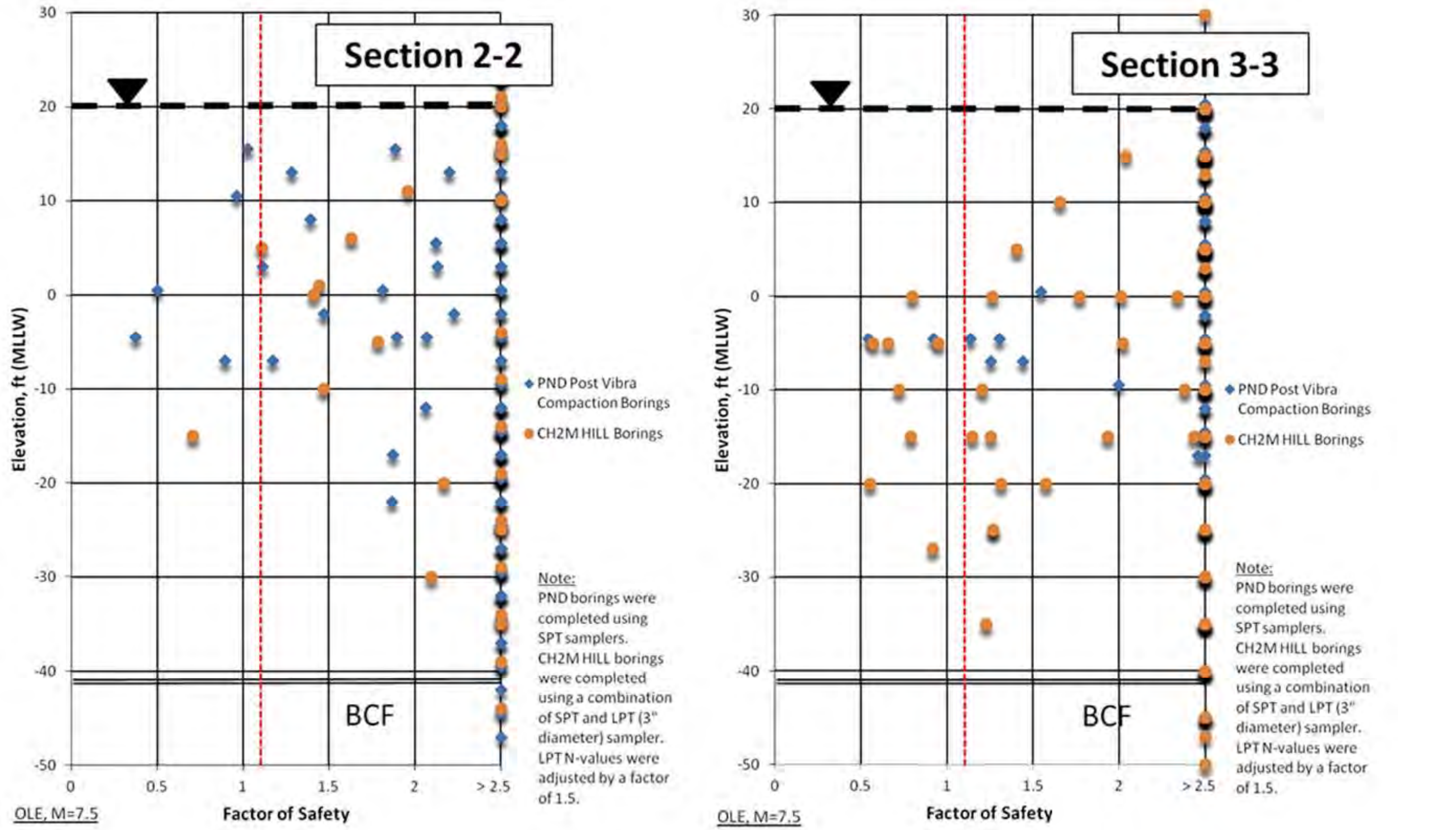

FIGURE 5.2-8. Liquefaction Factor of Safety for Granular Backfill at OLE Event (M7.5)

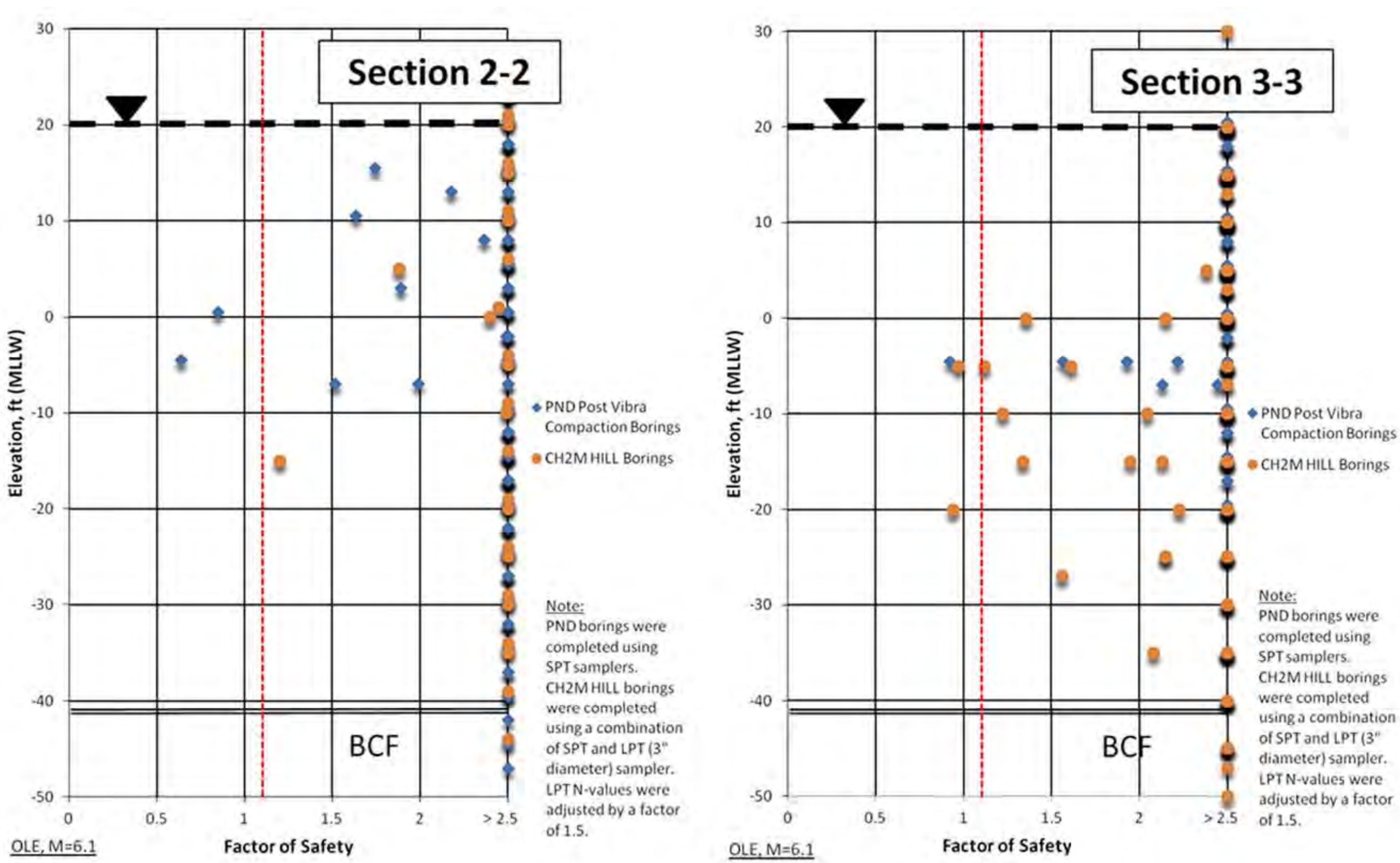

FIGURE 5.2-9. Liquefaction Factor of Safety for Granular Backfill at OLE Event (M6.1)

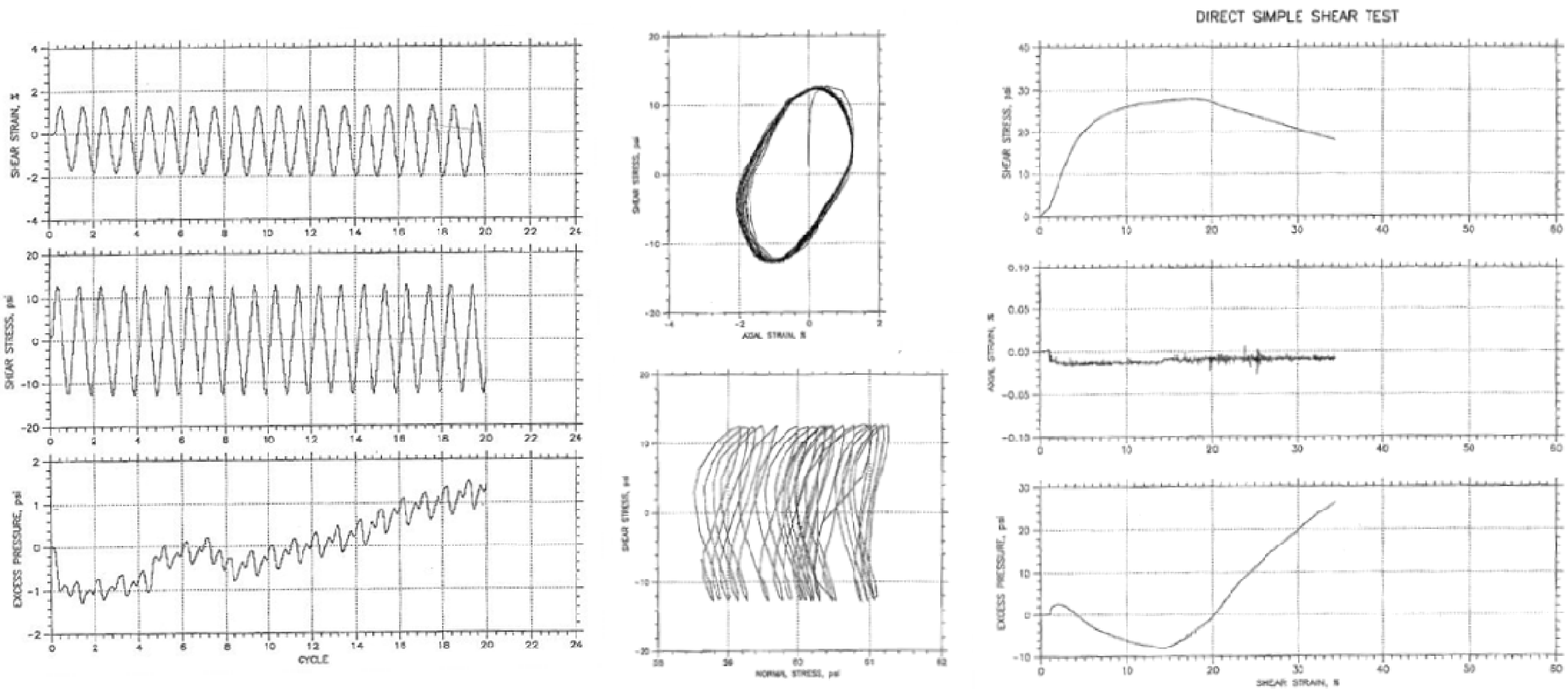

FIGURE 5.2-10a. Results from the Cycle-Controlled CyDSS Test (20 Cycles) Conducted on the BCF Clay below 50 feet from the Mudline (Terracon, 2004b; PND, 2008b)

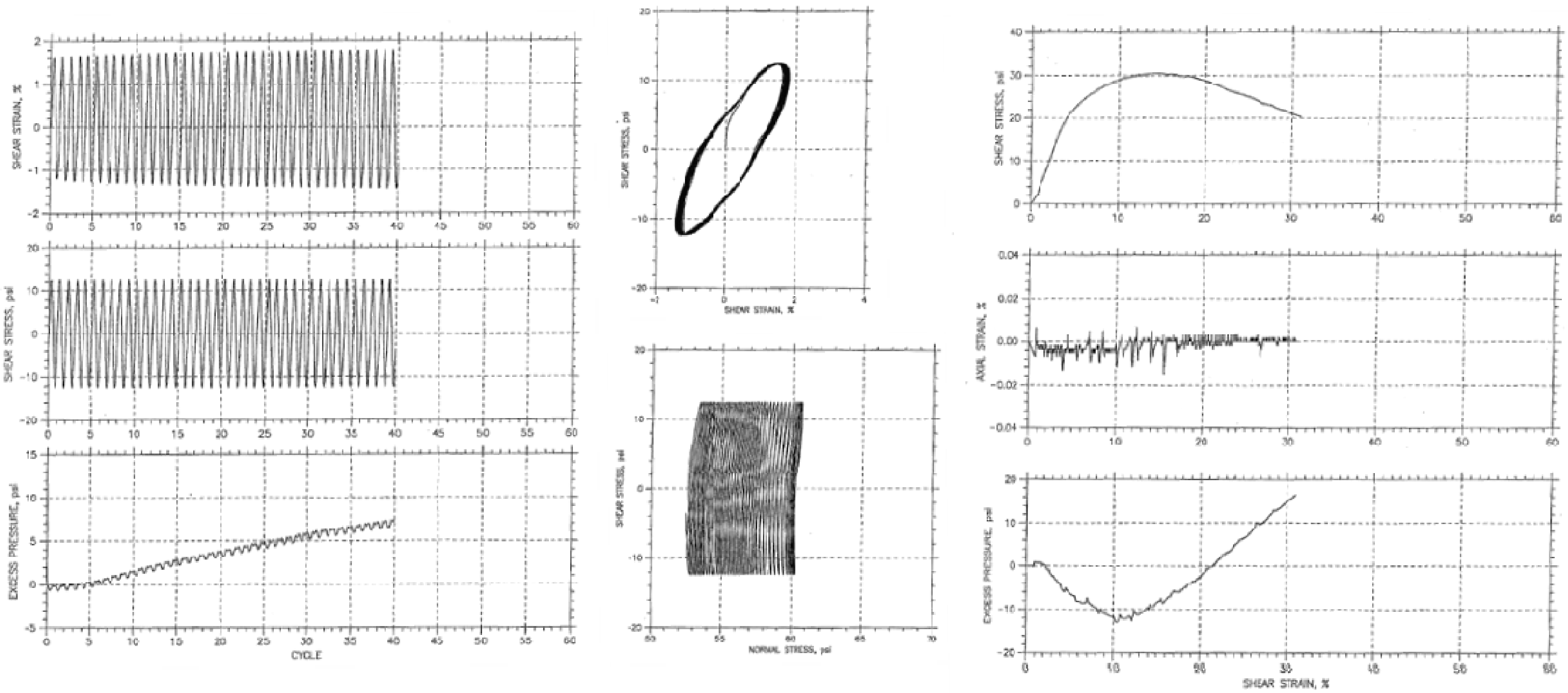

FIGURE 5.2-10b. Results from the Cycle-Controlled CyDSS Test (40 Cycles)
Conducted on the BCF Clay below 50 feet from the Mudline (Terracon, 2004b; PND, 2008b)

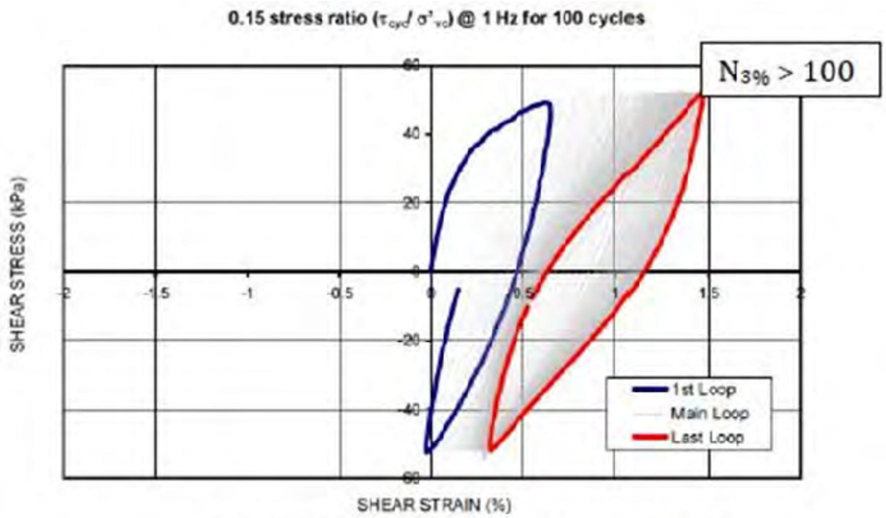

Results of Cyclic-DSS Test at OLE Stress Level

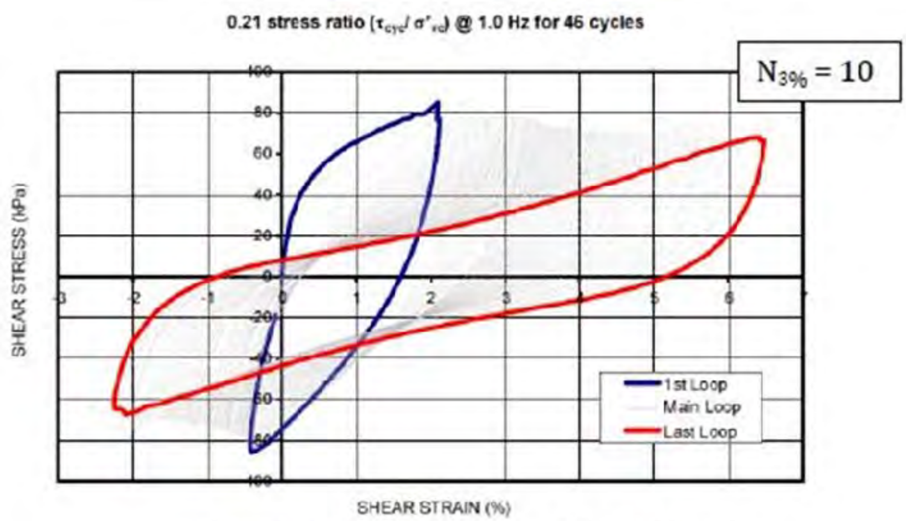

Results of Cyclic-DSS Test at CLE Stress Level

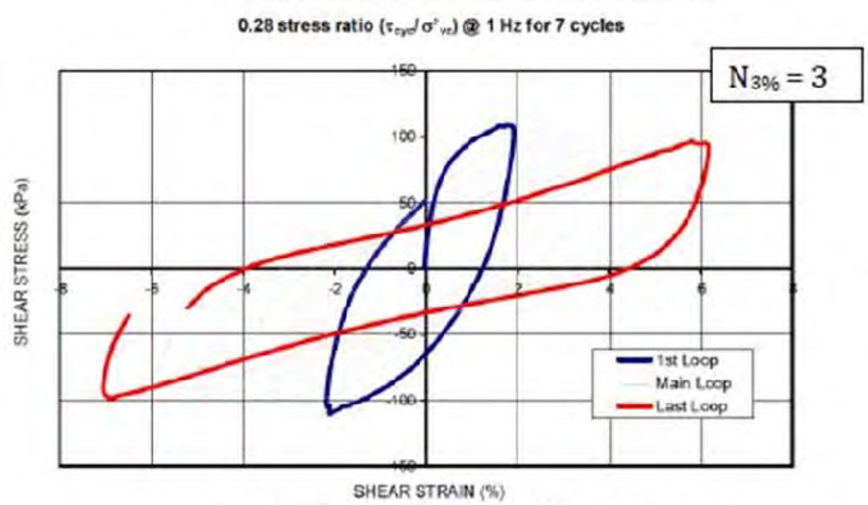

Results of Cyclic-DSS Test at MCE-Stress Level

FIGURE 5.2-10c. Stress-Controlled CyDSS Test Results Conducted on BCF Clay in the Upper 20 feet (PND, 2010)

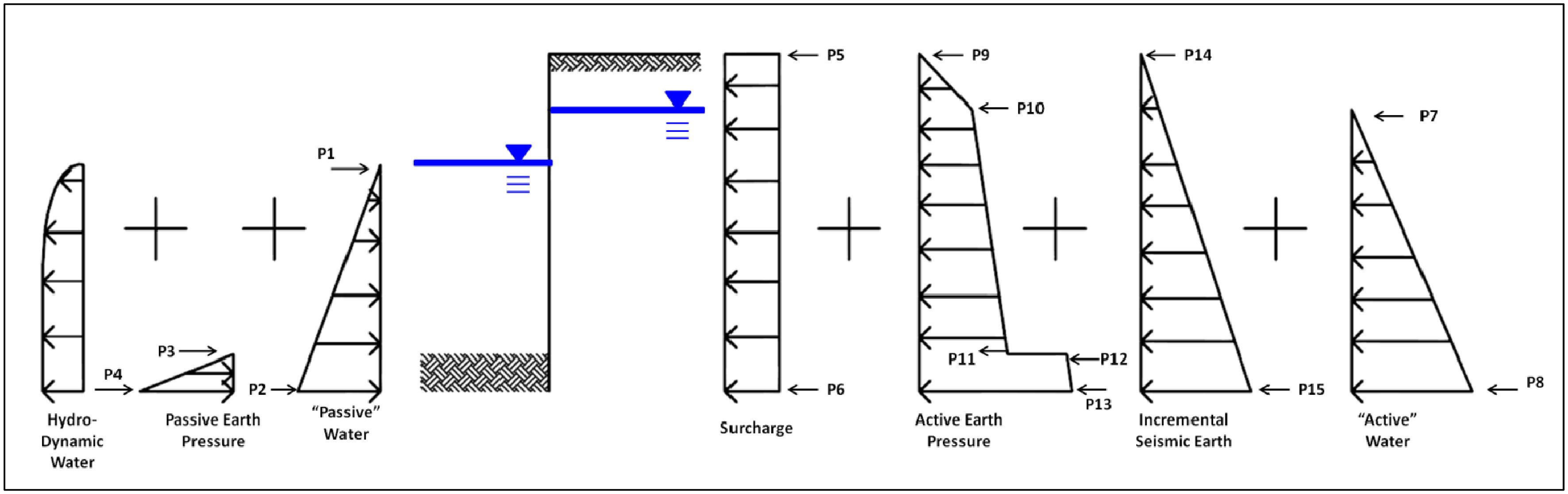

FIGURE 5.2-11. Static and Seismic Lateral Pressures Acting on OCSP® Face Sheets

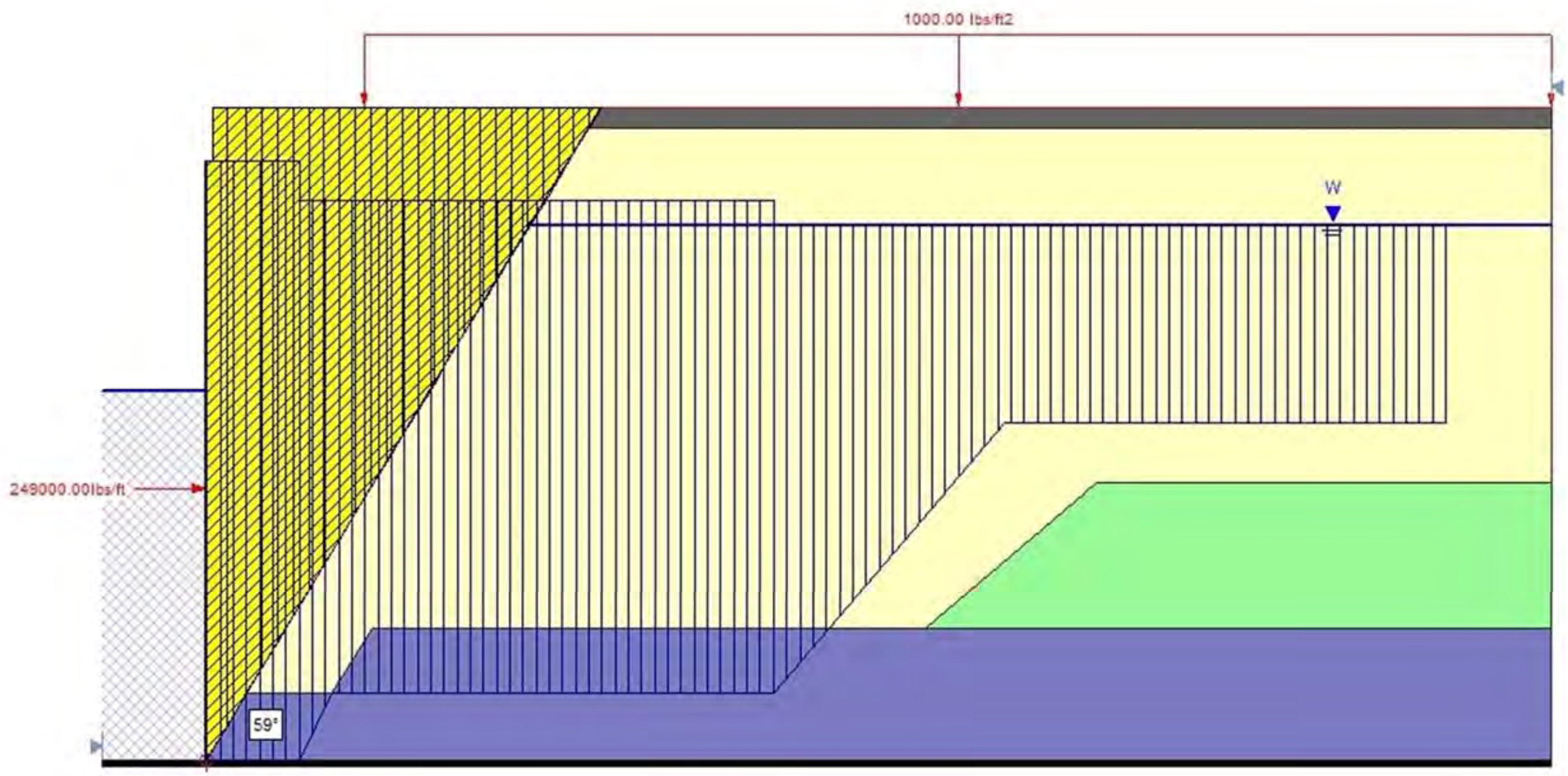

FIGURE 5.2-12. Example Generalized Limit Equilibrium Model and Resultant Lateral Force Solution for Long-Term Static-Undrained Case (Section 2-2)

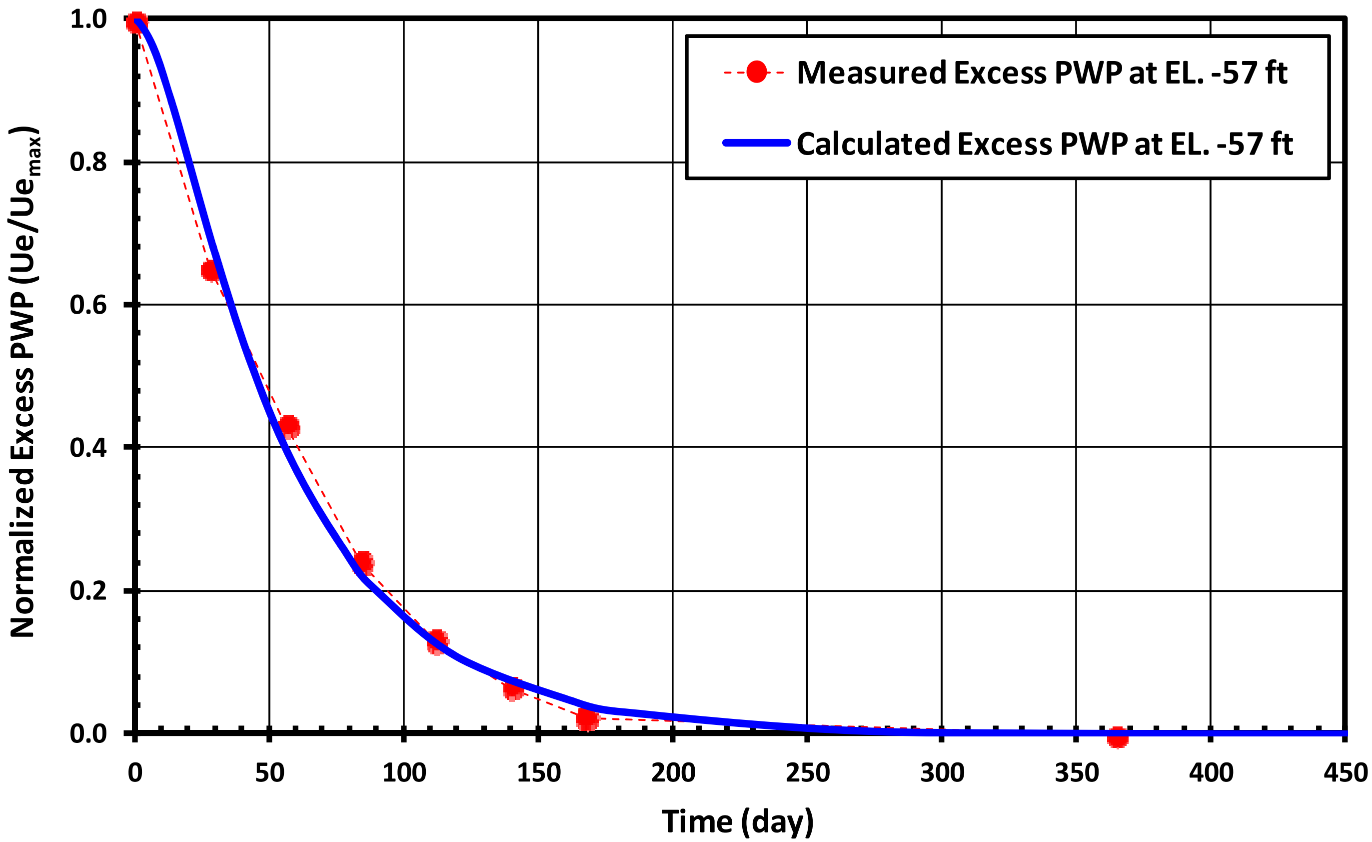

FIGURE 5.2-13. Normalized Excess Porewater Pressure at EL -57 ft (Cell No. 58)

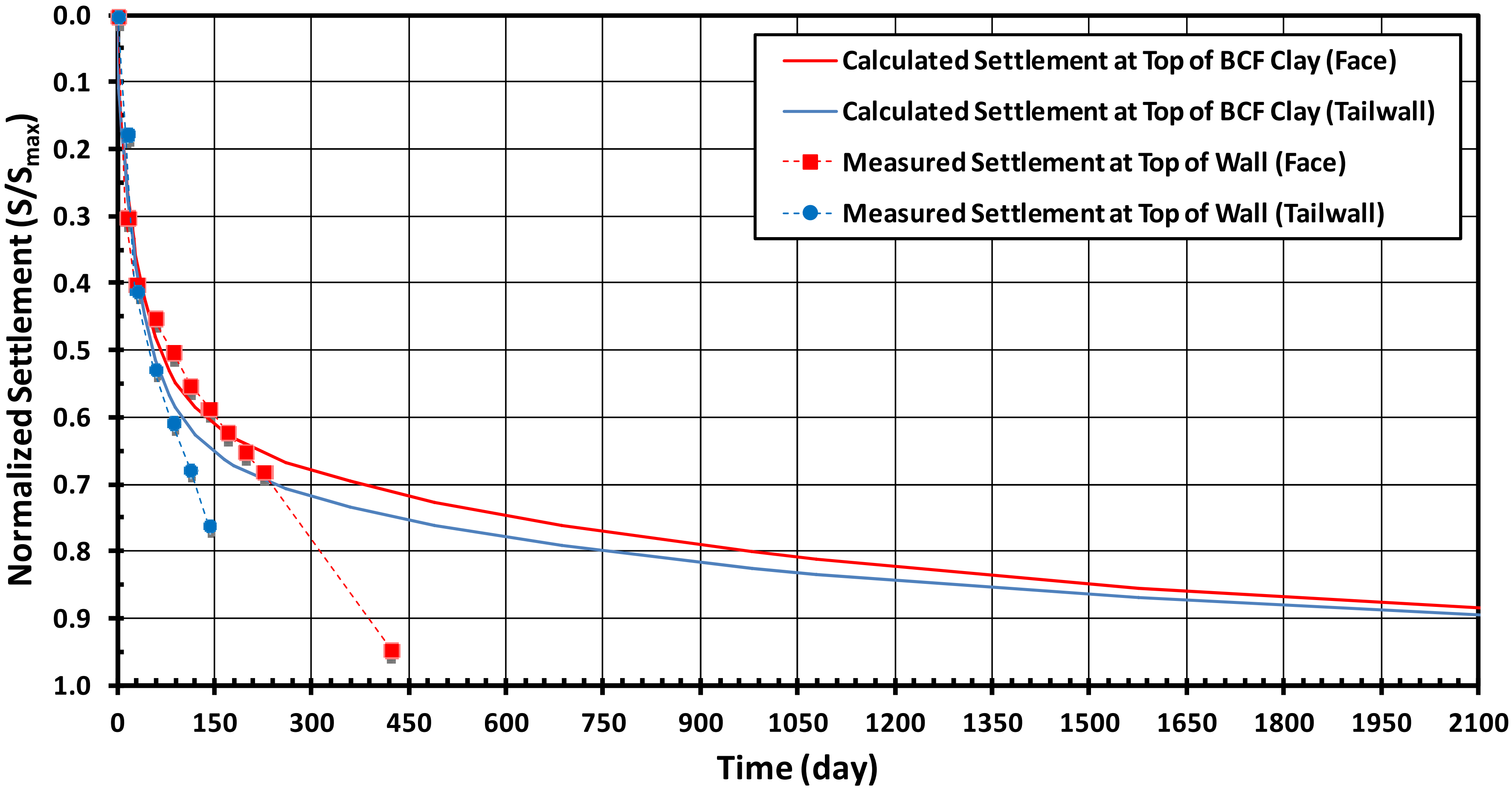

FIGURE 5.2-14. Normalized Settlement at the Top of the BCF Clay (Cell No. 61)

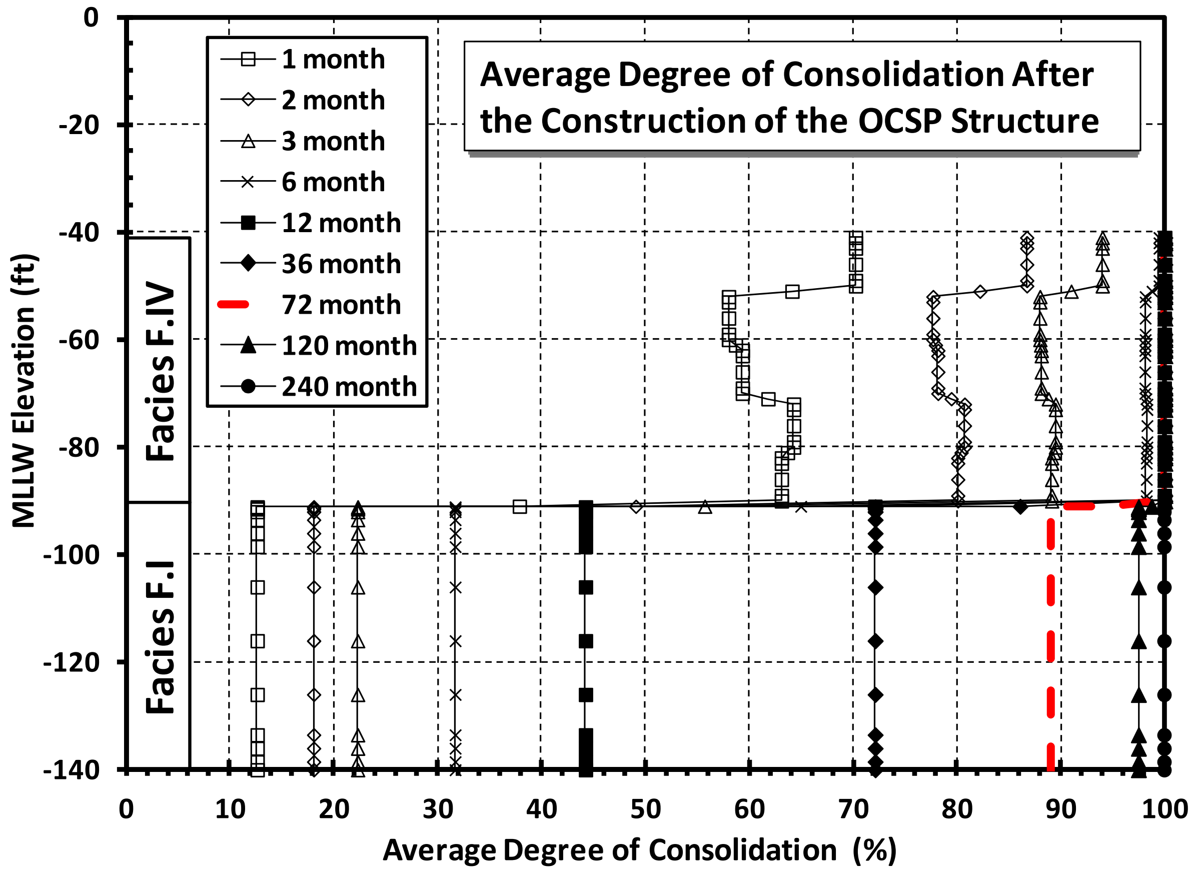

FIGURE 5.2-15. Calculated Degree of Consolidation at Section 2-2 After the Construction of the OCSP® Structure

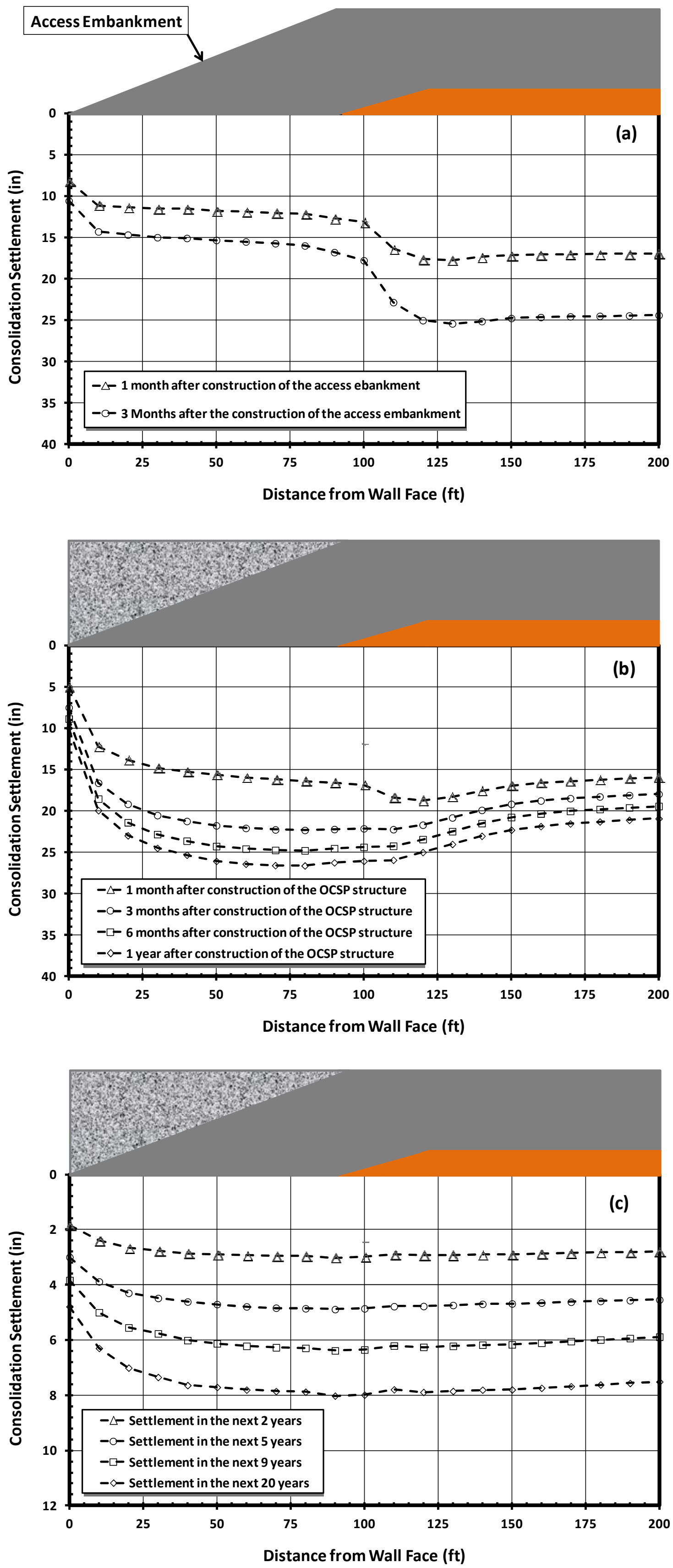

FIGURE 5.2-16. Calculated Settlement Profile in the BCF Clay at Section 2-2 after (a) Construction of the Access Embankment; (b) Construction of the OCSP® Structure; and (c) the Next 20 Years

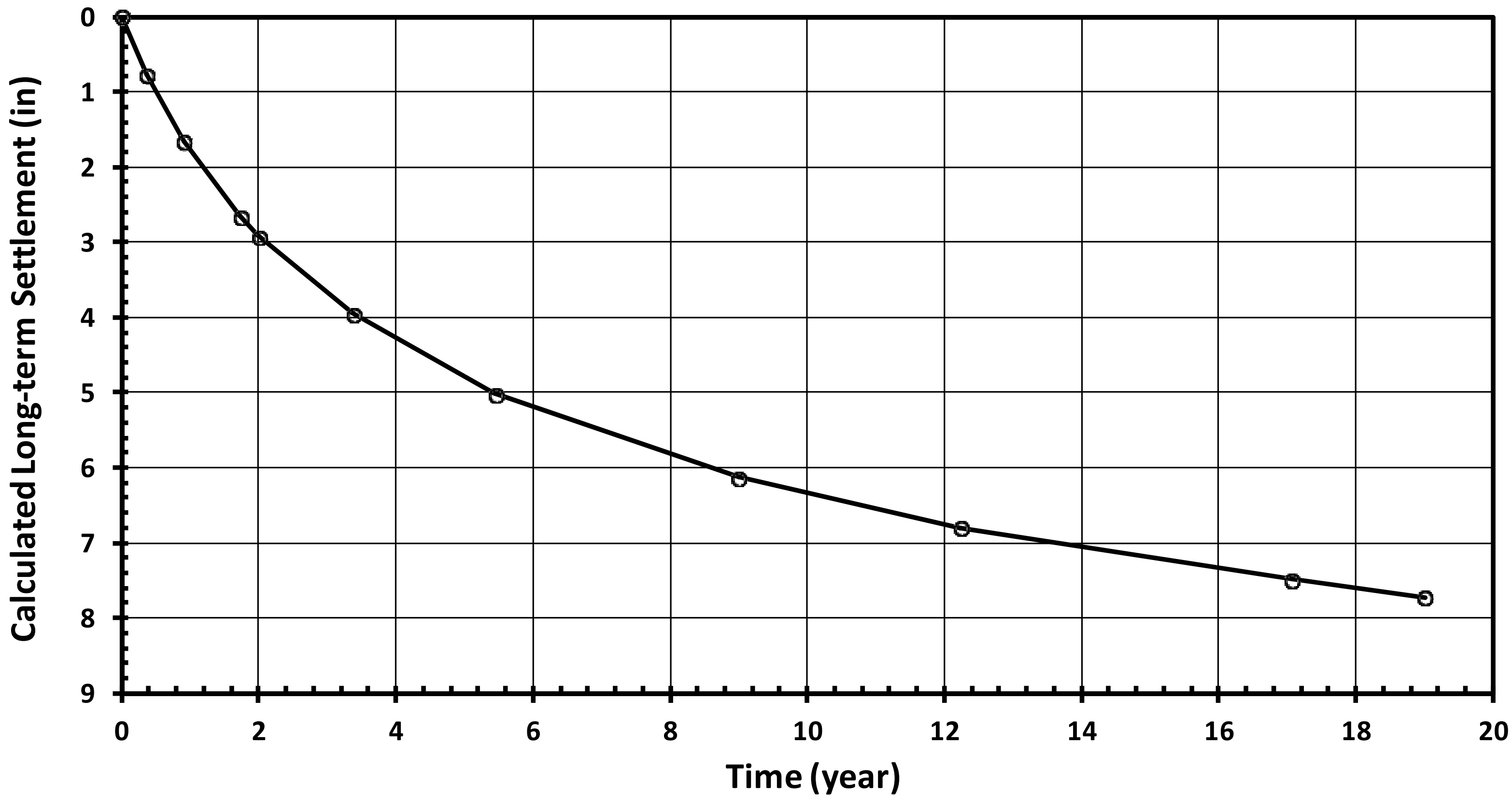

FIGURE 5.2-17. Predicted Post-Construction Settlement in the BCF Clay Layer from Present Time

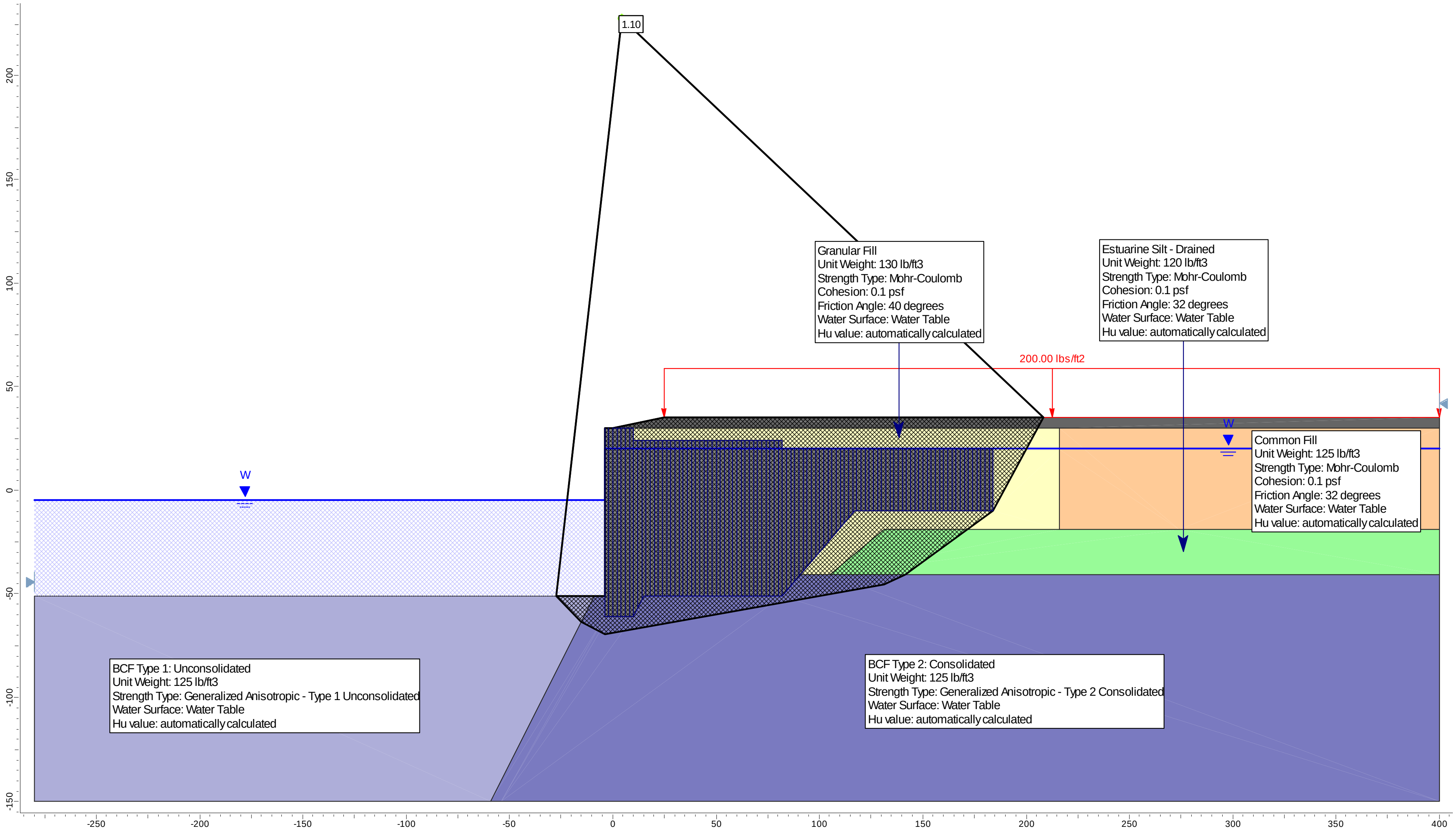

FIGURE 5.2-18a. Global Stability at End-of-Construction Condition (Section 2-2)

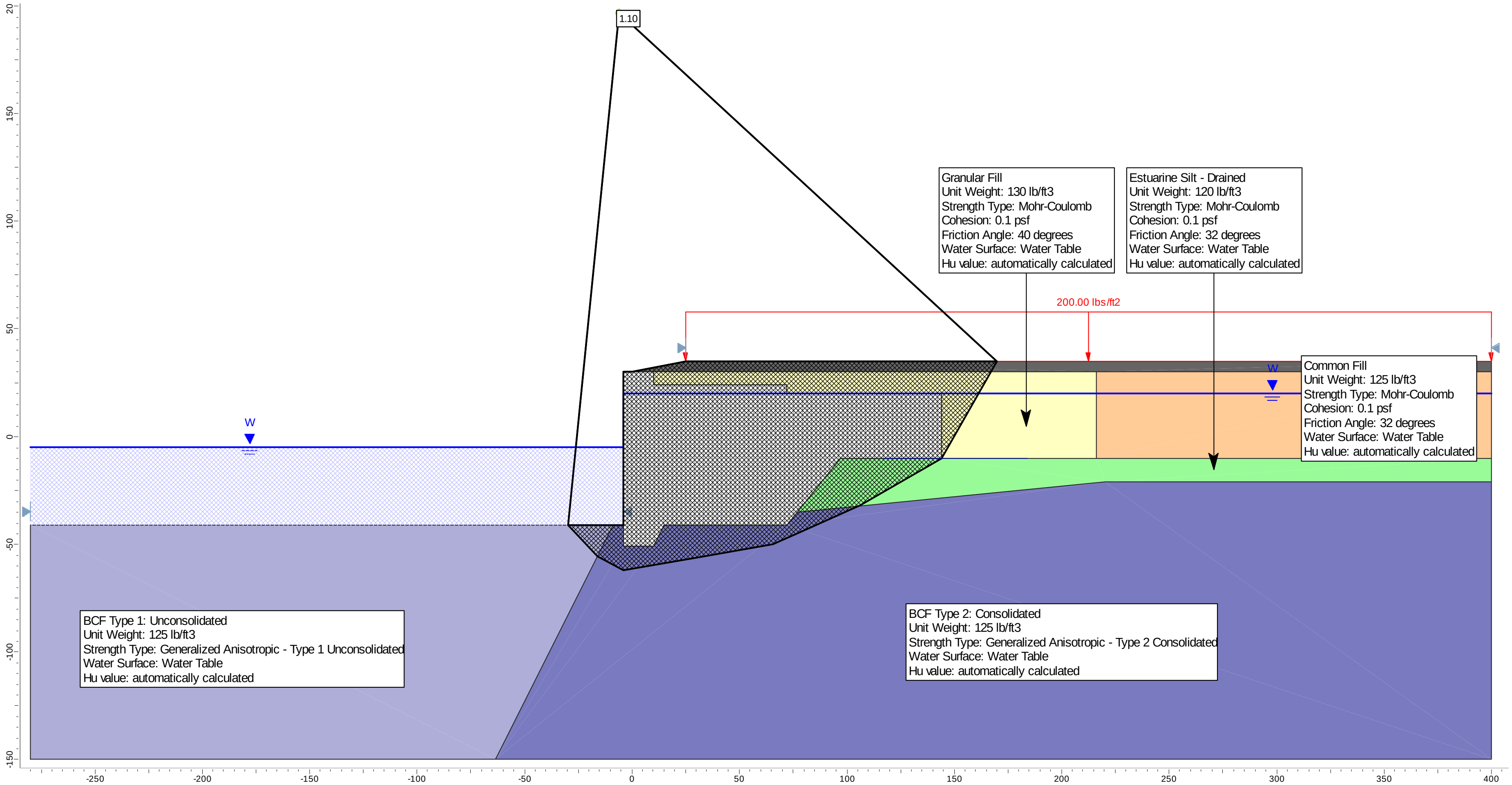

FIGURE 5.2-18b. Global Stability at End-of-Construction Condition (Section 3-3)

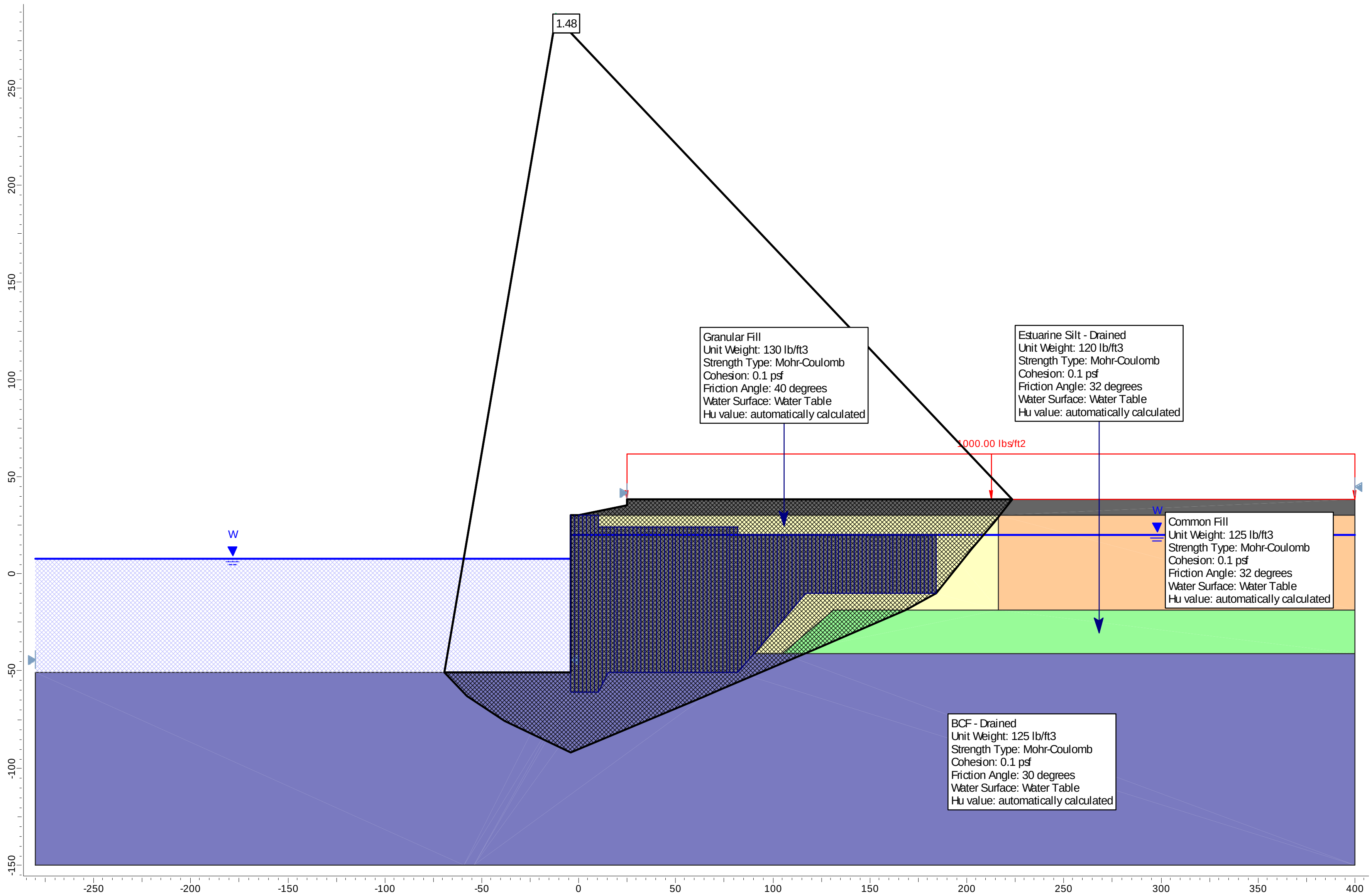

FIGURE 5.2-19a. Global Stability at Long-Term Static-Drained Condition (Section 2-2)

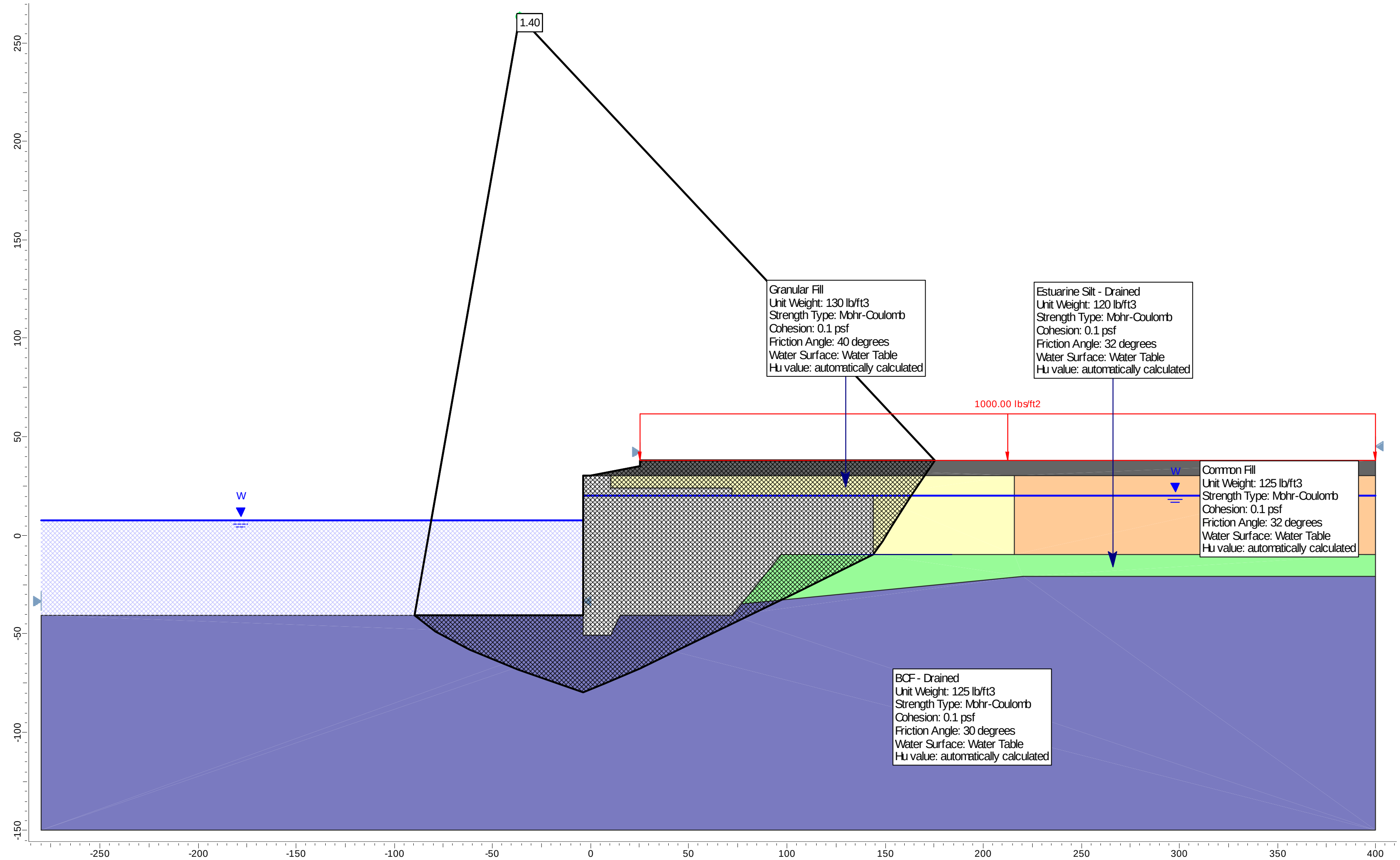

FIGURE 5.2-19b. Global Stability at Long-Term Static-Drained Condition (Section 3-3)

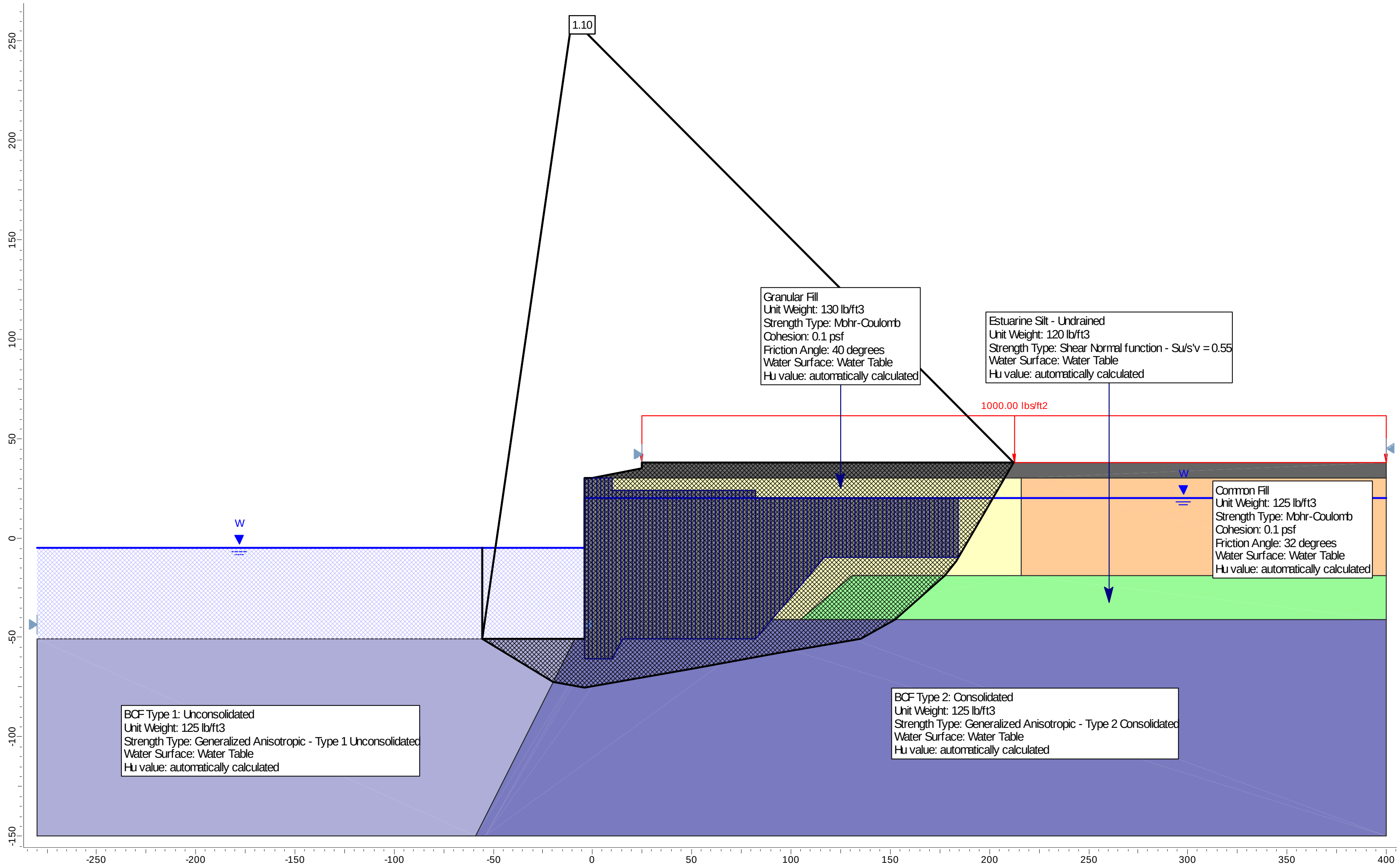

FIGURE 5.2-20a. Global Stability at Long-Term Static-Undrained Condition (Section 2-2)

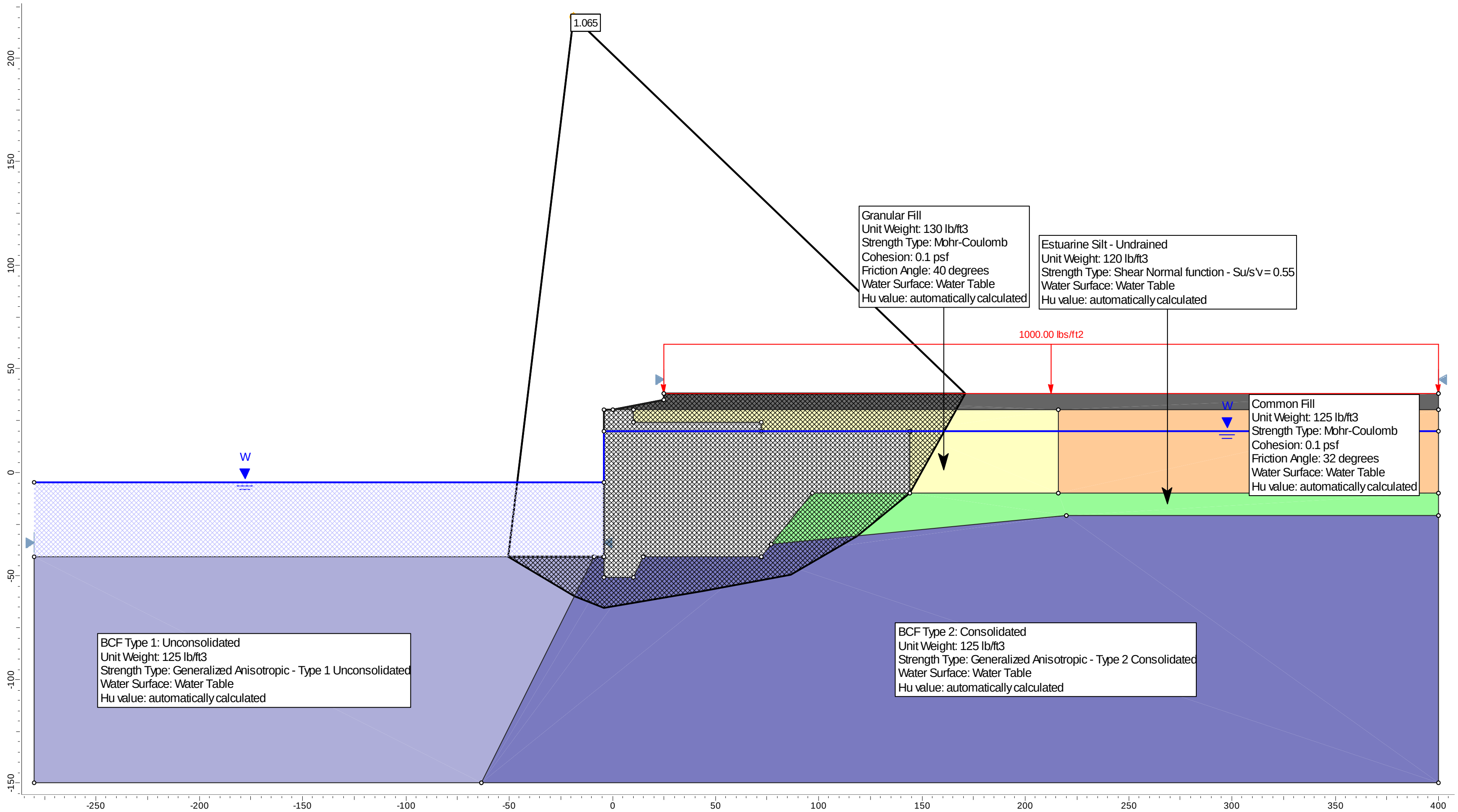

FIGURE 5.2-20b. Global Stability at Long-Term Static-Undrained Condition (Section 3-3)

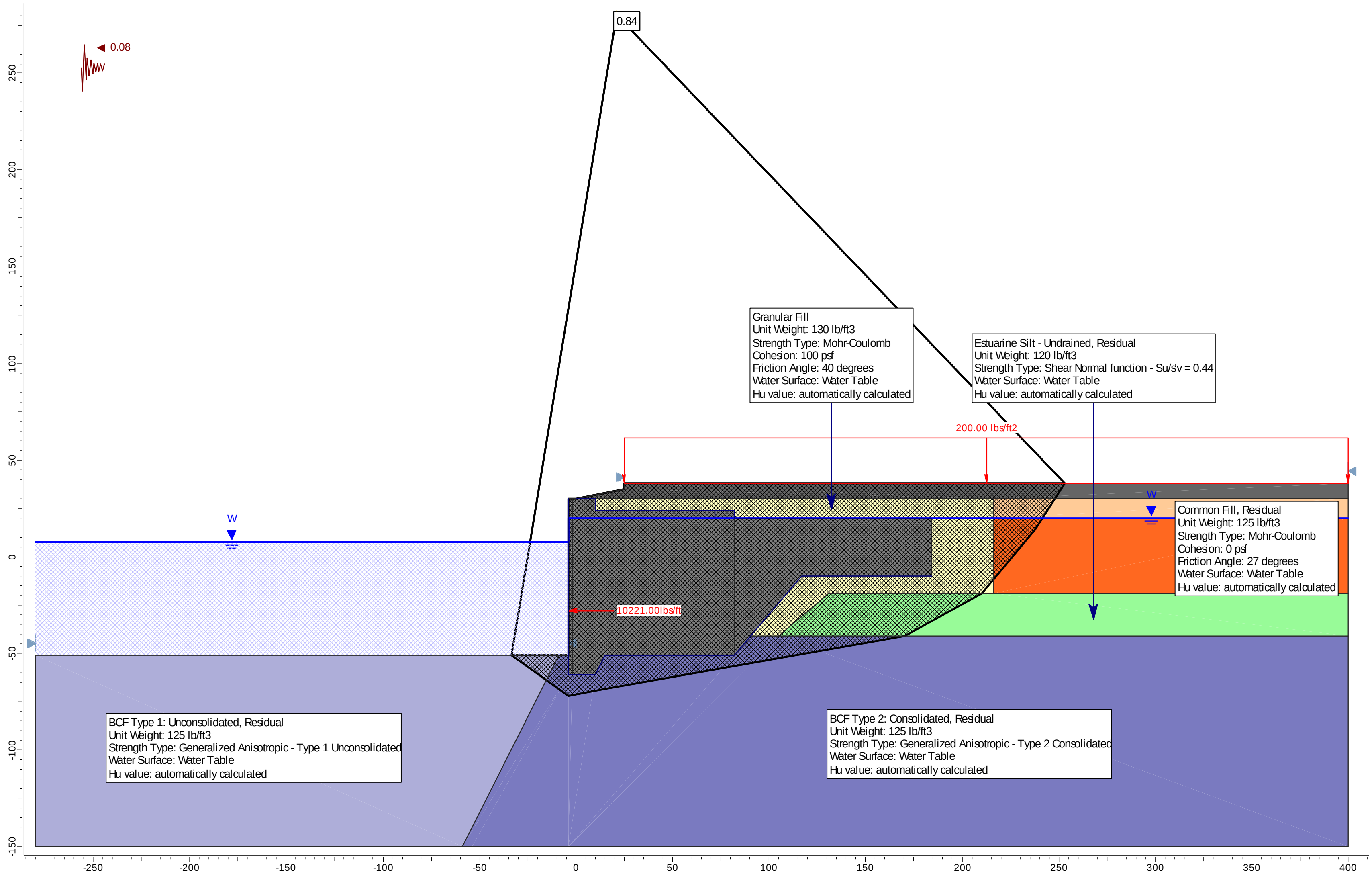

FIGURE 5.2-21a. Global Stability During the OLE Seismic Event (Section 2-2)

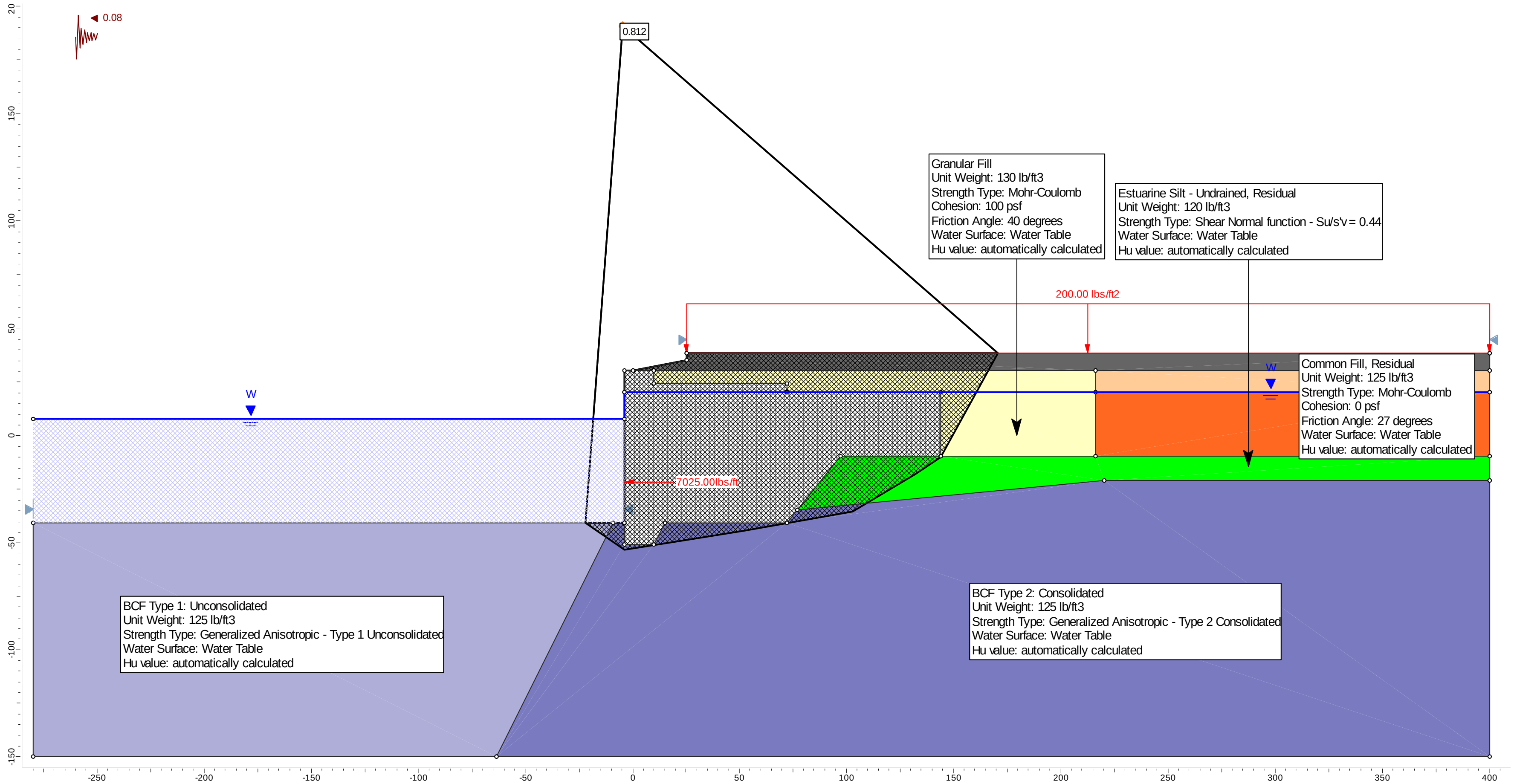

FIGURE 5.2-21b. Global Stability During the OLE Seismic Event (Section 3-3)

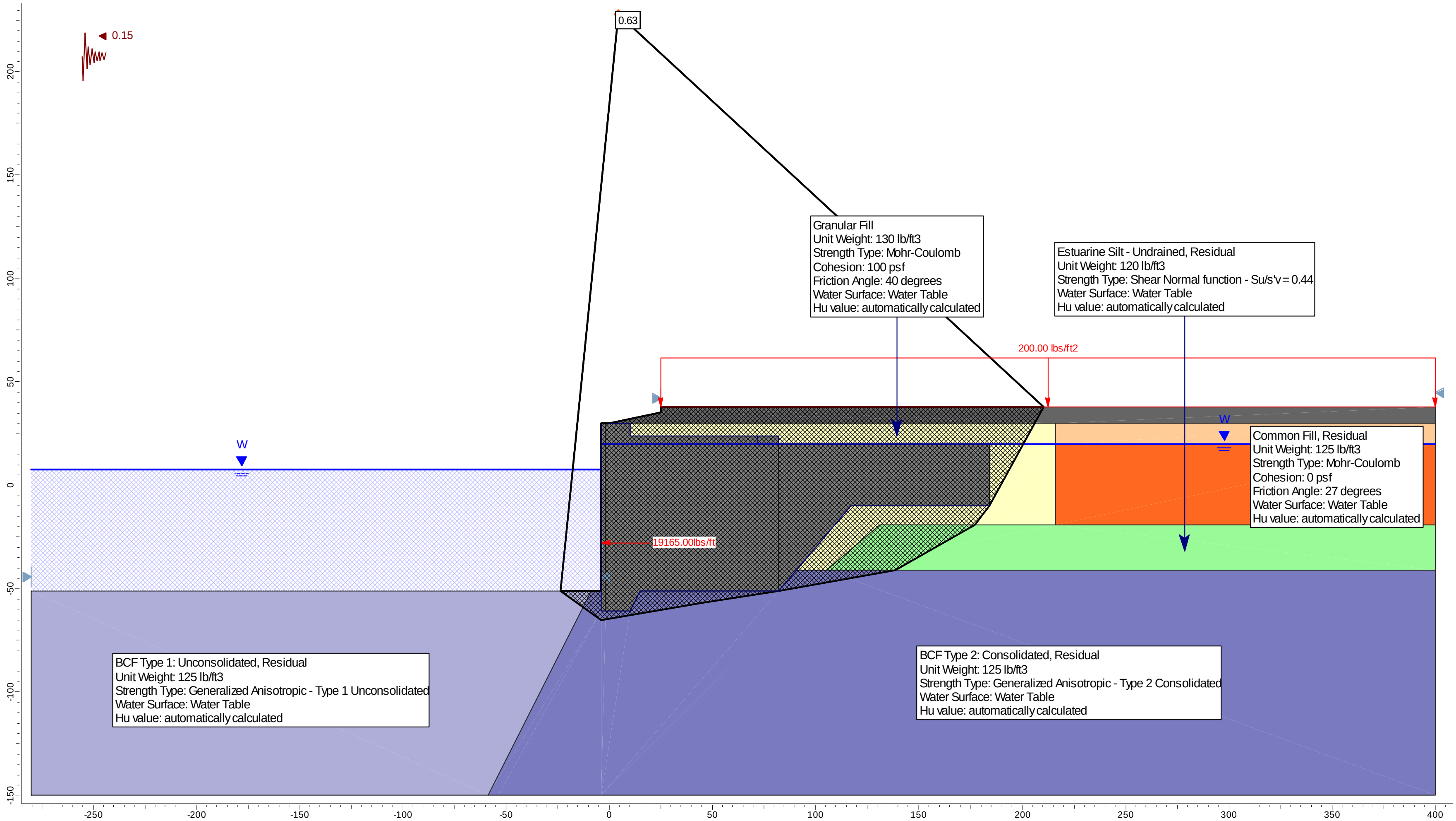

FIGURE 5.2-22a. Global Stability During the CLE Seismic Event (Section 2-2)

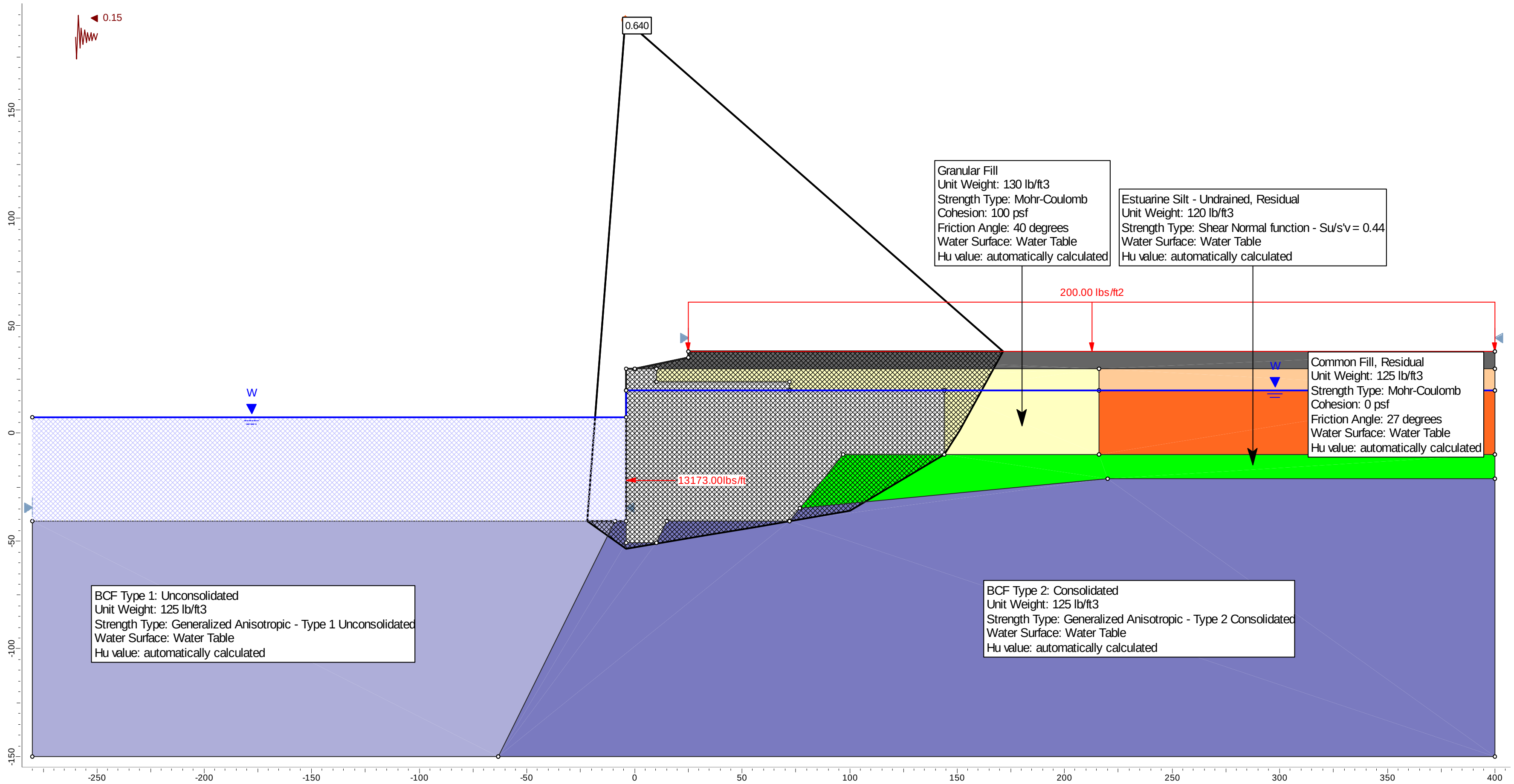

FIGURE 5.2-22b. Global Stability During the CLE Seismic Event (Section 3-3)

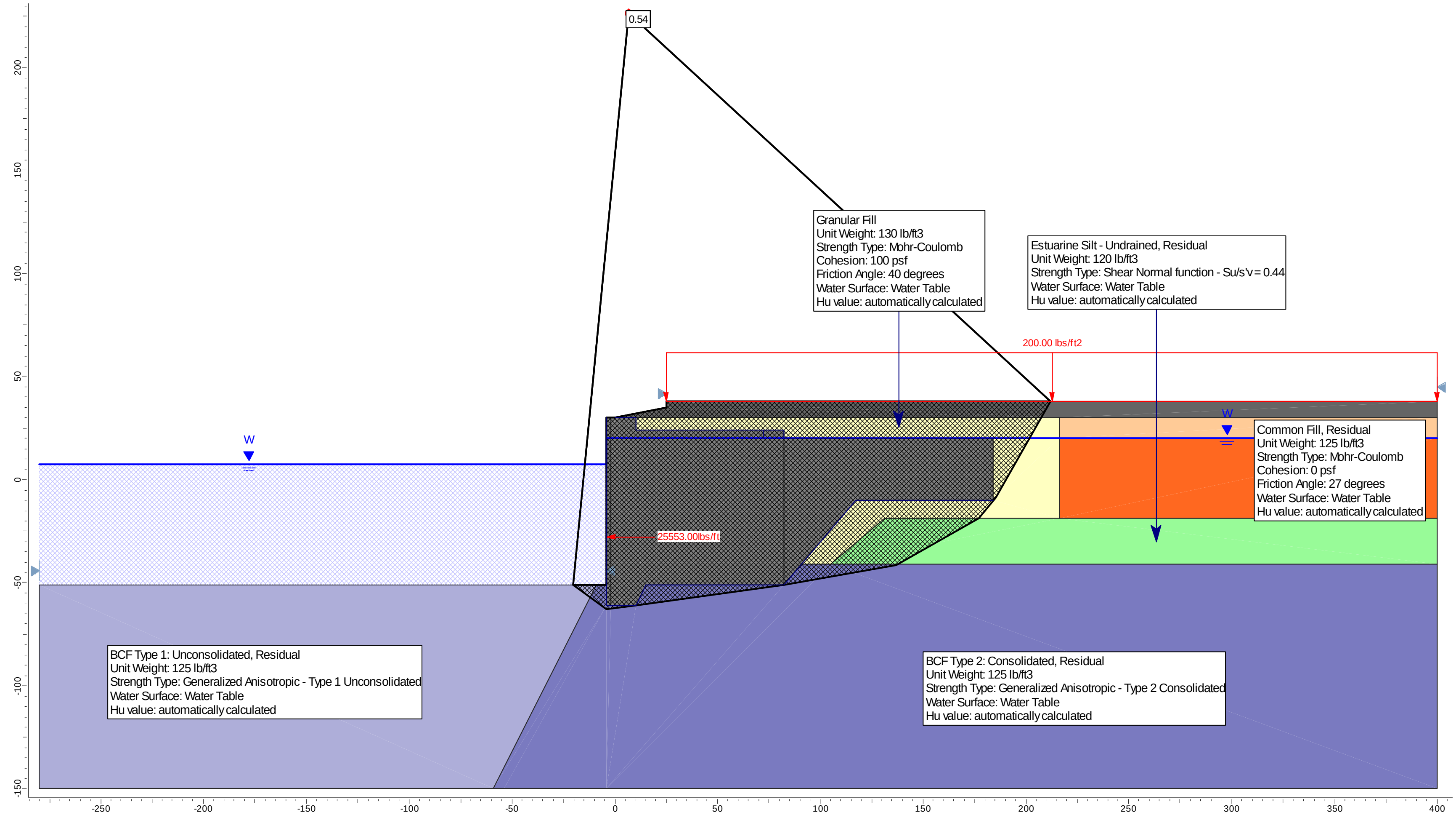

FIGURE 5.2-23. Global Stability During the MCE Seismic Event (Section 2-2)

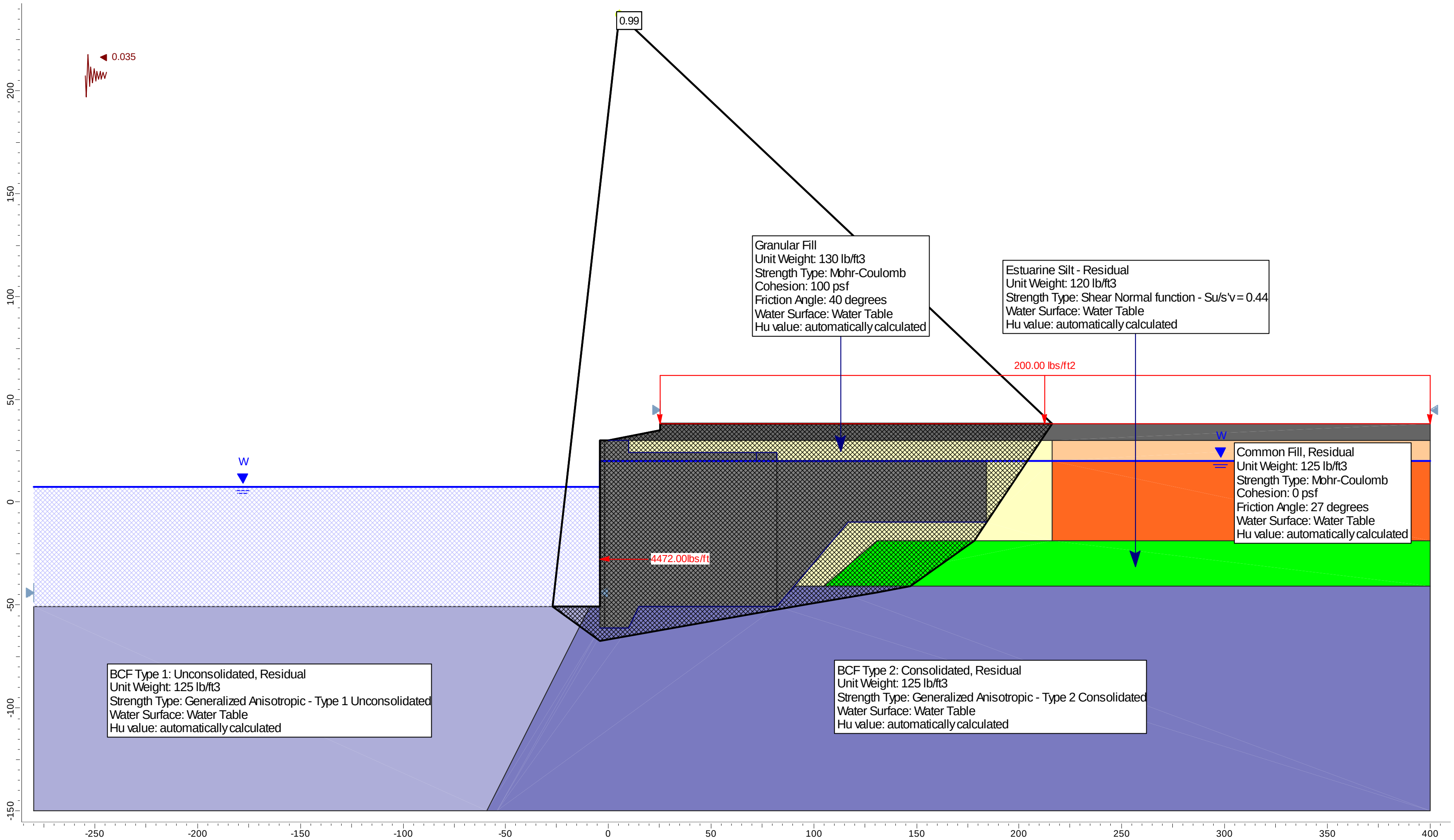

FIGURE 5.2-24a. Determination of the Yield Acceleration (Section 2-2)

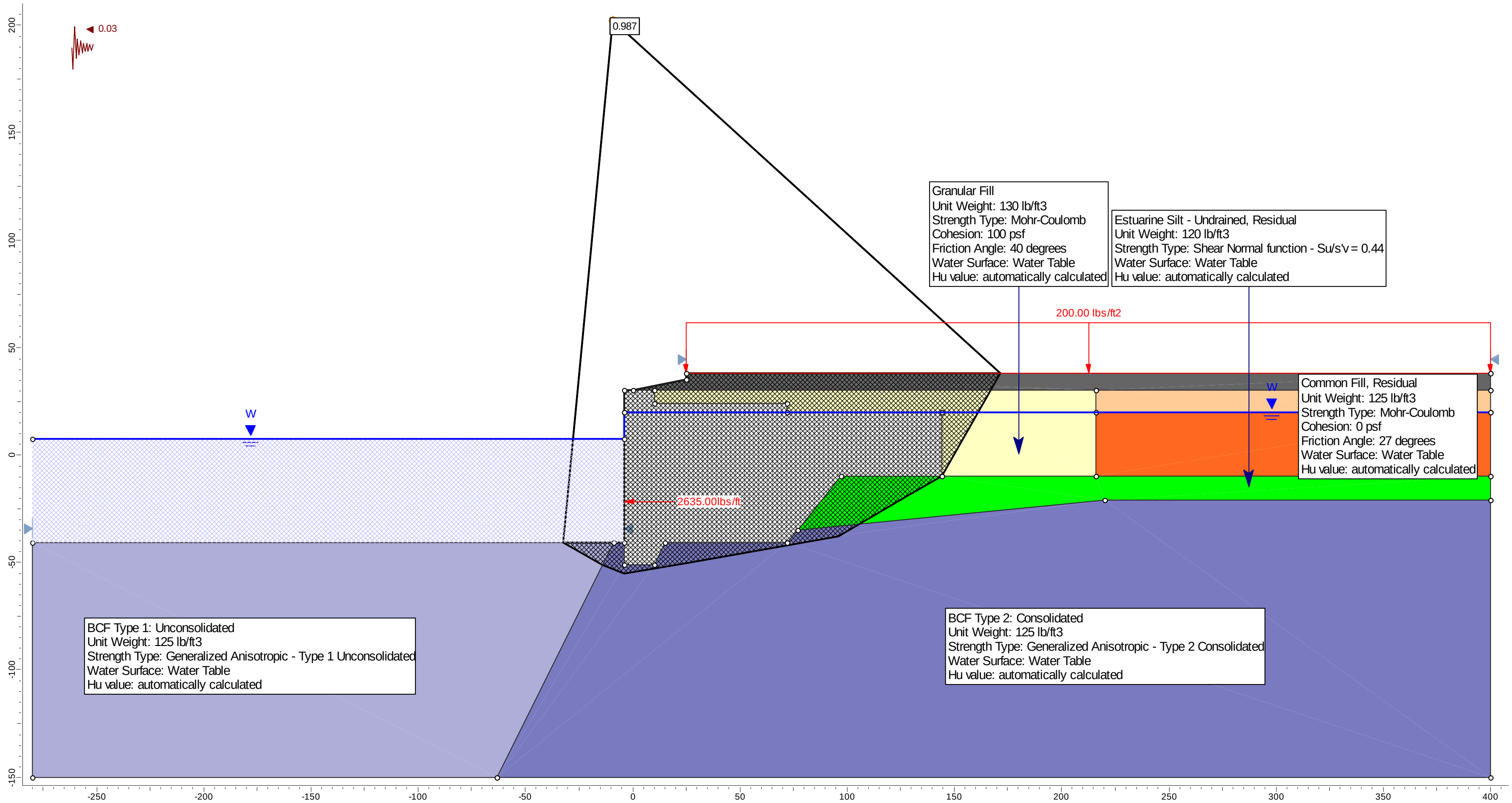

FIGURE 5.2-24b. Determination of the Yield Acceleration (Section 3-3)

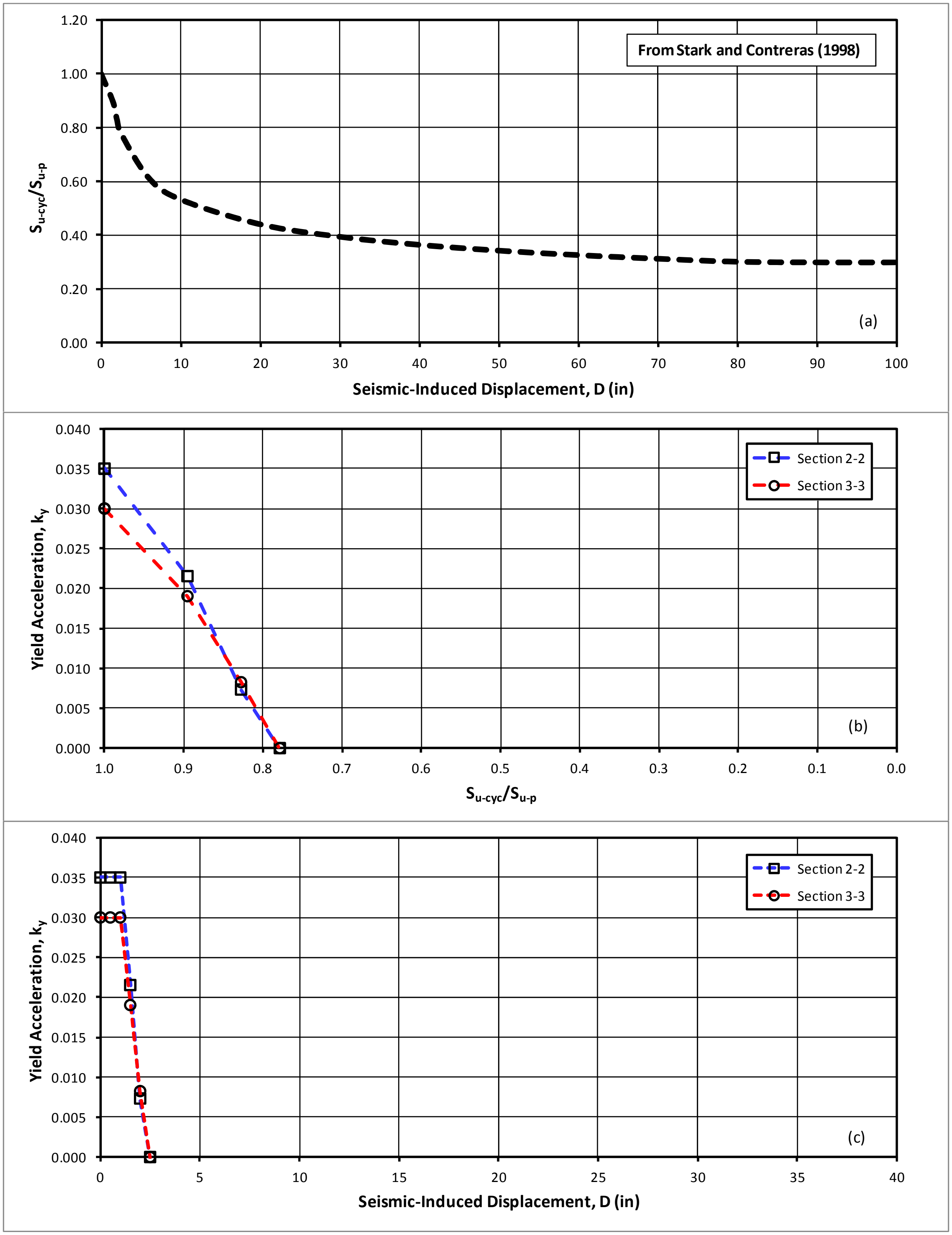

FIGURE 5.2-25. Yield Acceleration as a Function of Seismic-Induced Displacement for the BCF Clay (per Stark and Contreras 1988)

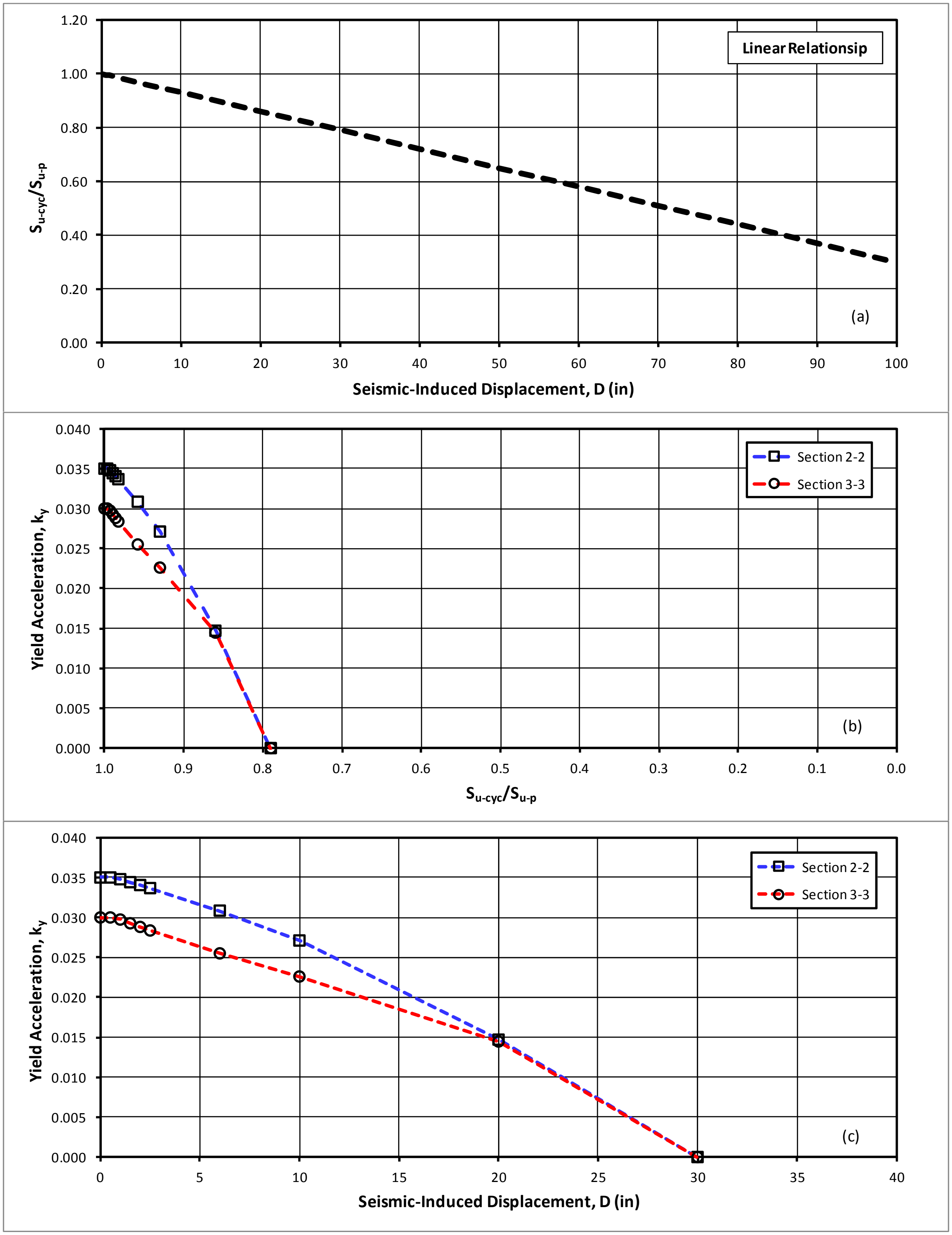

FIGURE 5.2-26. Yield Acceleration as a Function of Seismic-Induced Displacement for the BCF Clay (Linear Shear Strength Reduction)

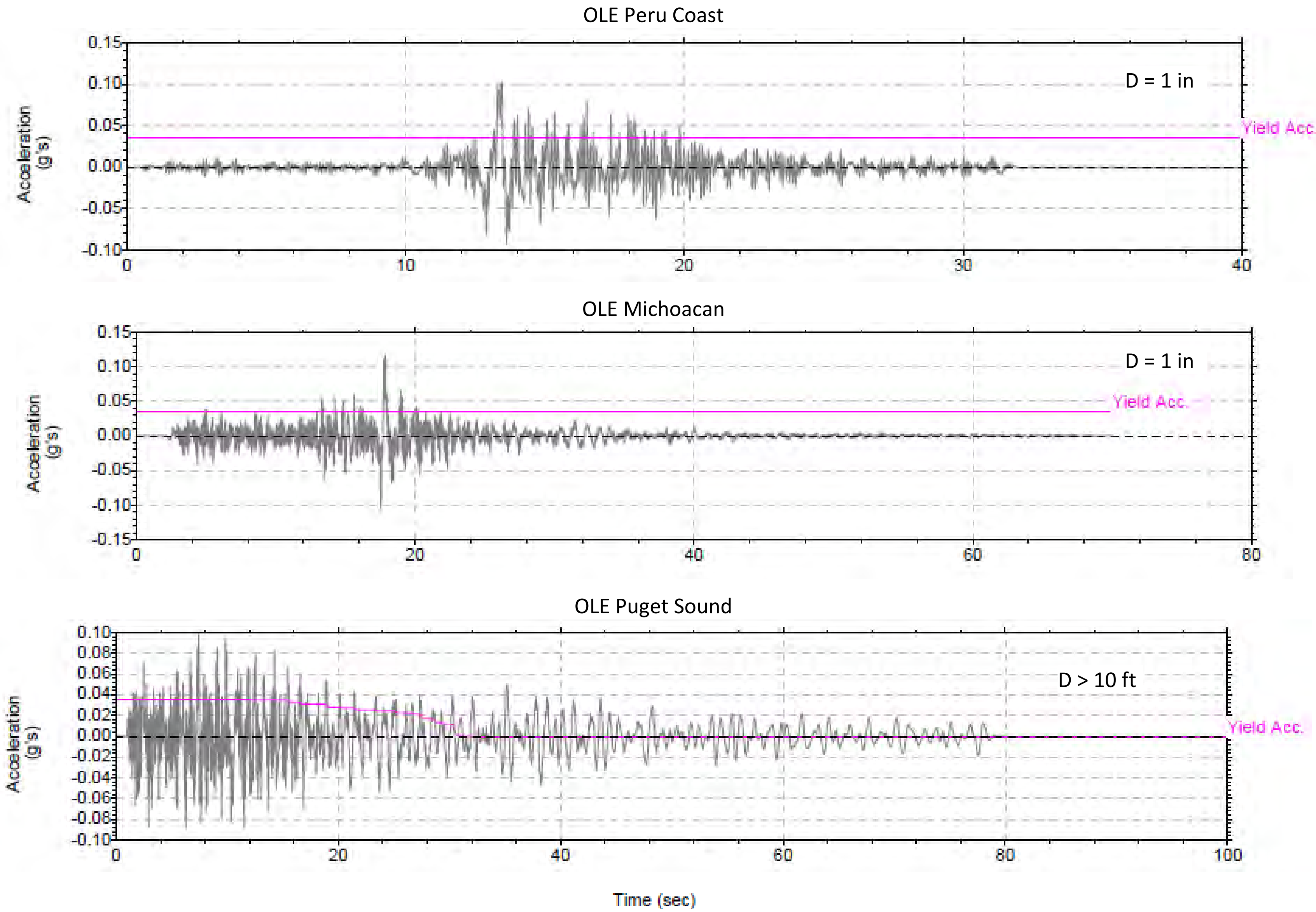

FIGURE 5.2-27. Modified Newmark Analysis for Section 2-2 Based on OLE Time Histories (Stark and Contreras 1998)

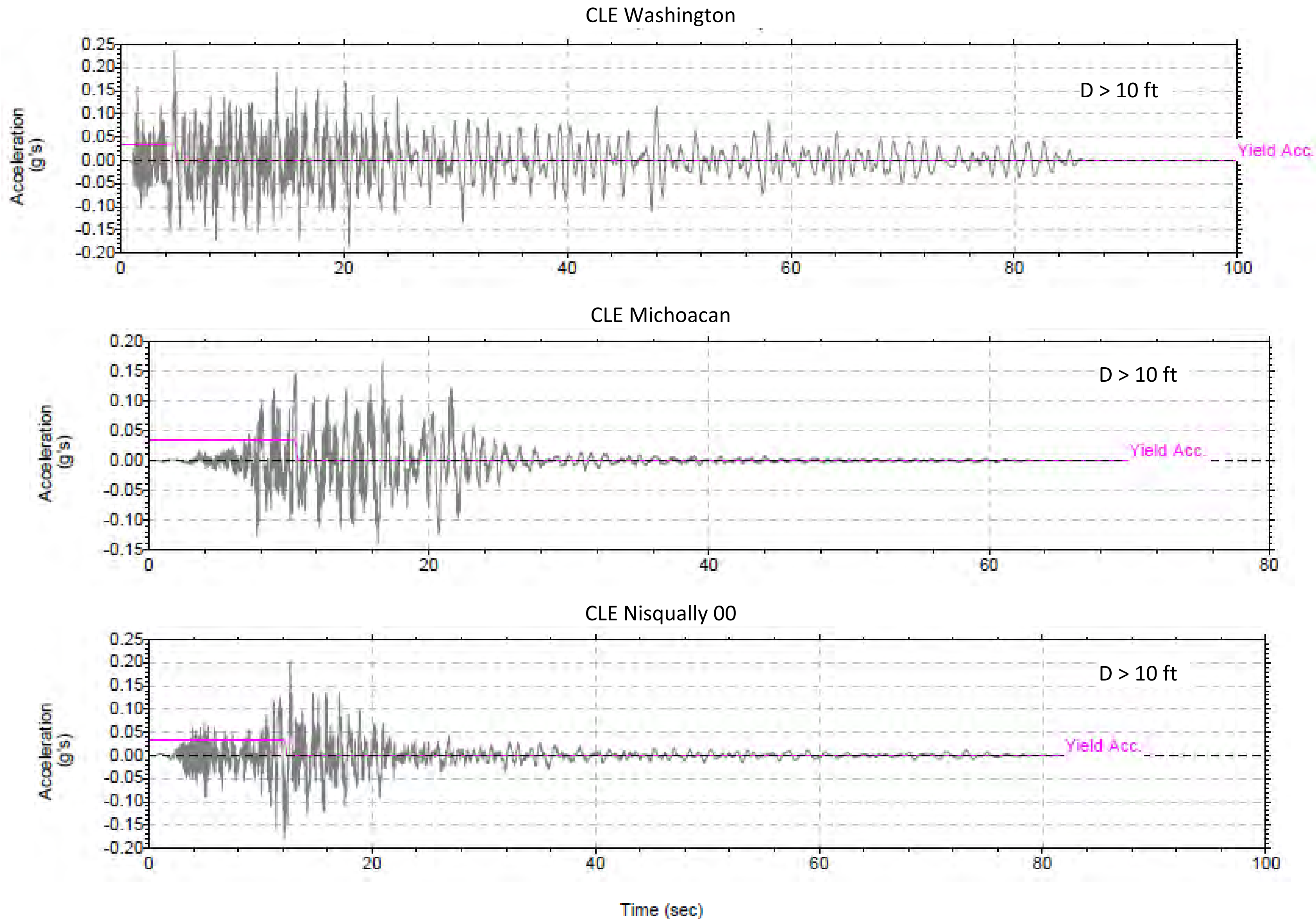

FIGURE 5.2-28a. Modified Newmark Analysis for Section 2-2 Based on CLE Time Histories (Stark and Contreras 1998)

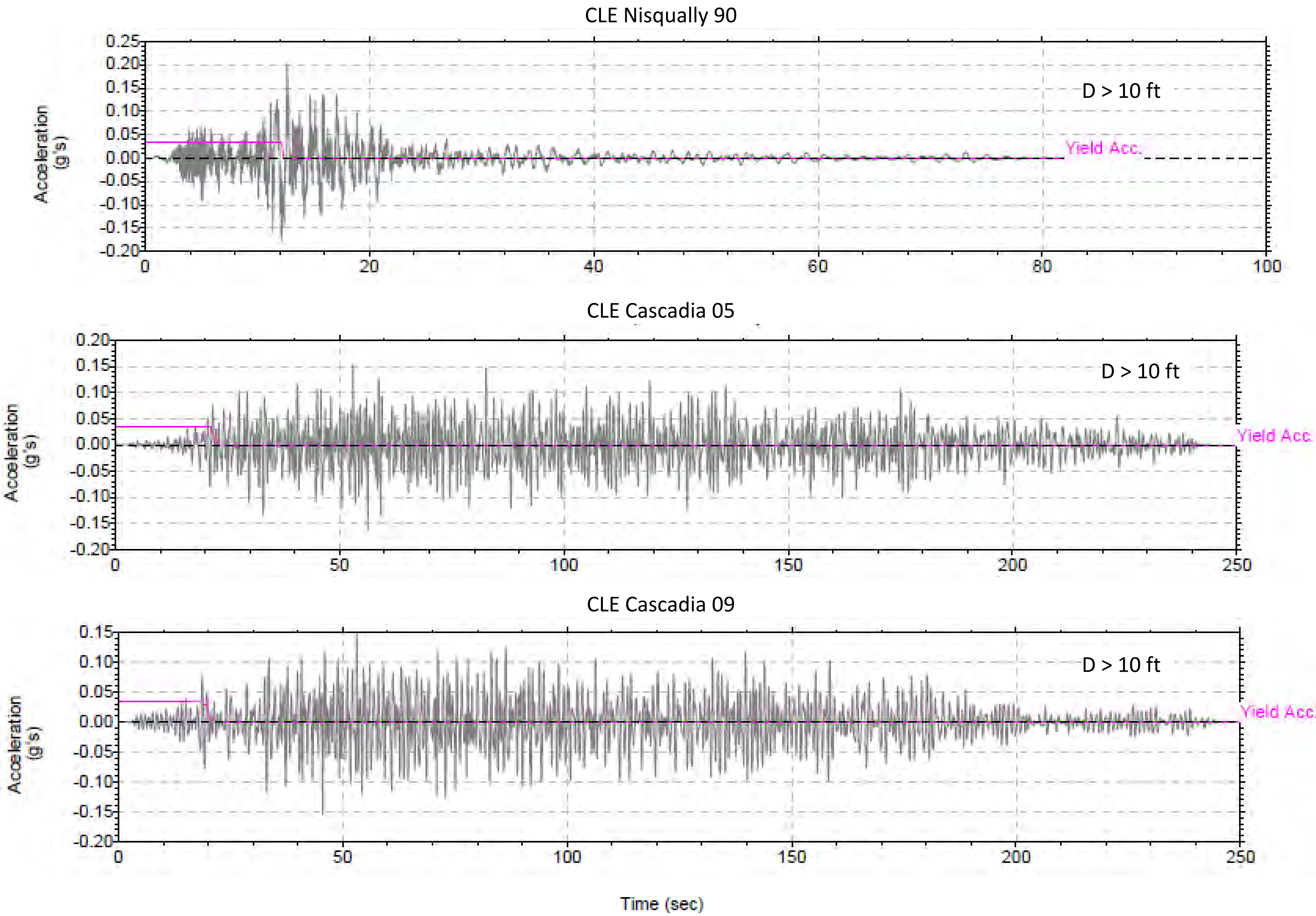

FIGURE 5.2-28b. Modified Newmark Analysis for Section 2-2 Based on CLE Time Histories (Stark and Contreras 1998)

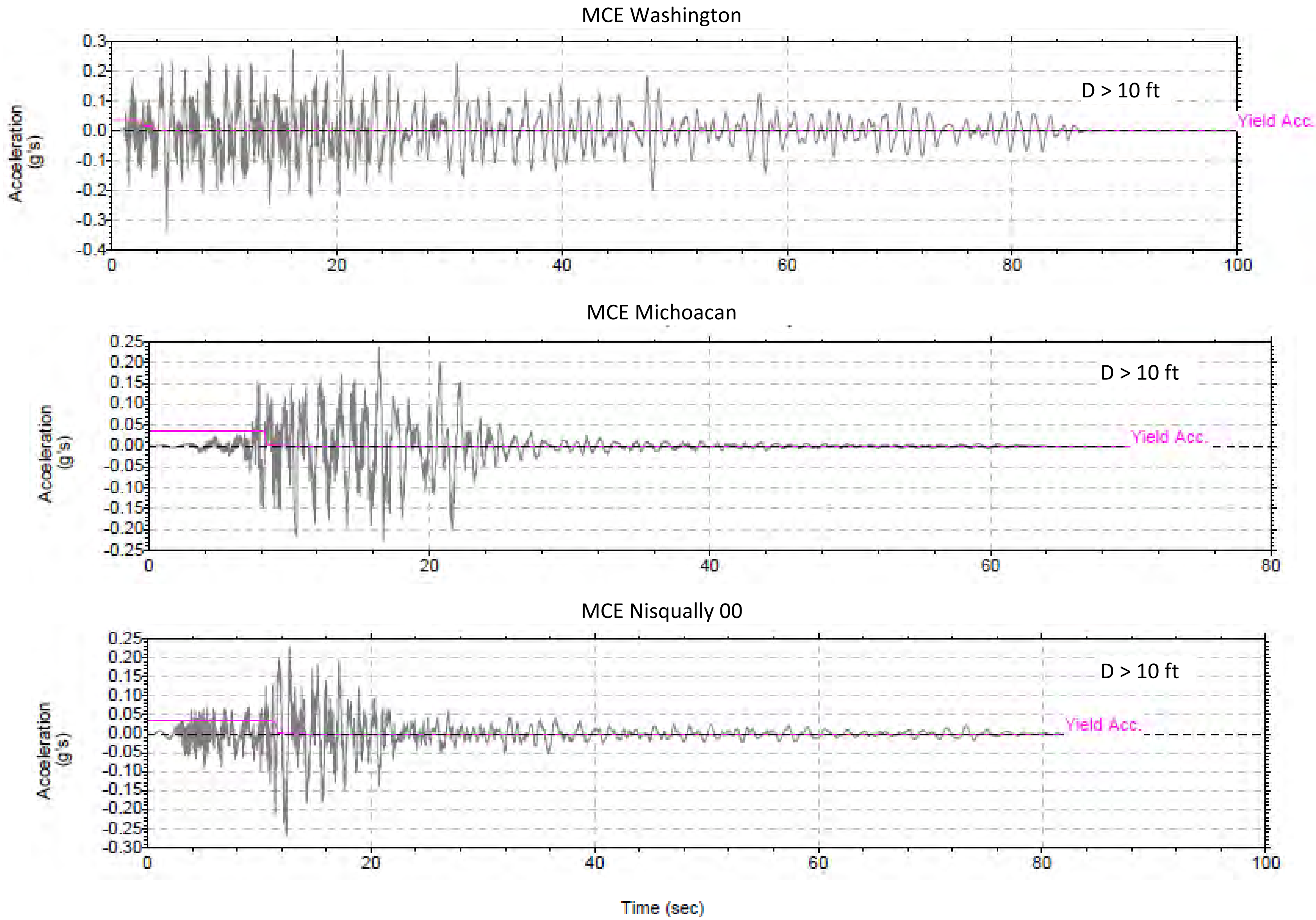

FIGURE 5.2-29a. Modified Newmark Analysis for Section 2-2 Based on MCE Time Histories (Stark and Contreras 1998)

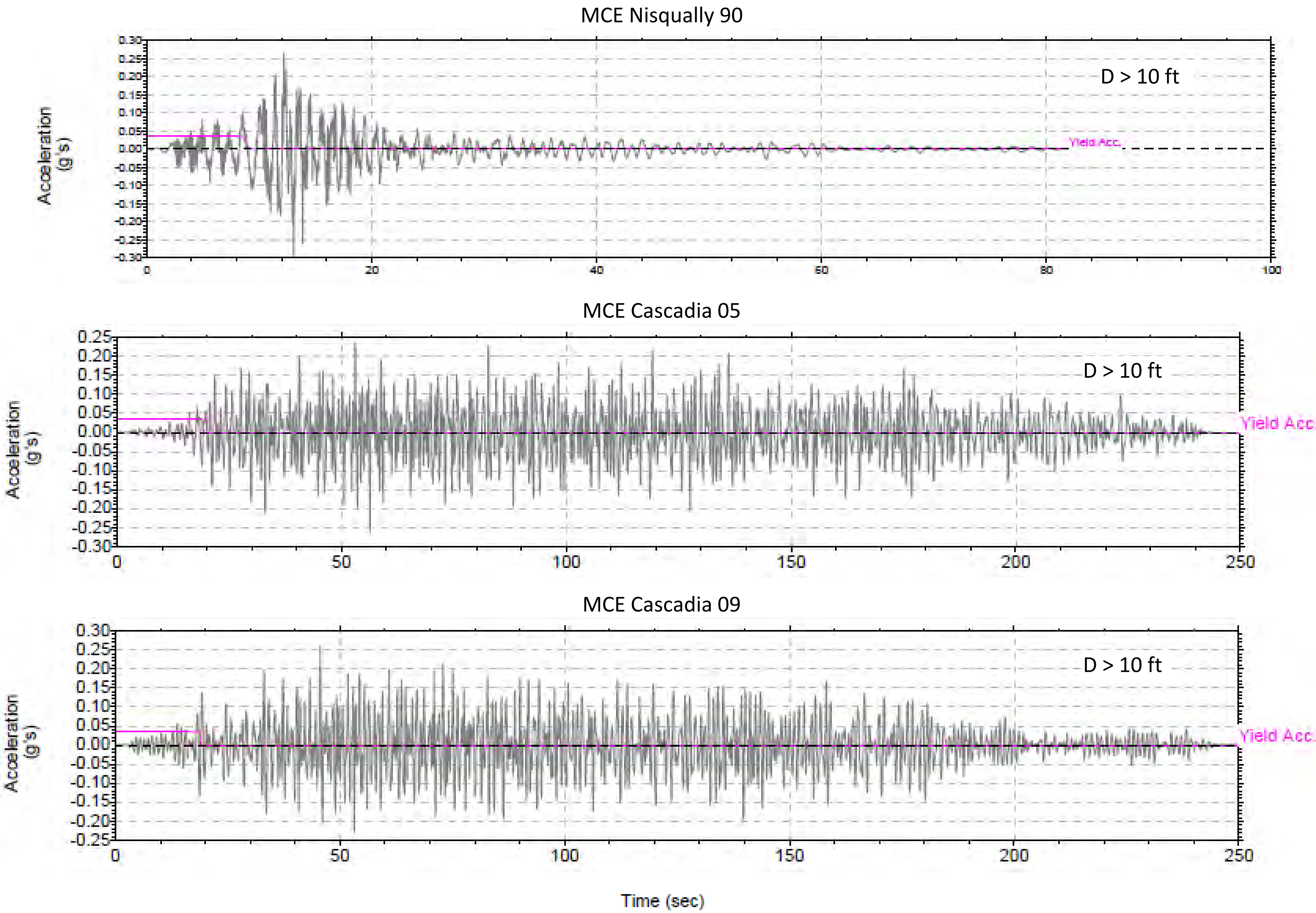

FIGURE 5.2-29b. Modified Newmark Analysis for Section 2-2 Based on MCE Time Histories (Stark and Contreras 1998)

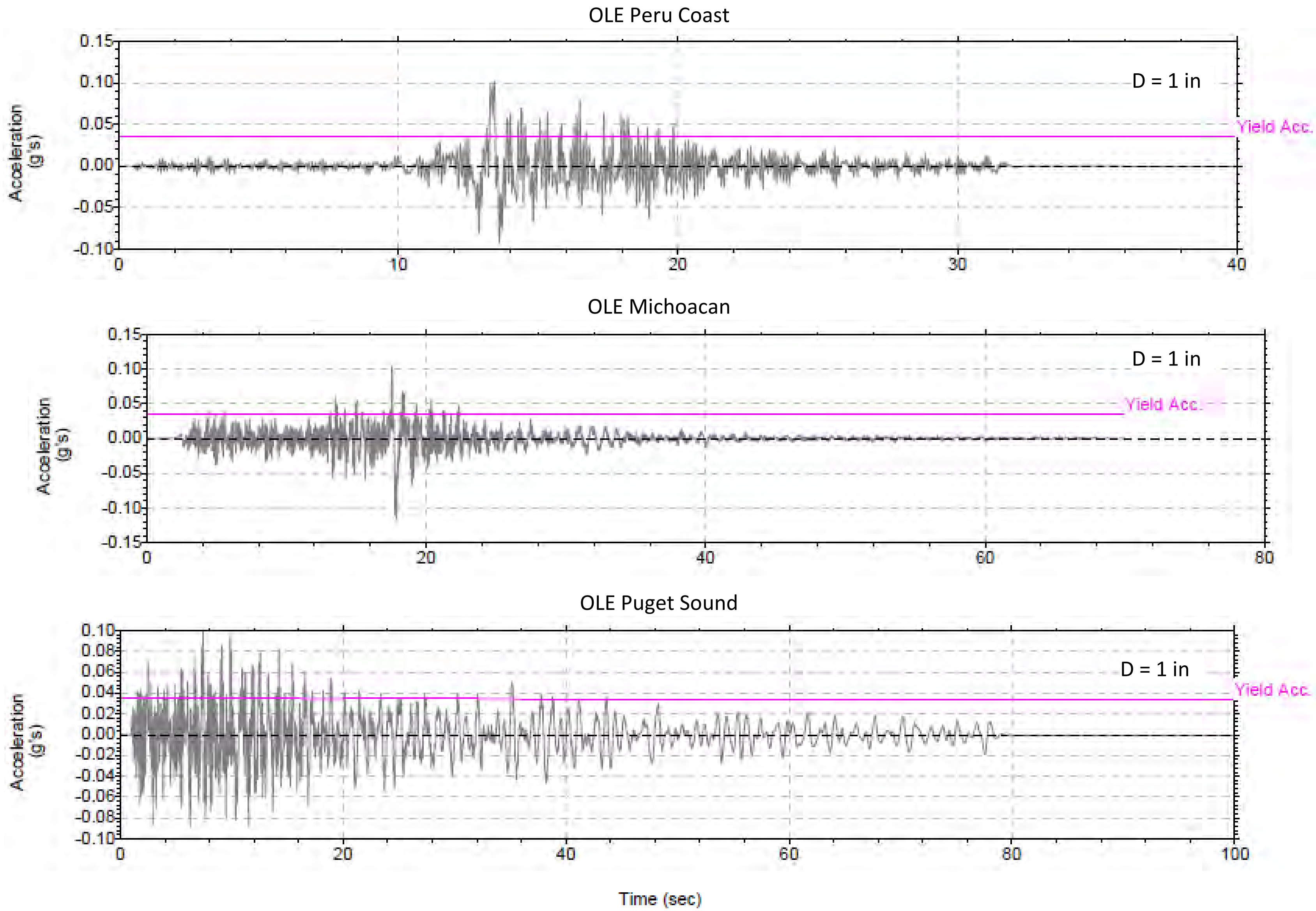

FIGURE 5.2-30. Modified Newmark Analysis for Section 2-2 Based on OLE Time Histories (Linear Shear Strength Reduction)

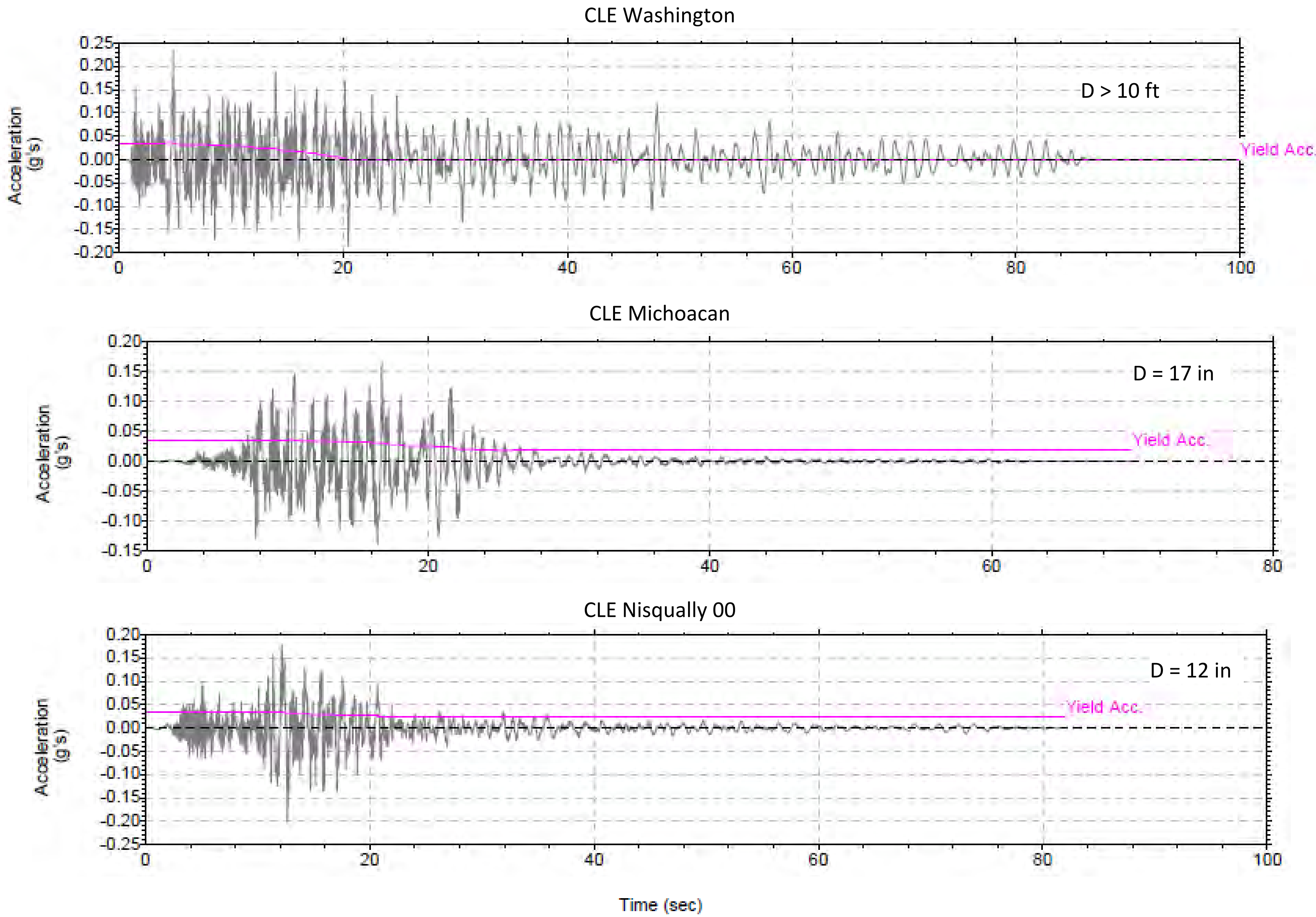

FIGURE 5.2-31a. Modified Newmark Analysis for Section 2-2 Based on CLE Time Histories (Linear Shear Strength Reduction)

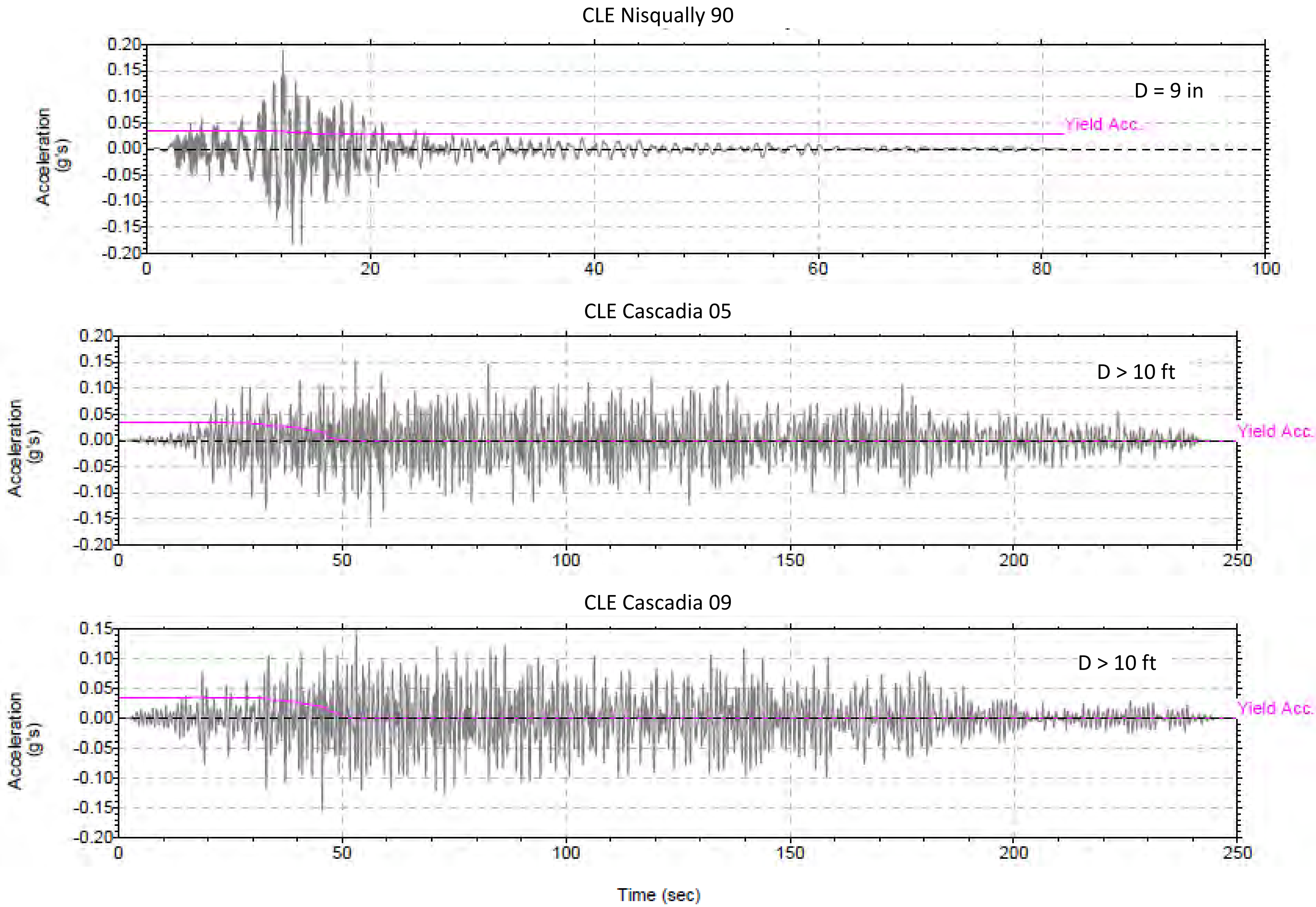

FIGURE 5.2-31b. Modified Newmark Analysis for Section 2-2 Based on CLE Time Histories (Linear Shear Strength Reduction)

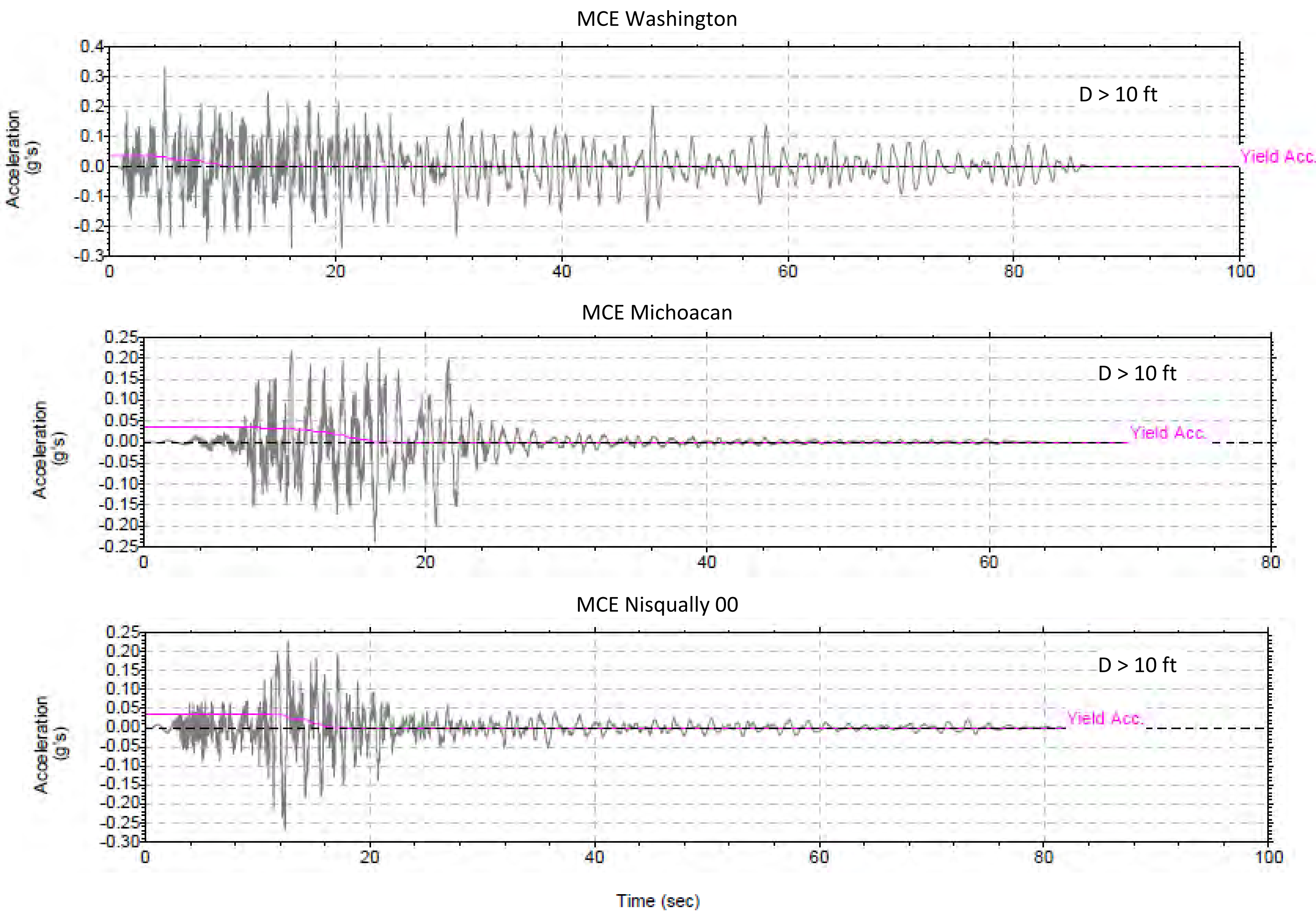

FIGURE 5.2-32a. Modified Newmark Analysis for Section 2-2 Based on MCE Time Histories (Linear Shear Strength Reduction)

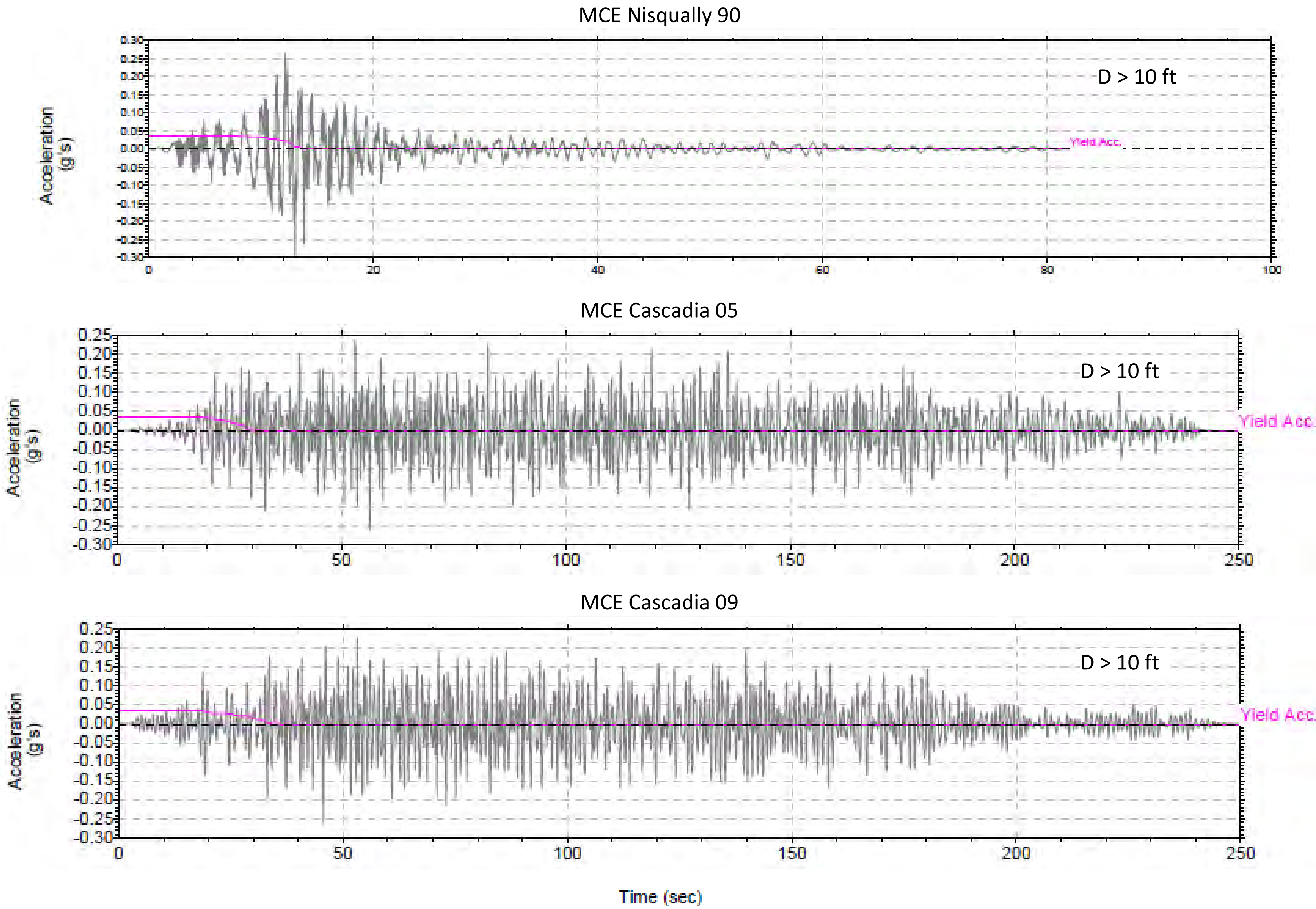

FIGURE 5.2-32b. Modified Newmark Analysis for Section 2-2 Based on MCE Time Histories (Linear Shear Strength Reduction)

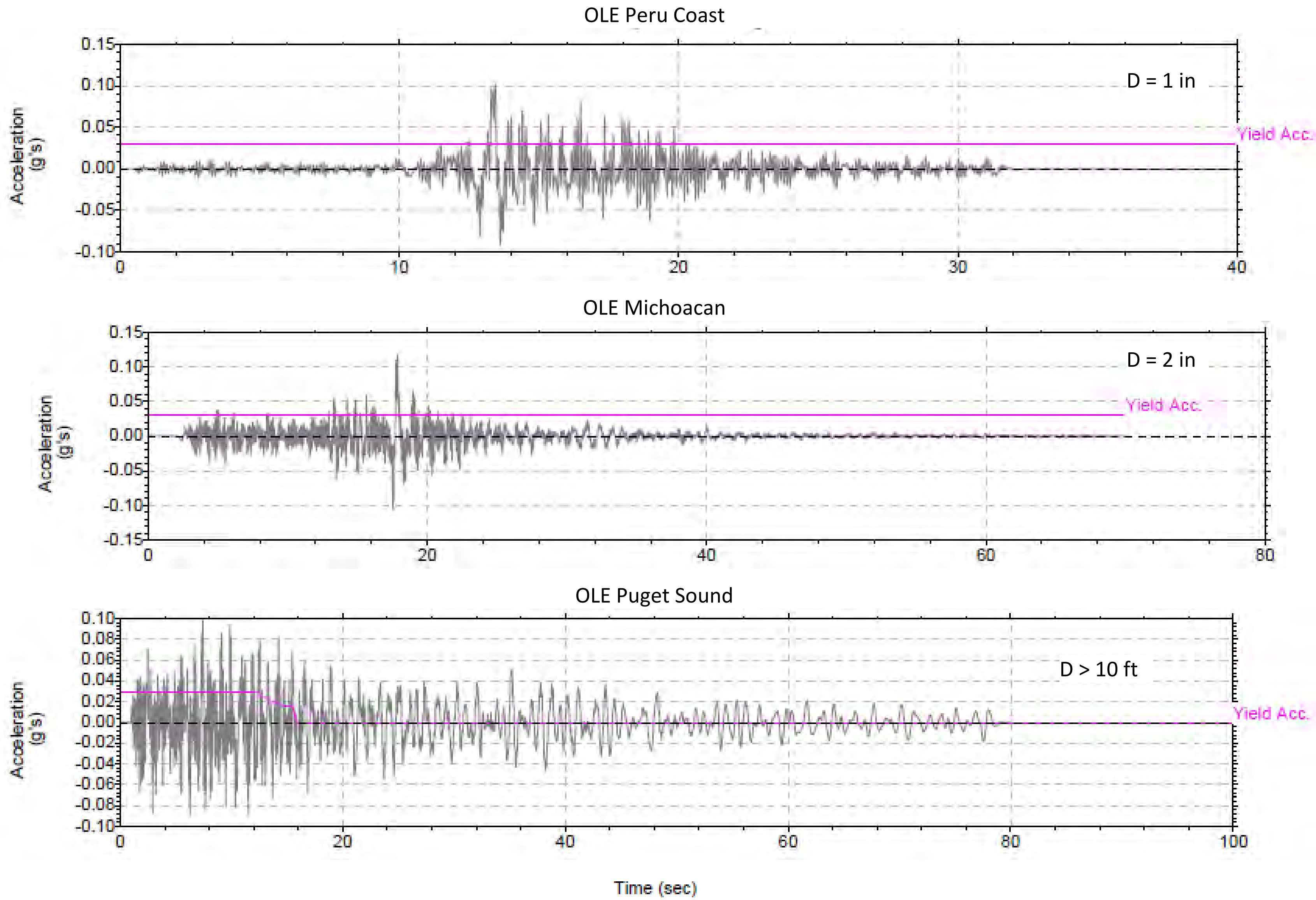

FIGURE 5.2-33. Modified Newmark Analysis for Section 3-3 Based on OLE Time Histories (Stark and Contreras 1998)

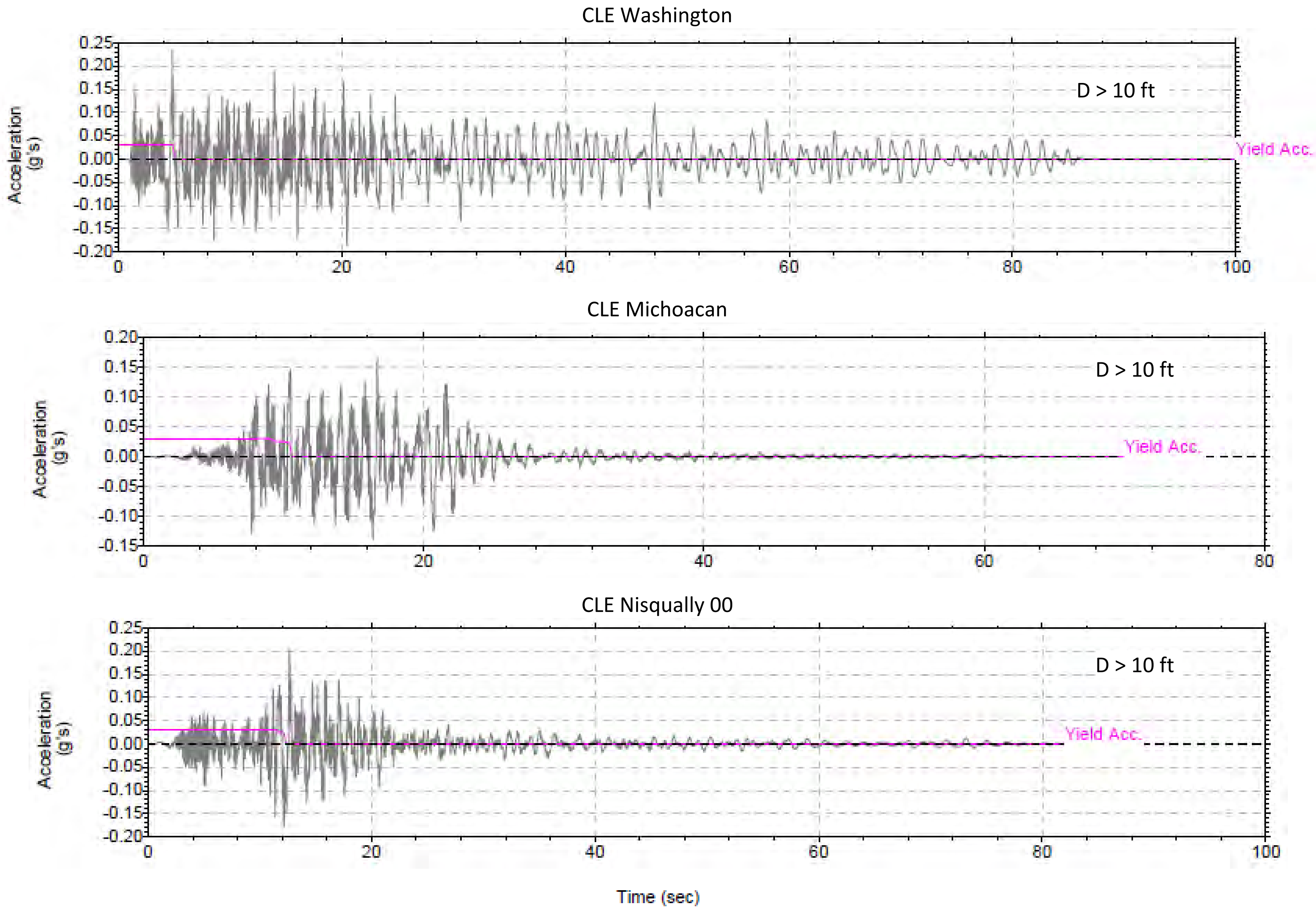

FIGURE 5.2-34a. Modified Newmark Analysis for Section 3-3 Based on CLE Time Histories (Stark and Contreras 1998)

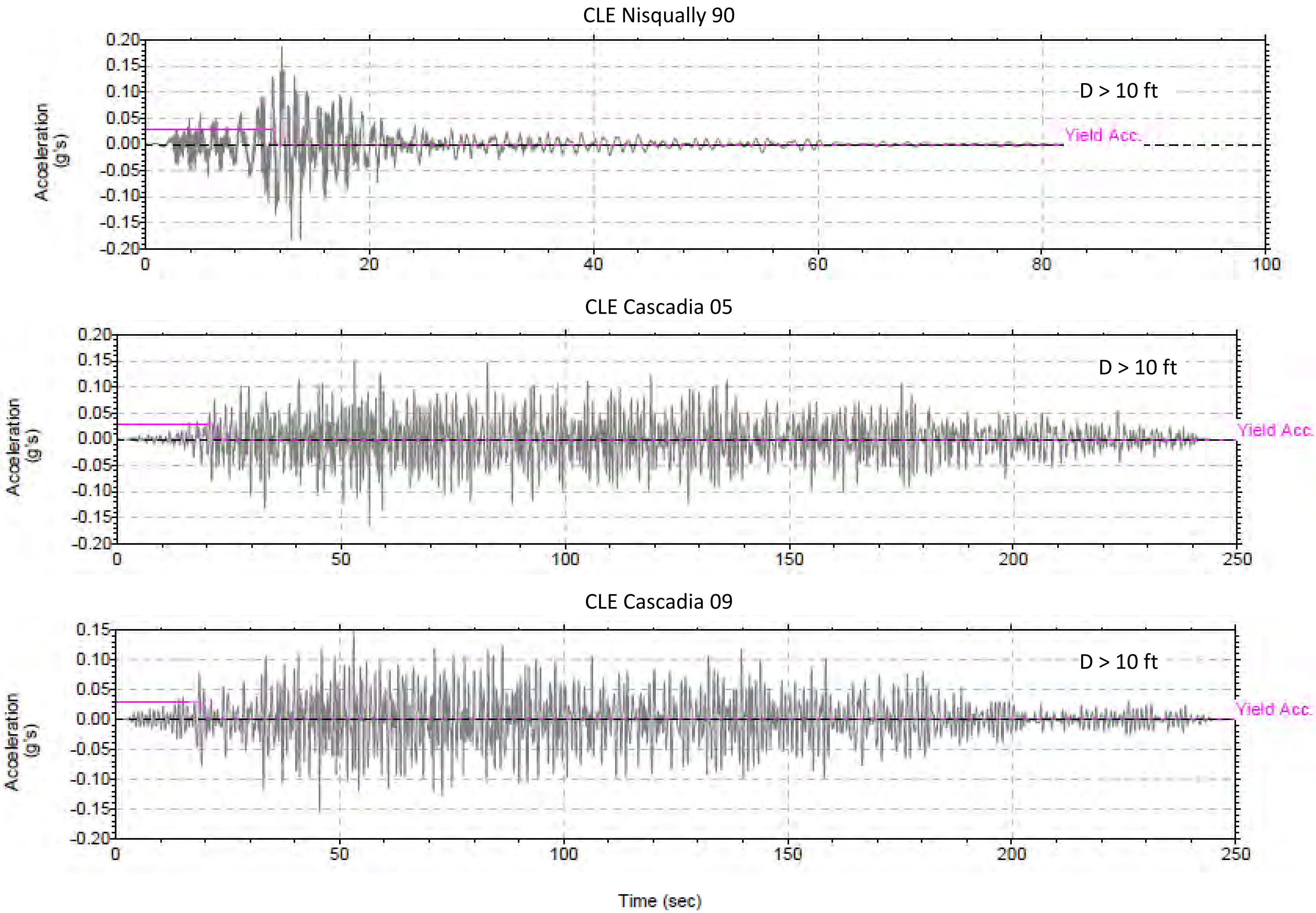

FIGURE 5.2-34b. Modified Newmark Analysis for Section 3-3 Based on CLE Time Histories (Stark and Contreras 1998)

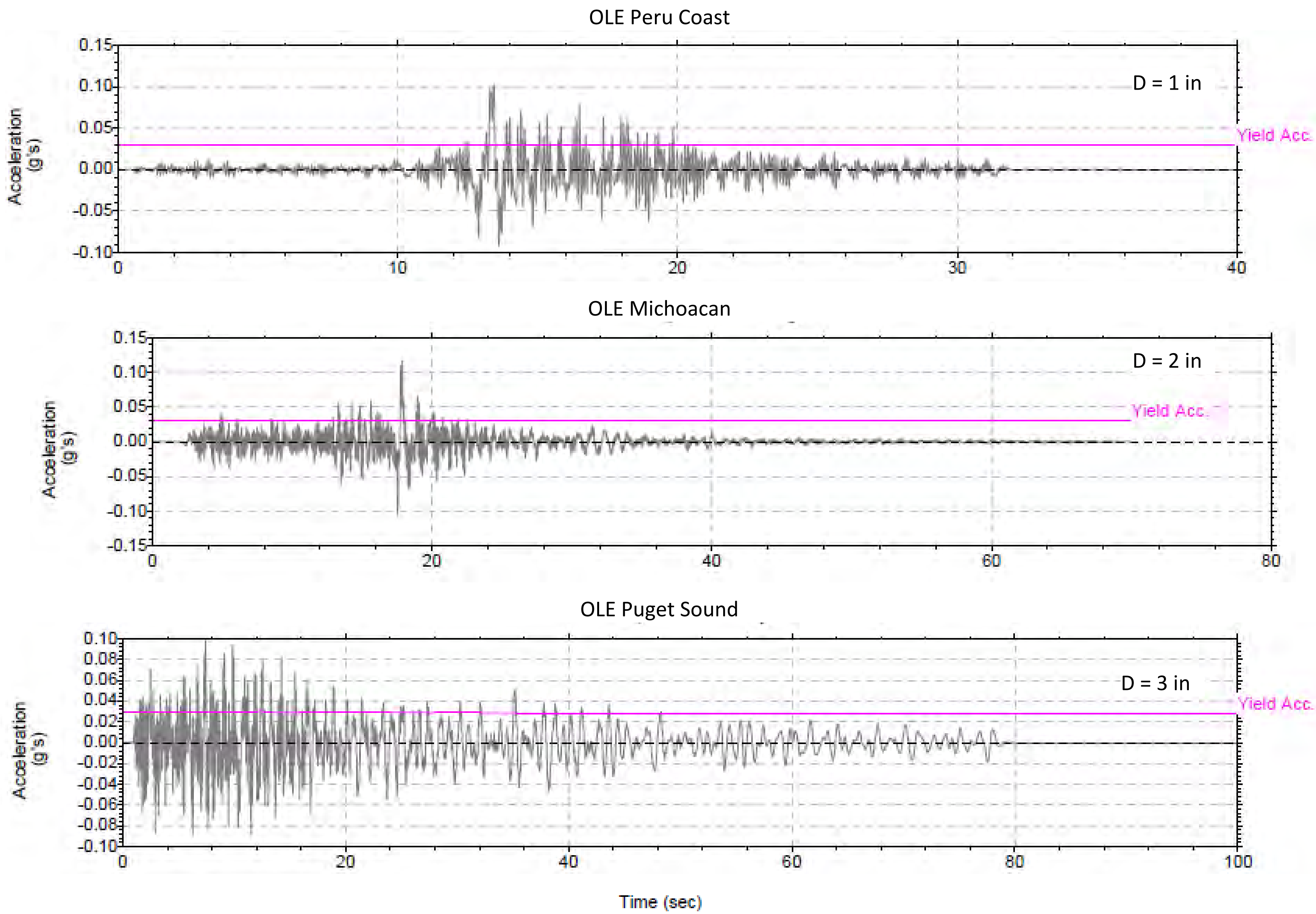

FIGURE 5.2-35. Modified Newmark Analysis for Section 3-3 Based on OLE Time Histories (Linear Shear Strength Reduction)

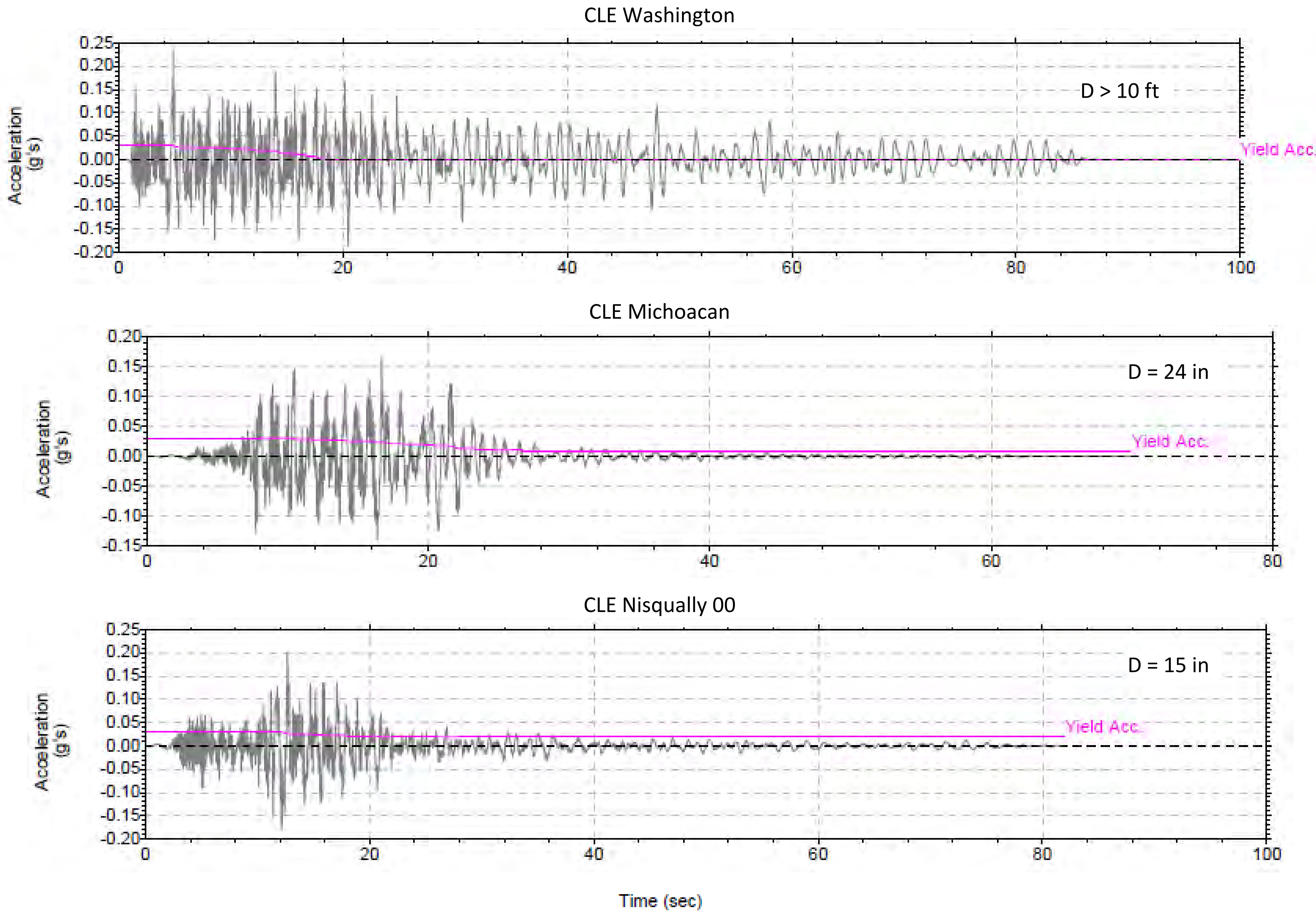

FIGURE 5.2-36a. Modified Newmark Analysis for Section 3-3 Based on CLE Time Histories (Linear Shear Strength Reduction)

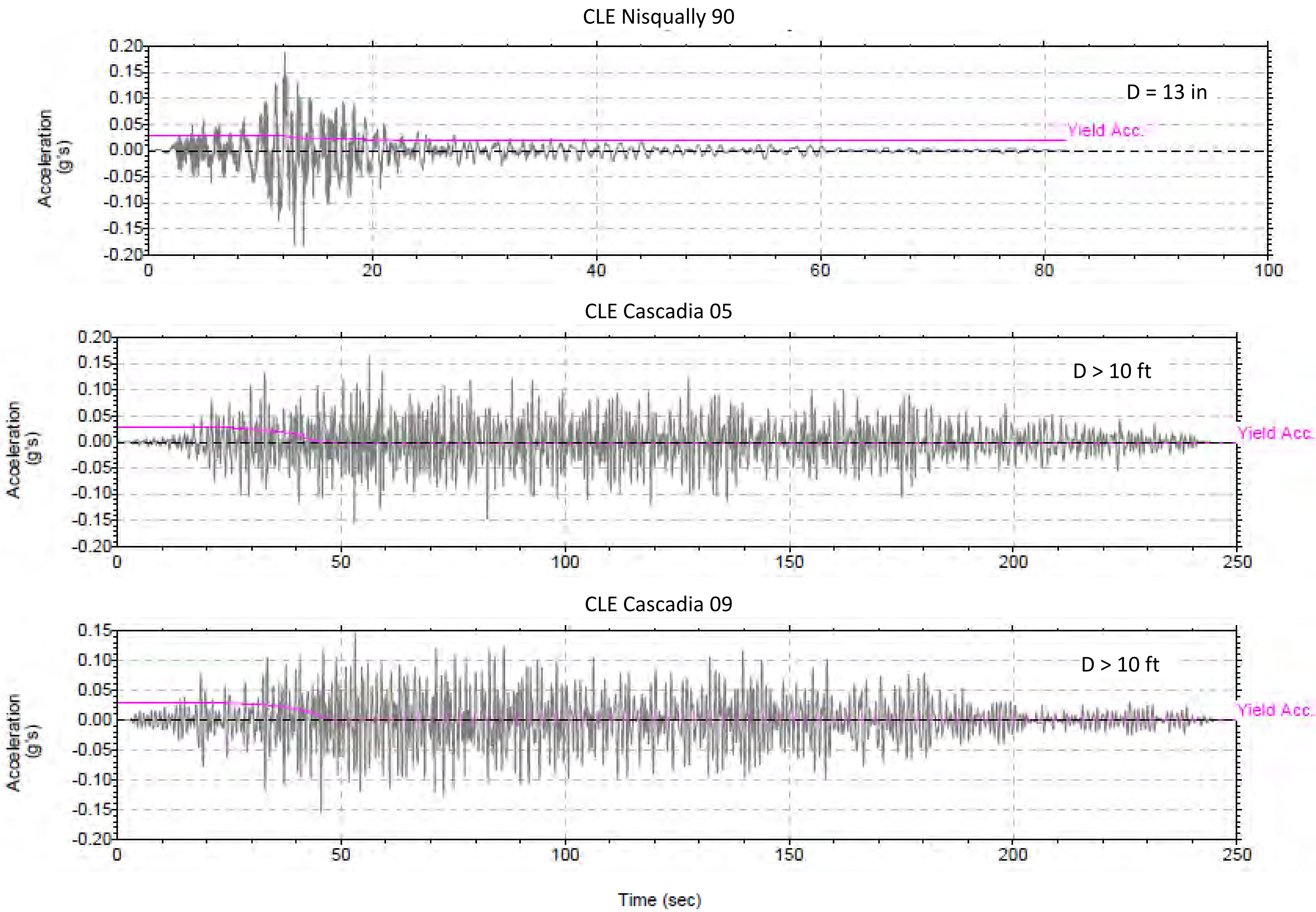

FIGURE 5.2-36b. Modified Newmark Analysis for Section 3-3 Based on CLE Time Histories (Linear Shear Strength Reduction)

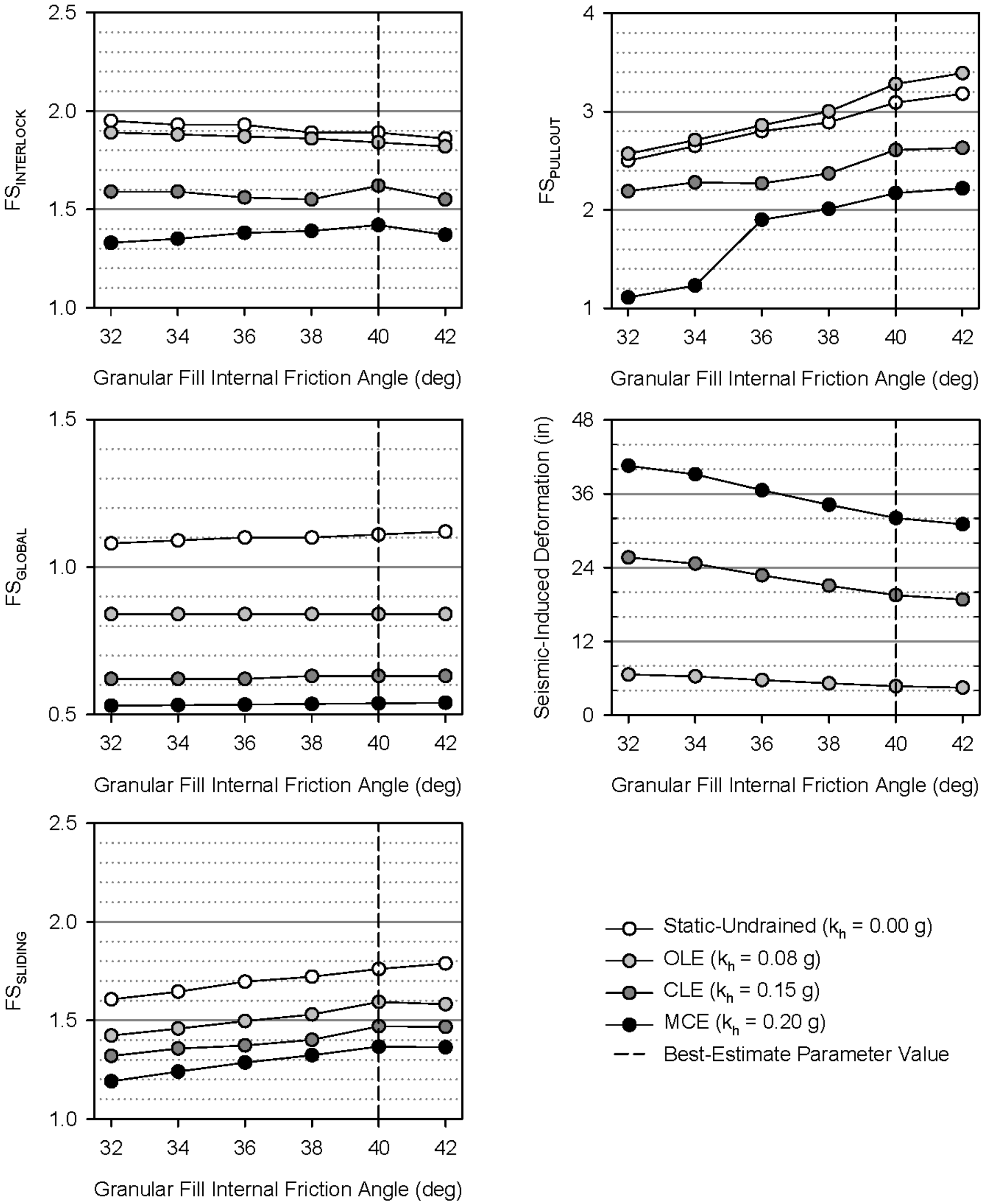

FIGURE 5.3-1. Effect of Granular Fill Friction Angle on Internal, External, and Global Stabilities

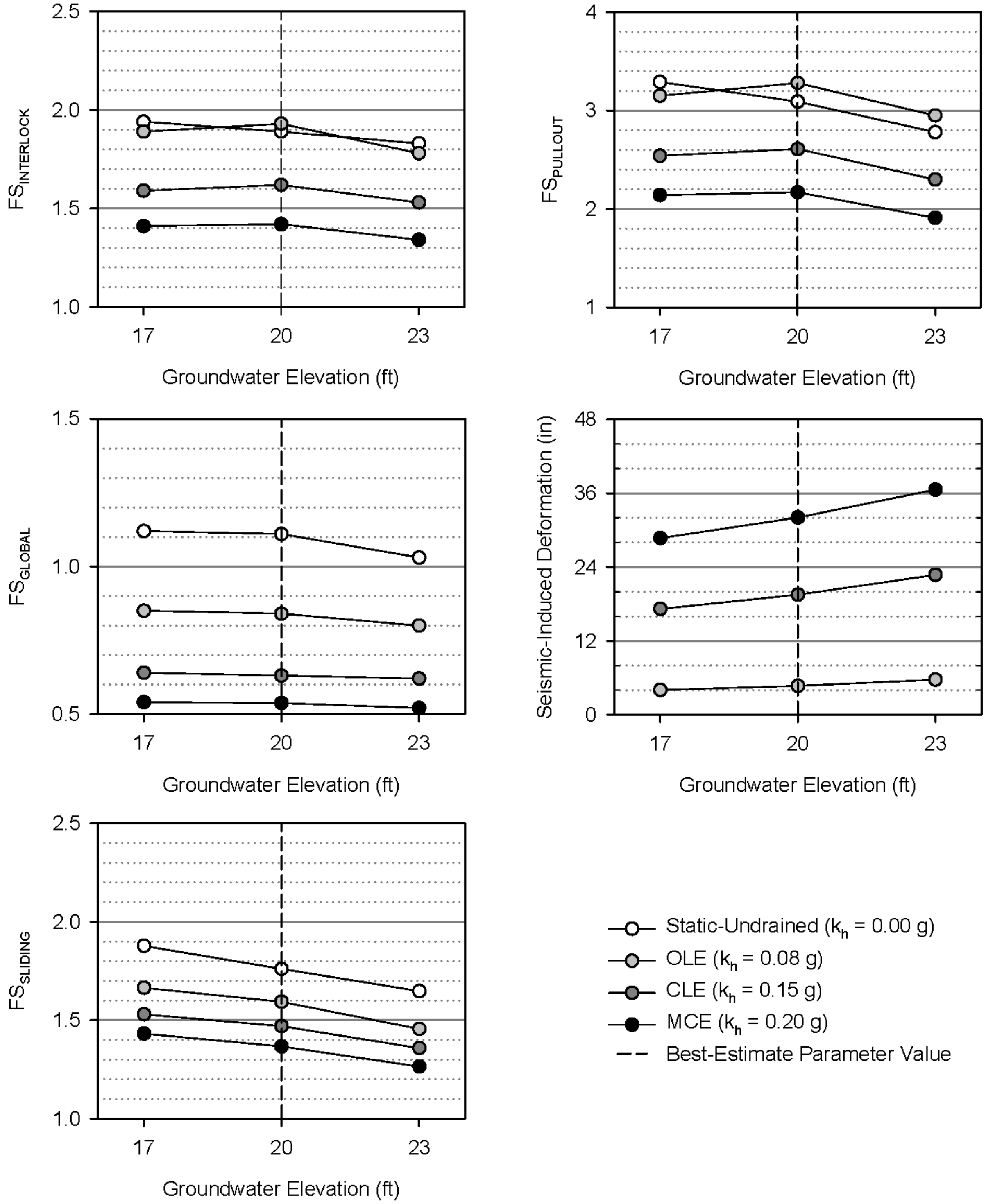

FIGURE 5.3-2. Effect of Landside Groundwater Elevation on Internal, External, and Global Stabilities

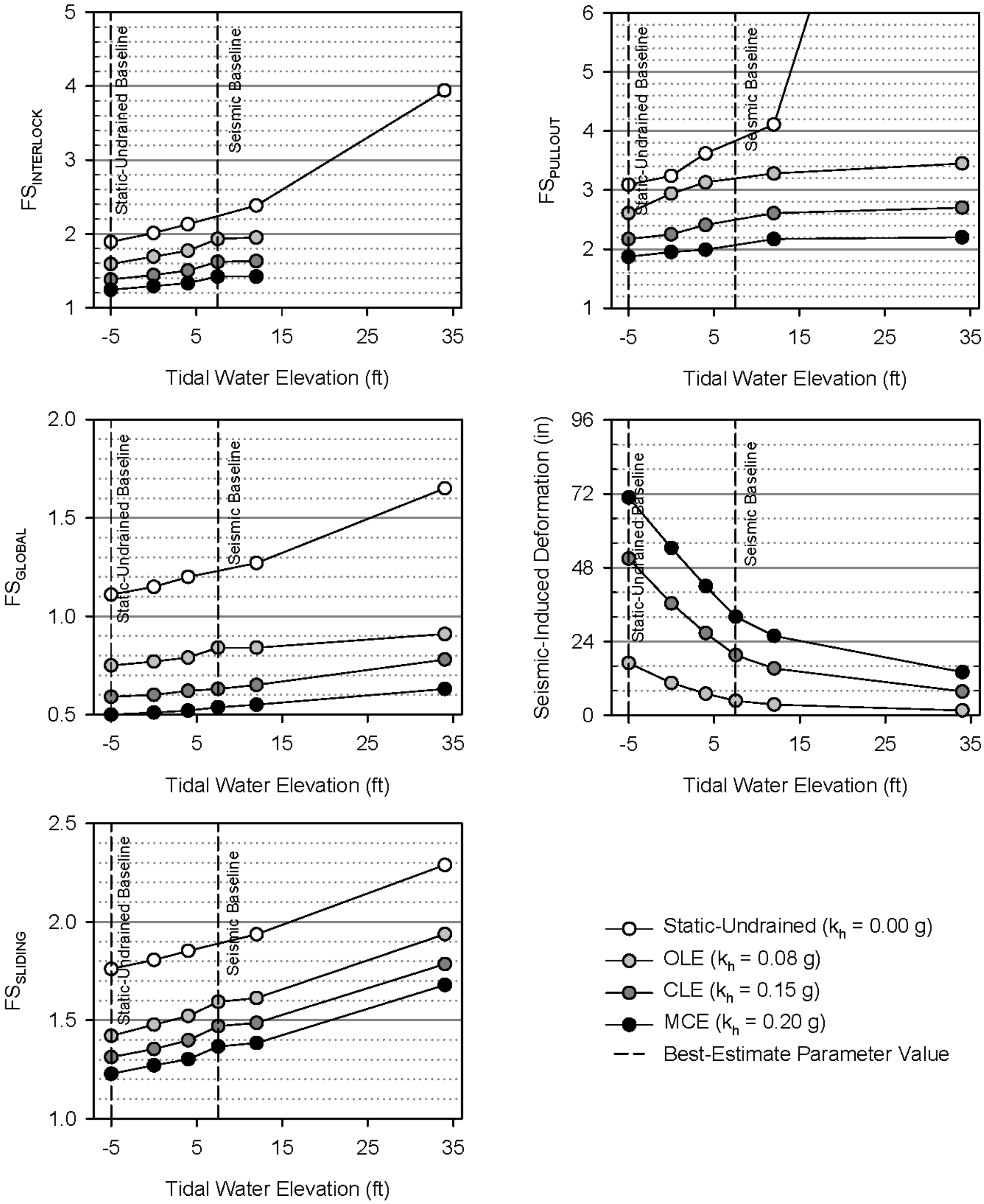

FIGURE 5.3-3. Effect of Tidal Water Elevation on Internal, External, and Global Stabilities

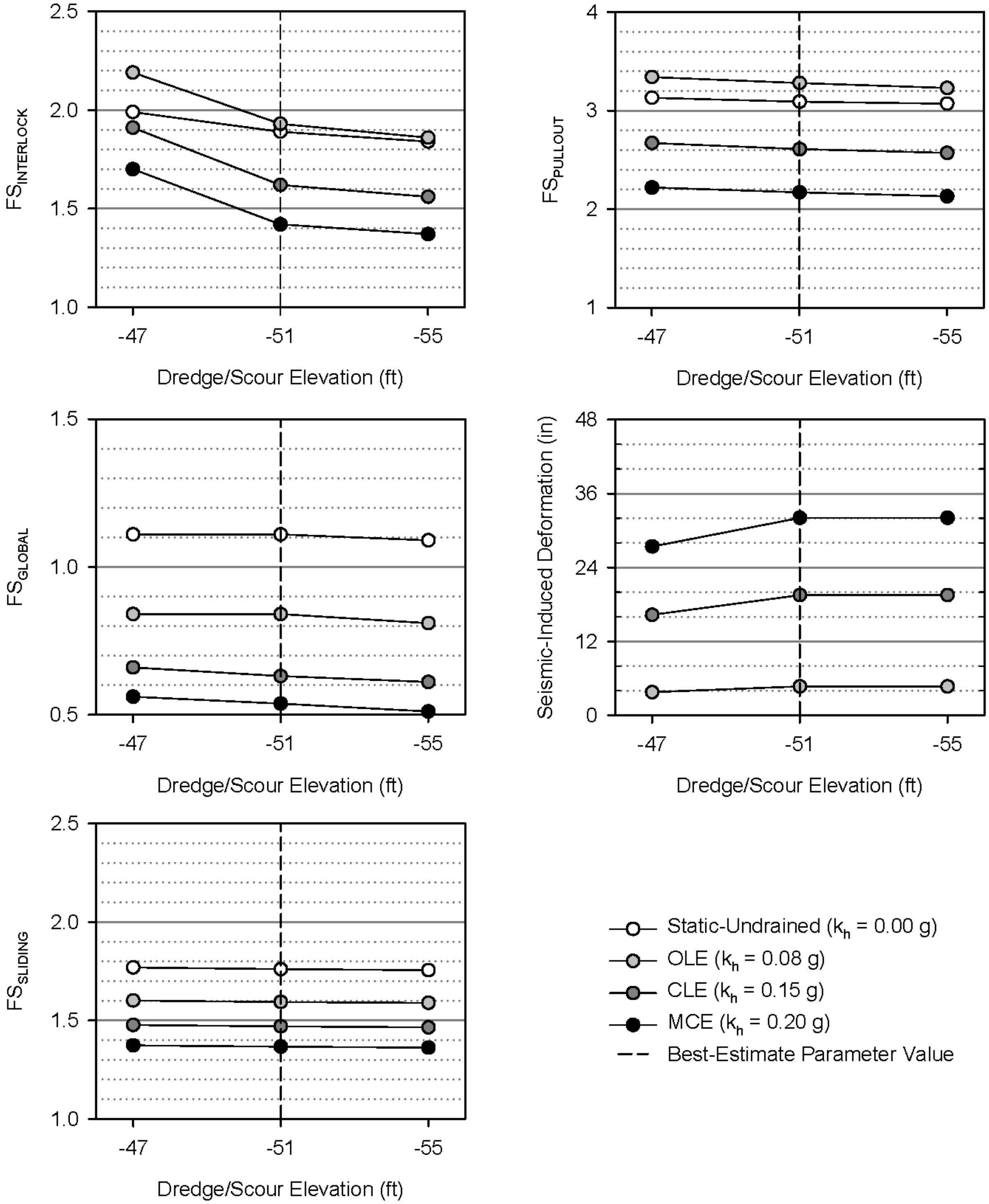

FIGURE 5.3-4. Effect of Dredge/Scour Elevation on Internal, External, and Global Stabilities

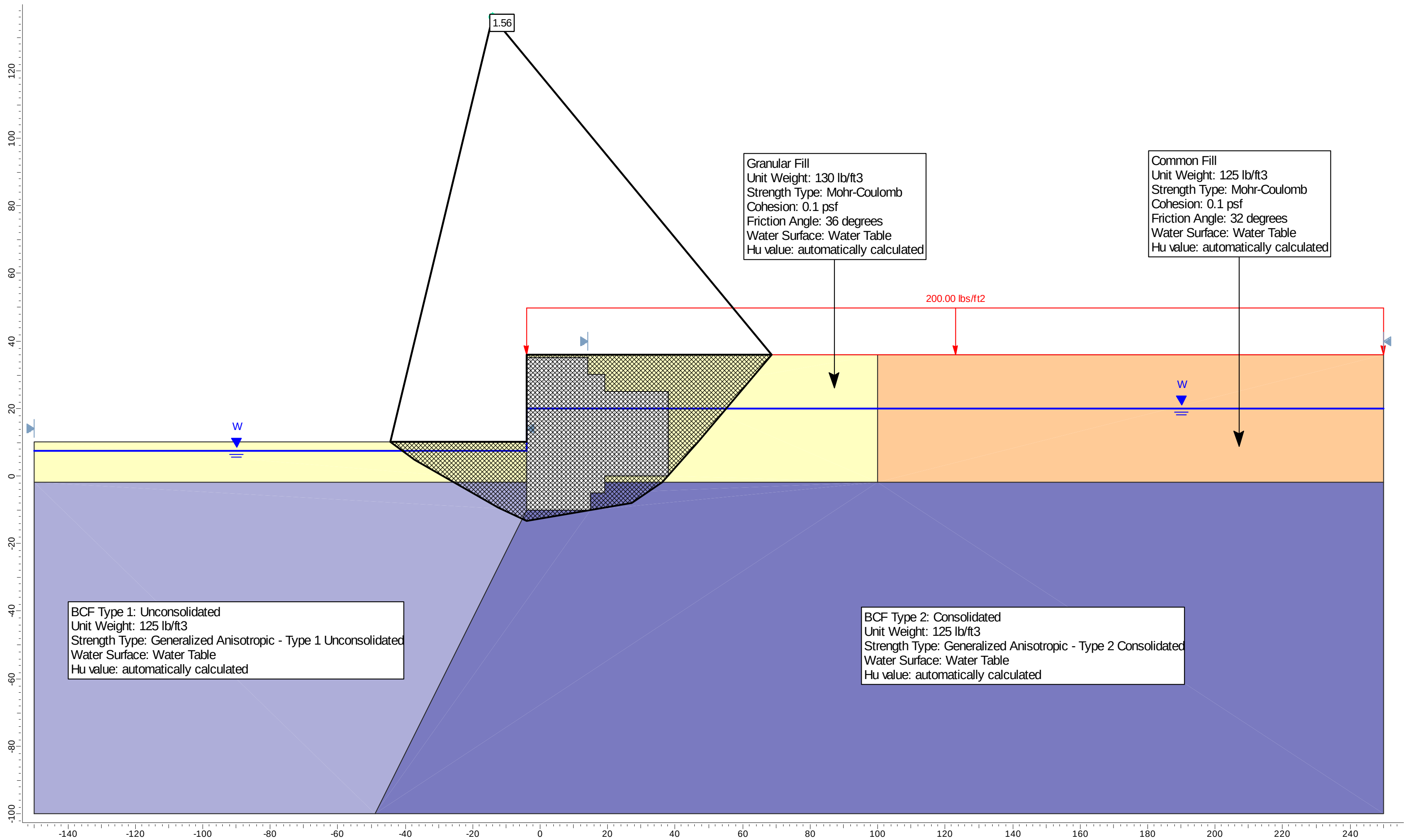

FIGURE 5.4-1a. Global Stability of the Dry Barge Berth at End-of-Construction Condition (Section C-C)

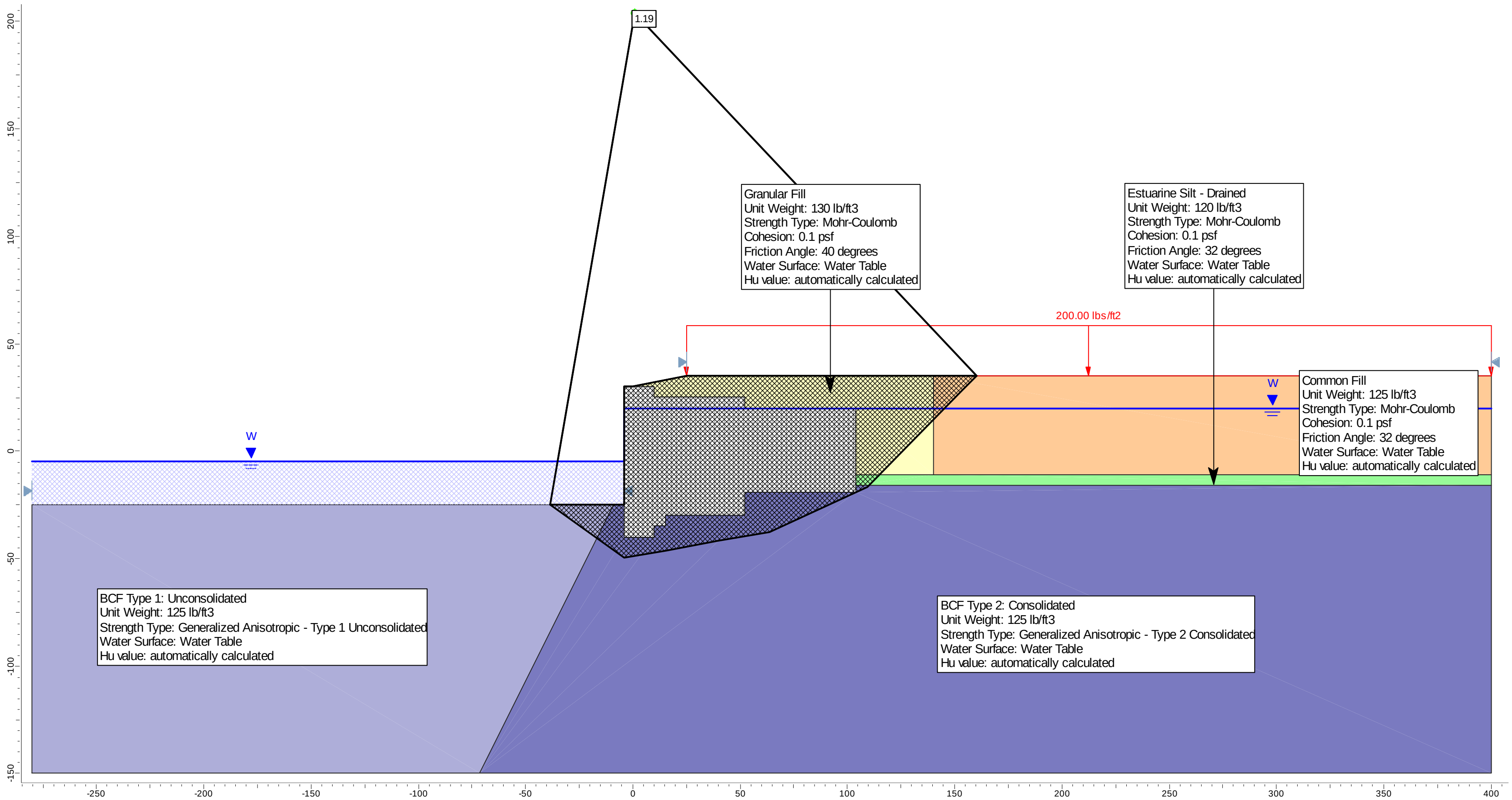

FIGURE 5.4-1b. Global Stability of the Wet Barge Berth at End-of-Construction Condition (Section D-D)

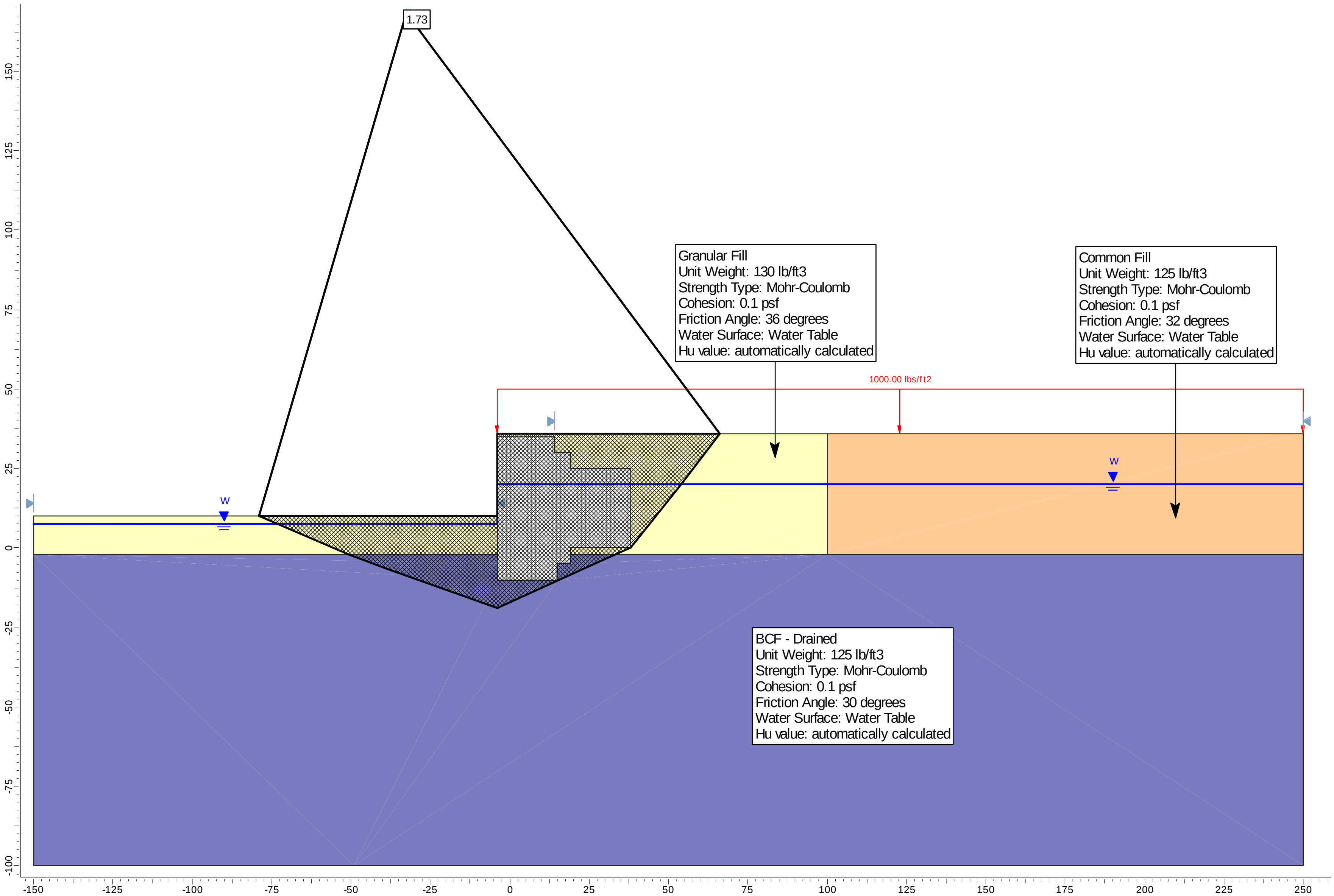

FIGURE 5.4-2a. Global Stability of the Dry Barge Berth at Long-term Static-Drained Condition (Section C-C)

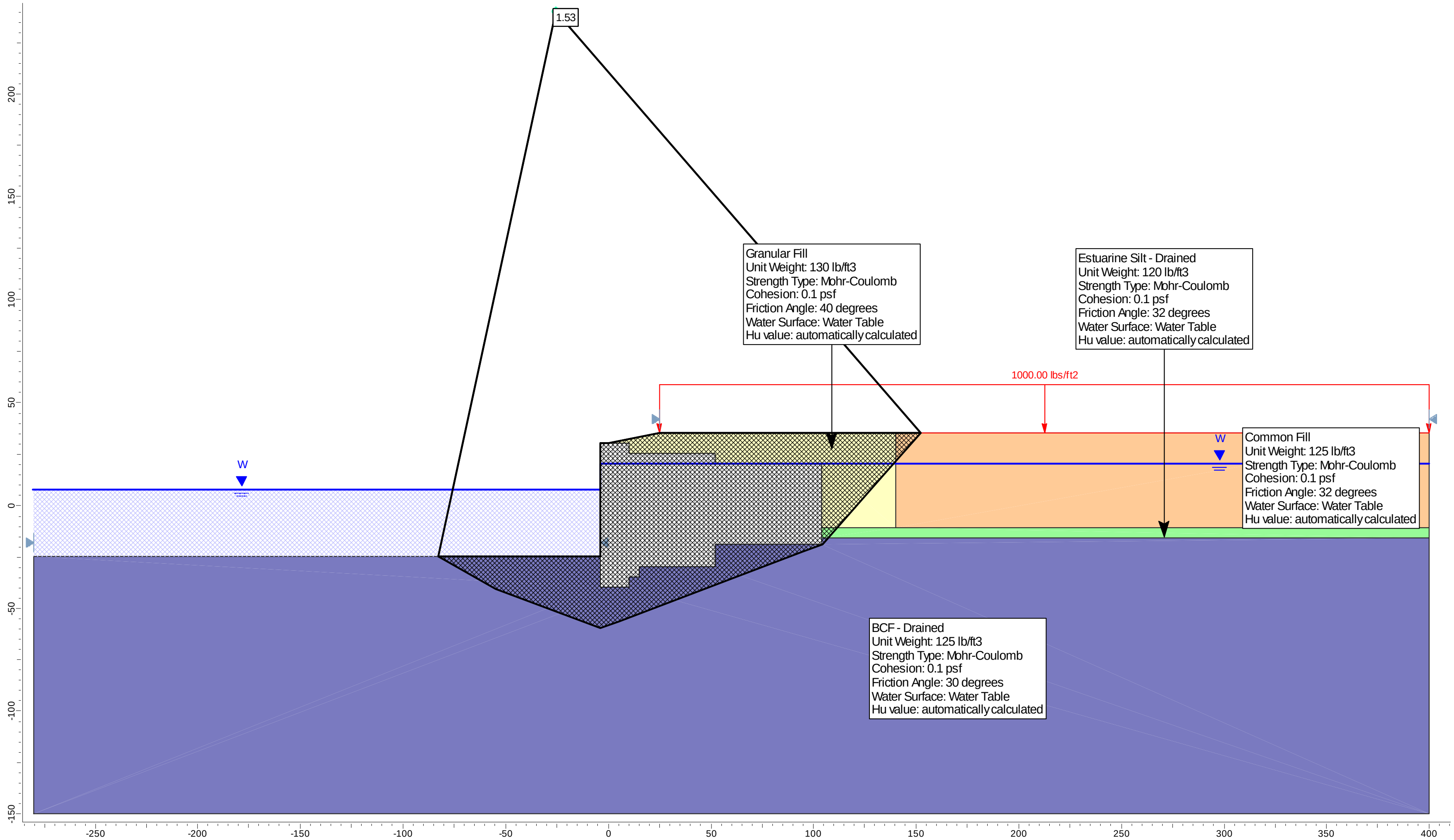

FIGURE 5.4-2b. Global Stability of the Wet Barge Berth at Long-term Static-Drained Condition (Section D-D)

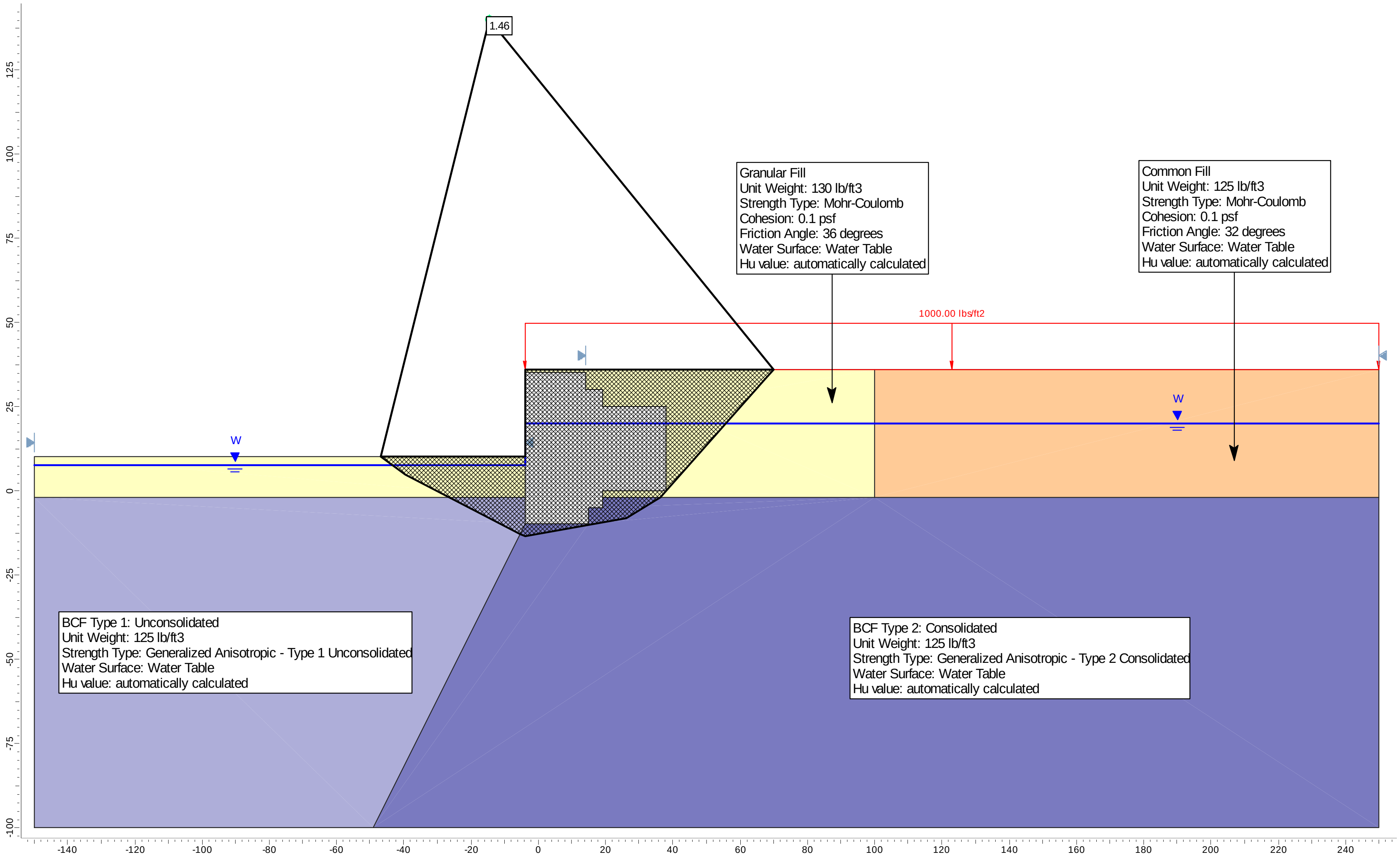

FIGURE 5.4-3a. Global Stability of the Dry Barge Berth at Long-term Static-Undrained Condition (Section C-C)

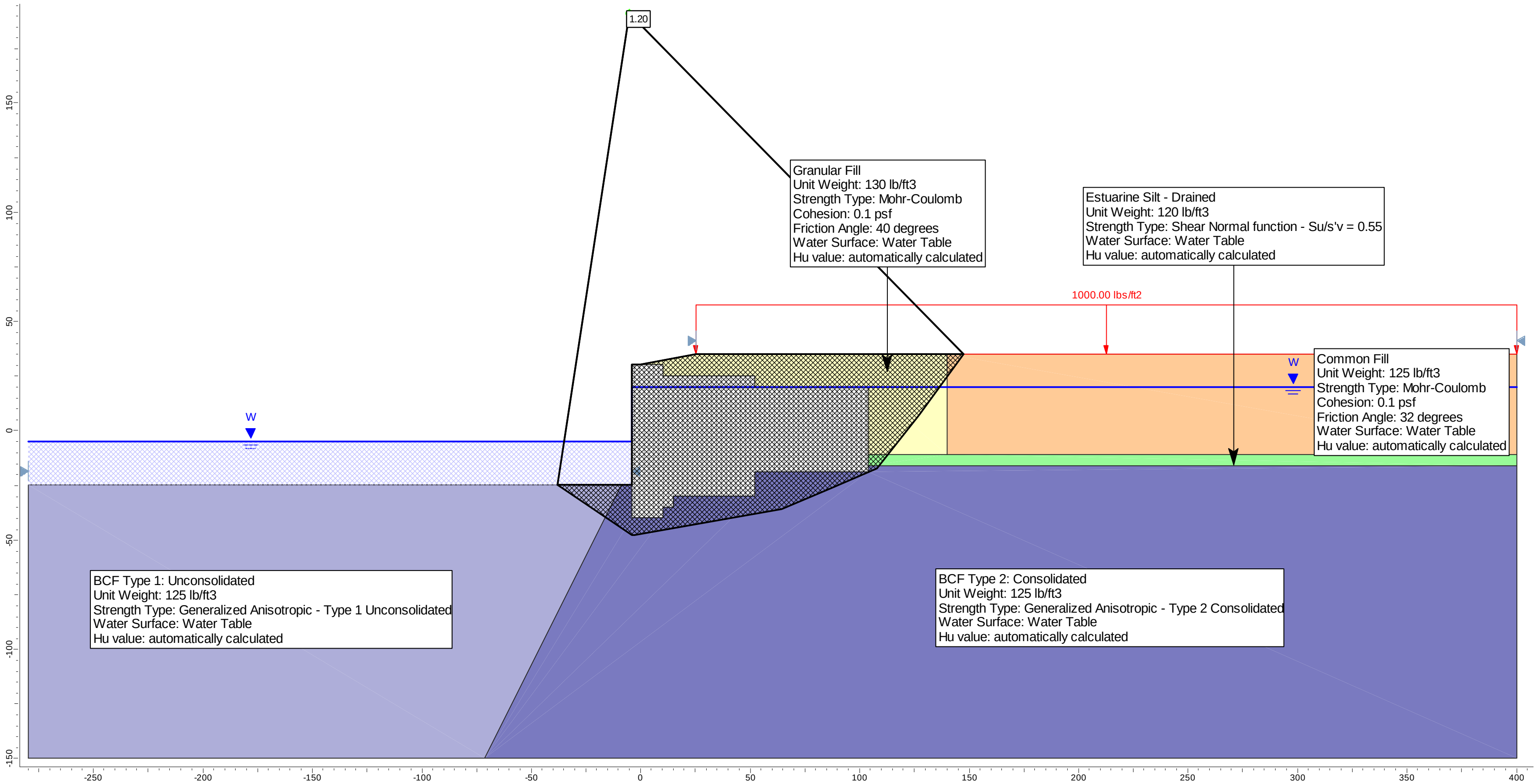

FIGURE 5.4-3b. Global Stability of the Wet Barge Berth at Long-term Static-Undrained Condition (Section D-D)

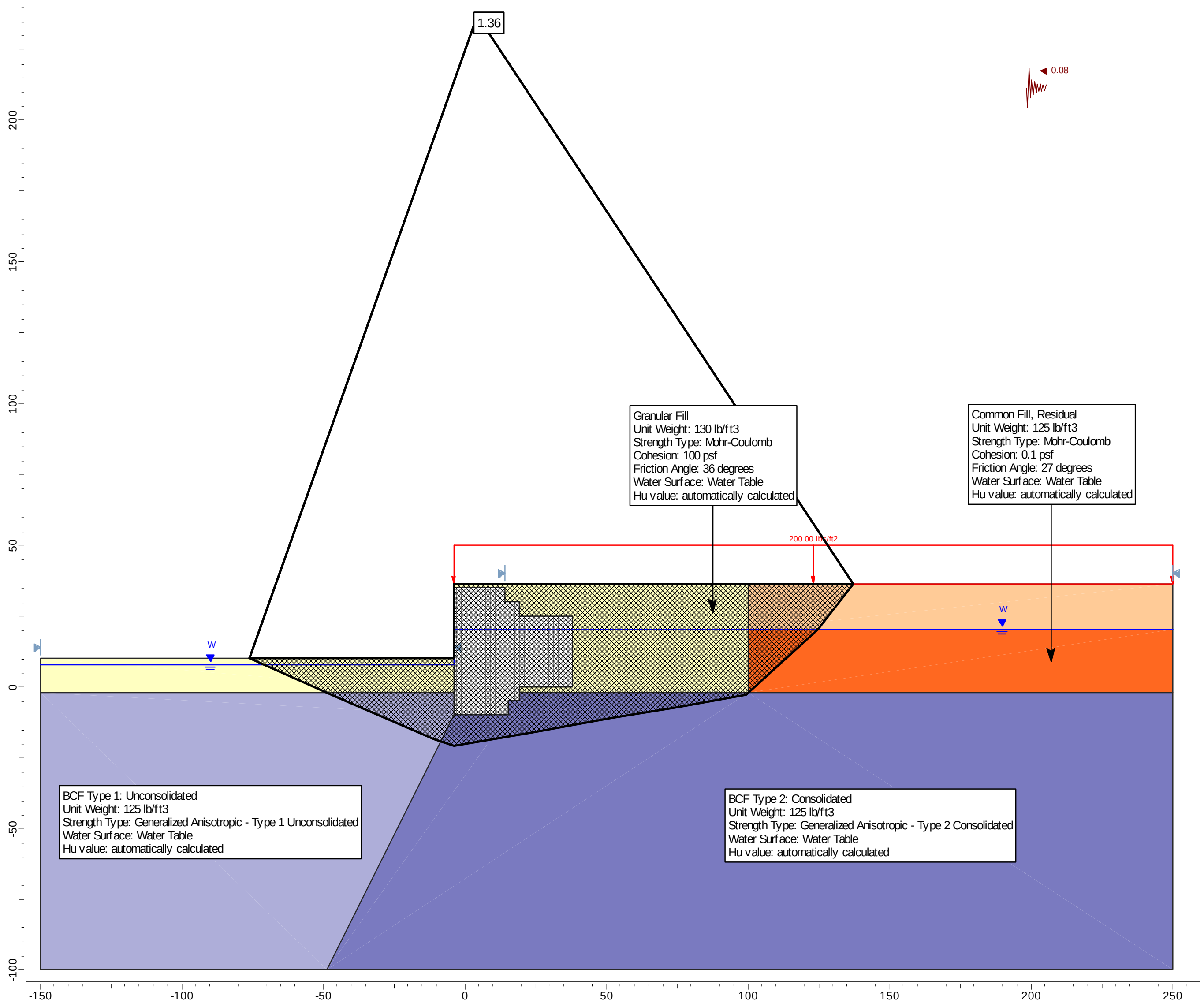

FIGURE 5.4-4a. Global Stability of the Dry Barge Berth During OLE Seismic Event (Section C-C)

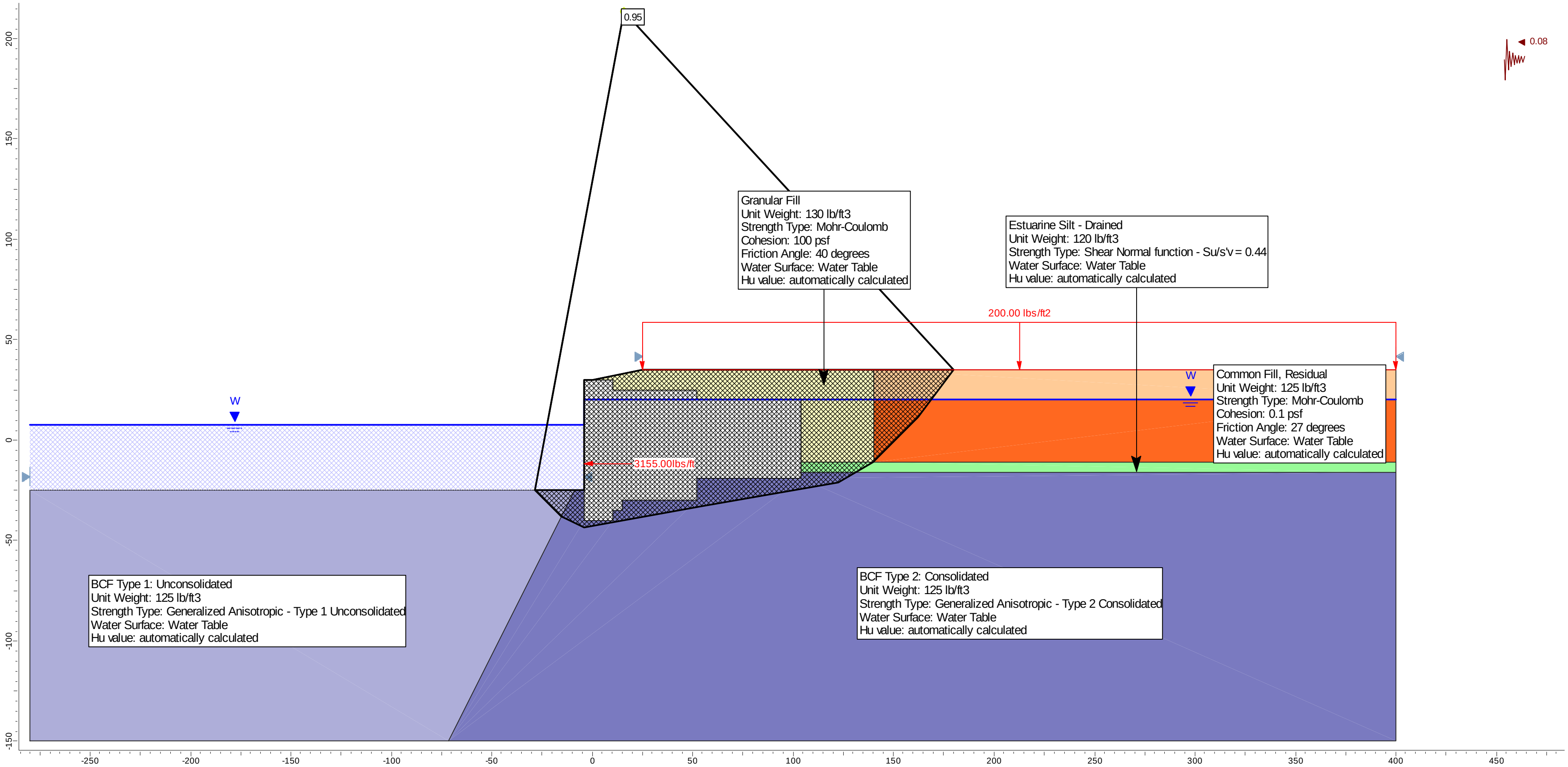

FIGURE 5.4-4b. Global Stability of the Wet Barge Berth During OLE Seismic Event (Section D-D)

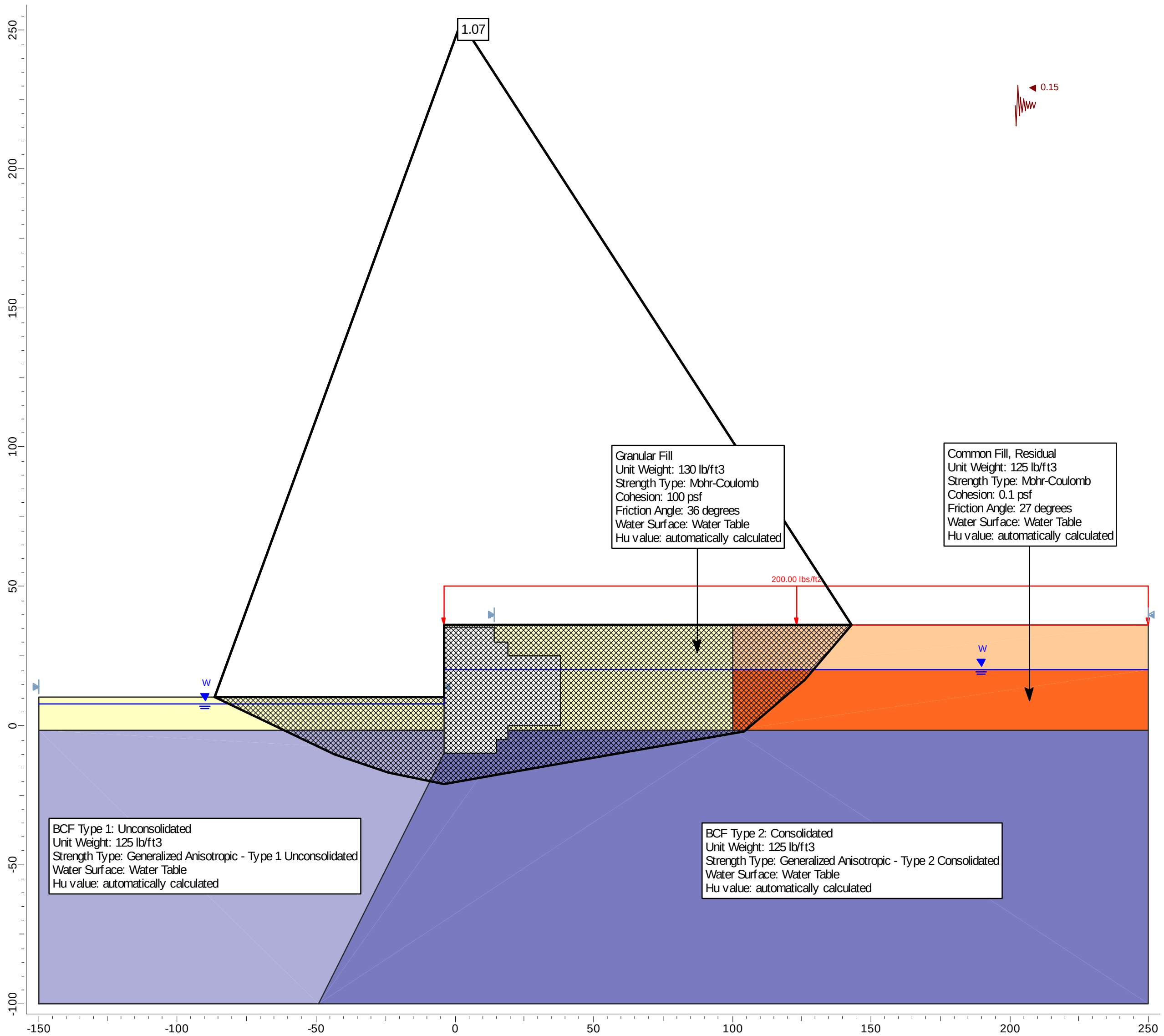

FIGURE 5.4-5a. Global Stability of the Dry Barge Berth During CLE Seismic Event (Section C-C)

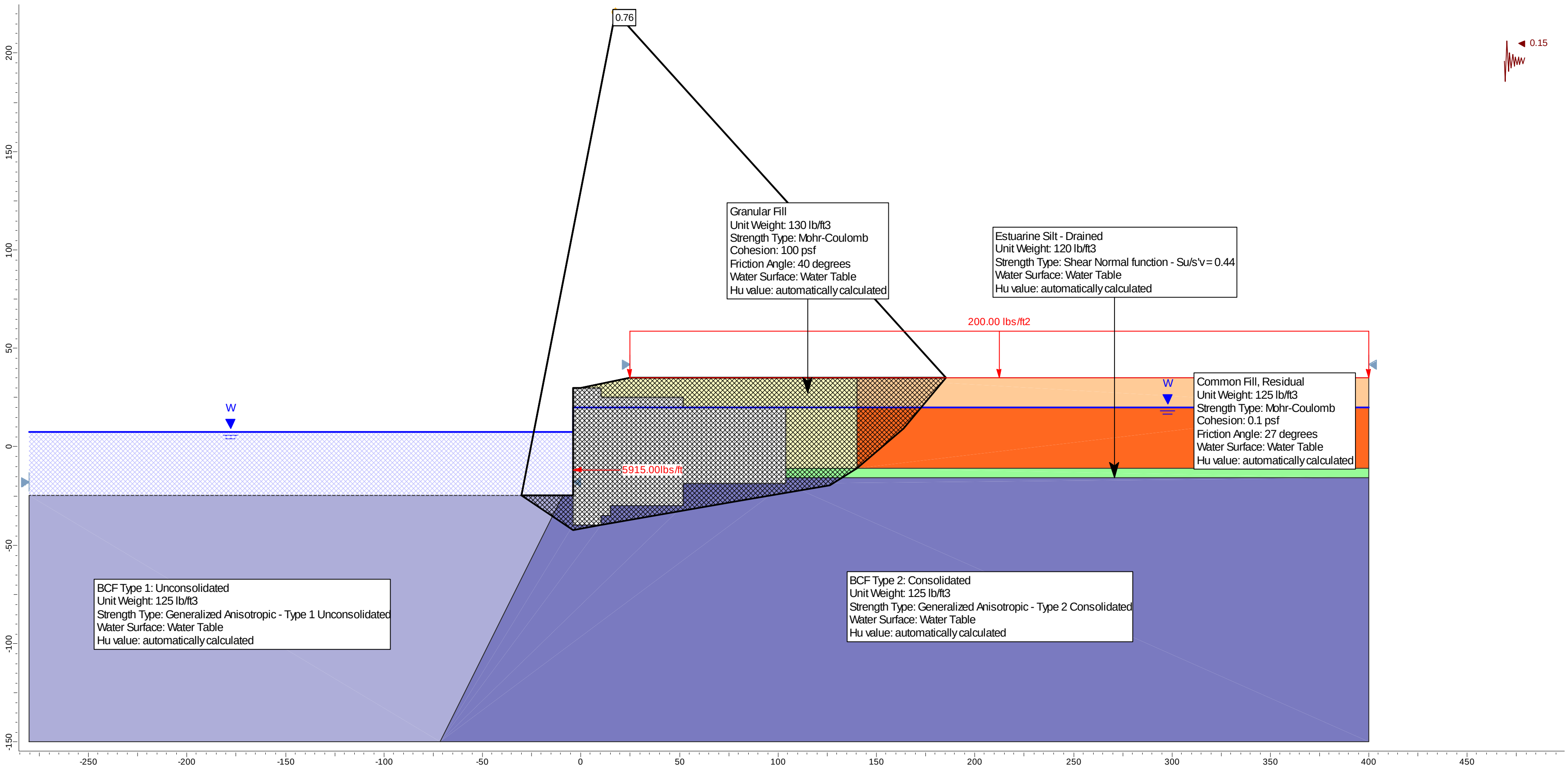

FIGURE 5.4-5b. Global Stability of the Wet Barge Berth During CLE Seismic Event (Section D-D)

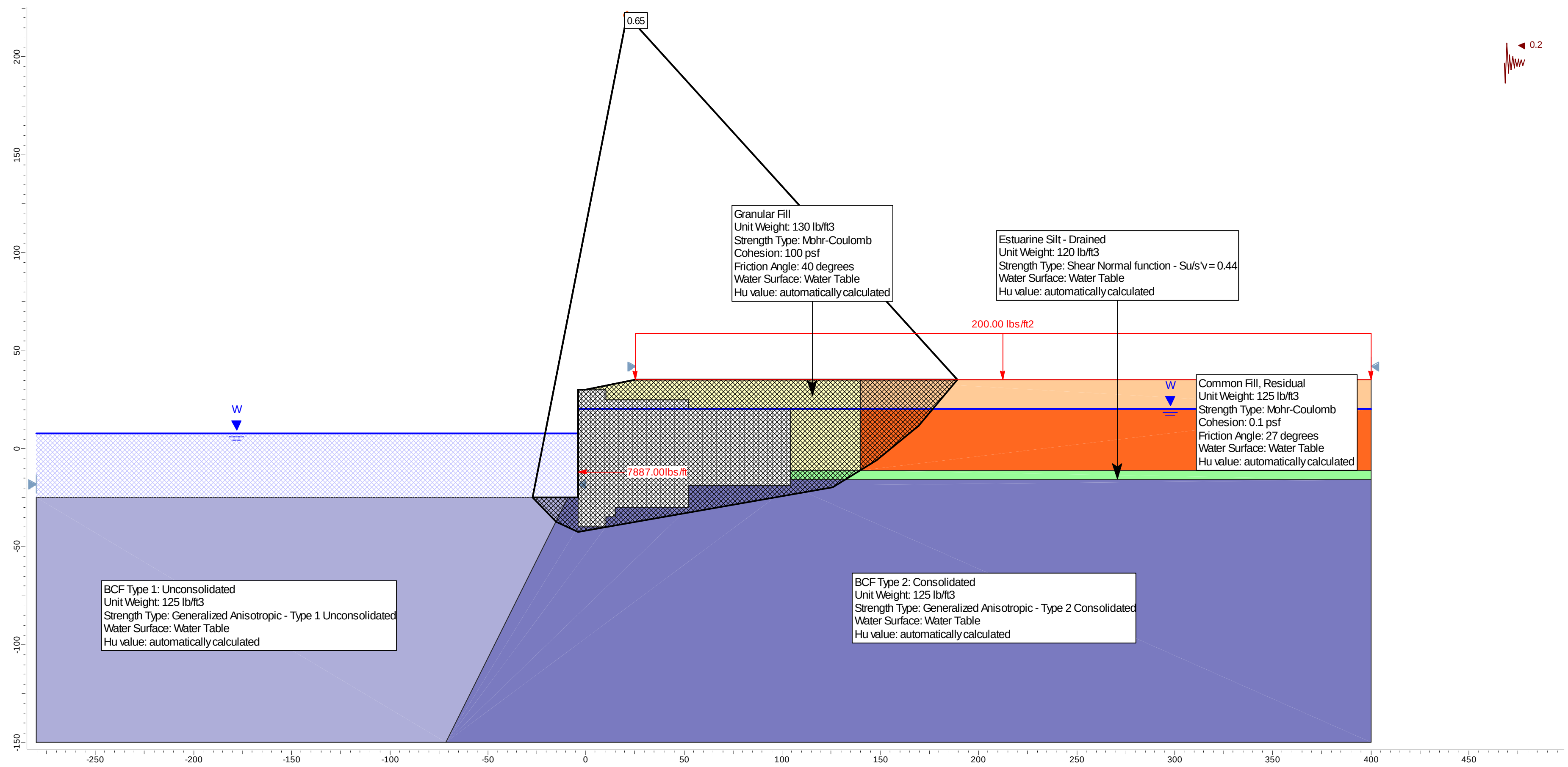

FIGURE 5.4-6. Global Stability of the Wet Barge Berth During MCE Seismic Event (Section D-D)

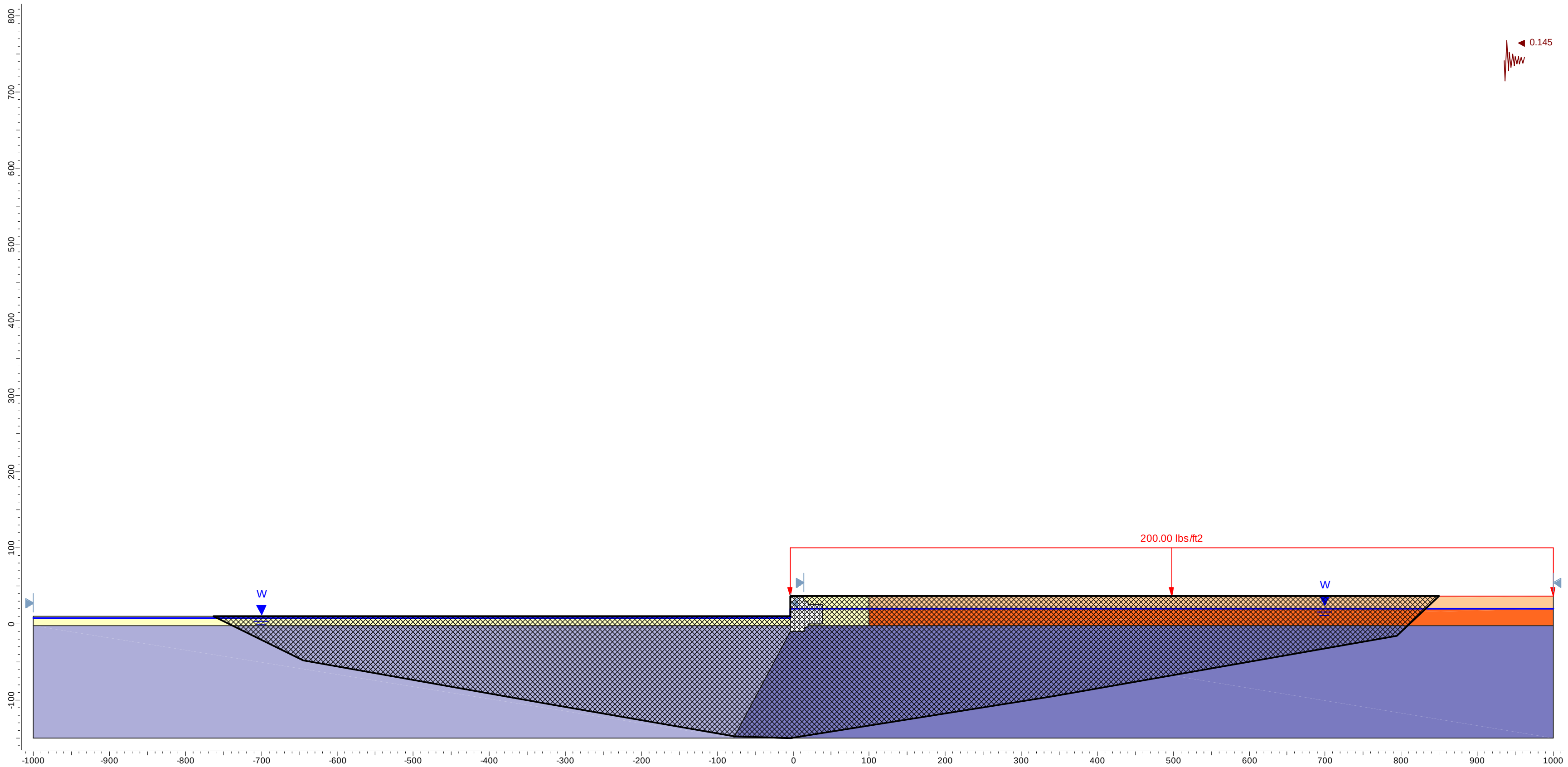

FIGURE 5.4-7a. Yield Acceleration of the Dry Barge Berth During Seismic Event (Section C-C)

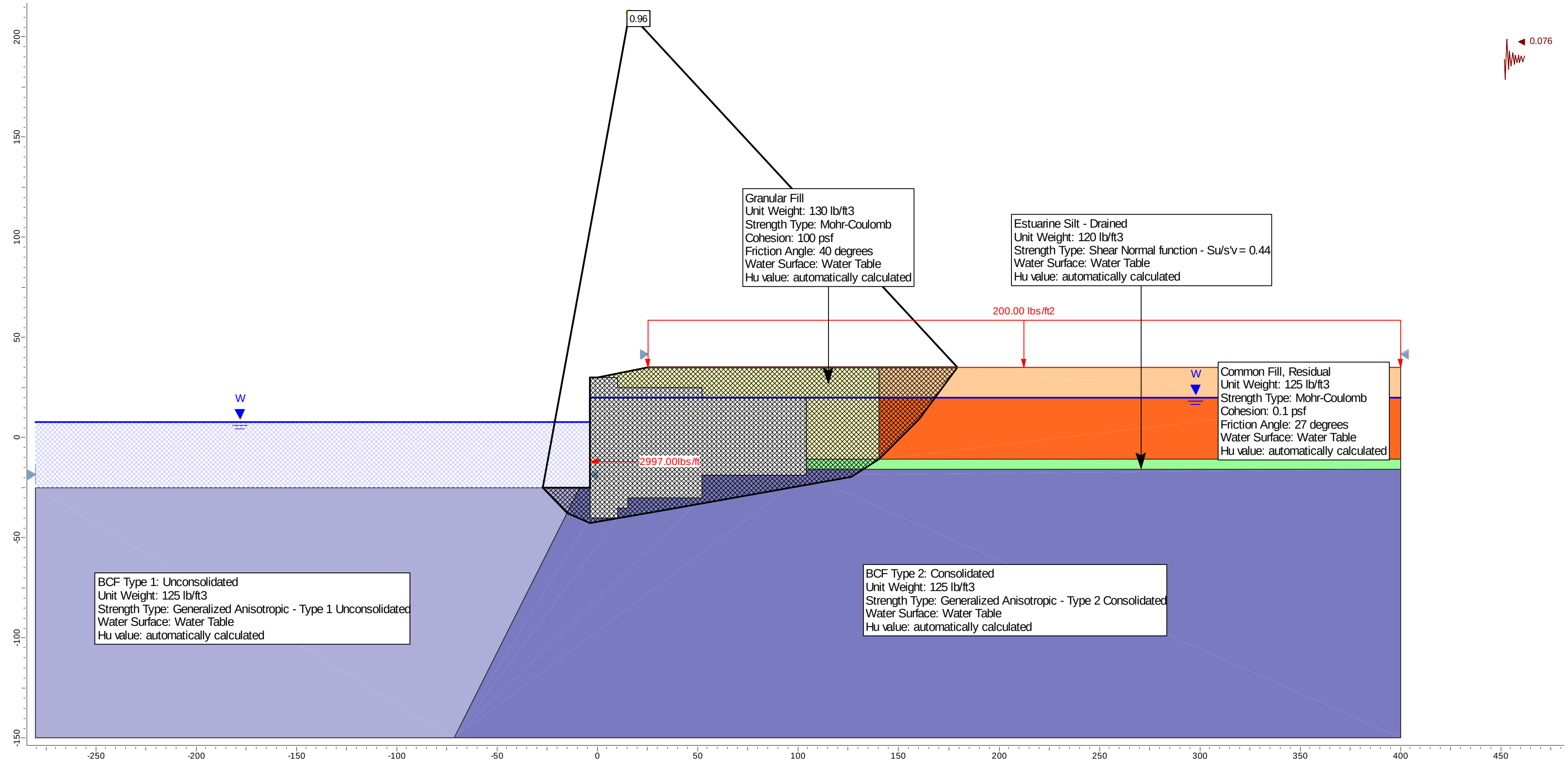

FIGURE 5.4-7b. Yield Acceleration of the Wet Barge Berth During Seismic Event (Section D-D)